# FAILURE ANALYSIS OF COLD-FORMED STEEL SECTIONS

**Xiao-ting Chu,** ***BEng, MEng***

Doctor of Philosophy


School of Engineering and Applied Science
Aston University
Birmingham, UK
2004

Aston University

# FAILURE ANALYSIS OF COLD-FORMED STEEL SECTIONS

**Xiao-ting Chu,** ***BEng, MEng***
Doctor of Philosophy
2004

## SUMMARY

The purlin-sheeting system has been the subject of numerous theoretical and experimental investigations over the past 30 years, but the complexity of the problem has led to great difficulty in developing a sound and general model. The primary aim of the thesis is to investigate the failure behaviours of cold-formed zed and channel sections for use in purlin-sheeting systems. Both the energy method and finite strip method are used to develop an approach to investigate cold-formed zed and channel section beams with partial-lateral restraint from the metal sheeting when subjected to a uniformly distributed transverse load.

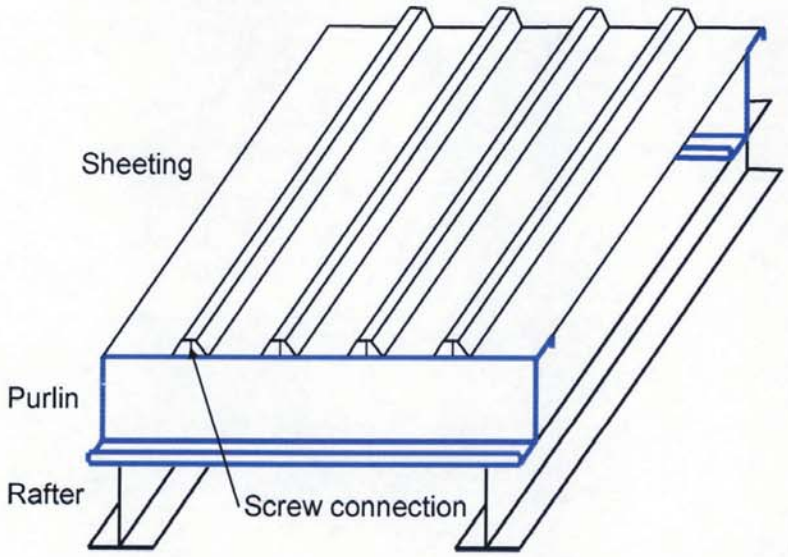


The stress analysis of cold-formed zed and channel section beams with partially-lateral restraint from the metal sheeting when subjected to a uniformly distributed transverse load is investigated firstly by using the analytical model based on the energy method in which the restraint actions of the sheeting are modelled by using two springs representing the translational and rotational restraints. The numerical results have showed that the two springs have significantly different influences on the stresses of the beams. The influence of the two springs has also been found to depend on the anti-sag bar and the position of the loading line.

A novel method is presented for analysing the elastic local buckling behaviour of cold-formed zed and channel section beams with partial-lateral restraint from metal sheeting when subjected to a uniformly distributed transverse load, which is carried out by inputting the cross sectional stresses with the largest compressive stress into the finite strip analysis. By using the presented novel method, individual influences of warping stress, partially lateral restraints from the sheeting and the dimensions of the cross section and position of the loading line on the local buckling behaviour are investigated.

The semi-analytical finite strip method is presented to investigate the buckling behaviour of the cold-formed steel zed and channel section beams when subjected to different loads. The focus of the study is on local and distortional buckling, for which existing results are only for sections subjected to pure compression and/or pure bending. The results obtained from this study have shown that, for local buckling there is no practical difference in the critical loads between pure bending and uniformly distributed loading. For distortional buckling, however, remarkable differences are found. The critical load for the uniformly distributed load is generally higher than that for the pure bending. The difference between these two loading cases is found to decrease with the beam length.

An analytical model is presented for predicting the lateral-torsional buckling of cold-formed zed and channel section beams, partial-laterally restrained by metal sheeting, subjected to uniformly distributed transverse loading with various boundary conditions. The individual influences of restraints provided by the sheeting and by interval anti-sag bars, boundary conditions, warping stress, loading position and the dimensions of cross section on the lateral-torsional buckling behaviour of the beams have been investigated. Further development of the analytical model is carried out to determine the load capacity for the lateral-torsional buckling of statically indeterminate zed purlins (a single span beam with one or two ends fixed), with partial lateral restraint from metal sheeting, when subjected to a uniformly distributed uplift load. The model takes account of the influence of the "softening" of the section stiffness due to local buckling and/or local material yielding. The analytical model developed in this paper, together with the numerically or experimentally obtained curves describing the local stiffness softening, can be used to determine the critical load for lateral-torsional buckling of the statically indeterminate purlin.

**Keywords:** cold-formed steel, local buckling, distortional buckling, lateral-torsional buckling, thin-walled.

# ACKNOWLEDGEMENTS

First and foremost, I am truly indebted to my supervisor, Dr. Long-Yuan Li, who has provided me an excellent study and working environment. I would like to thank him for directing me into this challenging and interesting research field. Without his consistent encouragement and help, this work would have never been completed.

I would like to acknowledge the financial support provided partly by the Committee of Vice-Chancellors and Principals of the universities of U.K. through the Overseas Research Studentship (ORS) awards and by research scheme of Dr. Long-yuan Li. Additional expenses for conference travels were also provided by research scheme.

I am most fortunate to have been enrolled in the Group of Civil Engineering and Logistics, as the support the Group gives postgraduate students helps to make the PhD process a more fruitful one. Many thanks go to the Head of Group, Professor Roger Kettle, not only for the Group's continued support of postgraduate students but also for providing helpful discussion and comments for my first year report and following several published papers throughout the project within his valuable time.

The work involved in this research was predominately theoretical and numerical which is mostly reliant on computers, and we depend on the support staff to keep the computers running. I am most grateful to Rob Poole, who helped me with numerous computer and net work problems, and particularly for maintaining the UNIX computer system. Thanks also to Nic Doran in the Computer Science Group. I also gave my thanks to Mr. John White and Dr. Neil Short for their generous support and advice during the time I was doing postgraduate demonstration at their lectures. I am grateful to the secretaries, Mrs Joy Atkins, Mrs Hellen Mallinson and Mrs Diane Markley, for their kind assistance.

Thanks to my postgrad colleagues and dear friends, Mr Bai-sen He, Ms Ling Zhang, Dr Qi-cheng Sun and Mr Dinh-tuan Tran, who gave generous support at various stages. Whether they gave me the direct advice about my subject or helped me with my personal problems, I enjoyed the time being with them. Baisen is really a good sport player and an excellent chef, thanks to you, I felt warm and comfortable during

my beginning period in UK. Ling helped me to learn a lot of things in the university and provided useful information about life in UK. I very much cherish the friendship with Dr Sun and his family who generously offered so much to me and my husband. Tuan was always a fountain of information when it came to computer software and I admire your aspiration for learning. I also acknowledge the kindness provided by my colleagues, particularly Betty Tam in MB171 from Bio-mechanical Engineering after we moved from Sumpner building to main building.

I also wish to express my thanks to Ms Qiaohong Lu, my best friend for her continuous support during the past five years, whose friendship encouraged me to carry on with the job and got me through the difficult time.

Finally, my sincere appreciation attributes to my family. My husband, Zhi-zhou Zhong, provided great support and encouragement and understanding throughout the whole period of my study. But most importantly, I would like to give my best acknowledgment and honour to my parents for their love. It is to them that this thesis is dedicated.

# CONTENTS

# LIST OF FIGURES & TABLES

# NOMENCLATURE

## Roman Characters

| | |
|---|---|
| $a$ | distance between loading line and web central line (mm) |
| $A$ | area of the cross section |
| $A_o$, $B_o$, $C_o$ | coefficients obtained from the calculation of the strain energy |
| $A_1$, $B_1$, $C_1$ | coefficients obtained from the calculation of the work done by the pre-buckling stress |
| $A_g$ | gross area of the cross section |
| $A_{ij}$ | coefficient matrices obtained from the calculation of the strain energy |
| $[A]$ | stiffness matrix |
| $b$ | flange width along the middle line (mm) |
| $b_1$ | overall width of flange (mm) |
| $b_{e1}$, $b_{e2}$, $b_{eff}$ | effective width (mm) |
| $B_{ij}$ | coefficient matrices obtained from the calculations of work done by the externally applied load through buckling displacements |
| ${}^kB$ | transverse bending stiffness |
| $[B]$ | Appropriate derivatives of the shape functions [N] |
| $c$ | lip length along the middle line (mm) |
| $c_1$ | overall lip length (mm) |
| $C_{eff}$ | effective length of the stiffening lip (mm) |
| $C_w$ | warping constant ($mm^6$) |
| ${}^kC$ | generalised warping constant |
| $d$ | web depth along the middle line (mm) |
| $d_1$ | overall depth of the cross section (mm) |
| $\{d\}$ | vector of nodal degrees of freedom |
| $D_w$ | section property ($mm^6$) |
| ${}^kD$ | generalised torsional constant |
| $[D]$ | plate rigidities matrix |
| $E$ | Young's modulus (MPa=$N/mm^2$) |
| $f_1$, $f_2$ | linear edge stresses (MPa) |
| $f_i$ | coefficient columns obtained from the calculations of work done by the externally applied load through the pre-buckling displacements |
| $f_i(x,x_i)$ | spline interpolation function |
| $f_{yi}$, $f_{zi}$ | coefficients obtained from the calculation of the work done by the externally applied loads |
| $\{f\}$ | vector of nodal forces |

| | |
|---|---|
| $f(y)$ | function defining the variation of the compressive stress along the longitudinal axis |
| $F_y$ | yield stress |
| $G$ | shear modulus (MPa) |
| $[G]$ | matrix resulting from differentiating the shape functions |
| $h$, $h_s$ | perpendicular distance from a tangent at the point under consideration to the centroid and shear centre (mm) |
| $I_y$, $I_z$ | second moments of the cross-section area about $y$ and $z$ axes ($mm^4$) |
| $I_{yz}$ | product moment of the cross-section area ($mm^4$) |
| $I_\omega$ | warping constant calculated based on the sectional coordinate with respect to the centroid ($mm^6$) |
| $I_{\omega z}$ | sectorial product of inertia with respect to $z$ axis calculated based on the sectional coordinate with respect to the centroid ($mm^5$) |
| $J$ | torsion constant ($mm^4$) |
| $k$ | total length of the middle lines of the cross-section (mm) |
| $k_1$, $k_2$ | constants of the two rotational springs applied at the ends of beam (N) |
| $k_x$, $k_z$ | translational spring stiffness along $x$ and $z$ axis (MPa) |
| $k_\phi$ | rotational spring stiffness (N) |
| $k_\sigma$ | buckling factor |
| $[K]$ | initial stiffness matrix |
| $[K_g]$ | geometric stiffness |
| $[K_{gmn}]$, $[K_{gnm}]$ | coupled global geometric stiffness matrix associated with wave number m and n |
| $[K_M]$, $[K_{gMM}]$ | global stiffness matrix and global geometric stiffness matrix associated with wave number M |
| $[K_{uv}]$, $[K_{w\theta}]$ | initial stiffness submatrices for plane stress and bending |
| $l$ | span length of the beam (mm) |
| $M_{cr}$ | critical buckling moment (MPa) |
| $M_{crd}$ | critical elastic distortional buckling moment (N mm) |
| $M_{cre}$ | critical elastic lateral-torsionalal buckling moment (N mm) |
| $M_{crl}$ | critical elastic local buckling moment (N mm) |
| $M_n$ | nominal flexural strength (N mm) |
| $M_{nd}$ | nominal flexural strength for distortional buckling (N mm) |
| $M_{ne}$ | nominal flexural strength for lateral-torsional buckling (N mm) |
| $M_{nl}$ | nominal flexural strength for local buckling (N mm) |
| $M_T$ | twisting moment (N mm) |
| $M_{oy}$, $M_{oz}$ | pre-buckling moment about $y$ and $z$ axes (N mm) |
| $M_y$, $M_z$ | bending moments about y and z axis (N mm) |
| $M_{yield}$ | yielding moment (N mm) |

| | |
|---|---|
| $M_{yo}$, $M_{yl}$, $M_{zo}$, $M_{zl}$ | concentrated moments about y and z axes, applied at the ends of the purlin (N mm) |
| $M_{\omega}$ | warping moment (N mm) |
| $N$ | number of modes |
| $[N]$ | shape functions |
| $[N']$ | appropriate derivatives of the shape functions $[N]$ |
| $p_0$ | limiting compression stress (MPa) |
| $p_{cr}$ | local buckling stress (MPa) |
| $P_{crd}$ | critical elastic distortional column buckling load (N) |
| $P_{cre}$ | minimum of the critical elastic column buckling load in flexural, torsional, or torsional-flexural buckling (N) |
| $P_{crl}$ | critical elastic local column buckling load |
| $P_n$ | nominal axial strength (N) |
| $P_{nd}$ | nominal axial strength for distortional buckling (N) |
| $P_{ne}$ | nominal axial strength for flexural, torsional, or torsional-flexural buckling (N) |
| $P_{nl}$ | nominal axial strength for local buckling (N) |
| $[P]$ | load column matrix |
| $q_y$ | density of uniformly distributed load (N/mm) |
| ${}^{k}q$ | uniformly distributed load |
| $R_y$, $R_z$ | radii of curvature of the centroidal axis in the *xz* and *xy* planes |
| $s$ | distance from some chosen origin to the point along the section's middle line (mm) |
| $S_f$ | gross section modulus referenced to the extreme fiber in first field |
| $t$ | thickness (mm) |
| $T_1$, $T_2$ | tractions (N/mm) |
| $u(x,y)$, $v(x,y)$, $w(x,y)$ | displacements of a finite strip at a point (x,y) (mm) |
| $\bar{u}(x, y, z)$, $u_b(x)$ | longitudinal displacements of the beam at points $(x,y,z)$ and $(x,o,o)$ (mm) |
| $[u]$ | nodal displacement column matrix |
| $(u_{1m}, v_{1m}, w_{1m}, \theta_{1m})$, $(u_{2m}, v_{2m}, w_{2m}, \theta_{2m})$ | nodal displacements associated with wave number m (mm) |
| $U$ | total strain energy (N mm) |
| $U_0$ | total strain energy (N mm) |
| $U_1$ | strain energy generated by the buckling displacements (N mm) |

| | |
|---|---|
| $U_{0\_beam}$ | strain energy of the beam due to deflections and rotation (N mm) |
| $U_{0\_k}$ | strain energy stored in two rotational springs over the supports (N mm) |
| $U_{0\_spring}$ | strain energy stored in two springs (N mm) |
| $U_{1\_beam}$ | strain energy due to the deflections and rotation when buckling occurs (N mm) |
| $U_{1\_k}$ | strain energy stored in two rotational springs over the support when buckling occurs (N mm) |
| $U_{1\_spring}$ | strain energy stored in two springs when buckling occurs (N mm) |
| $v$, $w$ | pre-buckling deflections of the beam in $y$ and $z$ directions (mm) |
| $v_b$, $w_b$ | buckling deflections of the beam in $y$ and $z$ directions respectively (mm) |
| $v_i$, $w_i$ | to-be-determined horizontal and vertical deflections at interpolation points $x_i$ (mm) |
| $\{v_i\}$, $\{w_i\}$ | deflections of the purin centroid at $x=x_i$ (mm) |
| $\overline{v}$ , $\overline{w}$ | deflections of the beam at point $(x,y,z)$ during the buckling (mm) |
| ${}^{k}V$, ${}^{k}W$ | generalised deformation resultant and stress resultant |
| $W$ | strain energy generated by the membrane stresses through the nonlinear strains of the buckling displacements (N mm) |
| $W_0$ | strain energy generated by the load (N mm) |
| $W_1$ | strain energy generated by the pre-buckling longitudinal stresses through the second-order strains (N mm) |
| $W_{\sigma xb}$, $W_{\sigma xw}$ | strain energy generated by bending stress and done by warping stress respectively (N mm) |
| $W_q$ | strain energy generated by the load due to the load that is not acting at the shear centre (N mm) |
| ${}^{i,k}W_{cr}$ | critical stress resultant |
| $x_i$ | spline interpolation points |
| $y_k$, $z_k$ | coordinate of the position where the springs are applied |
| $y_q$, $z_q$ | coordinate of the position where the load is applied |
| $Y_m$ | depth of compression zone (mm) |

## Greek Characters

| | |
|---|---|
| $\alpha$ | angle between z axis and loading line |
| $\alpha_1$ | imperfection factor |
| $\beta$ | warping function of St. Venant torsion |
| $\varepsilon_x$, $\gamma_{xy}$, $\gamma_{xz}$ | longitudinal strain and shear strains generated by the buckling displacements |
| $\varepsilon_{x2}$, $\gamma_{xy2}$, $\gamma_{xz2}$ | second-order non-linear longitudinal strain and shear strains |
| $\chi$ | reduction factor for buckling with respect to the unbuckled capacity |

| | |
|---|---|
| $\phi$ | angle of twist |
| $\phi_b$ | buckling angle of twist |
| $\phi_i$ | to-be-determined angle of twist at interpolation points |
| $\lambda$ | critical load factor |
| $\lambda_l$ | half buckling wavelength |
| $\overline{\lambda}$ | relative slenderness in the relevant buckling mode |
| $\overline{\lambda_p}$ | plate slenderness |
| $\omega$ , $\overline{\omega}$ | sectional coordinate ($mm^2$) and corresponding average value ($mm^3$) with respect to the centroid |
| $\omega_s$ , $\overline{\omega}_s$ | sectional coordinate ($mm^2$) and corresponding average value ($mm^3$) with respect to the shear centre |
| $\nu$ | Poisson's ratio |
| ${}^{ijk}\kappa$ | second-order section properties |
| $\sigma_o$ | maximum stress when $k_z=k_\phi=\infty$ (MPa) |
| $\sigma_c$ | maximum compressive stress in the plate element (MPa) |
| $\sigma_{cr}$ | critical stress for elastic buckling (MPa) |
| $\sigma_{eff}$ | maximum compressive stress in the plate element (MPa) |
| $\sigma_x$ | pre-buckling longitudinal stress (MPa) |
| $\sigma_{xb}$, $\sigma_{xw}$ | longitudinal stresses generated by the bending and twisting moments respectively (MPa) |
| $\sigma_y$ | yield stress (MPa) |

# Chapter 1

# 1 INTRODUCTION

## 1.1 GENERAL BACKGROUND

Cold-formed steel members are widely used as purlins or rails, the intermediate members between the main structural frame and the corrugated roof or wall sheeting, in buildings for farming and industrial use. Trapezoidal sheeting is usually fixed to these members in order to enclose the building. The shape of the cross-section of the members is mostly that of zed, channel or sigma. These types of cross-section are inherently sensitive to local, distortional, and lateral-torsional buckling. As a result of current trends, these sections are becoming more slender and more highly stiffened and therefore more prone to local and distortional buckling.

Historically, the load-bearing capacity of purlins and sheeting rails has generally been determined by carrying out full-scale testing (Moore, 1988; Rhodes, 1991; Trahair, 1993; Laine & Tuomala, 1999). However, the proliferation of new cladding systems, including those which offer little restriction to the supporting purlins (standing seam roofs, clip fix systems, etc.) requires that analytical design procedures should be developed. This is a problem that has not been addressed in British Codes of Practice (Leach & Robinson, 1993).

The recent Eurocode publication (EC 3: Part 1.3, 1996) presents a method which enables the designer to evaluate the ultimate load capacity of a purlin system. The method is largely based on the research work carried out in The Netherlands (Toma & Soetens, 1987), Germany (Schardt, 1982) and France (Sokol, 1979 & 1996). The method requires only a limited amount of small-scale testing to evaluate the lateral and torsional restraints offered by the roof cladding system to the purlin itself. Different end conditions are dealt by means of the effective length concept. Anti-sag bars are treated in a similar manner. The load tables calculated from EC3, however, have been found to be on average 20% to 25% less than those based on full-scale

testing (Leach & Robinson, 1993; Toma & Wittemann, 1994) and those obtained from finite strip analysis (Hancock, 1997a; Ye et al., 2002 & 2004). This implies that the method suggested in EC3 is rather conservative. Although any design method should be a conservative estimate of the true behaviour of a member, it is clear that, with an inherent conservatism in the design method of up to 30%, the method still needs considerable refinement before it becomes an acceptable and economical replacement for full-scale testing. In addition, the calculation method does not include the case where the beam is overlapped over interior supports (i.e., the sleeved system which is widely used today). The overlapping of beams results in an increase of stiffness in the overlap zone which can enhance the load capacity of the system, as has been demonstrated experimentally by Ghosn and Sinno (1995).

Cold-formed steel members have been increasingly used recently in various buildings because of the advantages such as lightness, high strength and stiffness, fast and easy erection/installation, economy in transportation and handing. Although it is not yet so evident in the UK, in other parts of the developed world there is an extremely rapid development in the use of cold-formed framing systems for houses and other low-rise construction (Davies, 2000). It was reported that, in the USA, about 500 homes were built in light gauge steel in 1992, which increased to 15,000 in 1993 and 75,000 in 1994, while by 2002 the increase has reached to a further five-fold.

The cross-sections of thin-walled members consist usually of relatively slender parts. Instead of failure through material yielding, compressed parts tend to loose their stability. Steel sections may be subject to one of three basic types of buckling, namely local, distortional and global.

The term *global buckling* (or long mode buckling) embraces flexural buckling, torsional and flexural-torsional buckling and lateral-torsional buckling. The half-wave lengths of these modes are of the order of magnitude of the length of the member. Rigid body movements of the whole member characterize global buckling such that individual cross-sections rotate and translate but do not distort in shape. Local and distortional buckling are sometimes called sectional buckling because they depend very much of the geometry of the cross-section. *Local buckling* is characterized by relatively short half-wave length of the order of magnitude of individual plate

elements and the displacements only perpendicular to plane elements and redistribution of stresses while the fold lines remain straight. In this mode the shape of the section is only slightly distorted, because only rotations at plane element junctures are involved. *Distortional buckling* occurs at a half-wave length intermediate to local and global mode buckling. The half-wave length is typically several times larger than the largest characteristic dimension of the cross-section. Distortional buckling involves both translation and rotation at the fold lines of a member leading to a distortion of the cross-section.

With the increasing use of higher strength steels it is inevitable to reduce the thickness of the section and therefore considerations of local stability lead logically to the development of highly stiffened sections with more folds and rolled in stiffeners. The consequence of this is that design procedures are becoming more complicated and engineers will experience difficulty if they try to obtain results by hand calculation. In addition, some cases may arise which are not adequately covered by the available codes or where the codes are over-conservative and more efficient designs can be obtained by improving the design procedure (Davies, 2000).

## 1.2 BACKGROUND OF THE PROJECT

The purlin-sheeting system has been the subject of numerous theoretical and experimental investigations over the past 30 years, but the complexity of the problem has led to great difficulty in developing a sound and general model (Rhodes, 1991; Pekoz, 1999; Davies, 2000). The complexity shows itself in three main aspects. Firstly, the purlin is either a channel or zed section, which is not doubly symmetric, with very thin thickness and therefore the failure mode could be either a local buckling at short half-wavelengths, or a lateral-torsional buckling at long half-wavelengths, or even a distortional buckling at intermediate half-wavelengths. Interactions between these buckling modes and between buckling and yielding may also occur. Secondly, the nature of the purlin-sheeting connection makes the shear and rotational stiffness provided by the sheeting to the purlin difficult to quantify. The rotational stiffness, in particular, varies with sheeting type, purlin type and dimensions, screw spacing, and other connection details. Thirdly, most pulins are

fixed with cleats by bolt connection at each end through their web, which behave neither as simply supported nor as fixed boundaries. Although existing whole-section models based on the finite strip method (FSM) (Hancock, 1997a; Schafer, 2001c & 2003a) or on the generalized beam theory (GBT) (Davies, 2000) using half sine wave displacement functions are very effective in dealing with local and distortional buckling and the interaction between them, they are not very suitable for handling lateral-torsional buckling, particularly where anti-sag bars are present because the influence of end boundary conditions and point supports provided by the anti-sag bars is not appropriately treated in these methods.

In addition, bifurcation analyses in finite strip method and GBT only provide the critical stress for elastic buckling of the beams with pure bending and/or pure compression. For economic design, it is necessary to consider the moment gradient along the longitudinal axis of the beam (that is, the uniformly distributed load rather than the uniformly distributed stress). In most current design codes, the design focus is placed on the local buckling behaviour. This may be correct for beams that are laterally restrained by either cladding and/or anti-sag bars. For beams that have little or no lateral restraints the failure of the beams is likely to be dominated by the lateral-torsional and distorsional buckling. Therefore, how to quantity the influence of the lateral restraints on the lateral-torsional buckling of the beams becomes critical for providing economic design of a purlin sheeting system.

## 1.3 AIMS OF THE THESIS

The primary aim of the thesis is to investigate the failure behaviours of cold-formed zed and channel sections for use in purlin-sheeting systems. The main task is to develop an approach to investigate cold-formed zed and channel section beams with partially-lateral restraint from metal sheeting when subjected to a uniformly distributed transverse load.

The main aim can be subdivided into further sub-sections:

1. To develop an analytical model based on the energy method for the stress analysis of cold-formed steel zed and channel sections within purlin-sheeting systems.

2. To study the elastic local buckling behaviour of cold-formed steel zed and channel sections by introducing a novel approach by use of the method described in (1) and the finite strip method. To review the existing design specifications and to compare the relevant clauses with results obtained by the presented approach.

3. To examine the local and distortional buckling behaviour of cold-formed steel zed and channel section beams by using the semi-analytical finite strip method.

4. To investigate the elastic lateral-torsional buckling of cold-formed steel zed and channel sections using the analytical model based on the energy method.

5. To study inelastic lateral-torsional buckling of cold-formed steel zed and channel sections by developing a spring model to simulate the local softening of the section stiffness due to local buckling and/or local material yielding.

6. To study the effects of various factors, such as, dimensions of cross-sections, internal and external restraints, warping stress, loading positions and span lengths, on the behaviour of cold-formed steel zed and channel beams.

## 1.4 ORDER OF PRESENTATION

The main body of the thesis contains the introduction, a literature review of previous research, the theoretical (based on energy method) and numerical (design specifications, finite strip method) investigations, recommendations, and conclusions. There are four appendices which include more comprehensive descriptions.

Chapter 2 provides an introduction to the characteristics of cold-formed steel structures, including aspects such as the buckling behaviour and the developments in

technology and application, past research on local buckling, distortional buckling and lateral-torsional buckling, and the examination of existing approaches for research and development.

The stress analysis of cold-formed zed and channel section beams is described in Chapter 3. The investigations are carried out based on the analytical method which provides the full formulations for calculating the longitudinal stresses due to bending and warping. The effects of various restraints on the pre-buckling stress are also studied.

In Chapter 4, the local buckling behaviours of cold-formed steel zed and channel sections are studied. The basic design process of BS 5950 (1998) and finite strip method-CUFSM (Schafer, 2001c & 2003a) are introduced and three types of loading conditions are considered. A novel model based on the combination of energy method and finite strip method is presented to investigate the local buckling behaviour of the purlin-sheeting systems.

An investigation on the buckling behaviour of the cold-formed steel zed and channel section beams when subjected to different loads using a semi-analytical finite strip method is presented in Chapter 5. The focus of the study is on the local and distortional buckling, while existing results are available only for sections subjected to pure compression and/or pure bending.

An analytical model for predicting the elastic lateral-torsional buckling of cold-formed zed and channel section beams partial-laterally restrained by metal sheeting when subjected to a uniformly distributed load is discussed in Chapter 6. The effects of warping stress, boundary conditions, internal supports and loading positions on lateral-torsional buckling are studied.

A novel analytical model is presented in Chapter 7 for predicting the lateral-torsional buckling of statically indeterminate zed section purlins. The model together with experimentally or numerically obtained stiffness softening curves for local buckling or local material yielding can be used to determine the critical load of lateral-torsional buckling of the purlin with statically indeterminate boundary conditions.

Conclusions drawn from the work that has been done during this research project and future work on this topic are given in Chapter 8.

In addition to the chapters in the main body of this thesis, there are four appendices dealing with various topics, as noted by the appendix heading in the contents. In Appendix 1, the basic theory and formulations used in the finite strip software CUFSM and the present semi-analytical finite strip program are described, including a version of CUFSM modified by the thesis author. The expressions of sectional properties for zed and channel sections are presented in Appendix 2. MATLAB programming Scheme for the analytical model based on the energy method for investigating cold-formed steel zed and channel section beams partially-lateral restrained by the metal sheeting is presented in Appendix 3. Finally, several papers that have been published or submitted based on the work in this thesis are listed in Appendix 4.

# Chapter 2

# 2 LITERATURE REVIEW

## 2.0 CHAPTER SYNOPSIS

The following chapter provides an introduction to the characteristics of cold-formed steel structures, including aspects such as the buckling behaviour and the developments in technology and application.

In particular, this chapter reviews the previous research in the occurrence of local buckling, distortional buckling and lateral-torsional buckling and examines existing approaches for research and development.

It is a consequence of the increasing complexity of section shapes that local bucking calculations are becoming more complicated and that distortional buckling takes on increasing importance. Whereas much has been written about local and lateral buckling, and codes of practice for the design of structural steelwork contain the relevant clauses, distortional buckling and lateral-torsional buckling are less well known and less well documented. This, however, should not be taken as an indication of its lack of importance.

# 2.1 INTRODUCTION

The major research developments in cold-formed steel structures over the recent years as published in leading journals on steel structures and thin-walled structures are reviewed and summarized by Hancock (1997 & 2003), Rondal (2000) and Davies (2000) which provide the latest information on developments in, and the design of cold-formed steel structural members and sections. Hancock summarizes the publication and development of the American Iron and Steel Institute Specification for the design of light gauge cold-formed steel structural members (1996, 1999, 2001), publication of the CEN document Eurocode 3, Part 1.3 for cold-formed thin gauge members and sheeting (1996), and the publication of the Australian/New Zealand Standard AS/NZS 4600:1996 for cold-formed steel structures (1996). The general report by Rondal (2000) deals with stability problems of cold-formed members, and joints between cold-formed. The paper by Davies (2000) includes developments in cold-formed section technology, developments in applications, and developments in design procedures for cold-formed sections, current design models and their deficiencies, and design using whole-section models.

# 2.2 COLD-FORMED STEEL SECTIONS

## 2.2.1 Characteristics Of Cold-Formed Steel Sections

### 2.2.1.1 Peculiarities

In general, cold-formed steel structural members provide the following advantages in building construction (Yu, 1985):

- As compared with thicker hot-rolled shapes, cold-formed light members can be manufactured for relatively light loads and/or short spans;
- Unusual sectional configurations can be produced economically by cold-forming operations and, consequently, favourable strength-to-weight ratios can be obtained;
- Nestable sections can be produced, allowing for compact packaging and shipping;

- Load-carrying panels and decks can provide useful surfaces for floor, roof, and wall construction, and in other cases, they can also provide enclosed cells for electrical and HVAC conduits;
- Load-carrying panels and decks not only withstand loads normal to their surfaces, but they can also act as shear diaphragms to resist force in their own planes if they are adequately interconnected to each other and to supporting members.

Compared with other materials such as timber and concrete, the cold-formed steel structural members have the following qualities:

- Lightness;
- High strength and stiffness;
- Ease of prefabrication and mass production;
- Fast and easy erection and installation;
- Substantial elimination of delays due to weather;
- More accurate detailing;
- Nonshrinking and noncreeping at ambient temperature;
- Uniform quality;
- Economy in transportation and handling.

However, because cold-formed members are usually thin-walled, special care must be given to design. Compared to classical hot-rolled sections, they are characterized by some peculiarities, e.g.:

- Large width to thickness ratios;
- Singly symmetrical or unsymmetrical shapes;
- Unstiffened or partially unstiffened parts of sections, which can lead to complicated buckling problems;
- Combined torsional and flexural buckling;
- Local plate buckling;
- Distortional buckling;
- Interaction between local and global buckling;
- Fire resistance,...

Also, connections must be designed with care because of the thinness of the members that can lead to local failures.

For these reasons, dedicated specifications have been published in United States first, followed in Europe, Australia and in other countries to cover these important questions.

### 2.2.1.2 Materials

The type of steel used should be suitable for cold-forming and, if required, for galvanising. For cold-formed sections and sheeting it is preferable to use cold-rolled continuously galvanized steel with yield stresses in the range of 280-320-350 $N/mm^2$, and with a total elongation of at least 10% for a 12.5 mm wide strip, referred to a gauge length 80 mm, and a ratio of ultimate tensile strength to yield stress of at least 1.1.

Under normal conditions, zinc protection Z275 (275 $g/m^2$) is sufficient; in more corrosive environments, improved protection using suitable coating systems may be necessary. Continuously applied zinc protective coating systems are generally limited in core thickness to about 3.5 mm. For increased material thickness, hot-dip galvanizing and site- or shop-applied top coats may be used.

### 2.2.1.3 Mechanical properties

Thin-walled steel sections are fabricated by means of folding, press-braking of plates or cold-rolling of coils made in carbon steel. Cold-forming techniques allow the geometrical properties of a shape to be readily varied. It is possible, therefore, to influence the load-bearing behaviour of the element with respect to strength, stiffness and failure modes by, for example, the introduction of intermediate stiffeners or by ensuring adequate width-to-thickness ratios in adjacent flat parts of the section.

For these members which are now very frequently used in modern steel construction, the initial $\sigma-\varepsilon$ relations of the steel are considerably changed by the cold-straining due to the manufacturing processes. Fig.2.1 shows the modification of the $\sigma-\varepsilon$ diagram when a carbon steel specimen is first strained beyond the yield plateau and then unloaded. If strain aging is now very rare, or at least limited, with modern steels, the

cold-straining however modified the apparent σ–ε diagram which is pertinent for cold-formed steel members.

However, the stain-hardening can vary considerably along the cross-section due to the forming process shown in Fig.2.2. When a steel section is cold-formed from flat sheet or strip, the yield strength, and to a lesser extent the ultimate strength, are increased as a result of this cold working, particularly in the bends of the section. The yield and ultimate strength are unaffected in the area where little cold work has taken place and the strength is much higher in the corners, which have been strongly cold-worked in the forming process. Many authors have investigated the influence of cold work on the distribution of the yield strength along the cross-section (Karren 1967; Karren & Winster, 1967; EC 3, 1996).

### 2.2.2 Developments In Cold-Formed Section Technology

As a "high-tech" product, a cold-formed steel section is more open to development than its more mundane hot-rolled counterpart. This section reviews some recent developments which have been summarised by Pekoz (1999) and Davies (2000).

#### 2.2.2.1 Trend to higher quality steels

The trends to higher quality steel is primarily seen in an increased yield stress and there has been a continuing increase in the yield stress of typical mass-produced products such as purlins, sheeting and decking in recent years. The steel used for such applications now typically has yield stress in the range 280 to 550 N/mm$^2$. This trend of increasing yield stress is likely to continue. There are also some steels available with ultra-high yield stress. These are generally only economic for special applications such as lightweight bridges for the military. Hoglund (1995) discusses the welding of quenched and tempered (QT) steel produced in Sweden with yield strength up to 1100 N/mm$^2$. The application of steels with a very high yield stress is often limited by considerations of stiffness and Nippon Steel in Japan is reputed to have produced steels with a 30% increase of Young's modulus in the direction of rolling though with a corresponding decrease in the transverse direction. Steels with better fire resistance, including less creep at elevated temperature, are also being introduced.

#### 2.2.2.2 Trend to more complex section shape

The use of higher strength steels is inevitably accompanied by a reduction in thickness and considerations of local stability lead logically to the development of highly stiffened sections with more folds and rolled in stiffeners. This trend can be conveniently illustrated by the development of sections for purlins. Early purlin shapes were simple lipped channels and Zed sections. As shown in Fig.2.3, the simple channel has evolved into Multibeam Marks I, II and III, the last having a compound lip. A similar trend can be seen in the evolution of Zed into the Zeta and Ultrazed shapes.

A similar evolution can be obtained in cassette sections with stiffened flanges and webs, the (perforated) uprights in pallet racks, slotted wall studs and the 2nd and 3rd generation decking profiles. The use of high strength steels in thinner, highly stiffened sections inevitably leads to more demanding design requirements.

#### 2.2.2.3 Better corrosion resistance

Undoubtedly, one of the primary reasons for the increase in the practical usage of cold-formed sections is improved corrosion resistance. This is the result of improved galvanising and other coating technology, bearing in mind that the protective coating system is undamaged by the cold-forming process. There is also an increasing use of cold-formed stainless steel. A 12% chromium steel with no nickel has been used for housing in Japan. This steel does not have the shiny surface usually associated with stainless steel but is less prone to rust.

#### 2.2.2.4 Improved rolling and forming technology

Modern rolling lines are generally computer controlled from the design office so that not only can highly accurate complex shapes of precise lengths be produced to order but also holes, perforations and slots (e.g. web openings for services) can be punched in precise positions during the rolling process. A significant recent development is the automatic end forming of beams at the time of rolling.

The rolling of transverse stiffeners in the wide top flange of 3rd generation decking profiles, has been available for some time. Similar technology allows the rolling of vertical web stiffeners in beam sections. Even more complex sections may now be

formed in two or more parts in which the individual parts are formed and assembled using high frequency welding in a single operation. This may involve the combination of different material qualities and thickness in a single component.

#### 2.2.2.5 Improved connection technology

Because of the comparative thinness of the material, connection technology plays an important role in the development of structures formed using cold-formed sections. The conventional methods of connection, such as bolting and arc-welding are, of course, available but are generally less appropriate and the emphasis is on special techniques more suited to thin material. Long-standing methods for connecting two elements of thin material are blind rivets and self-drilling, self-tapping screws. Fired pins are often used to connect thin material to a thicker supporting member. More recently, clinching technology (Davies et al., 1996) has been taken from automotive industry and applied to building construction. An even more recent and significantly stronger innovation is the "Rosette" (Makelainen & Kesti, 1999; Pasternak & Komann, 1999).

### 2.2.3 Developments In Applications

The use of cold-formed steel members in building construction began in the middle of the eighteenth century in the United States and United Kingdom. However such steel members were not widely used as structural members until around 1946 and the publication of the first edition of the "Specification for the Design of Light Gauge Steel Structural Members" by the American Iron and Steel Institute (AISI). Since that period, thousands of researches in the field have led to a wide use of cold-formed metal elements in all types of buildings.

Historically, the main applications have been such elements as: purlins and sheeting rails and associated components; cladding and decking; pallet racking and shelving etc. The developments in technology outlined above are all applicable to components of this type and their evolution will undoubtedly continue. However, the main current and foreseeable developments are in a rather different sphere which have been summarised by Davies (2000).

### 2.2.3.1 Applications in residential and other low-rise buildings

Although this is not yet so evident in Europe, in other parts of the developed world there is an extremely rapid development in the use of cold-formed framing systems for houses and other low-rise construction. This development is being led by the USA where the rise may be said to be "exponential". Pekoz (1999) states that, in the USA, about 500 homes were built in light gauge steel in 1992. This number rose to 15000 in 1993 and 75000 in 1994. A further five-fold increase was estimated by 2002. The primary framing elements for this form of construction are cold-formed steel wall studs and floor joists. Light gauge steel roof trusses or rafters are also used. There is a vast amount of literature on the subject, a good deal of which is summarised in the "Residential Steel Framing Manual" published by the American Iron and Steel Institute [AISI, undated].

Surprisingly, this major evolution has been accompanied by little development in cold-formed section technology. The majority of steel framing systems have evolved from timber framed solutions and have merely involved replacing timber sections by cold formed steel sections of similar overall size connected together by conventional methods such as bolting and welding. More recently, advantage has been taken of the clinching connection methods (Davies et al., 1996), particularly where factory prefabrication is used. A recent important development is the use of wall studs with perforated webs (Hoglund, 1998; Kesti & Makelainen, 1998). These studs have been developed in the Scandinavian countries in order to reduce thermal bridging in external walls. The web perforations take the form of arrays of slots which, of course, significantly weaken the web in transverse bending and shear. This has several effects, including a reduced resistance to distortional buckling, and thus leads to rather complex design problems.

Another significant development is the use of cassette walls (Davies, 1998). These have the advantage of providing a weather proof wall as well as a structural frame and avoid many of the stability problems of stud wall construction. They also act as a shear diaphragm with regard to horizontal (wind) load and thus avoid the necessity of providing bracing systems in the plane of the walls. This leads to much simpler detailing and more rapid construction.

### 2.2.3.2 Factory assembly of prefabricated units

Closely associated with the trend outlined above is the related trend to maximise prefabrication in the factory. Using jigs and appropriate jointing technology such as clinching and Rosettes, cold-formed steel components can be rapidly and accurately assembled into complete structural units for delivery to the site. Such units can take the form of wall and floor panels and roof trusses. Even more dramatic is the increasing factory prefabrication of complete building modules such as complete hotel rooms. These may be built and fitted out with bathroom units, furniture and fittings before being shipped to the site complete and requiring only the connection of external services (Davies et al., 1995). In the UK, most out of town hotels and motels are now built in this way.

### 2.2.3.3 Interaction of cold-formed steel with other materials and components

It is inherent in the nature of thin-walled steel construction that this material is often seen at its best when it interacts with other materials and building components. Familiar applications of this principle are: purlins stabilised by cladding; wall studs stabilised by sheathing; composite decks where embossed metal decking acts together with in-situ concrete; and sandwich panels where two thin metal faces interact with a lightweight insulating core. Stressed skin (diaphragm action) offers another instance of this important principle in which the thin metal cladding of a building can act to stabilise the framing members and even provide the primary stability of the complete structure. Various forms of frameless construction take this principle a stage further.

There are a number of current developments which utilise the interaction of cold-formed steel members with other materials. There are double skin roofing constructions which use profiled rigid insulation to completely fill the space between liner and weather sheets. Even in some roof systems there is no metal liner sheet and a rigid self supporting polyisocyanurate insulation board laid in metal tees is used instead. Also, filled cassettes, which are substantial C-shaped sections used for wall construction may be filled with rigid thermal insulation in order to provide improved stability and resistance to denting. Another important application is in dry flooring systems in which cold-formed steel floor joists (or profiled steel decking) act together with a built-up walking surface to provide enhanced structural performance as well as meeting the requirements of building physics (acoustic, fire, vibration etc). It is

significant that these two examples are both particularly applicable to residential and low-rise steel construction.

### 2.2.4 Structural Behaviour Of Cold-Formed Members

The cross-sections of thin-walled members consist usually of relatively slender parts, i.e. of flat plate fields and edge stiffeners. Instead of failure through material yielding, compressed parts tend to loose their stability. Steel sections may be subject to one of three basic types of buckling, namely local, distortional and global.

The term *global buckling* (or long mode buckling) embraces flexural buckling, torsional and flexural-torsional buckling and lateral-torsional buckling. The half-wave lengths of these modes are of the order of magnitude of the length of the member. Rigid body movements of the whole member characterize global buckling such that individual cross-sections rotate and translate but do not distort in shape. The displacements of the entire cross-section are large, leading to overall loss of stability of the member. Flexural buckling usually in the direction of minimum flexural stiffness is common also for cold formed members. Low torsional stiffness is typical for open thin-walled members, so buckling modes associated with torsion may be critical. Pure torsional buckling is possible for example in the case of a point symmetric cross-section (e.g. Z-section), where the centre of the cross-section and the shear centre coincide. In torsional buckling, the cross-section rotates around the shear centre. A mixed flexural-torsional buckling mode, where the cross-section also translates in plane, is possible in the case of single symmetric cross-sections (e.g. U, C and hat). Due to the low torsional stiffness of open thin-walled cross-sections, lateral-torsional buckling is a very probable failure mode of beams.

Local and distortional buckling are sometimes called sectional buckling because they depend very much of the geometry of the cross-section. *Local buckling* is characterized by relatively short half-wave length of the order of magnitude of individual plate elements and the displacements only perpendicular to plane elements and redistribution of stresses while the fold lines remain straight. In this mode the shape of the section is only slightly distorted, because only rotations at plane element junctures are involved.

*Distortional buckling* occurs at a half-wave length intermediate to local and global mode buckling. The half-wave length is typically several times larger than the largest characteristic dimension of the cross-section. Distortional buckling involves both translation and rotation at the fold lines of a member leading to a distortion of the cross-section. The displacements of the cross-section parts are largely due to buckling of e.g. flange stiffeners. In both local and distortional buckling modes, the stiffness properties of the cross-section may be changed, but the member probably still has some post-buckling capacity since translation and/or rotation of the entire cross-section is not involved.

A selection of buckling modes produced using the finite strip analysis at different half wavelengths is shown in Fig.2.4 by Hancock (1997a). The modes range from lateral buckling at long half-wavelengths (>10d) shown in the top left of the figure through distortional buckling at intermediate half-wavelengths to local buckling at short half-wavelengths (<d) shown in the bottom right of the figure (*d* is the web depth).

It is a consequence of the increasing complexity of section shapes that local buckling calculations are becoming more complicated and that distortional buckling takes on increasing importance. These two modes of buckling may, of course, interact with each other as well as with global buckling. Whereas much has been written about local and global buckling, and codes of practice for the design of structural steelwork contain the relevant clauses, distortional buckling is less well known and less well documented. This, however, should not be taken as an indication of its lack of importance. In many cold-formed sections, distortional buckling is at least as likely as local buckling and warrants similar consideration in design.

There are other untypical buckling modes, such as shear buckling, interactive buckling, etc. There is an increasing need for the understanding of them. Naturally, plastic or elastic-plastic static behaviour of compressed or bent members are possible when loaded to failure, but with normal structural geometry and loading, stability is critical in the design of thin-walled members.

## 2.3 LOCAL BUCKLING BEHAVIOUR

### 2.3.1 Models For Local Buckling

#### 2.3.1.1 Effective width concept

In this mode the shape of the section is only slightly distorted, because only rotations at plane element junctures are involved. Local buckling of thin-walled sections has been known for many years and has been well understood. For such plate elements, local buckling is not the same as overall beam or column buckling. Although the element begins to deflect out of its original straight or plane shape, it does not fail when the initial buckling stress is reached. On the contrary it can still resist increasing compression stresses often well in excess of those at which local buckling first appears.

The basic phenomenon of local buckling in a cassette column is illustrated in Fig.2.5 which shows local buckling in a cassette column with an intermediate stiffener in the wide flange. As shown, plate elements that are adequately stiffened along both longitudinal edges tend to buckle into approximately square waves. For economic design, it is essential to consider the post-buckled condition and the primary "building block" for cold-formed section design is the concept of effective width illustrated in Fig.2.6.

Considering the element as the compression flange of some member (see Fig.2.6), the total compressive force is the area under this stress distribution curve, times the thickness of the element. What is needed in design, really, is only this total compressive force. It is convenient to replace the actual variable stress distribution with a fictitious uniform stress distribution, of the same intensity of the edge stress, $\sigma_{eff}$ as in the real element.

In order to get the same total compression force in the fictitious as in the real distribution, the areas under the two must be equal. This means adjusting the width of each of the two fictitious rectangles, $b_{eff}/2$, until the combined area of the two rectangles is equal to that under the solid curve. This width is known as the effective width, $b_{eff}$.

Once this effective width, $b_{eff}$, is known, structural members, such as beams or columns, can be designed simply by replacing the real width, $b$, of each compression element by its effective width, $b_{eff}$. Then, effective section properties, such as area, section modulus, and moment of inertia, can be calculated by using for each compression element its effective width, $b_{eff}$, instead of its real width, $b$.

#### 2.3.1.2 Effective cross-sections

The effects of local buckling shall be taken into account in the determination of the design strength and stiffness of the members. Using the concept of effective width of individual elements prone to local bucking, the effective cross-sectional properties can be calculated. The first step is to evaluate the effective width of the compression elements of the section, based on the appropriate stress distribution over the cross-section; the next step is to calculate the geometric properties of the effective section, taking into account the shift of the neutral axis caused by disregarding the ineffective parts of the section. In general, the resistance of a thin-walled effective cross-section is limited by the design yield stress at any part of the section, based on an elastic analysis. Deviations from this rule are only permitted in special cases.

### 2.3.2 Analysis Approaches

#### 2.3.2.1 Design specification

Elastic local buckling is typically treated by ignoring any interaction between elements (flanges and web). Each element is considered independently and classical plate buckling equations based on isolated simply supported plates are generally used. The result of this approach is that each element of the section is predicted to buckle at a different stress. This approach, called the element model, can lead to rather conservative predictions.

The usual effective width formula is the semi-empirical formula due to Winter (1947):

$$\begin{aligned} &if\ \overline{\lambda_p} \le 0.673 && b_{eff} = b \\ &if\ \overline{\lambda_p} > 0.673 && b_{eff} = (1.0 - \frac{0.22}{\overline{\lambda_p}})\frac{1}{\overline{\lambda_p}} b \end{aligned} \tag{2.1}$$

in which the plate slenderness $\overline{\lambda_p}$ is given by:

$$\overline{\lambda_p} = \sqrt{\frac{\sigma_c}{\sigma_{cr}}} = 1.052\frac{b}{t}\sqrt{\frac{\sigma_c}{Ek_\sigma}} \tag{2.2}$$

where $\sigma_c$ = the maximum compressive stress in the plate element;

$\sigma_{cr}$ = the critical stress for elastic buckling of the plate element given by the well-known Von Karmen formula;

E = the Young's modulus;

$k_\sigma$ = the buckling factor which is 4.0 for a simply supported plate in uniform compression and 0.43 for an outstand plate element with one edge free.

Elements stiffened on one side only are much less stable and can also be treated by an analogous effective width approach. However, such unstiffened elements rarely arise in practice because lips usually restrain the free edges. The modern tendency is to use compound lips.

Eurocode 3: Part 1.3 (1996) gives some comprehensive rules for the determination of effective widths under different stress conditions. In principle, the effective widths of the individual plate elements may be combined to give an effective section and member design completed using conventional techniques. However, this apparent simplicity conceals a number of difficulties. As illustrated by Fig.2.5, individual plate elements do not buckle in isolation but interact with each other. Although some codes (e.g. BS 5950 (1998)) give an approximate treatment of this phenomenon, it can only be dealt with accurately by a whole-section analysis.

Furthermore, Fig.2.5 suggests that both the intermediate stiffener in the wide flange and the compound lip stiffeners are "fully effective" so that they remain straight during local buckling of the plate elements. With modern, highly stiffened sections, this is often not the case. Stiffeners may be partially effective so that stiffener buckling interacts with local plate buckling. Eurocode 3: Part 1.3 (1996) gives some design rules for more general situations but these are complicated to use and not particularly accurate (Kesti & Davies, 1999). Evidently, this is the situation where design based on an analysis of the whole section is to be preferred.

#### 2.3.2.2 Finite strip method

The best known of numerical methods developed for analysing thin-walled beams based on the separation of variables is perhaps the finite strip method. In the finite strip method the displacement interpolation is built up of two parts, a polynomial defined on a cross-section and a truncated Fourier series part governing the behaviour of displacement function in the axial direction with the latter satisfying a priori the boundary conditions at the ends of the beam. This provides "whole section" solutions for the full range of buckling phenomena, leading to relatively new design procedures.

If the thin-walled beam is prismatic and the boundary and loading conditions are suitable, the finite strip method is quite economical with respect to computational efficiency. Several well-known researchers have developed user-friendly computer software (Schafer, 2001c & 2003a) for this calculation, which is available to practical designers.

Unfortunately, the applicability of the finite strip method to various geometries or boundary and loading conditions introduced is weak. In the buckling analysis of thin-walled beams using the finite strip method difficulties are experienced, for example, when dealing with non-periodic buckling modes or unequal loading in the axial direction.

A brief introduction to the finite strip model employed in the program CUFSM (Schafer, 2001c & 2003a) is presented in Section 2.8.5.

## 2.4 DISTORTIONAL BUCKLING BEHAVIOUR

### 2.4.1 Models For Distortional Buckling

Distortional buckling involves both translation and rotation at the fold lines of a member leading to a distortion of the cross-section. Recently, distortional buckling has received the attention of a number of researchers. The research has now reached the point where design procedures suitable for inclusion in codes of practice are beginning to emerge. Both columns and beams will be considered in turn. Mention

will also be made of the special case of beams (purlins or sheeting rails) which are partially restrained by the cladding that they support as this is an important practical case.

#### 2.4.1.1 Model for distortional column buckling

Distortional buckling of compression members such as lipped channels usually involves rotation of each flange and lip about the flange-web junction in opposite directions as shown in Fig.2.7. The web undergoes flexure at the same half-wavelength as the flange buckles, and the whole section may translate in a direction normal to the web also at the same half-wavelength as the flange and web buckling deformations. The web buckling involves single curvature transverse bending of the web.

A simplified analytical expressions for the distortional elastic buckling stress was originally developed by Lau and Hancock (1987), as is shown in Fig.2.7, which were based on a flange buckling model in which the flange was treated as a compression member restrained by a rotational and a translational spring. The rotational spring stiffness $k_\phi$ represents the torsional restraint from the web and the translational spring stiffness $k_x$ represents the restraint to translational movement of the cross section.

In Lau and Hancock's analysis (1987), it is shown that the translational spring stiffness $k_x$ does not have much influence on the buckling mode under consideration and the value of $k_x$ was thus assumed to be zero. The key to evaluating this model is to consider the rotational spring stiffness $k_\phi$ and the half buckling wavelength $\lambda_l$, while taking account of symmetry. Lau and Hancock (1987) give a detailed analysis in which the effect of the local buckling stress in the web and of shear and flange distortion were taken into account in determining expressions for $k_\phi$ and $\lambda_l$. This gave rise to a rather long and detailed series of explicit equations for the distortional buckling stress. Not withstanding their cumbersome nature, these are now included in the Australian code (AS/NZS 4600, 1996).

A similar set of explicit equations has also proposed by Schafer (2001a).

### 2.4.1.2 Model for distortional buckling in beams

Analytical expressions for the distortional buckling of thin-walled beams of general section geometry under a constant bending moment about the major axis have been developed by Hancock (1995). These analytical expressions were based on the simple flange buckling model shown in Fig.2.8 (together with an improvement proposed by Davies and Jiang (1996a & 1996b)), in which the flange was treated as a compression member with both rotational and translational spring restraints in the longitudinal direction. The rotational spring stiffness $k_\phi$ and the translational spring stiffness $k_x$ represent the torsional restraint and translational restraint from the web respectively. In his analysis, Hancock again assumed the translational spring stiffness $k_x$ to be zero.

These beam models are, of course, directly analogous to the column model shown in Fig.2.7. The only significant difference lies in the stiffness of the rotational spring and the necessary modifications to the design expressions for the rotational spring stiffness $k_\phi$ and the buckling length $\lambda_l$ are given in Hancock's paper (1995). This then leads to the similar equations for the critical stress for distortional buckling.

Explicit expressions for the prediction of the distortional buckling of beams have also been proposed by Schafer and Pekoz (1999a).

### 2.4.1.3 Models for the buckling of restrained beams

When one flange is elastically restrained, the buckling behaviour is more complex and there are two distortional modes to consider in design. Pekoz and Soroushian (1982) have described a model for the combined torsional-distortional mode. And Hancock's distortion buckling model in Fig.2.8 can be readily modified further to include the additional torsional restraint from the cladding (Davies, 1996).

## 2.4.2 Useful Data On The Distortional Buckling Mode

Three recent papers have provided more useful data on the distortional buckling mode where the edge stiffened element fails by transverse bending of the stiffener, which has been called *flange-distortional* to distinguish it from the *lateral-distortional* mode that can occur in flexure as shown in Fig.2.9 by Hancock (2003). The first paper by Badawy Abu-Sena et al. (2001) provides an interesting study where the torsional-

flexural mode interacts with the lip buckling (flange-distortional) mode for lip-stiffened compression members. Useful formulae based on an energy method are provided for design and compared with finite element analyses (FEA) to test their accuracy.

The second paper by Kesti and Davies (1999) investigates local and distortional buckling of thin-walled short columns. An investigation of the design method in Eurocode 3 Part 1.3 (1996) for lip-stiffened channels versus design based on distortional buckling and GBT has been performed to show that the latter provides a better estimate of strength than EC3. The third paper by Schafer and Peköz (1999b) investigates laterally braced cold-formed steel flexural members with edge stiffened flanges with similar buckling modes to those shown in Fig. 2.9. New procedures for hand calculation of the buckling stress in the local and distortional modes are presented and verified. Comparisons with tests show that the methods are more reliable than the existing methods in the design standards and specifications (AISI, 1996; AS/NZS, 1996).

## 2.5 LATERAL-TORSIONAL BUCKLING BEHAVIOUR

### 2.5.1 Research on Lateral-torsional Buckling Behaviour

The lateral-torsional buckling is characterized by the mode of rigid body movements of the whole member in which individual cross-sections rotate and translate but do not distort in shape. It is well known that long beams with low lateral stiffness and low torsional stiffness are very prone to buckling laterally. Further, the sections are often loaded eccentrically from their shear centres. Because of the geometry of the cross section, which gives great flexural rigidity about one axis at the expense of low torsional rigidity and low flexural rigidity about a perpendicular axis, cold-formed members are particularly susceptible to lateral-torsional buckling.

Compared to the local and distortional buckling, the lateral-torsional buckling has been little concerned. This is partly because cold-formed steel members are usually used together with metal sheeting that restrains the lateral movement of the members

and thus reduces the possibility of the occurrence of lateral-torsional buckling, and partly because the lateral-torsional buckling is traditionally prevented by the use of inexpensive anti-sag bars.

Recently, there have been many experimental, numerical and analytical studies of torsion and lateral-torsional buckling (Davies, 2000; Gotluru et al., 2000; Hancock, 2003). Put et al. (1998) performed lateral buckling tests on unbraced, simply supported cold-formed lipped channel beams. Experiments on braced cold-formed steel channel and zed purlin beams were also undertaken at Cornell University (Schafer, 2001b). Pi et al. (1998) investigated the lateral buckling and biaxial bending behaviour of both channel and zed sections using finite element methods. A pilot study of laterally braced C-sections as used in wall studs was performed by Beshara and LaBoube (2001). The effect of a lateral brace at mid length to restrain the C-section from rotation was investigated experimentally.

Channel and Zee (Zed) sections are the most common members used as purlins and girts in roof and wall systems with sheeting attached and so the effect of the sheeting in preventing torsion and lateral-torsional buckling needs to be quantified. Considerable research has been performed in this area over many years. Lucas et al. (1997a & 1997b) investigated the influence of sheeting on the performance of the cold-formed sections using the finite element method. Linder and Aschinger (1994) proposed some alternative design procedures for the load-carrying capacity of cold-formed beams subjected to overall lateral-torsional buckling and local plate buckling. Laine and Tuomala (1999) studied Z, Zeta, C and Hat shaped sections to determine experimentally the influence of internal supports and sheeting on the top flange for purlins under gravity load. In design specifications such as BSI (1998) the lateral-torsional buckling of cold-formed members is calculated based on the theory of a detached beam, the result of which is obviously too conservative as it neglects the influence of sheeting restraints.

The recently developed finite strip analysis packages are aimed to predict more accurate elastic buckling stresses related to local, distortional, and lateral-torsional buckling (Loughlan, 1996; Hancock, 1997a; Schafer, 2001c&2003a; Ye, 2002). However, at the present, these packages can be only applied to the case where the

member is subjected to pure compression and/or pure bending. For local buckling, it may be acceptable to assume constant stresses along the longitudinal axis because of its relatively short half-wavelength. For distortional buckling and particularly for lateral-torsional buckling, however, the stress gradient along the longitudinal axis should be considered if the result of finite strip analysis is going to be used for the design purpose.

Recently, Li (2004) developed an analytical model for predicting the lateral-torsional buckling of cold-formed zed-purlins partially restrained by metal sheeting for both downward and uplift loadings. The details are given in Section 2.5.2.

### 2.5.2 Analytical Model For Cold-Formed Steel Beams

An analytical model for predicting the lateral-torsional buckling of cold-formed steel members is presented by Li (2004). The model is constructed for the practical case where the cold-formed member is subjected to transverse loads and is restrained partial-laterally by sheeting and interval anti-sag bars. The focus is to investigate the influence of the restraints provided by the sheeting and by the interval anti-sag bars, and the variation of moment along the longitudinal axis on the lateral-torsional buckling behaviour of the cold-formed steel member.

#### 2.5.2.1 Analytical model

Consider a purlin that is partially restrained by the sheeting on its upper flange. The restraint of the sheeting can be simplified by one translational spring and one rotational spring, as shown in Fig.2.10. Let the origin of the coordinate system ($x$, $y$, $z$) be the centroid of the cross-section, with x axis being along the longitudinal direction of the beam, and y and z axes taken in the plane of the cross-section. For an arbitrary axis system, the relationship between bending moments and radii of curvature can be expressed as:

$$\begin{Bmatrix} M_y \\ M_z \end{Bmatrix} = E \begin{bmatrix} I_y & I_{yz} \\ I_{yz} & I_z \end{bmatrix} \begin{Bmatrix} 1/R_z \\ 1/R_y \end{Bmatrix} \tag{2.3}$$

where $M_y$ and $M_z$ = the bending moments about $y$ and $z$ axes;

$E$ = the Young's modulus;

$I_y$ and $I_z$ = the second moments of the cross-section area about $y$ and $z$ axes;

$I_{yz}$ = the product moment of the cross-section area;

$R_y$ and $R_z$ = the radii of curvature of the centroidal axis in the $xz$ and $xy$ planes, respectively.

The moment in Eq.(2.3) is defined as positive if it creates a tensile stress for positive $y$ and $z$ values. Thus, $M_y$ has the same direction as $y$ axis, while $M_z$ has an opposite direction to $z$ axis.

Note that for small deflections the radii of curvature can be expressed in terms of deflections of the centroidal axis as follows:

$$\frac{1}{R_y} = -\frac{d^2v}{dx^2}, \quad \frac{1}{R_z} = -\frac{d^2w}{dx^2} \tag{2.4}$$

where $v$ and $w$ = the deflections of the beam centroidal axis in $y$ and $z$ directions, respectively.

The strain energy of the beam due to deflections and rotation can be expressed as:

$$U_{0\_beam} = \frac{1}{2}\int_o^l (\frac{M_y}{R_z} + \frac{M_z}{R_y})dx + \frac{GJ}{2}\int_o^l (\frac{d\phi}{dx})^2 dx + \frac{EC_w}{2}\int_o^l (\frac{d^2\phi}{dx^2})^2 dx \tag{2.5}$$

where $G$ = the modulus of elasticity in shear;

$J$ = the torsion constant;

$C_w$ = the warping constant;

$\phi$ = the angle of twist;

$l$ = the span length of the beam.

The first term in Eq. (2.5) represents the strain energy due to bending about y and z axes, the second term represents the strain energy due to twisting, and the third term represents the warping strain energy, respectively.

The strain energy stored in the two springs due to the deformation of the beam can be expressed by

$$U_{0\_spring} = \frac{k_z}{2}\int_o^l (w - \frac{d\phi}{2})^2 dx + \frac{k_\phi}{2}\int_o^l \phi^2 dx \tag{2.6}$$

where $k_z$ and $k_\phi$ = the per-unit length stiffness constants of the translational and rotational springs;

$d$ = the depth of the section.

It is assumed that the purlin is subjected to the external loads of a vertical uniformly distributed load within the span and concentrated moments at its ends. The potential energy generated by these external loads can be expressed by

$$W_o = \int_o^l q_y(v - a\phi)dx + (M_{yo}\frac{dw}{dx}\bigg|_{x=0} - M_{yl}\frac{dw}{dx}\bigg|_{x=l}) + (M_{zo}\frac{dv}{dx}\bigg|_{x=0} - M_{zl}\frac{dv}{dx}\bigg|_{x=l}) \tag{2.7}$$

where $q_y$ = the density of uniformly distributed load;

$a$ = the distance between loading line and web central line;

$M_{yo}$, $M_{yl}$, $M_{zo}$, $M_{zl}$ = the concentrated moments about y and z axes, applied at the ends of the purlin.

The deflections, $v(x)$ and $w(x)$, and the angle of twist, $\phi(x)$ due to the externally applied loads can be determined by employing the stationary principle as follows:

$$\delta(U_0 - W_o) = \delta(U_{0\_beam} + U_{0\_spring} - W_o) = 0 \tag{2.8}$$

After the deflections and rotation are determined the pre-buckling moment distributions along the longitudinal axis can then be calculated using Eq. (2.3).

The analysis of linear elastic buckling can be done using a similar energy method. Let $M_{oy}$ and $M_{oz}$ be the pre-buckling moment distributions that are obtained from the pre-buckling stress analysis. The pre-buckling longitudinal stress due to $M_{oy}$ and $M_{oz}$ can be calculated by using the bending formula of the asymmetric beam:

$$\sigma_x(x,y,z) = \frac{M_{oz}I_y - M_{oy}I_{yz}}{I_yI_z - I_{yz}^2}y + \frac{M_{oy}I_z - M_{oz}I_{yz}}{I_yI_z - I_{yz}^2}z \tag{2.9}$$

Note that $\sigma_x$ is the function of $y$ and $z$ as well as of $x$. Now, let $v(x)$ and $w(x)$ be the buckling deflections of the beam centroidal axis in y and z directions and $\phi(x)$ as the buckling twisting about x axis. Thus, the strain energy generated by the buckling displacements can be calculated using Eq. (2.5) for the purlin and Eq. (2.6) for the springs.

The buckling deflections of the beam at any point $(x,y,z)$ during buckling can be expressed in terms of the buckling displacements of the beam centroidal axis, $v_b$, $w_b$ and $\phi_b$, as follows (Ressner, 1989; Li, 2004):

$$\begin{aligned} \overline{v}(x,y,z) &= v_b - z\sin\phi_b + y(\cos\phi_b - 1) \approx v_b - z\phi_b - \frac{1}{2}y\phi_b^2 \\ \overline{w}(x,y,z) &= w_b + z(\cos\phi_b - 1) + y\sin\phi_b \approx w_b + y\phi_b - \frac{1}{2}z\phi_b^2 \end{aligned} \tag{2.10}$$

where $\overline{v}(x,y,z)$ and $\overline{w}(x,y,z)$ = the deflections of the beam at point $(x,y,z)$ during the buckling.

The longitudinal displacement at point (x,y,z) can be expressed as follows:

$$\begin{aligned} \overline{u}(x,y,z) &= u_b - (y\cos\phi_b - z\sin\phi_b)\frac{dv_b}{dx} - (z\cos\phi_b + y\sin\phi_b)\frac{dw_b}{dx} + \beta(y,z)\frac{d\phi_b}{dx} \\ &\approx u_b - y\frac{dv_b}{dx} - z\frac{dw_b}{dx} + \beta\frac{d\phi_b}{dx} + z\phi_b\frac{dv_b}{dx} - y\phi_b\frac{dw_b}{dx} \end{aligned} \tag{2.11}$$

where $\beta(y,z)$ = the warping function of St. Venant torsion;

$\overline{u}(x,y,z)$ and $u_b(x)$ = the longitudinal displacements of the beam at points $(x,y,z)$ and $(x,o,o)$, respectively.

The longitudinal strain and shear strains generated by the buckling displacements can be calculated by

$$\varepsilon_x(x,y,z) = \frac{\partial \overline{u}}{\partial x} + \frac{1}{2}[(\frac{\partial \overline{v}}{\partial x})^2 + (\frac{\partial \overline{w}}{\partial x})^2]$$
$$\gamma_{xy}(x,y,z) = \frac{\partial \overline{u}}{\partial y} + \frac{\partial \overline{v}}{\partial x} + \frac{\partial \overline{w}}{\partial x}\frac{\partial \overline{w}}{\partial y} \tag{2.12}$$
$$\gamma_{xz}(x,y,z) = \frac{\partial \overline{u}}{\partial z} + \frac{\partial \overline{w}}{\partial x} + \frac{\partial \overline{v}}{\partial x}\frac{\partial \overline{v}}{\partial z}$$

Substituting Eqs. (2.10) and (2.11) into (2.12) and splitting them into linear and nonlinear terms in terms of the buckling displacements, it leads to the following second-order nonlinear strains:

$$\varepsilon_{x2}(x,y,z) = \frac{1}{2}[(\frac{dv}{dx})^2 + (\frac{dw}{dx})^2 + (y^2+z^2)(\frac{d\phi}{dx})^2] + z\phi\frac{d^2v}{dx^2} - y\phi\frac{d^2w}{dx^2}$$
$$\gamma_{xy2} = 0 \tag{2.13}$$
$$\gamma_{xz2} = 0$$

The non-linear strain energy generated by the pre-buckling longitudinal stress through the second-order strains is calculated by:

$$W_{\sigma xb} = -\int_o^l \int_A \sigma_x(x,y,z)\varepsilon_{x2}(x,y,z)dAdx \tag{2.14}$$

where $A$ = the area of the cross section.

The negative sign in Eq. (2.14) is because $\sigma_x$ and $\varepsilon_{x2}$ are in opposite direction. Substituting Eq. (2.13) into (2.14) and noting that for the zed purlin that is symmetric about its centroid.

$$\int_A \sigma_x(x,y,z)dA = 0$$
$$\int_A \sigma_x(x,y,z)(y^2+z^2)dA = 0 \tag{2.15}$$

the following equation is obtained,

$$W_{\sigma xb} = \int_o^l \int_A \sigma_x(x,y,z)(y\frac{d^2w}{dx^2} - z\frac{d^2v}{dx^2})\phi dAdx = \int_o^l \phi(M_{oz}\frac{d^2w}{dx^2} - M_{oy}\frac{d^2v}{dx^2})dx \tag{2.16}$$

Note that $W_{\sigma xb}$ does not include the strain energy generated due to the lowering of the distributed load during the rotation which is due to the load that is not acting at the shear center (Timoshenko & Gere, 1961). When this is considered the strain energy should be expressed by

$$W_1 = W_{\sigma xb} + W_q = \int_o^l \phi(M_{oz}\frac{d^2w}{dx^2} - M_{oy}\frac{d^2v}{dx^2})dx + \frac{d}{4}\int_o^l q_y\phi^2 dx \tag{2.17}$$

It is known that for any infinitesimal buckling displacements if the strain energy generated by the buckling displacements is less than the strain energy generated by the pre-buckling stresses then buckling will occur. Mathematically, this means that buckling occurs at:

$$\lambda W_1 = \lambda(W_{\sigma xb} + W_q) \geq U_1 = U_{1\_spring} + U_{1\_beam} \tag{2.18}$$

where $\lambda$ = the critical load factor;

$U_1$ = the total strain energy of the system.

$U_{1\_beam}$ and $U_{1\_spring}$ = the stain energy of the beam when the buckling occurs, which have the same expression as $U_{0\_beam}$ and $U_{0\_spring}$ except for that the deflections and the angle of twist are now the buckling deflections and the buckling angle of twist.

The minimum buckling critical load thus is calculated by

$$\delta(U - \lambda W) = 0 \tag{2.19}$$

#### 2.5.2.2 Numerical implementation

Eqs. (2.8) and (2.19) can be applied to the general case where the purlin can have any boundary conditions and subjected to any distribution loads and moments. Variational Eq. (2.8) is equivalent to the pre-buckling equilibrium equation, whereas variational Eq. (2.19) is equivalent to the secondary equilibrium of the system, that is, so-called buckling equation. For a given problem, one can determine the pre-buckling displacement functions $v(x)$, $w(x)$ and $\phi(x)$ and thus the pre-buckling moment distributions, $M_{oy}$ and $M_{oz}$ by solving the variational Eq. (2.8) and then determine the critical load factor and corresponding buckling displacements $v(x)$, $w(x)$ and $\phi(x)$ by

solving the variational Eq. (2.19). It should be mentioned here that the strain energies, $U$, in Eqs. (2.8) and (2.19) have different meanings although they have the same expression. In the former, the strain energy is generated by the pre-buckling deflections and rotation which are caused by the loads externally applied to the purlin; while in the latter, the strain energy is the buckling strain energy generated by the buckling displacements, which are determined from the buckling Eq. (2.19).

In Li's numerical study focus is on the purlin that is laterally restrained in the translational direction but free in the rotational direction (that is, $k_z = \infty, k_\phi = 0$), which is a case of most practical applications. For the purlin with its upper flange being laterally restrained the rotational displacement can be expressed in terms of the deflection in the horizontal direction as follows:

$$\phi(x) = \frac{2}{d} w(x) \tag{2.20}$$

For this particular case the strain energy expression (2.5) and (2.7) and (2.17) can be simplified into:

$$U = \frac{E}{2} \int_o^l [(I_y + \frac{4C_w}{d^2})(\frac{d^2w}{dx^2})^2 + 2I_{yz} \frac{d^2w}{dx^2} \frac{d^2v}{dx^2} + I_z (\frac{d^2v}{dx^2})^2] dx + \frac{2GJ}{d^2} \int_o^l (\frac{dw}{dx})^2 dx \tag{2.21}$$

$$W_o = \int_o^l q_y (v - \frac{2aw}{d}) dx + (M_{yo} \frac{dw}{dx}\Big|_{x=0} - M_{yl} \frac{dw}{dx}\Big|_{x=l}) + (M_{zo} \frac{dv}{dx}\Big|_{x=0} - M_{zl} \frac{dv}{dx}\Big|_{x=l}) \tag{2.22}$$

$$W = \frac{2}{d} \int_o^l w(M_{oz} \frac{d^2w}{dx^2} - M_{oy} \frac{d^2v}{dx^2}) dx + \frac{1}{d} \int_o^l q_y w^2 dx \tag{2.23}$$

The horizontal and vertical deflections of the purlin at the centroid can be constructed by using cubic spline interpolations as follows:

$$\begin{aligned} v(x) &= \sum_{i=1}^{n} v_i f_i(x, x_i) \\ w(x) &= \sum_{i=1}^{n} w_i f_i(x, x_i) \end{aligned} \tag{2.24}$$

where $v_i$ and $w_i$ = the to-be-determined horizontal and vertical deflections at interpolation points $x_i$;

$f_i(x,x_i)$ = the spline interpolation function which is constructed in terms of the function values at $n$ internal interpolation points ($x_1$, $x_2$, ..., $x_n$) and function and derivative values at two end points ($x_o$, $x_{n+1}$).

The function values used for constructing $f_i(x,x_i)$ are defined as:

$$\begin{aligned} f_i(x,x_i) &= 1 \quad for \quad x = x_i \qquad i = 1,2,...,n \\ f_i(x,x_i) &= 0 \quad for \quad x = x_j \neq x_i \qquad j = 0,1,\ldots,n+1 \end{aligned} \tag{2.25}$$

The derivative values used at end points are dependent upon the real boundary conditions of the member. For each end it is divided into two cases:

$$\frac{df_i(x,x_i)}{dx} \equiv 0 \qquad \text{for a fixed boundary at end } x=x_j \tag{2.26}$$

$$\frac{d^2 f_i(x,x_i)}{dx^2} \equiv 0 \qquad \text{for a simply supported boundary at end } x=x_j \tag{2.27}$$

Fig.2.11 graphically shows the profiles of the spline interpolation employed for two different boundaries. It can be seen that the influence of the boundary on the function distribution profile is mainly in the region close to the boundary. The superior of using spline functions over the traditional trigonometric series is obvious. Firstly, it can easily fit the required boundary conditions. Secondly, it is convenient to simulate intermediate point restraints provided by the anti-sag bars.

Substituting Eq. (2.24) into (2.21)-(2.23) and then into the variational Eqs. (2.8) and (2.19), it yields two algebra equations,

$$\begin{bmatrix} A_o & B_o \\ B_o & C_o \end{bmatrix} \begin{bmatrix} \{v_i\} \\ \{w_i\} \end{bmatrix} = \begin{bmatrix} \{f_{yi}\} \\ \{f_{zi}\} \end{bmatrix} \tag{2.28}$$

$$\begin{bmatrix} A_o & B_o \\ B_o & C_o \end{bmatrix} \begin{bmatrix} \{v_i\} \\ \{w_i\} \end{bmatrix} = \lambda \begin{bmatrix} A_1 & B_1 \\ B_1 & C_1 \end{bmatrix} \begin{bmatrix} \{v_i\} \\ \{w_i\} \end{bmatrix} \tag{2.29}$$

where $A_o$, $B_o$ and $C_o$ = the coefficients obtained from the calculation of the strain energy;

$f_{yi}$ and $f_{zi}$ = the coefficients obtained from the calculation of the work done by the externally applied loads;

$A_1$, $B_1$ and $C_1$ = the coefficients obtained from the calculation of the work done by the pre-buckling stress.

Equation (2.28) is the pre-buckling equilibrium equation and the corresponding solutions $\{v_i\}$ and $\{w_i\}$ represent the deflections of the purlin centroid at $x=x_i$. Whereas Eq. (2.29) is the buckling equation and the corresponding solutions $\{v_i\}$, $\{w_i\}$ and $\lambda$ represent the buckling modes and corresponding critical load factors. The smallest eigenvalue of Eq. (2.29) represents the buckling critical load factor of the member.

## 2.6 UNTYPICAL BUCKLING MODES

### 2.6.1 Shear Buckling Mode

Shear buckling may also be either local or global. Local shear buckling can occur in the slender webs of members subjected to bending or in the wide flanges of sheeting and decking profiles subjected to diaphragm action. Global shear buckling generally only arises when relatively lightweight sheeting or lining profiles are subjected to diaphragm action. There is a need for greater understanding of both local and global shear buckling of stiffened tray and cassette sections subjected to diaphragm action (Davies, 2000).

### 2.6.2 Torsion And Distortion

Cold-formed open section steel members are more likely to undergo torsional deformation due to their low torsional rigidity resulting from their thin walls. Further, the sections are often loaded eccentrically from their shear centres and so are subjected to substantial torques. According to Hancock (2003), four recent papers provide valuable information on the torsional and distortional behaviour of thin-walled and cold-formed sections.

Gotluru et al. (2000) have performed simple geometric nonlinear analyses, finite element analysis and finite strip analysis and compared their results with simple experiments. The influence of typical support conditions was studied and found to produce partial warping restraints. This effect is accounted for by introducing hypothetical springs. Put et al. (1999) have investigated the bending and torsion of cold-formed channel beams. The effect of loading eccentricity was investigated in detail and simple interaction equations have been developed for design.

Jönsson (1999a) has developed a distortional theory for thin-walled beams by extending the conventional torsional theory to include a distortional warping function. The extended theory works for open sections, closed sections and sections with open and closed parts.

### 2.6.3 Web Crippling

Web crippling often occurs in cold-formed members because the loading is eccentric from the web centreline due to the rounded corners of the sections, and because the webs are often slender and unstiffened unlike hot-rolled design where web stiffeners are often used (Hancock, 2003). A recent paper by Young and Hancock (2001) provides experimental data on cold-formed unlipped channels subjected to web crippling. The web slenderness of the channels was lower than that used in the calibration of the design standards (AISI, 1996; AS/NZS, 1996; CEN, 1996) and the results showed these standards to be quite lax for stockier webs. The results have been used as part of the calibration of the new web crippling rules in the NAS (AISI, 2001) to remove the current laxity.

Webs may often contain openings especially if they are part of residential construction as floor joist or studs. A recent experimental investigation of the effect of circular holes on web strength was conducted by LaBoube et al. (1999), from which new design rules have been developed and incorporated in the NAS (AISI, 2001).

## 2.7 DESIGN ISSUES

Currently the design of thin-walled cold-formed steel members relies on the effective width approach. This powerful empirical method has been used successfully since the inception of the cold-formed steel design specification in the 1940's and continues to be used in the design of a variety of thin-walled structures. The method works by considering the strength reduction due to local plate buckling as a reduced (or effective) width for each element of a member.

In developing new rules for elements with intermediate and edge stiffeners difficulty in extending the effective width approach was encountered. This includes that the number of effective portions increases significantly with the introduction of stiffeners, and the competition between multiple buckling modes (i.e., local vs. distortional) is difficult to capture in an effective width approach.

The classical elastic buckling analysis on isolated structural elements could provide over conservative or under conservative results. For design purposes, it is generally necessary to consider the interaction of bucking and yielding. Furthermore, for economic design, it is also necessary to consider the beneficial effect of post-buckling. There are two complementary approaches which are available to deal with this situation.

### 2.7.1 The Ayrton-Perry Equation

The Ayrton–Perry equation (EC3, 1996) is used in most modern codes to combine yielding and global buckling (lateral or lateral-torsional). Solutions of practical accuracy can generally be obtained by combining the theoretical load (or stress) for elastic (bifurcation) buckling with the corresponding yield load (or stress) using the equation:

$$\chi = \frac{1}{\phi + [\phi^2 - \overline{\lambda}^2]^{0.5}} \; but \; \chi \leq 1 \; with \; \phi = 0.5[1 + \alpha_1(\overline{\lambda} - 0.2) + \overline{\lambda}^2] \qquad (2.30)$$

where $\chi$ = the reduction factor for buckling with respect to the unbuckled capacity;

$\alpha_1$ = an imperfection factor;

$\bar{\lambda}$ = the relative slenderness in the relevant buckling mode.

In Eurocode 3: Part 1.3 (1996), this equation is applied to the flexural buckling of columns and to the lateral torsional buckling of beams with $\bar{\lambda}$ equal to $\sqrt{P/P_{cr}}$ or $\sqrt{M/M_{cr}}$ respectively.

However, the Ayrton–Perry approach does not include any allowance for post local buckling so that it is likely to be over-conservative when applied to situations where local buckling is significant. It is with this in mind that Schafer and Pekoz (1998) have recently proposed the "direct strength" approach.

### 2.7.2 Direct Strength Design Of Cold-Formed Sections

Schafer and Pekoz (1998) have recently proposed a new procedure which works only with the gross properties of a member and can take into account not only the interaction between local and global buckling but also the interaction between distortional and global buckling.

Formulae are proposed for beams (Schafer & Pekoz, 1998) and for columns (Schafer, 2001a) and were approved in 2003 by the American Iron and Steel Institute Committee on Specifications and finalized in 2004 as Appendix 1 of the North American Specification for the Design of Cold-Formed Steel Structural Members (AISI, 2004).

The Direct Strength Method requires determing of the elastic buckling behaviour of the member, and then provides a series of nominal strength [resistance] curves for predicting the member strength based on the elastic buckling behaviour. The procedure does not require effective width calculations, nor iteration, and instead uses gross properties and the elastic buckling behaviour of the cross-section to predict the of the whole section.

The provisions of the method are applicable for determinng of the nominal axial ($P_n$) and flexural ($M_n$) strengths of cold-formed steel members. A list of pre-qualified

beams and columns with geometric and material limitations and their corresponding calibrated safety factor and resistance factor are given in (AISI, 2004). Other beams and columns shall be permitted to use the provisions, but the standard factors for rational analysis apply.

### 2.7.2.1 Direct strength for columns

The nominal axial strength, $P_n$, is the minimum of $P_{ne}$, $P_{nl}$ and $P_{nd}$ as give below.

- Flexural, Torsional, or Torsional-Flexural Buckling

The nominal axial strength, $P_{ne}$, for flexural, torsional, or torsional-flexural buckling is

$$P_{ne}/P_y = \begin{cases} 0.658^{\lambda_c^2} & \sqrt{P_y/P_{cre}} \le 1.5 \\ 0.877/\lambda_c^2 & \sqrt{P_y/P_{cre}} > 1.5 \end{cases} \tag{2.31}$$

where $P_y = A_g F_y$;

$P_{cre}$ = Minimum of the critical elastic column buckling load in flexural, torsional, or torsional-flexural buckling.

- Local Buckling

The nominal axial strength, $P_{nl}$, for local buckling is

$$P_{nl}/P_{ne} = \begin{cases} 1 & \sqrt{P_{ne}/P_{crl}} \le 0.776 \\ [1-0.15(\frac{P_{crl}}{P_{ne}})^{0.4}](\frac{P_{crl}}{P_{ne}})^{0.4} & \sqrt{P_{ne}/P_{crl}} > 0.776 \end{cases} \tag{2.32}$$

where $P_{crl}$ = Critical elastic local column buckling load.

- Distortional Buckling

The nominal axial strength, $P_{nd}$, for distortional buckling is

$$P_{nd}/P_y = \begin{cases} 1 & \sqrt{P_y/P_{crd}} \le 0.561 \\ [1-0.25(\frac{P_{crd}}{P_y})^{0.6}](\frac{P_{crd}}{P_y})^{0.6} & \sqrt{P_y/P_{crd}} > 0.561 \end{cases} \tag{2.33}$$

where $P_{crd}$ = Critical elastic distortional column buckling load.

### 2.7.2.2 Direct strength for beams

The nominal flexural strength, $M_n$, is the minimum of $M_{ne}$, $M_{nl}$ *and* $M_{nd}$ as given below.

- Lateral-torsional Buckling

The nominal flexural strength, $M_{ne}$, for lateral-torsional buckling is

$$M_{ne} = \begin{cases} M_{cre} & if\ M_{cre} < 0.56M_{yield} \\ \frac{10}{9}M_y(1-\frac{10M_y}{36M_{cre}}) & if\ 2.78M_y \geq M_{cre} \geq 0.56M_{yield} \\ M_y & if\ M_{cre} > 2.78M_{yield} \end{cases} \quad (2.34)$$

where $M_{yield} = S_f F_y$;

$S_f$ = the gross section modulus referenced to the extreme fiber in first field;

$M_{cre}$ = Critical elastic lateral-torsional buckling moment.

- Local Buckling

The nominal flexural strength, $M_{nl}$, for local buckling is

$$M_{nl}/M_{ne} = \begin{cases} 1 & \sqrt{M_{ne}/M_{crl}} \leq 0.776 \\ [1-0.15(\frac{M_{crl}}{M_{ne}})^{0.4}](\frac{M_{crl}}{M_{ne}})^{0.4} & \sqrt{M_{ne}/M_{crl}} > 0.776 \end{cases} \quad (2.35)$$

where $M_{crl}$ = Critical elastic local buckling moment.

- Distortional Buckling

The nominal flexural strength, $M_{nd}$, for distortional buckling is

$$M_{nd}/M_y = \begin{cases} 1 & \sqrt{M_y/M_{crd}} \leq 0.673 \\ [1-0.22(\frac{M_{crd}}{M_y})^{0.5}](\frac{M_{crd}}{M_y})^{0.5} & \sqrt{M_y/M_{crd}} > 0.673 \end{cases} \quad (2.36)$$

where $M_{crd}$ = Critical elastic distortional buckling moment.

#### 2.7.2.3 The limitations of direct strength method

Currently, the Direct Strength Method provides no explicit provisions for members in tension, shear, combined bending and shear, web crippling, combined bending and web crippling, or combined axial load and bending (bending-columns).

A more profound understanding of the method's conception can be gained on this basis. As a result, the Direct Strength Method assumes the plastic reserve of the section shape to influence the cross-section capacity of locally buckled members. This assumption has been checked by Rusch and Lindner (2001) using the test results on thin-walled I-sections, who pointed out that the Direct Strength Method is limited to cases where no shift of the effective centroid occurs. This is presupposed by the fundamental similarity to the other concepts. Therefore, caution is necessary in all cases, where the shift leads to an additional bending moment. Especially if the additional bending moment increases an exiting external moment, an interaction formula, which does not take into account the shift, overestimates the load carrying capacity significantly.

## 2.8 OUTLINE OF APPROACHES FOR RESEARCH

### 2.8.1 Tests

*Tests are suitable for the determination of the design strength of all kinds of cold-formed steel structures.*

Historically, design by testing has been more widely used for cold-formed sections than for most other building components. There are a number of reasons for this, both practical and economic. As analytical methods have improved, testing is now used less frequently. However, it is still widely used for particular cases such as: purlins clad with sheeting; perforated racking uprights; (slotted) studs with sheathing attached; composite decks; sandwich panels etc. It is notable that almost all of these examples involve the interaction of light gauge steel components with other materials or parts of the structure as discussed above. These situations are, of course,

notoriously difficult to analyse satisfactorily although much progress is being made in this area. Other situations which are difficult to analyse and where testing may still be appropriate are those involving significant holes or openings through the member and those where economic design requires consideration of ultimate limit states in which there is interaction between buckling and yielding.

### 2.8.2 Design Specifications

*Design specifications are suitable for the determination of the design strength of most cases.*

The research and development engineer has a range of tools available to him when considering the design of a new range of cold-formed sections or new applications of existing sections. Evidently, most cases of practical importance are covered by modern design codes such as Eurocode 3: Part 1.3 (1996); The American Specification (1996), The Australian and New Zealand Standard (1996) and the British Standard BS 5950: Part 5 (1998).

However, cases may arise which are not adequately covered by the available codes or where the codes are over-conservative and more efficient designs can be obtained by an investment in a more detailed design.

### 2.8.3 Classic Methods

*They are applicable to various buckling behaviours.*

Although the differential equations which govern the behaviour of thin-walled metal sections have been known for many years, explicit solutions have been found for relatively few practical situations. The main application of explicit solutions is in the analysis of the global buckling (lateral and lateral-torsional) of beams and columns. Explicit solutions are also useful in some simple cases of shear buckling.

An analytical model for predicting the lateral-torsional buckling of cold-formed steel members is presented by Li (2004). The model is constructed for the practical case where the cold-formed member is subjected to transverse loads and is restrained

partial-laterally by sheeting and interval anti-sag bars. The details are given in Section 2.5.2.

Generalised beam theory is also applicable to all three generic modes of buckling as well as their interaction for prismatic members. The essential concept of GBT is the separation of the behaviour of a prismatic member into a series of orthogonal displacement modes. Some details are given in Section 2.8.6.

### 2.8.4 The Finite Element Method

*The finite element method can model all of the required phenomena.*

The most general method is the finite element method, which provides solutions to the governing differential equations. In principle, all of the required phenomena can be modelled using appropriate finite element techniques. However, this method is generally considered to be too cumbersome for practical design and therefore may only be seen as a primary method for researchers.

The primary building-block for the analysis of cold-formed sections is the second-order thin shell element which can accommodate the full range of section shapes and buckling phenomena. If a non-linear stress-strain relationship is incorporated into the analysis, such elements can also model yielding and elastic-plastic buckling. Contact elements, connection elements and large deflection theory add to the huge range of facilities that are available to the analyst so that all the relevant practical problems can be solved using the finite element method. The disadvantage is, of course, the considerable cost. This is mainly a consequence of the time spent in data preparation and post-processing although non-linear problems may take a long time to run. It should be noted that great care is needed in formulating the correct boundary conditions and this can also consume a considerable amount of time.

The seven degrees of freedom, prismatic finite element was developed by Barsoum and Gallagher (1970). It adds the first derivative of rotation about the longitudinal axis to a conventional six degree of freedom, second-order beam-column element and thus introduces consideration of lateral torsional buckling. This provides a rational

approach to "rigid body" buckling when the available solutions based on explicit solutions of the governing differential equations are not sufficient.

### 2.8.5 The Finite Strip Method

*The finite strip method is applicable to elastic local, distortional and global buckling of the structures with uniform stress distribution along the longitudinal axis of the member.*

The finite strip method falls into the category of numerical methods that are specifically designed for prismatic members. Cold-formed sections are generally prismatic and so the finite strip method has the advantage over the finite element method of requiring less computer time and memory as well as less data preparation.

From the practical point of view, the second-order finite strip method is particularly important because bifurcation buckling solutions may be obtained relatively easily using simple half sine wave displacement functions. This provides "whole section" solutions for the full range of buckling phenomena, leading to relatively new design procedures which will be considered later. Several well-known researchers (e.g. Hancock, Pekoz, Rhodes) have developed user-friendly computer software codes for this calculation which are available to practical designers.

Y.K. Cheung originally promoted the finite strip method. An excellent summary of the method, and the theory behind it, can be found in his book (Cheung, 1976). The use of the finite strip method for understanding and predicting the behaviour of hot-rolled steel members, and cold-formed steel members has been greatly extended by G. Hancock (1994). Hancock used the stiffness matrices derived in Cheung's book, and with some modification, created BFINST- a computer program for solving the elastic buckling problem of open thin-walled members via the finite strip. His early work in the field on I-Beams led to the acceptance and understanding of the use of the finite strip method, which was further developed particularly on cold-formed steel design.

A basic introduction to the finite strip model employed in the program CUFSM is presented here, which includes the theoretical development and derivation of the

initial stiffness and geometric stiffness within the finite strip method (Schafer, 2001c & 2003a). The coordinate directions and degrees of freedom for a typical strip are shown in Fig.2.12. Note the rather unusual choice of the x-z coordinate system and this is consistent with Cheung's original derivation.

Since a box structure may be considered as an assembly of rectangular plates which are capable of undergoing both bending and in-plane deformations, in a linear elastic analysis, it is assumed that no interaction takes place between these two systems. The stiffness and force matrices for a finite strip in the analysis of box structures can therefore be obtained by combining the bending and in plane analysis.

### 2.8.5.1 Initial stiffness matrix for plates

The standard definition of an initial stiffness matrix is apparent from: $\{f\} = [K]\{d\}$, or, expanded to explicitly show the nodal forces, nodal degrees of freedom, and the initial stiffness submatrices: $[K_{uv}]$ (plane stress) and $[K_{w\theta}]$ (bending) are:

$$\begin{Bmatrix} F_{u_1} \\ F_{v_1} \\ F_{u_2} \\ F_{v_2} \\ F_{w_1} \\ M_{\theta_1} \\ F_{w_2} \\ M_{\theta_2} \end{Bmatrix} = \begin{bmatrix} [K_{uv}] & \begin{matrix} 0 & 0 & 0 & 0 \\ 0 & 0 & 0 & 0 \\ 0 & 0 & 0 & 0 \\ 0 & 0 & 0 & 0 \end{matrix} \\ \begin{matrix} 0 & 0 & 0 & 0 \\ 0 & 0 & 0 & 0 \\ 0 & 0 & 0 & 0 \\ 0 & 0 & 0 & 0 \end{matrix} & [K_{w\theta}] \end{bmatrix} \begin{Bmatrix} u_1 \\ v_1 \\ u_2 \\ v_2 \\ w_1 \\ \theta_1 \\ w_2 \\ \theta_2 \end{Bmatrix} \tag{2.37}$$

The initial stiffness matrix may be expressed as:

$$[K] = \int [B]^T [E][B] dV \quad \text{or} \quad \int [N']^T [E][N'] dV \tag{2.38}$$

where $[B]$ or $[N']$ = the appropriate derivatives of the shape functions $[N]$, which is defined from $(u\ v\ w)^T = [N]\{d\}$, where $(u\ v\ w)^T$ is the displacement field and $\{d\}$ is a vector of the nodal degrees of freedom.

For an orthotropic plate, and assuming no variation in the thickness ($t$) of the strip, $[K]$ may be expressed as: $[K] = t\int[B]^T[D][B]dA$, where the plate rigidities are defined as:

$$[D] = \begin{bmatrix} D_x & D_1 & 0 \\ D_1 & D_y & 0 \\ 0 & 0 & D_{xy} \end{bmatrix} \tag{2.39}$$

$$D_x = \frac{E_x t^3}{12(1-\nu_x\nu_y)}, D_y = \frac{E_y t^3}{12(1-\nu_x\nu_y)}, D_{xy} = \frac{Gt^3}{12}, D_1 = \frac{\nu_y E_x t^3}{12(1-\nu_x\nu_y)} = \frac{\nu_x E_y t^3}{12(1-\nu_x\nu_y)}.$$

The finite strip solution used here employs a polynomial in the transverse direction and a harmonic function in the longitudinal direction. In this derivation, the longitudinal direction is assumed to take the form of a half sine wave. This is consistent with the boundary condition of simply supported ends. The advantage of such an assumption is that the integrals used in forming the stiffness matrix decouple, and the solution is simplified.

The derivation of the initial stiffness matrix is in two completely decoupled parts. A pure plane stress conditions is assumed for the in plane $u$ and $v$ degrees of freedom. The $w$ and $\theta$ degrees of freedom are derived using classical small defection plate theory to arrive at the bending initial stiffness matrix. The two matrices $[K_{uv}]$ and $[K_{w\theta}]$ are combined to form the total initial stiffness matrix.

- **Plane stress initial stiffness matrix $[K_{uv}]$**

The shape functions for use in determining the in-plane stiffness matrix are:

$$u = \begin{bmatrix} (1-\frac{x}{b_s}) & (\frac{x}{b_s}) \end{bmatrix} \begin{Bmatrix} u_1 \\ u_2 \end{Bmatrix} Y_m$$
$$v = \begin{bmatrix} (1-\frac{x}{b_s}) & (\frac{x}{b_s}) \end{bmatrix} \begin{Bmatrix} v_1 \\ v_2 \end{Bmatrix} \frac{a}{m\pi} Y'_m \qquad Y_m = \sin(\frac{m\pi y}{a_s}) \tag{2.40a}$$

The expressions can be put in the general form $[N]$ such that:

$$\begin{Bmatrix} u \\ v \end{Bmatrix} = [N] \begin{Bmatrix} u_1 \\ v_1 \\ u_2 \\ v_2 \end{Bmatrix} = [N]\{d\} \tag{2.40b}$$

With the shape functions in that form, the strain-displacement matrix $[B]$ can be write in terms of derivatives of $[N]$:

$$\begin{Bmatrix} \varepsilon_x \\ \varepsilon_y \\ \gamma_{xy} \end{Bmatrix} = \begin{Bmatrix} \partial u / \partial x \\ \partial v / \partial y \\ \partial u / \partial y + \partial v / \partial x \end{Bmatrix} = [B]\{d\} = [N']\{d\} \tag{2.41}$$

Using these definitions, and performing the necessary substitutions into the expression for the stiffness matrix presented before, the explicit plane stress matrix for an element, or strip is given in Appendix 1.

- **Bending initial stiffness matrix** $[K_{w\theta}]$

The shape functions for use in determining the bending stiffness matrix are:

$$w = Y_m \left[ (1 - \frac{3x^2}{b_s^2} + \frac{2x^3}{b_s^3}) \quad x(1 - \frac{2x}{b_s} + \frac{x^2}{b_s^2}) \quad (\frac{3x^2}{b_s^2} - \frac{2x^3}{b_s^3}) \quad x(\frac{x^2}{b_s^2} - \frac{x}{b_s}) \right] \begin{Bmatrix} w_1 \\ \theta_1 \\ w_2 \\ \theta_2 \end{Bmatrix} \tag{2.42}$$

With the shape functions in this form, the strain-displacement matrix $[B]$ can be written in terms of derivatives of $[N]$:

$$\{\varepsilon\} = \begin{Bmatrix} -\partial^2 w / \partial x^2 \\ -\partial^2 w / \partial y^2 \\ \partial^2 w / \partial x \partial y \end{Bmatrix} = [B]\{d\} = [N']\{d\} \tag{2.42}$$

The explicit bending stiffness matrix for an element or strip is also given in Appendix 1.

### 2.8.5.2 Geometric stiffness matrix for plates

The geometric stiffness matrix for a plate strip subjected to linearly varying edge traction can be determined by either directly considering the higher order strain terms, or equivalently by forming the potential energy due to in-plane forces. The latter is the method for use here.

Consider a strip with linear edge traction as shown in Fig.2.13. The tractions correspond to linear edge stresses $f_1$ and $f_2$ via $T_1 = f_1 t$ and $T_2 = f_2 t$.

The expression for the potential energy (U) due to the in-plane forces is

$$U = \frac{1}{2}\int_0^{a_s}\int_0^{b_s}[T_1 - (T_1 - T_2)\frac{x}{b_s}]\left(\left[\frac{\partial u}{\partial y}\ \frac{\partial v}{\partial y}\ \frac{\partial w}{\partial y}\right]\left\{\frac{\partial u}{\partial y}\ \frac{\partial v}{\partial y}\ \frac{\partial w}{\partial y}\right\}^T\right)dxdy \tag{2.44}$$

The derivatives in the expression for U, may be expressed in terms of the nodal degrees of freedom $\{d\}$. The matrix resulting from differentiating the shape functions in this case is called $[G]$, for which we have

$$\{\frac{\partial u}{\partial y}\ \frac{\partial v}{\partial y}\ \frac{\partial w}{\partial y}\}^T = [G]\{d\} \tag{2.45}$$

The potential energy may now be expressed in terms of $\{d\}$ and a matrix known as the geometric stiffness $[K_g]$,

$$U = \frac{1}{2}\{d\}^T[K_g]\{d\},\quad [K_g] = \int_0^{a_s}\int_0^{b_s}(T_1 - (T_1 - T_2)\frac{x}{b_s})[G]^T[G]dxdy \tag{2.46}$$

And its explicit form is given in Appendix 1.

### 2.8.5.3 Finite strip solution methods

In the previous two sections explicit matrices are given for the initial stiffness and geometric stiffness of a discrete finite strip. For a member composed of multiple strips the contribution of each strip must be formed into the global initial stiffness and geometric stiffness. Thus:

$$[K] = \sum_{n=1}^{\#strips} [k]_n \quad \text{and} \quad [K_g] = \sum_{n=1}^{\#strips} [k_g]_n \tag{2.47}$$

The summation implies proper coordinate transformations and correct addition of the stiffness terms in the global coordinates according to the degrees of freedom. The elastic buckling problem is a standard eigenvalue problem of the following form:

$$[K]\{d\} = \lambda[K_g]\{d\} \tag{2.48}$$

Where the eigenvalue $\lambda$, are the buckling load factor, and the eigenvectors are the buckling modes. Solution of such an eigenvalue problem may readily be solved in such programs as MATLAB.

Both $[K]$ and $[K_g]$ are a function of the length. Therefore, the elastic buckling stress and the corresponding buckling modes are also a function of the length. The problem can be solved for several lengths and thus a complete picture of the elastic buckling stress and modes can be determined. The minima of such of curve could be considered as the critical buckling loads and modes for the member.

#### 2.8.5.4 The limitation of the finite strip method

It should be mentioned here that, in the finite strip method the stress distribution is assumed as constant along the half wavelength, while in the practical case the longitudinal stress varies along the span. However, it is conceivable that for a beam subjected to a varying stress distribution along its span the local and distortional buckling will occur only at a worst place. Obviously, the finite strip method proposed here is not suitable for analyzing global buckling of the structures with a varying stress distribution along its span.

However, local buckling can be carried out by the finite strip method if the pre-buckling stress distribution on the cross-section at the worst place is known, since it has a relatively short half wavelength.

### 2.8.6 Generalised Beam Theory

*Generalised Beam Theory is applicable to local, distortional and global buckling as well as their interaction.*

The essential concept of GBT is the separation of the behaviour of a prismatic member into a series of orthogonal displacement modes (Davies et al., 1994a; Davies & Leach, 1994; Davies et al., 1994b; Davies, 2000). It is a particular strength of GBT that these modes may be considered separately or in any combination in order to investigate different aspects of the structural response. In GBT, each mode has an equation and, in the second-order format, neglecting the shear deformation terms, the equation for mode "$k$" is:

$$E\,{}^{k}C\,{}^{k}V'''' - G\,{}^{k}D\,{}^{k}V'' + {}^{k}B\,{}^{k}V + \sum_{i=1}^{n}\sum_{j=1}^{n} {}^{ijk}\kappa({}^{i}W\,{}^{j}V) = {}^{k}q \quad \text{for } k = 1,2,...n \tag{2.49}$$

where the left superscript $k$ denotes the mode;

$^{k}C$ is the generalised warping constant;

$^{k}D$ is the generalised torsional constant;

$^{k}B$ is the transverse bending stiffness.

These are the generalised section properties which depend only on the cross-section geometry. In addition:

$^{ijk}\kappa$ = second-order section properties which relate the cross-section deformations to the stress distributions;

$E$ and $G$ = the modulus of elasticity and the shear modulus respectively;

$^{k}V$ and $^{k}W$ = the generalised deformation resultant and stress resultant;

$^{k}q$ = the uniformly distributed load;

$n$ = the number of modes in the analysis.

For simple cross-sections, the section properties and the $^{ijk}\kappa$ values may be calculated manually but this is cumbersome.

If the right hand side term ${}^{k}q$ of Eq.(2.49) is zero, the solution gives the critical stress resultant ${}^{i}W$. In general, this requires the solution of an eigenvalue problem in which the analyst is free to choose which modes to include in the analysis. Various mode interactions can be studied in this way for prismatic members of varying lengths.

When a constant stress resultant, such as an axial load or a constant bending moment, is applied along a member which is assumed to buckle in a half sine wave of wavelength $\lambda_l$, GBT allows some particularly simple results to be obtained. Thus the critical stress resultant for single mode buckling is (Davies et al., 1994):

$$ {}^{i,k}W_{cr} = \frac{1}{{}^{ikk}\kappa}\left(\frac{\pi^2}{\lambda_l^2} E\,{}^{k}C + G\,{}^{k}D + \frac{\lambda_l^2}{\pi^2}\,{}^{k}B\right) \tag{2.50} $$

As the wavelength is varied, the minimum critical stress resultant is

$$ {}^{i,k}W_{cr} = \frac{1}{{}^{ikk}\kappa}\left(2\sqrt{E\,{}^{k}CB} + G\,{}^{k}D\right) \tag{2.51} $$

and the corresponding half wavelength is

$$ {}^{k}\lambda_l = \pi\left(\frac{E\,{}^{k}C}{{}^{k}B}\right)^{0.25} \tag{2.52} $$

Eqs. (2.49), (2.50) and (2.51) allow a particularly simple examination to be made of any individual buckling mode, including the distortional modes. No other method known to the author allows the distortional modes to be isolated in this way. In particular, it can be seen that critical stress resultant for either local or distortional buckling in mode $k$ is dependant only on readily calculable section properties. The second-order coupling term ${}^{ikk}\kappa$ is dependant on the load mode $i$ but the buckling half wavelength depends only on the cross-section properties ${}^{k}C$ and ${}^{k}B$ which are independent of the type of load (e.g. axial or bending). The design expressions based on simplified models, which will be discussed later, have the same pattern.

There are three different applications of second-order GBT which may be used to investigate buckling phenomena in cold-formed sections. These are: (1) the above

explicit expressions for single-mode buckling; (2) simple mode interaction based on the half sine wave assumption which gives rise to elementary eigenvalue problems; and (3) the general case, without any assumed displacement function, which gives rise to larger eigenvalue problems based on a finite difference solution of the coupled differential equations. However, at the present time, GBT is not readily available to the structural designer.

### 2.8.7 Direct Strength Method

*The direct strength method is suitable for the determination of the design strength based on the known elastic buckling load for those cases where no shift of the effective centroid occurs.*

The direct strength method makes a more formal allowance for post-buckling and is evidently more appropriate when local buckling is significant. The "direct strength method" recognises that the available models for local and distortional buckling design are far from simple and have significant limitations. It also recognises that the current trend is to increase the complexity of section shapes and also increases the complexity of the required mathematical models. It therefore proposes a formal design procedure based on elastic bucking solutions for the complete cross-section. The particular characteristic of this procedure is that for economic design, it is necessary to take advantage of the post-buckling strength.

However, the Direct Strength Method is limited to cases where no shift of the effective centroid occurs (Rusch & Lindner, 2001).

## 2.9 SUMMARY

This chapter contains three aspects. First, it summarises the characteristics of cold-formed structures and the developments in cold-formed structural technology and applications. Cold-formed steel structures are structural products that are made by bending flat sheets of steel at ambient temperature into shapes which will support more than the flat sheets themselves. They have been produced for more than a

century since the first flat sheets of steel were produced by the steel mills. However, in recent years, higher strength materials and a wider range of structural applications have caused a significant growth in cold-formed steel relative to the traditional heavier hot-rolled steel structural members.

Secondly, the structural behaviour of cold-formed structures is reviewed, which includes local, distortional and global buckling modes. The available approaches based on the previous research are summarised. Development in technology and applications make demands on a more sophisticated treatment of local, distortional and global buckling and the interactions between them.

Finally, the main tools for research and development into the buckling phenomena are described by means of their availability and uncertainty.

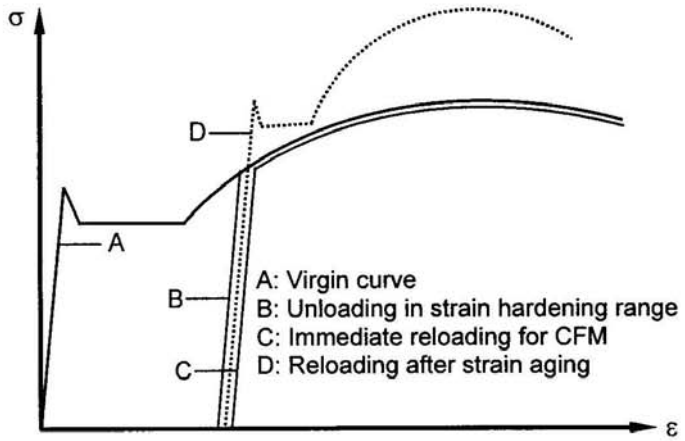


**Fig.2.1 Effects of cold straining and strain aging on σ–ε characteristics of carbon steel.**

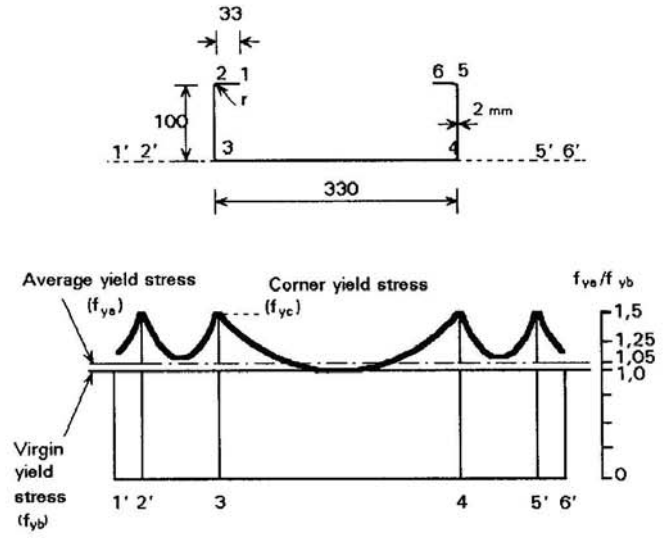


**Fig.2.2 Example of cold forming effects on the yield stress.**

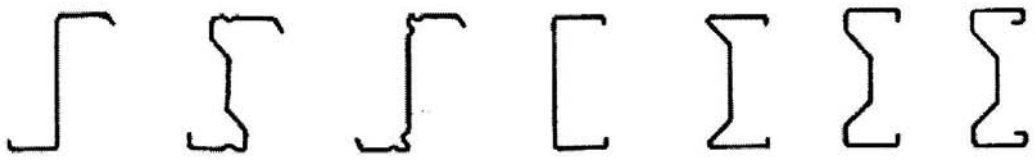


**Fig.2.3 Evolution of cold-formed purlin sections.**

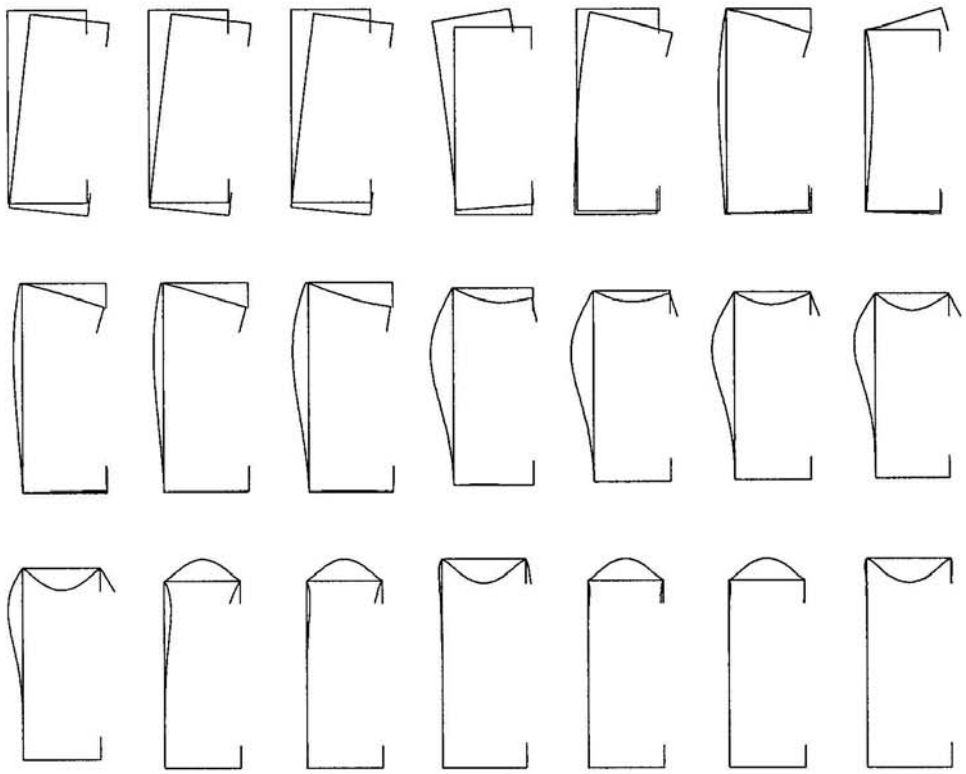

**Fig.2.4 Buckling modes of channel section purlin.**

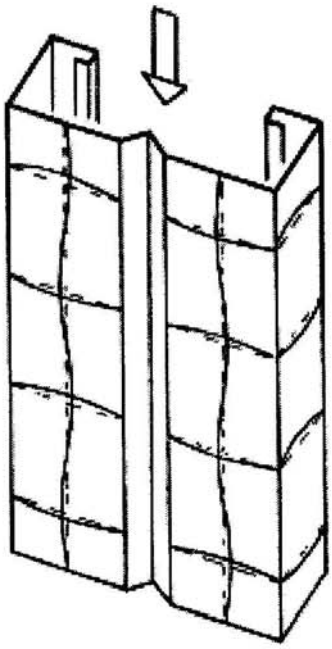

**Fig.2.5 Local buckling in a cassette section column (Davies, 2000).**

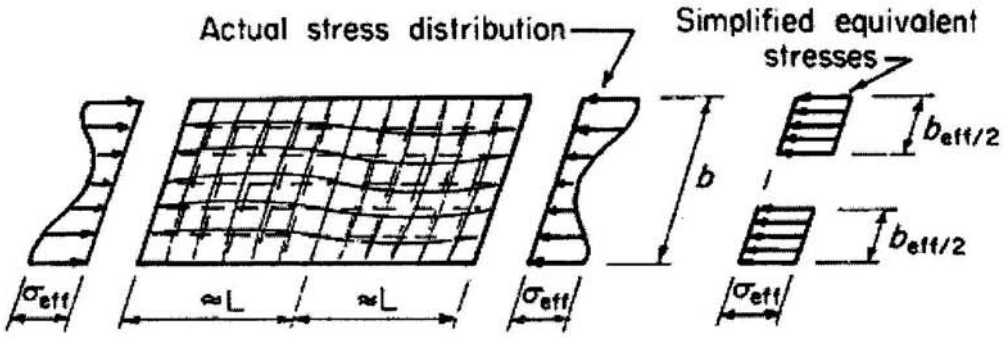


**Fig.2.6 Effective width of plane element stiffened along both edges.**

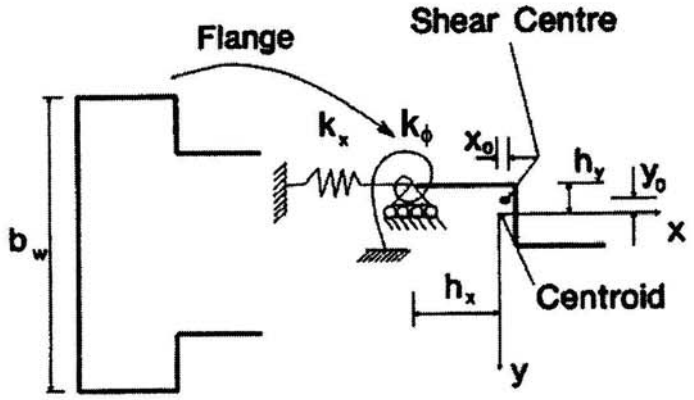


**Fig.2.7 Analytical model for distortional column buckling.**

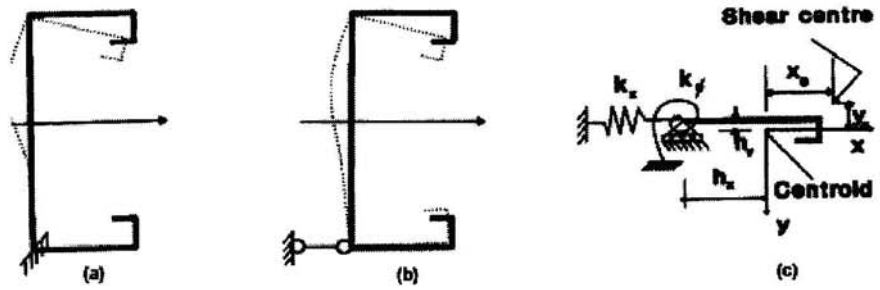


**Fig.2.8 Distortional buckling models. (a) Hancock's model; (b) Davies's model; (c) Analytical model.**

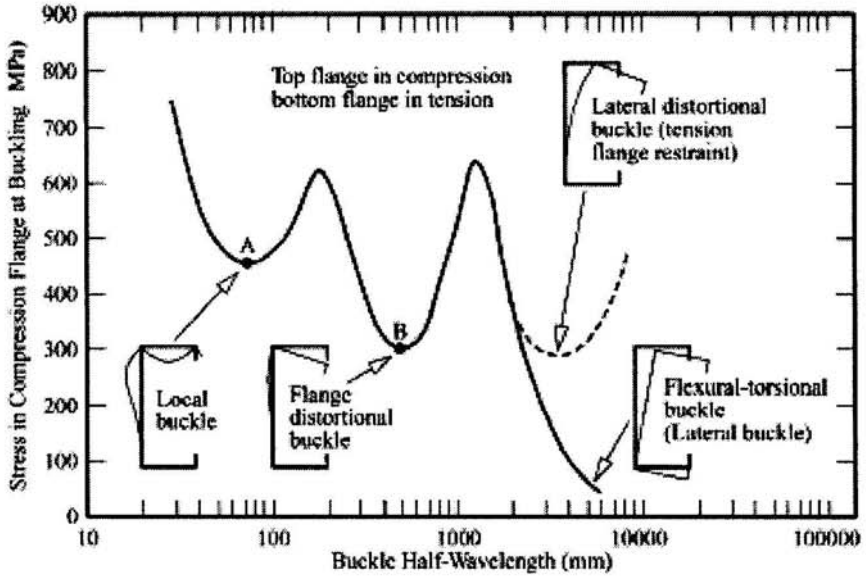


**Fig.2.9 Buckling modes of lipped channel in bending.**

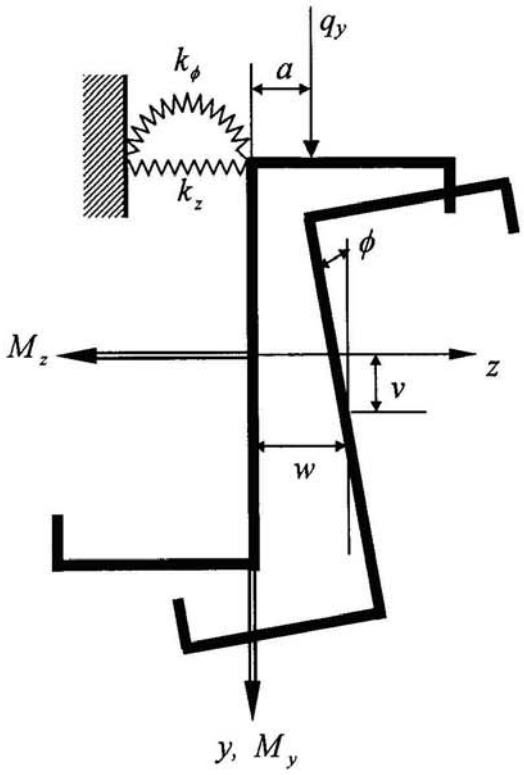


**Fig.2.10 An analytical model for lateral-torsional buckling analysis.**

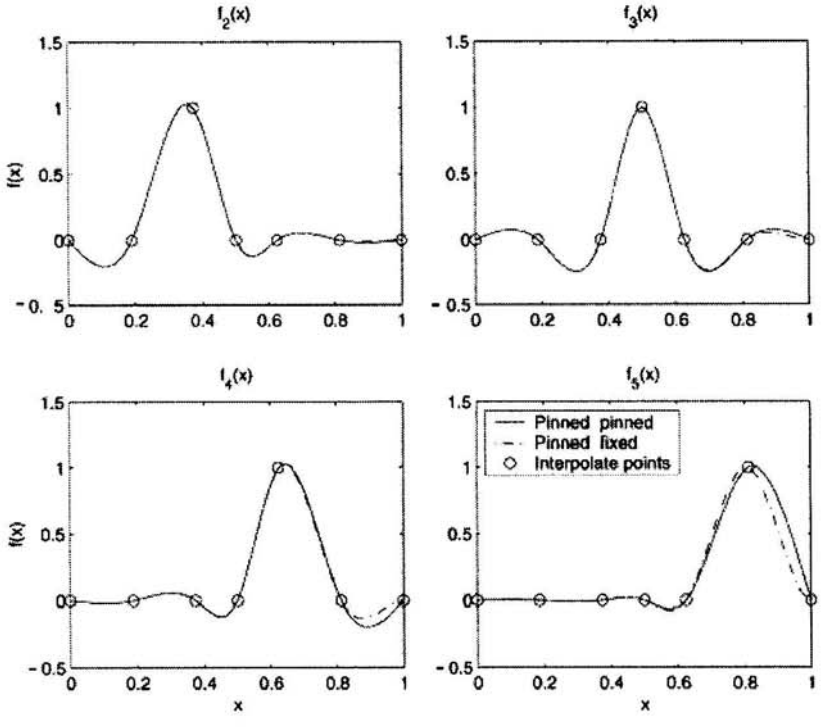


**Fig.2.11 Profiles of spline interpolations(n=5).**

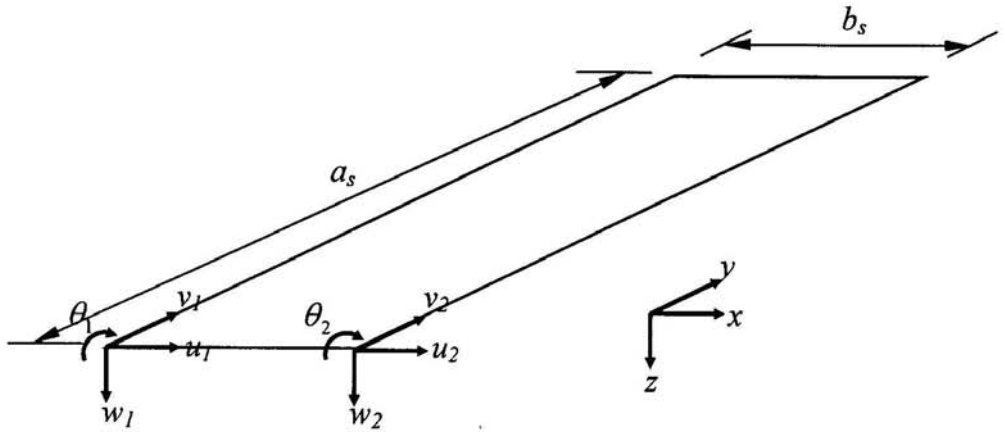


**Fig.2.12 Displacement field for typical simply supported finite strip.**

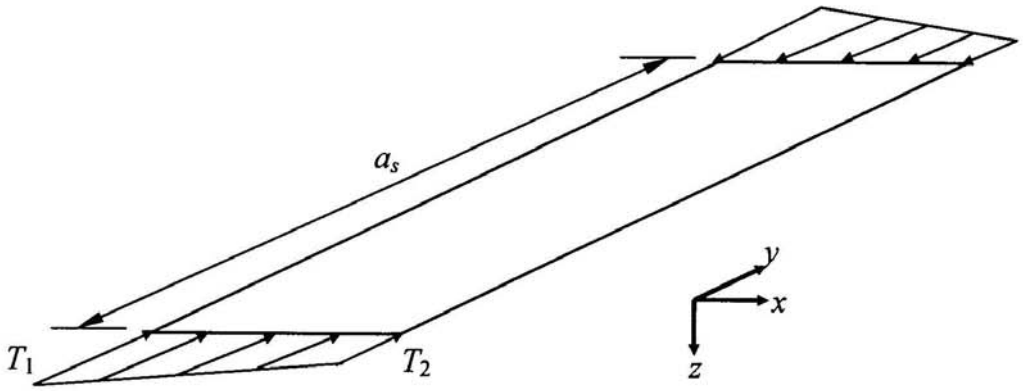


**Fig.2.13 Strip with edge traction.**

# Chapter 3

# 3 STRESS ANALYSIS OF PURLIN-SHEETING SYSTEMS

## 3.0 CHAPTER SYNOPSIS

This chapter describes the stress analysis of cold-formed zed and channel section beams. An analytical model for the stress analysis of cold-formed zed and channel section beams, subjected to a uniformly distributed transverse load, is proposed, in which the restraints from the sheeting to the purlin is taken into account by using translational and rotational springs. The influence of spring stiffnesses on the maximum tensile and compressive stresses is discussed. The effects of boundary conditions, interval restraints provided by anti-sag bars and the position of the loading point on the pre-buckling stress are also examined.

The results obtained from this study not only highlight the influence of the sheeting restraints on the results of stresses but also can be used as an input for carrying out the linear elastic buckling analysis of the sections.

## 3.1 INTRODUCTION

As most cold-formed sections are restrained by cladding or metal sheeting, the loads acting on the sections not only cause the bending of the member about its two principal axes but also torsion of the cross-section. Chapter 2 introduced an analytical model proposed by Li (2004) which uses energy methods for predicting the lateral-torsional buckling of cold-formed zed-purlins partially restrained by the sheeting. The model considers the bending and torsion of the member for pre-buckling analysis but in the buckling analyses the warping stress is ignored.

It is well known that, when a thin-walled beam has one or more cross-sections that are constrained against warping, a complex distribution of longitudinal warping stresses can be developed. These warping stresses together with the longitudinal stresses generated by bending moments may cause the beam to have local, distortional, or lateral-torsional buckling.

In this chapter, a further development of Li's model (2004) to carry out the stress analysis of cold-formed zed and channel section beams is proposed. The importance of the stress analysis is obvious as it provides the base for both strength and buckling analyses. The focus of this study is on the influence of the sheeting stiffness on the stress distribution in the cross-section of the member when it is subjected to a uniformly distributed transverse load. This problem has not been addressed in most current design codes (Leach & Robinson, 1993; BS 5950, 1998). In the British Codes of Practice (1998) the stress of a cold-formed member is calculated based on the bending in its web plane using the bending formula of symmetric beams. The compressive stresses calculated are then used to check if they would cause the compressed flanges to buckle locally. This design procedure is theoretically correct only if the member is fully restrained in both the translational and rotational directions. If it is not so, the member will be bent asymmetrically and therefore the stress should be calculated based on the bending of asymmetric beams. In addition to the asymmetric bending, torsion also needs to be considered due to the loads that are not applied at the shear centre. The twist creates not only shear stress but also warping

stress. This is a problem which has been recognized since 1970s (Kitipornchai & Trahair, 1980; Williams & Jemah, 1987; Walker, 1995; Trahair & Bradford, 1998; Bradford, 2000; Ye et al., 2004) but has not been considered in practice until the recent publication of EC 3 (1996).

## 3.2 ANALYTICAL MODEL

Consider the zed or channel section beam that is partially restrained by the sheeting on its upper flange. The restraint of the sheeting can be simplified by one translational spring and one rotational spring, as shown in Fig.3.1, and the coordinate of the position where the springs are applied is ($y_k$, $z_k$). Let the origin of the coordinate system ($x$, $y$, $z$) be the centroid of the cross-section, with $x$ axis being along the longitudinal direction of the beam, and $y$ and $z$ axes taken in the plane of the cross-section.

The relationship between moments and generalized strains can be expressed as (Vlasov, 1961; Oden, 1967):

$$\begin{Bmatrix} M_y \\ M_z \\ M_\omega \\ M_T \end{Bmatrix} = \begin{bmatrix} EI_y & EI_{yz} & 0 & 0 \\ EI_{yz} & EI_z & EI_{\omega z} & 0 \\ 0 & EI_{\omega z} & EI_\omega & 0 \\ 0 & 0 & 0 & GJ \end{bmatrix} \begin{Bmatrix} -\dfrac{d^2w}{dx^2} \\ -\dfrac{d^2v}{dx^2} \\ \dfrac{d^2\phi}{dx^2} \\ \dfrac{d\phi}{dx} \end{Bmatrix} \tag{3.1}$$

which can be written in the matrix form:

$$\{M\} = [R]\{\kappa\} \tag{3.2}$$

where $M_y$ and $M_z$ = the bending moments about $y$ and $z$ axes;

$M_\omega$ is the warping moment;

$M_T$ is the twisting moment;

$v$ and $w$ denote the $y$ and $z$ components of displacement of the centroid of the cross section;

$\phi$ is the angle of twist;

$E$ is the Young's modulus;

$G$ is the shear modulus;

$J$ is the torsion constant;

$I_y$ and $I_z$ are the second moments of the cross-section with respect to $y$ and $z$ axes, respectively;

$I_{yz}$ is the product moment of the cross-section area;

$I_{\omega z}$ is the sectorial product of inertia with respect to $z$ axis;

$I_\omega$ is the warping constant.

Note that the angle of twist and the two displacements in the present system are defined at the centroid of the cross section and therefore $I_{\omega z}$ and $I_\omega$ are also calculated based on the sectional coordinate with respect to centroid coordinate system (for channel sections the shear centre is not at the centroid). The detailed expressions for the sectional properties of zed and channel sections are predicted in Appendix 2.

The strain energy of the beam due to deflections and rotation can be expressed as:

$$U_{o\_beam} = \frac{1}{2}\int_0^l \{\kappa\}^T \{M\} dx = \frac{1}{2}\int_0^l \{\kappa\}^T [R]\{\kappa\} dx$$

$$= \frac{E}{2}\int_o^l [I_y(\frac{d^2w}{dx^2})^2 + 2I_{yz}\frac{d^2w}{dx^2}\frac{d^2v}{dx^2} + I_z(\frac{d^2v}{dx^2})^2]dx \qquad (3.3)$$

$$+ \int_o^l [\frac{GJ}{2}(\frac{d\phi}{dx})^2 + \frac{EI_\omega}{2}(\frac{d^2\phi}{dx^2})^2 - EI_{\omega z}\frac{d^2v}{dx^2}\frac{d^2\phi}{dx^2}]dx$$

where $l$ = the span length of the beam.

The strain energy stored in the two springs due to the deformation of the beam can be expressed by

$$U_{o\_spring} = \frac{k_z}{2}\int_o^l (w + y_k\phi)^2 dx + \frac{k_\phi}{2}\int_o^l \phi^2 dx \qquad (3.4)$$

where $k_z$ and $k_\phi$ = the per-unit length stiffness constants of the translational and rotational springs.

For a purlin that is subjected only to a uniformly distributed transverse load at the point ($y_q$, $z_q$), the potential energy caused by the load can be expressed by

$$W_o = \int_o^l q[\sin\alpha(v - z_q\phi) + \cos\alpha(w + y_q\phi)]dx \tag{3.5}$$

where $q$ = the density of uniformly distributed load;

$\alpha$ = the angle between $z$ axis and loading line seen in Fig.3.1.

The deflections, $v(x)$ and $w(x)$, and the angle of twist, $\phi(x)$ due to the externally applied loads can be determined by employing the stationary principle as follows:

$$\delta(U_o - W_o) = \delta(U_{o\_beam} + U_{o\_spring} - W_o) = 0 \tag{3.6}$$

After the deflections and rotation are determined the pre-buckling moment distributions along the longitudinal axis can be calculated using Eq. (3.1). Then the pre-buckling longitudinal stresses can be calculated as follows:

$$\sigma_x(x, y, z) = \sigma_{xb} + \sigma_{xw} \tag{3.7}$$

where $\sigma_{xb}$ and $\sigma_{xw}$ = the longitudinal stresses generated by the bending and twisting moments, respectively, which are expressed by

$$\sigma_{xb} = \sigma_{xbz} + \sigma_{xby} = M_z \frac{I_y y - I_{yz} z}{I_y I_z - I_{yz}^2} + M_y \frac{I_z z - I_{yz} y}{I_y I_z - I_{yz}^2} \tag{3.8}$$

$$\sigma_{xw} = E(\overline{\omega} - \omega - y\frac{I_{\omega z}}{I_z})\frac{d^2\phi}{dx^2} = E(\overline{\omega}_s - \omega_s)\frac{d^2\phi}{dx^2} \tag{3.9}$$

where $M_y$ and $M_z$ = the bending moments calculated from Eq.(3.1);

$\omega$ and $\overline{\omega}$ = the sectorial coordinate and corresponding average value with respect to the centroid;

$\omega_s$ and $\overline{\omega}_s$ are the sectorial coordinate and corresponding average value with respect to the shear centre;

The sectorial coordinates are properties of the cross-sections and are calculated as follows (Timoshenko & Gere, 1961; Oden, 1967):

$$\omega(s) = \int_0^s h\,ds \qquad \overline{\omega} = \frac{1}{k}\int_0^k \omega\,ds$$
$$\omega_s(s) = \int_0^s h_s\,ds \qquad \overline{\omega}_s = \frac{1}{k}\int_0^k \omega_s\,ds \tag{3.10}$$

where $h$ and $h_s$ = the perpendicular distances from a tangent at the point under consideration to the centroid and shear centre, respectively;

$s$ = the distance from any chosen origin to the same point measured along the middle line of the section;

$k$ = the total length of the middle lines of the cross-section.

The details of calculations of Eq.(3.10) are given in Appendix 2.

Eq. (3.6) is solved using a numerical method in which cubic spline interpolations are used to construct the deflection distribution with a number of nodal displacements as the unknowns. The assumed deflection functions are required to pre-satisfy all the required displacement boundary conditions. In this way, the variational Eq.(3.6) are reduced to the matrix forms of a set of linear algebraic equations. The numerical treatment is similar to the one introduced in Section 2.5.2.2, except that here cubic spline interpolations is also needed to construct the angle of twist $\phi$,

$$\phi(x) = \sum_{i=1}^{n} \phi_i f_i(x, x_i) \tag{3.11}$$

where $\phi_i$ = the to-be-determined angle of twist at interpolation points $x_i$;

$f_i(x,x_i)$ = defined in Section 2.5.2.2.

By using this way, Eqs.(3.6) reduce to the following algebra equation,

$$\begin{bmatrix} A_{11} & A_{12} & A_{13} \\ A_{12} & A_{22} & A_{23} \\ A_{13} & A_{23} & A_{33} \end{bmatrix} \begin{bmatrix} \{v\} \\ \{w\} \\ \{\phi\} \end{bmatrix} = \begin{bmatrix} f_1 \\ f_2 \\ f_3 \end{bmatrix} \tag{3.12}$$

where $A_{ij}$ = the coefficients obtained from the calculation of the strain energy;

$f_{yi}$ and $f_{zi}$ = the coefficients obtained from the calculation of the work done by the externally applied loads.

Equation (3.12) is the pre-buckling equilibrium equation and the corresponding solutions $\{v_i\}$, $\{w_i\}$ and $\{\phi_i\}$ represent the deflections of the purlin centroid at $x=x_i$.

## 3.3 NUMERICAL EXAMPLES

Table 3.1 gives the details of the analyzed zed and channel sections, such as section dimensions, material properties, definition of boundary conditions and loading details.

For a given problem, one can use numerical methods to solve the variational Eq.(3.6) to determine the pre-buckling displacements $v(x)$, $w(x)$ and $\phi(x)$ and thus the pre-buckling bending moment distributions $M_y$ and $M_z$ and corresponding longitudinal stresses $\sigma_{xb}$ and $\sigma_{xw}$ from Eq.(3.8) and (3.9).

The symbols like 'Zd200_b60_c20_t20' represents the cross-section with a section depth of 200mm, a flange width of 60mm and a lip depth of 20mm and the thickness of the plate is 2.0mm. The members considered here have a length of 8m.

### 3.3.1 Influence Of The Rotational And Translational Springs

The influence of the translational and rotational spring stiffness is studied for the zed and channel section beams with or without anti-sag bars when subjected to a uniformly distributed downward load at the middle of the top flange.

#### 3.3.1.1 Zed section beams (Zd202_b75_c20_t20)

Figs.3.2a and b show the influence of the translational spring stiffness on the maximum tensile stress and the maximum compressive stress for the simply-supported zed purlin without anti-sag bars subjected to the uniformly distributed downward load. Fig.3.2a is for a zero rotational spring stiffness ($k_\phi$=0) and Fig.3.2b is for an infinite rotational spring stiffness ($k_\phi$=$\infty$). It can be seen from the figures that

the influence of the translational spring stiffness on the maximum tensile and compressive stresses only occurs in the range $10^{-10}<k_z/E<10^{-7}$ where both maximum stresses decrease with the increase of the translational spring stiffness. For the case of $k_\phi=0$, the maximum compressive stress is found to be higher than the maximum tensile stress, particularly when $k_z/E$ is very small. This is due to the contribution of the warping stress to the compressive stress. If the warping stress is ignored, the maximum tensile stress was found to always be equal to the maximum compressive stress. This is due to the central symmetry of the cross-section. As is to be expected, for the case of $k_\phi=\infty$, the warping stress is zero because the beam is fully restrained in the rotational degree and so all four curves in Fig.3.2b are coincident. Comparison of the results in Fig.3.2a and Fig.3.2b shows that the influence of the translational spring stiffness is much greater than that of the rotational stiffness.

Figs.3.2c and d show the influence of the rotational spring stiffness on the maximum tensile stress and the maximum compressive stress for the simply-supported zed purlin without anti-sag bars subjected to the uniformly distributed load. Fig.3.2c is for a zero translational spring stiffness ($k_z=0$) and Fig.3.2d is for an infinite translational spring stiffness ($k_z=\infty$). Again, it is shown that the rotational spring stiffness has little influence on both maximum stresses, particularly when the translational spring stiffness is very large.

Fig.3.3 shows the influence of the translational and rotational spring stiffness on the maximum tensile stress and the maximum compressive stress for the simply-supported zed purlin with one anti-sag bar. Again, it can be seen from the figures that the influence of the translational spring stiffness on the maximum tensile and compressive stresses only occurs in the range $10^{-8}<k_z/E<10^{-5}$ where both maximum stresses decrease with the increase of the translational spring stiffness, while the rotational spring stiffness has little influence on both maximum stresses, particularly when the translational spring stiffness is very large.

The comparisons of Fig.3.2 and Fig.3.3 show that the range where the influence of spring stiffness occurs for the beams with one anti-sag bar has larger spring stiffness than that for the beams without anti-sag bars, and the maximum compressive stress

for the beams with one anti-sag bar is smaller than those for the beams without anti-sag bars, particularly when the translational spring stiffness is very small. It can also be seen from Fig.3.2-3.3 a and c that when there is one anti-sag bar, the maximum tensile stress is much smaller than the maximum compressive stress particularly when $k_z$ and $k_\phi$ are small.

### 3.3.1.2 Channel section beams (Cd202_b75_c20_t20)

Fig.3.4 shows the influence of the translational and rotational spring stiffness on the maximum tensile stress and the maximum compressive stress for the simply-supported channel section beam without anti-sag bars.

From Fig.3.4a, it can be seen that the influence of the translational spring stiffness on the maximum tensile and compressive stresses only occurs in the range $10^{-10} < k_z/E < 10^{-7}$ where both maximum stresses decrease with the increase of the translational spring stiffness and the maximum compressive stress is found to be slightly lower than the maximum tensile stress when $k_z$ is large. This, again, is due to the contribution of the warping stress. If the warping stress is ignored, the maximum compressive stress was found to be higher than the maximum tensile stress, which is because that channel section is axial symmetry instead of central symmetry as for zed section. For the case of $k_\phi = \infty$, the warping stress is zero because the beam is fully restrained in the rotational degree and the translational spring stiffness has no influence on the maximum stresses, so all four curves in Fig.3.4b are coincident.

It can be seen from Fig.3.4c and d that the influence of the rotational spring stiffness on the maximum tensile and compressive stresses only occurs in the range $10^{-9} < k_\phi/(Ey_k^2) < 10^{-6}$ where both maximum stresses decrease with the increase of the rotational spring stiffness. It appears that the warping stress has significant contribution on the influence of the rotational spring stiffness for $k_z$=0. If the warping stress is ignored, the maximum tensile stress is always equal to the maximum compressive stress, in which case stresses are purely generated by $M_z$.

Fig.3.5 shows the influence of the translational and rotational spring stiffness on the maximum tensile and compressive stresses for the simply-supported channel section

beam with one anti-sag bar. The most features shown here are very much similar to those observed in Fig.3.4. The comparisons of results reflect the influence of anti-sag bars which is similar to those for zed section beams.

### 3.3.2 Influence Of Boundaries And Interval Restraints Produced By Anti-Sag Bars

The influence of anti-sag bars and boundary conditions on the zed and channel section beams, when subjected to the uniformly distributed downward load, is analyzed. The load here is assumed to act at the middle of the top flange. Four special cases with respect to the various restraints from the sheeting are considered: Case 1: $k_z$=0 and $k_\phi$=0; Case 2: $k_z$=0 and $k_\phi$=∞; Case 3: $k_z$=∞ and $k_\phi$=0; Case 4: $k_z$=∞ and $k_\phi$=∞. The stresses plotted within the cross-section are normalized and are defined as positive (tensile) if they are plotted above or on the right of the central line of the cross section.

#### 3.3.2.1 Zed section beams (Zd202_b75_c20_t20)

**Case 1:** $k_z$=0 and $k_\phi$=0

Fig.3.6 shows the distributions of the longitudinal bending stresses ($\sigma_{xbz}$, $\sigma_{xby}$) caused by the two bending moments ($M_y$ and $M_z$) and the longitudinal warping stress ($\sigma_{xw}$) caused by the warping torsion, both within the cross-section and along the axial direction, for zed section beams with 0, 1, and 2 anti-sag bars. Fig.3.6a is for the beam with both ends simply-supported and Fig.3.6b is for the beam with both ends fixed.

It can be seen from Fig.3.6a that the dominant stress is the bending stress $\sigma_{xbz}$ particularly when there is no anti-sag bar, which is generated by the bending moment about z axis. Although the loading line is not along any of the principal axes of the zed section, the bending moment about y axis generated by external load is very small when the anti-sag bar is absent. However, the bending stress $\sigma_{xby}$ becomes comparable with $\sigma_{xbz}$ when anti-sag bar is present which is due to the interference of the anti-sag bar on the existing bending moment about the y axis created by the external load. It is also apparent from the figure that the anti-sag bars have no influence on the

distribution and the magnitude of the bending stress $\sigma_{xbz}$ and $\sigma_{xw}$ although they do affect the distribution of $\sigma_{xby}$.

The similar distributions for the longitudinal stresses for zed section beams with both ends fixed are shown in Fig.3.6b. It is noticed that, for $\sigma_{xbz}$ the largest stress is always found at the fixed ends, while for $\sigma_{xby}$ this is interfered by the presence of anti-sag bars. Anti-sag bar has some influence on the magnitude but not much on the distribution of $\sigma_{xby}$ and it has no influence on both magnitude and distribution of $\sigma_{xbz}$ and $\sigma_{xw}$.

The comparisons of Fig.3.6a and b reflect the influence of the boundary conditions. It is interesting to notice that the boundary condition affects both the value and distribution of stresses in the longitudinal axis direction, but not the distribution of stresses within the cross-section.

**Case 2:** $k_z$=0 and $k_\phi$=$\infty$

Fig.3.7 shows the distributions of bending stresses ($\sigma_{xbz}$, $\sigma_{xby}$) and the warping stress ($\sigma_{xw}$) for zed section beams. As is to be expected, the warping stress is zero because the beam is fully restrained in the rotational degree. It is clear that the features of $\sigma_{xbz}$ and $\sigma_{xby}$ are very similar to those in Fig.3.6. The main difference between Fig.3.7a and b reflects the influence of the change in boundary conditions.

**Case 3:** $k_z$=$\infty$ and $k_\phi$=0

Fig.3.8 shows the distributions of $\sigma_{xbz}$, $\sigma_{xby}$ and $\sigma_{xw}$ for zed section beams.

It can be seen from Fig.3.8a that the warping stress is much lower than the two bending stresses, particularly when the anti-sag bar is present for which case the warping stress is almost negligible. It is also apparent that the anti-sag bars have little influence on the distribution of bending stress $\sigma_{xby}$, which is due to the full lateral restraint from the sheeting. It is interesting that the two bending stresses are in opposite direction. The bending stress, $\sigma_{xby}$, is generated by the lateral restraint

provided by the sheeting and this implies that the lateral restraint can actually reduce the bending stress, which is coincident with the results in Fig 3.2a.

It is found from Fig.3.8b that the distribution of $\sigma_{xby}$ and $\sigma_{xw}$ dramatically changed and the warping stress is higher than the results in Fig.3.8a, particularly near the fixed ends. Again, this is due to the influence of the fixed boundary conditions.

**Case 4:** $k_z=\infty$ and $k_\phi=\infty$

Fig.3.9 shows the distributions of $\sigma_{xbz}$, $\sigma_{xby}$ and $\sigma_{xw}$ for zed section beams. Again, the warping stress is zero because the beam is fully restrained in the rotational degree. It can also be seen the bending stress $\sigma_{xby}$ is comparable to $\sigma_{xbz}$ , which is due to the yx plane not being one of the principal planes of the zed section, although the beam can only bend in *yx* plane when $k_z=\infty$ and $k_\phi=\infty$.

### 3.3.2.2 Channel section beams (Cd202_b75_c20_t20)

**Case 1:** $k_z=0$ and $k_\phi=0$

Fig.3.10 shows the distributions of $\sigma_{xbz}$, $\sigma_{xby}$ and $\sigma_{xw}$ for channel section beams, in which the bending stress $\sigma_{xbz}$ is generated by the bending moment about z-axis directly due to the external load and the bending stress $\sigma_{xby}$ is generated by the bending moment about y-axis due to the lateral restraint. As is to be expected, the bending stress $\sigma_{xby}$ is zero because the loading line is parallel to one of the principal axes of the channel section so that only a bending moment about z axis and an additional torsion are generated. It can be seen that the warping stress is comparable with the bending stress $\sigma_{xbz}$. The anti-sag bars have no influence on both the magnitude and distribution of $\sigma_{xbz}$ and $\sigma_{xw}$.

**Case 2:** $k_z=0$ and $k_\phi=\infty$

Fig.3.11 shows the distributions of $\sigma_{xbz}$, $\sigma_{xby}$ and $\sigma_{xw}$ for channel section beams. As is to be expected, the warping stress is almost negligible because the beam is fully restrained in the rotational degree. It is clear that the features of $\sigma_{xbz}$ and $\sigma_{xby}$ are very

similar to those in Fig.3.10. The main difference between Fig.3.11a and b reflects the influence of the fixed boundary conditions.

**Case 3:** $k_z=\infty$ and $k_\phi=0$

Fig.3.12 shows the distributions of $\sigma_{xbz}$, $\sigma_{xby}$ and $\sigma_{xw}$ for channel section beams. It can be seen that lateral restraint from $k_z$ and anti-sag bars makes significant contribution to the bending stress $\sigma_{xby}$.

**Case 4:** $k_z=\infty$ and $k_\phi=\infty$

Fig.3.13 shows the distributions of $\sigma_{xbz}$, $\sigma_{xby}$ and $\sigma_{xw}$ for channel section beams. It can be seen that when the channel section beams are fully restrained by the sheeting, the bending stress $\sigma_{xby}$ and warping stress $\sigma_{xw}$ are almost negligible.

### 3.3.3 Comparison Of Bending Stress And Warping Stress

Figs.3.14 and 15 show the distributions of the pre-buckling stresses in the zed (Zd202_b75_c20_t20)and channel section (Cd202_b75_c20_t20) beams, respectively, both of which are simply-supported with 0, 1 and 2 anti-sag bars when $k_z=\infty$ and $k_\phi=0$, which are further illustrations of Fig.3.8a and Fig.3.12a. The beams are subjected to the uniformly distributed downward load at the middle of the top flange. The stresses plotted are defined as negative (compressive stress) if they are plotted above or on the right of the middle line of the cross-section in order to achieve visible effect.

It is found from the figures that the warping stress is much larger in the channel section than in the zed section. This is probably due to the loading point which is assumed to be at the middle of the top flange and so cause more severe torsion in the channel section than in the zed section. For both sections, however, the warping stress is found to be significantly reduced when anti-sag bars are present. It is interesting to notice from Fig.3.15 that their presence has remarkable influence on the pre-buckling bending stress of the channel section (both the value and distribution). However, fo the zed section, the influence of the anti-sag bars is not very remarkable (see Fig.3.14). And this is consistent with the results in Section 3.3.2.

### 3.3.4 Influence Of The Position Of The Loading Points

The influence of the position of the loading point on the maximum tensile stress and maximum compressive stress for simply-supported zed and channel section beams without anti-sag bars when subjected to the uniformly distributed downward load at the top flange is analyzed.

Figs.3.16a and b respectively show the influence of the position of the loading point on the maximum tensile stress and maximum compressive stress for zed section beams. Again, as expected, for the fully rotational restrained cases ($k_\phi = \infty$) the maximum tensile stresses are equal to the maximum compressive stresses because there is no warping stress and also the maximum stresses do not vary with the position of loading point.

However, when the beam is not rotationally restrained ($k_\phi$=0), warping stresses are generated due to the torsion caused by eccentric loading and so the position of the loading point does affect the stress results. The maximum tensile stresses decrease with the increase of the distance $z_q$ between the loading point and the y axis until $z_q$ is around $0.4b$ when the stresses start to rise. However the maximum compressive stresses always increase for $k_z$=0 and $k_\phi$=0 and slightly decrease for $k_z = \infty$ and $k_\phi$=0.

Figs.3.17a and b respectively show the influence of the position of loading point on the maximum tensile and compressive stresses for channel section beams. Again, for the fully restrained rotational cases ($k_\phi = \infty$), the maximum tensile stresses are equal to the maximum compressive stresses and also the maximum stresses do not vary with the position of loading point. It is also found that when $k_\phi = \infty$, $k_z$ has no influence on the maximum stresses which is consistent with the results shown before. On the other hand, for the cases of $k_\phi$=0, the greater the distance between the loading point and y axis, the higher the maximum compressive stress.

Further inspection of Fig.3.16 and 17 shows that, for the zed section beams, the maximum compressive stress is less dependent on the rotational spring stiffness than on the translational spring stiffness. For the maximum tensile stress, however, the rotational spring stiffness may have a similar influence to the translational spring

stiffness when the loading point is remote from y axis. In contrast, for the channel section beams, the maximum stresses are more dependent on the rotational spring stiffness than on the translational spring stiffness.

## 3.4 SUMMARY

The stress analysis of cold-formed zed and channel section beams has been presented in this chapter in which the restraint actions of the sheeting are modelled by using two springs representing the translational and rotational restraints. The numerical results have shown that the two springs have significantly different influences on the stresses of the beams. The influence of the two springs has also been found to depend on presence of anti-sag bars and the position of the loading line. For the reported beam examples, the following major conclusions can be drawn:

- For most of the cases, the maximum tensile and compressive stresses decrease with increase in the translational and rotational spring stiffnesses.

- The influence of translational and rotational spring stiffness on the maximum tensile and compressive stresses occurs only in a small range of stiffness value.

- As far as the maximum tensile and compressive stresses are concerned, for zed section beams the rotational spring stiffness has less influence than translational spring stiffness, while for channel section beams the rotational spring stiffness has more influence.

- The translational and rotational spring stiffnesses have more significant influence on the bending stress $\sigma_{xby}$ and warping stress $\sigma_{xw}$ than on the bending stress $\sigma_{xbz}$, particularly for the case where no bi-moments are generated by the external load.

- When there is no rotational restraint ($k_\phi$=0), the warping stress has a significant contribution on the pre-buckling stress. However, its contribution is reduced by the presence of anti-sag bars.

- The bending stress of zed section beams is less sensitive to anti-sag bars than those of channel section beams.

- The influence of the two spring stiffnesses on the stress and its distribution is found to be influenced by the anti-sag bars. The influence range for the spring stiffness moves from a low value to a high value when the anti-sag bars are present. The maximum stresses for the beams with anti-sag bars are smaller than those for the beams without anti-sag bars, particularly when the translational and rotational spring stiffnesses are very small.

- In terms of the generated stresses it appears that the best location for fixing (that is, the loading line) is close to the centre of the flange for zed section beams and to the web line for channel section beams, which provides the lowest maximum tensile and compressive stresses.

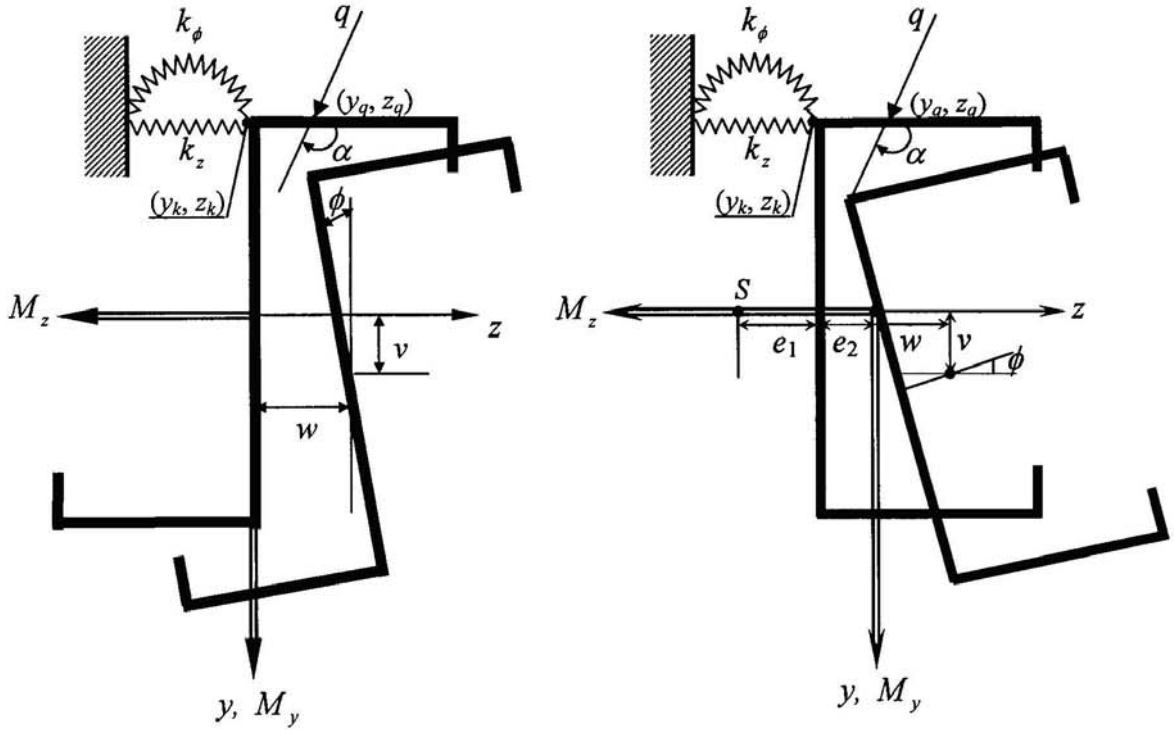


**Fig.3.1 Analytical models for stress analysis of zed and channel section beams.**

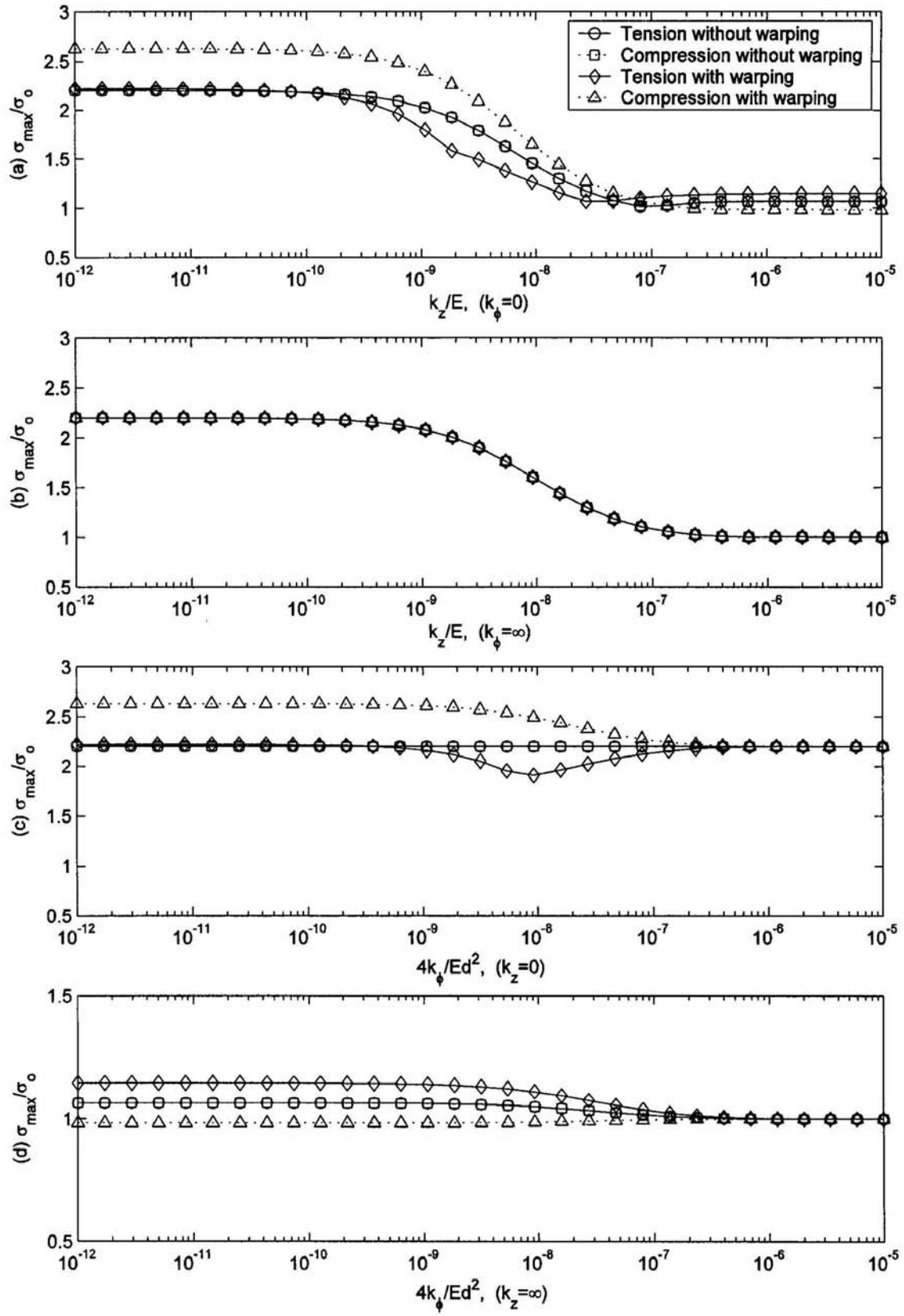


**Fig.3.2 Influence of translational and rotational spring stiffness on maximum tensile and compressive stresses of zed section beam without anti-sag bars ($y_q$=-d/2, $z_q$=b/2, $\sigma_o$ is the maximum stress when $k_z$=$k_\phi$=∞).**

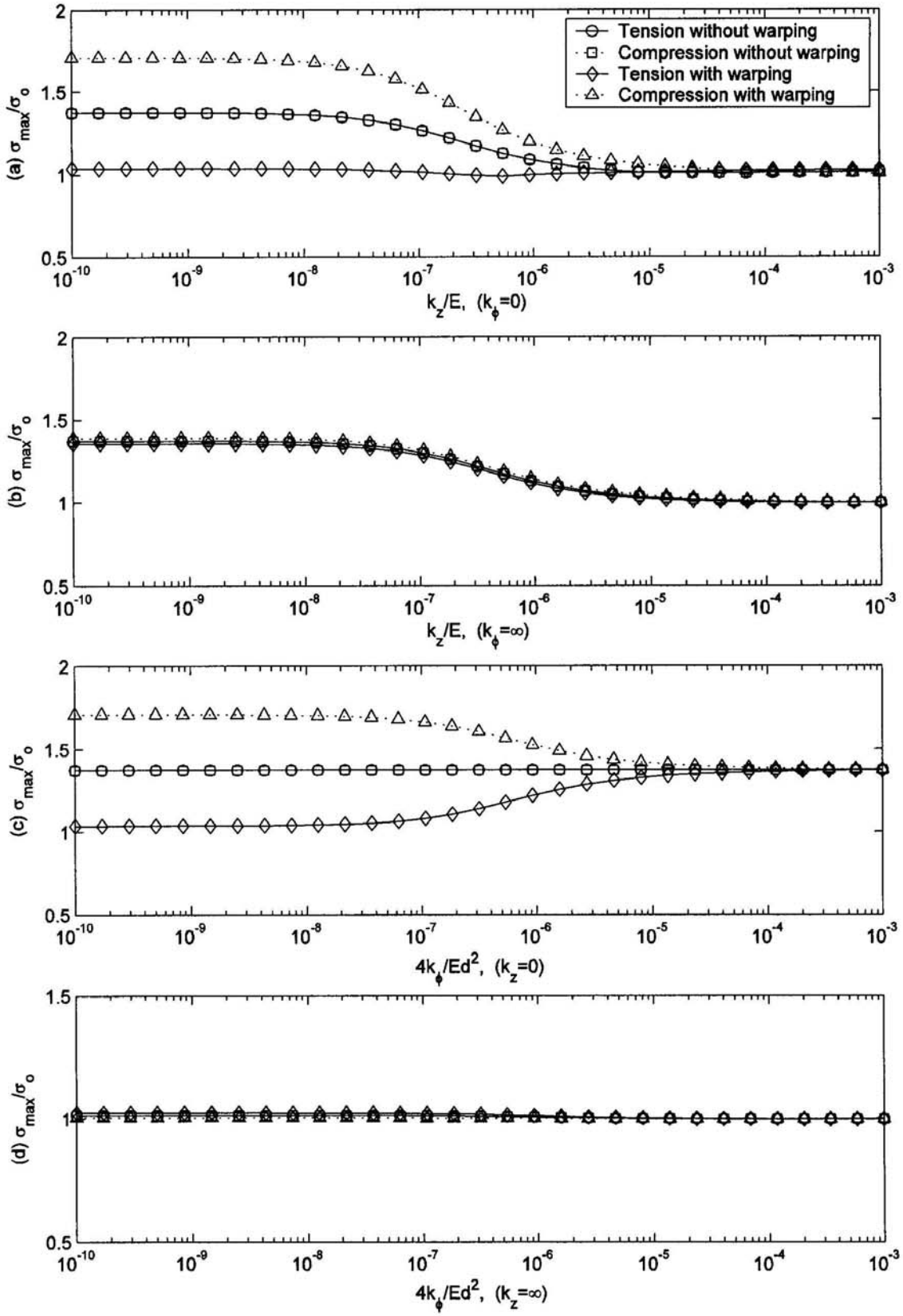


**Fig.3.3 Influence of translational and rotational spring stiffness on maximum tensile and compressive stresses of zed section beam with one anti-sag bar ($y_q$=-d/2, $z_q$=b/2, $\sigma_o$ is the maximum stress when $k_z$=$k_\phi$=∞).**

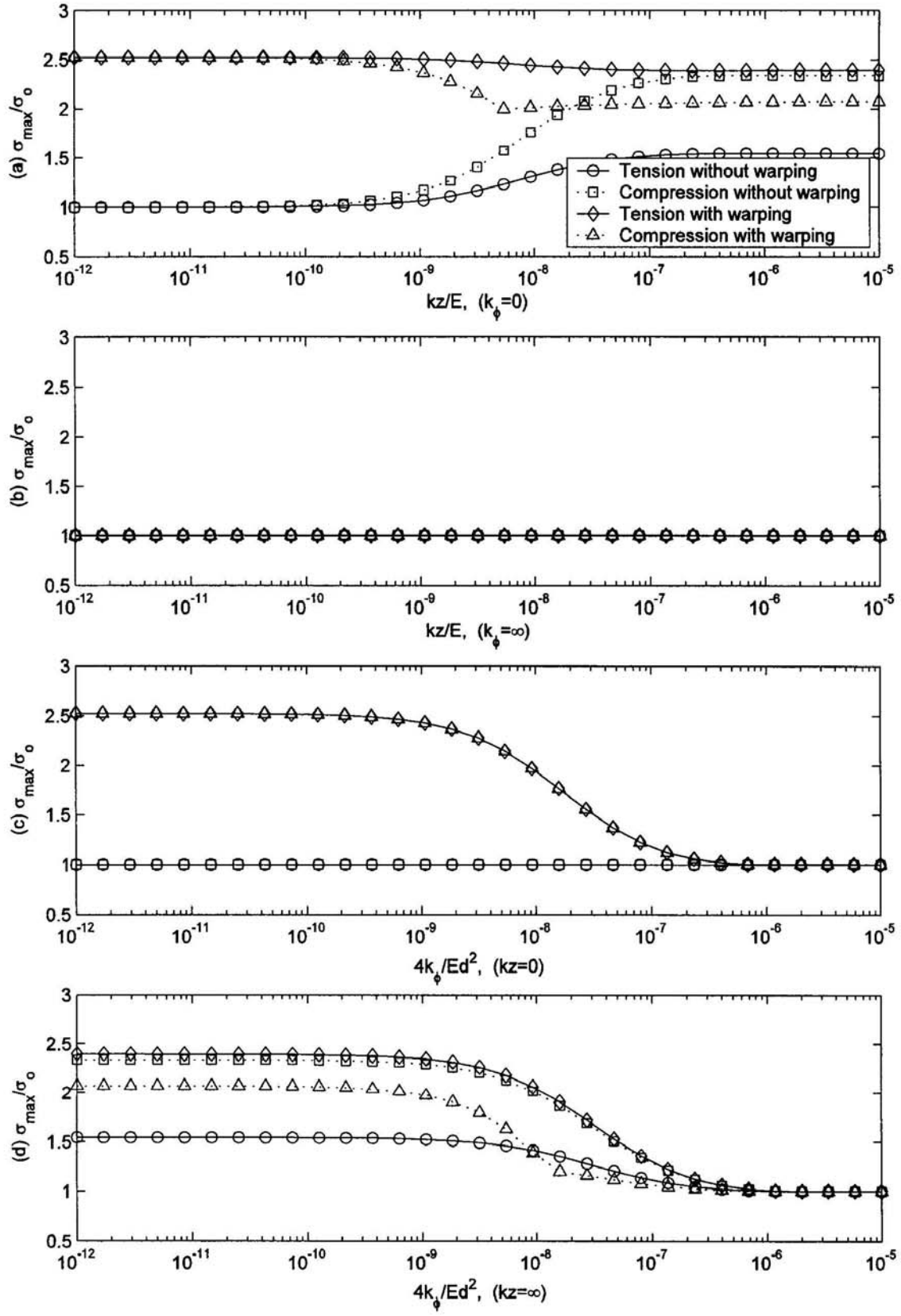


**Fig.3.4 Influence of translational and rotational spring stiffness on maximum tensile and compressive stresses of channel section beam without anti-sag bars ($y_q$=-d/2, $z_q$=b/2-$e_2$, $\sigma_o$ is the maximum stress when $k_z$=$k_\phi$=∞).**

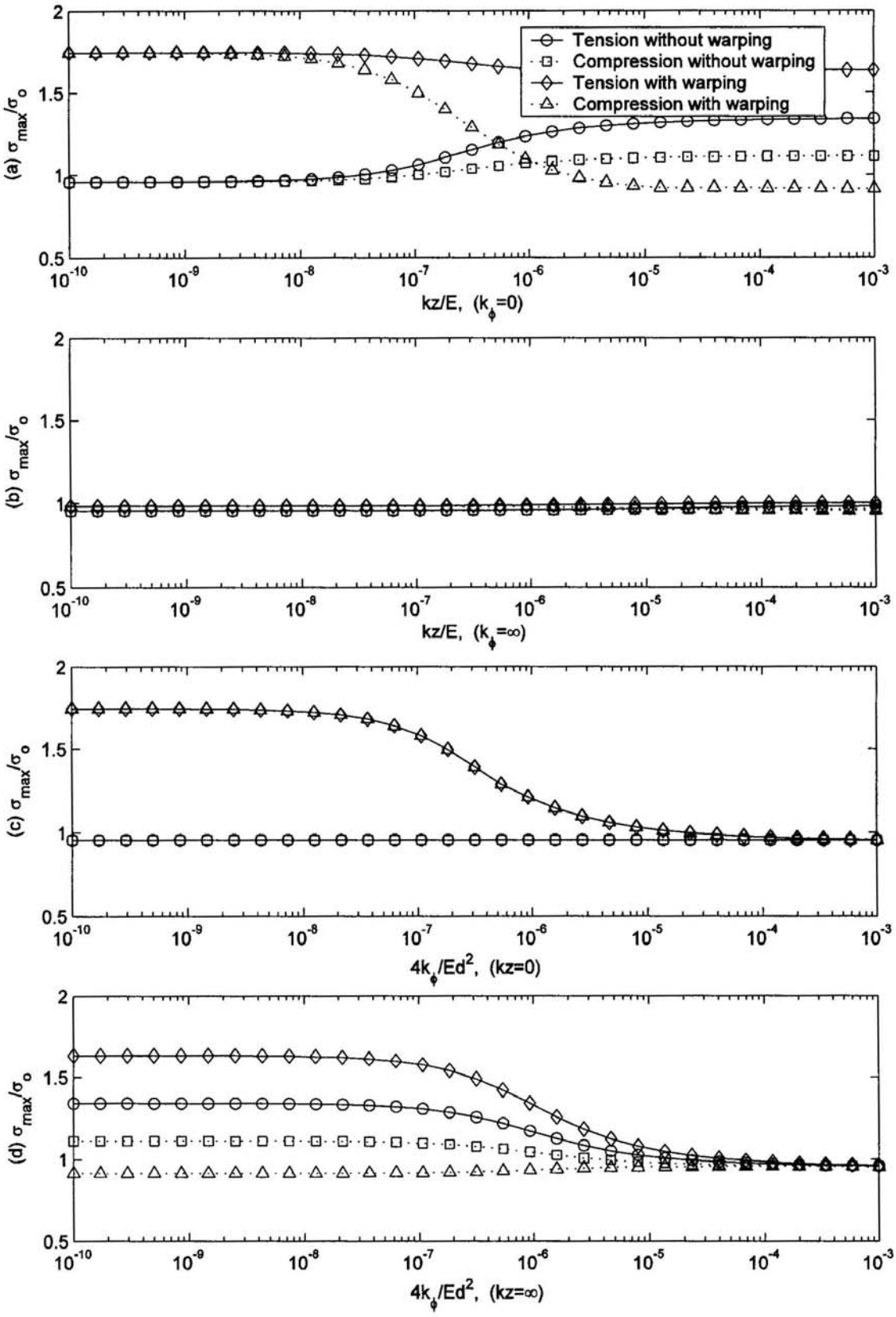


**Fig.3.5 Influence of translational and rotational spring stiffness on maximum tensile and compressive stresses of channel section beam with one anti-sag bar ($y_q$=-d/2, $z_q$=b/2-$e_2$, $\sigma_o$ is the maximum stress when $k_z$=$k_\phi$=∞).**

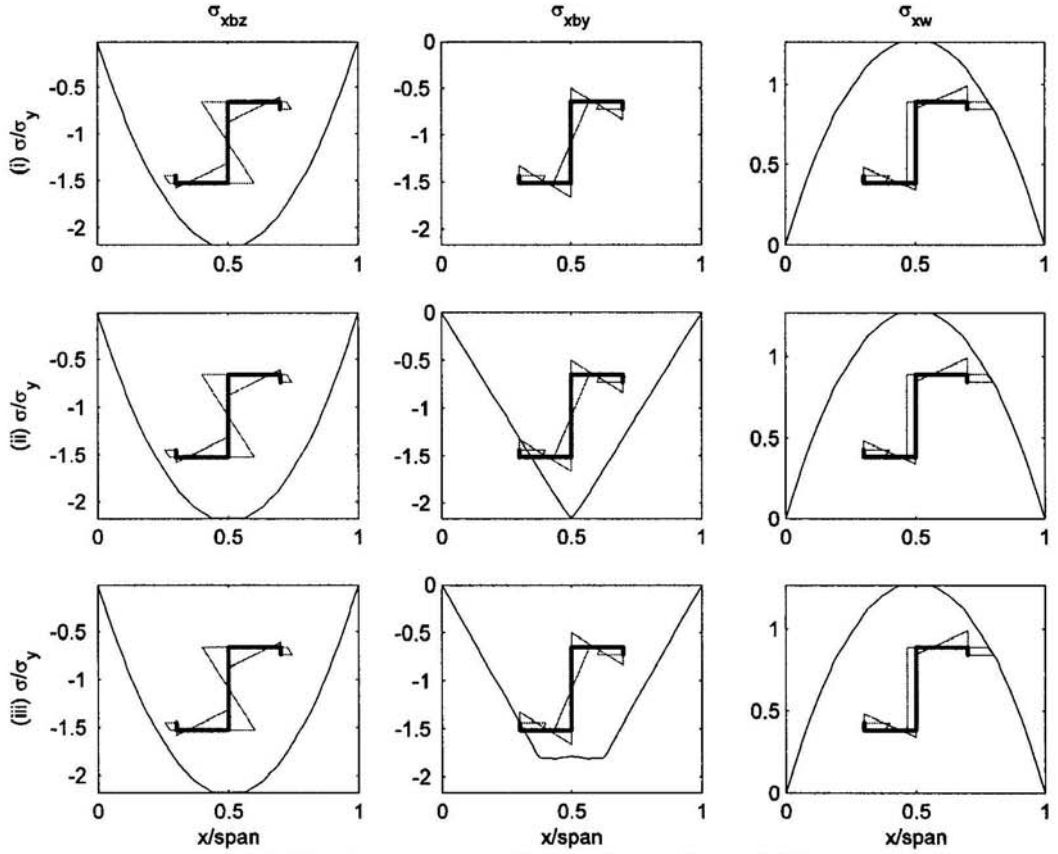


(a) Simply supported beam ($y_q$=-d/2, $z_q$=b/2).

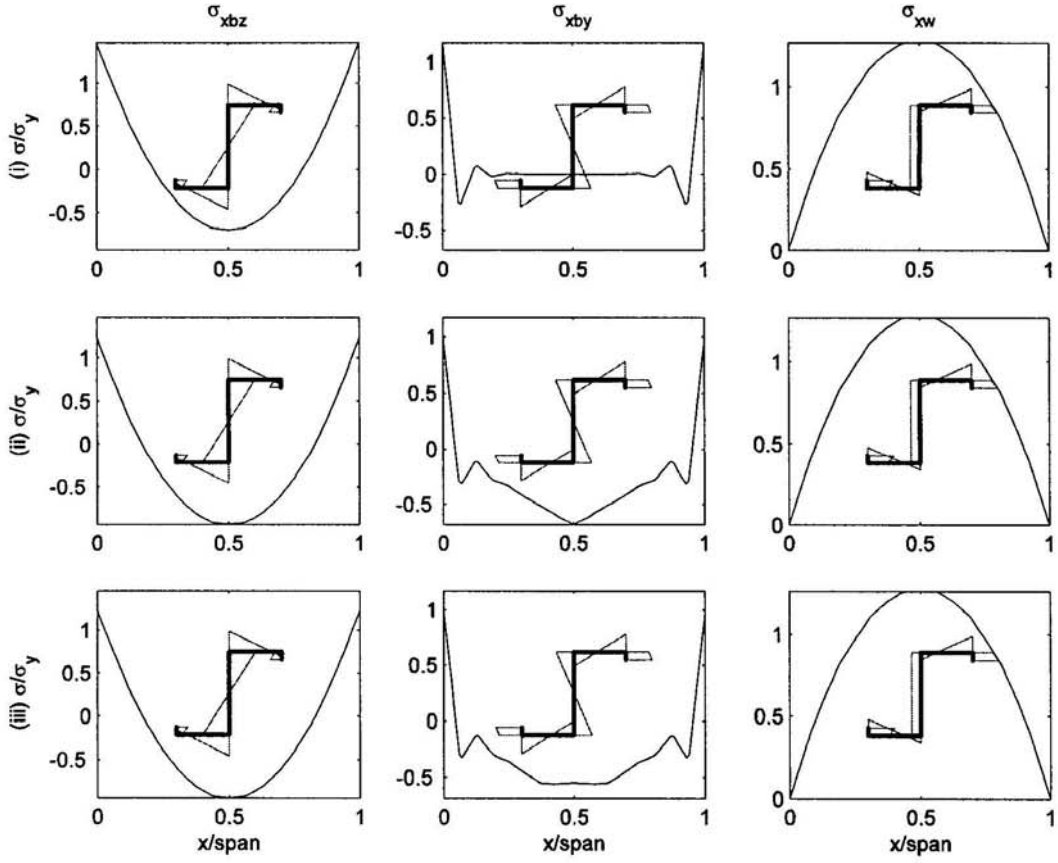


(b) Fixed beam ($y_q$=-d/2, $z_q$=b/2).

**Fig.3.6 Pre-buckling stress distribution for zed section beam when $k_z$=0 and $k_\phi$=0. (i) No anti-sag bars; (ii) One anti-sag bar; (iii) Two anti-sag bars.**

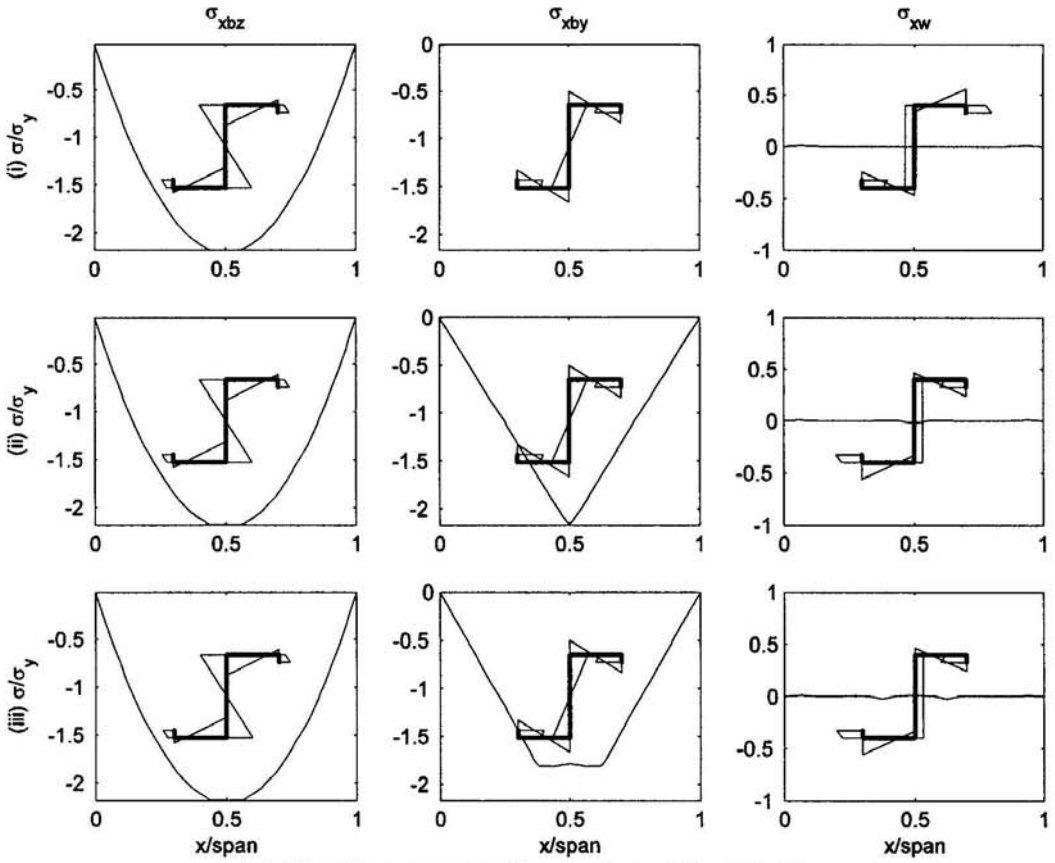


(a) Simply supported beam ($y_q$=-d/2, $z_q$=b/2).

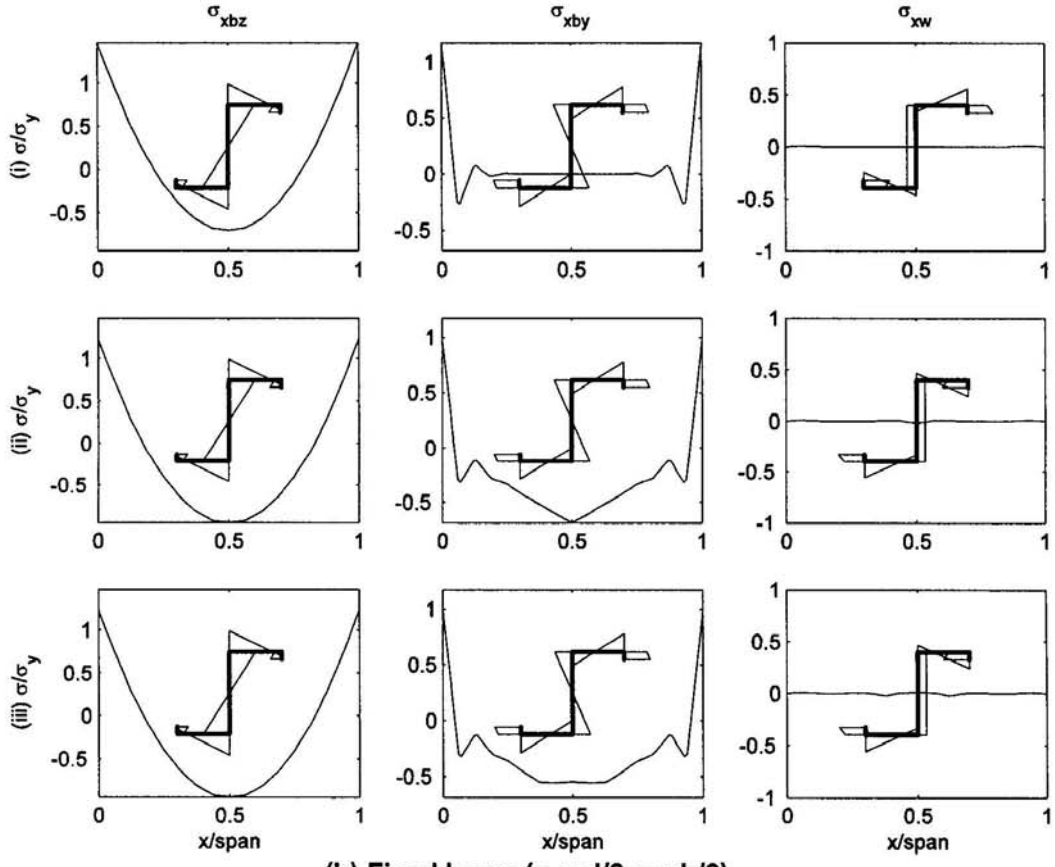


(b) Fixed beam ($y_q$=-d/2, $z_q$=b/2).

**Fig.3.7 Pre-buckling stress distribution for zed section beam when $k_z$=0 and $k_\phi$=∞. (i) No anti-sag bars; (ii) One anti-sag bar; (iii) Two anti-sag bars.**

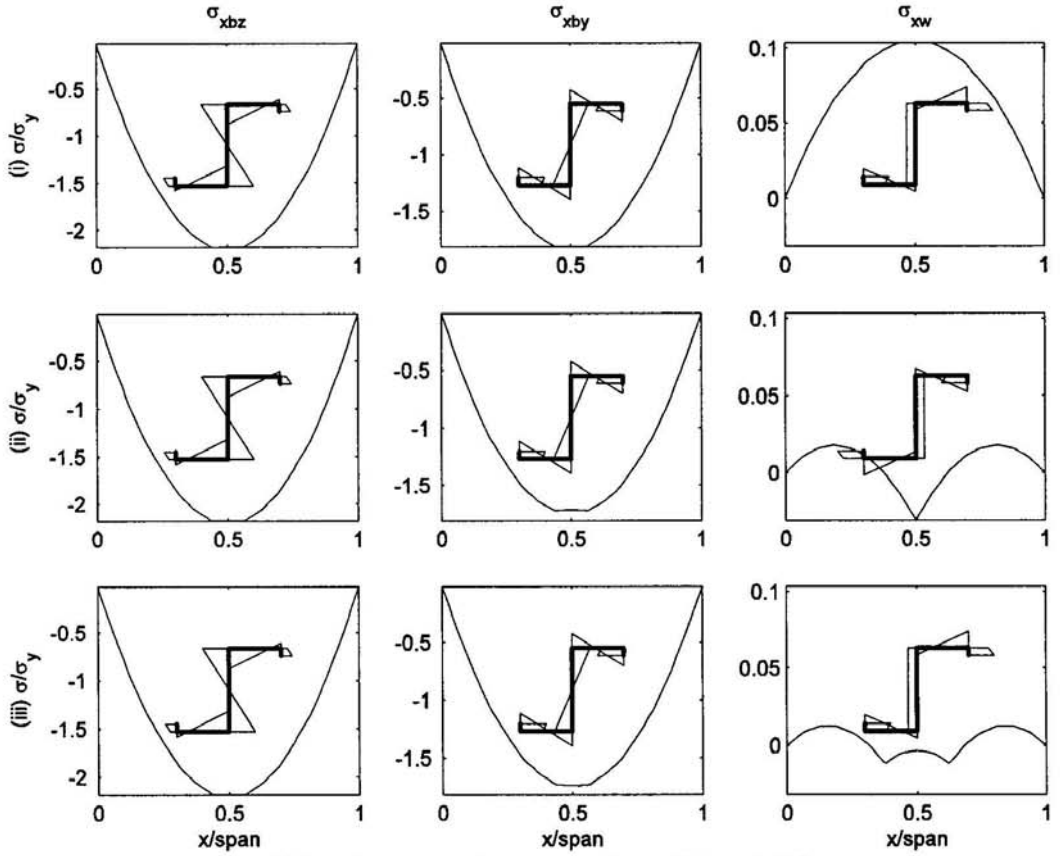


(a) Simply supported beam ($y_q$=-d/2, $z_q$=b/2).

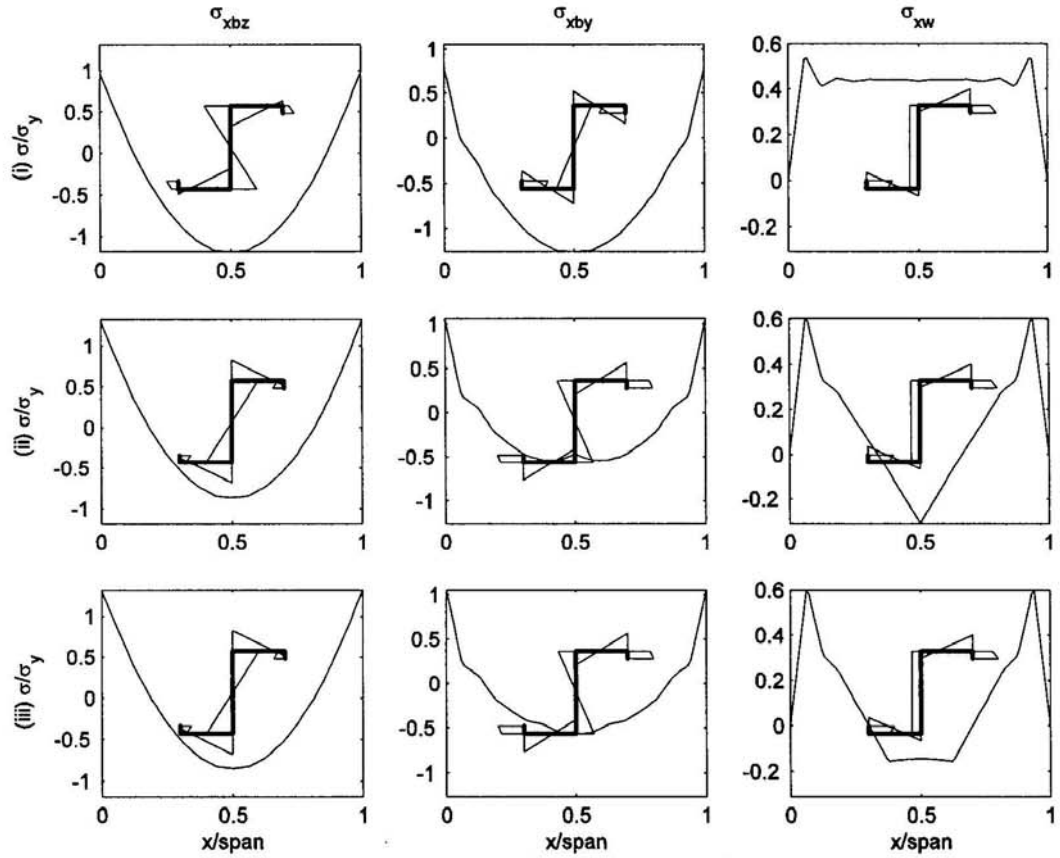


(b) Fixed beam ($y_q$=-d/2, $z_q$=b/2).

**Fig.3.8 Pre-buckling stress distribution for zed section beam when $k_z=\infty$ and $k_\phi$=0. (i) No anti-sag bars; (ii) One anti-sag bar; (iii) Two anti-sag bars.**

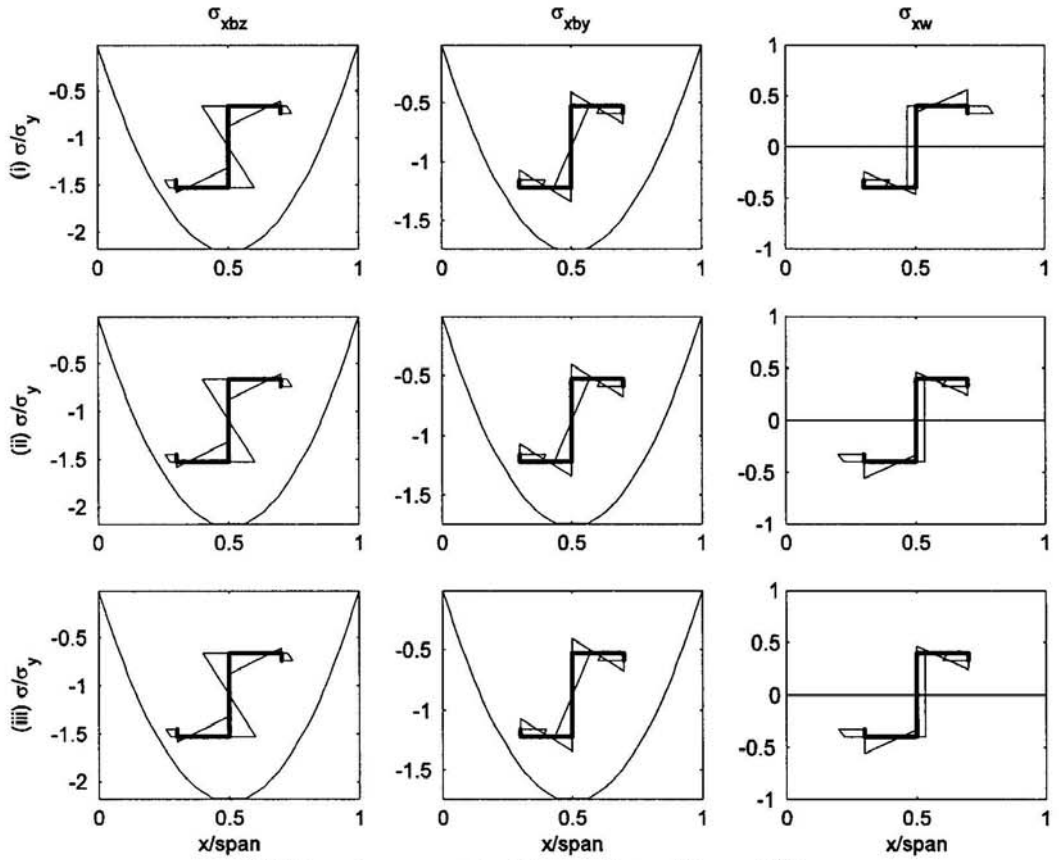


(a) Simply supported beam ($y_q$=-d/2, $z_q$=b/2).

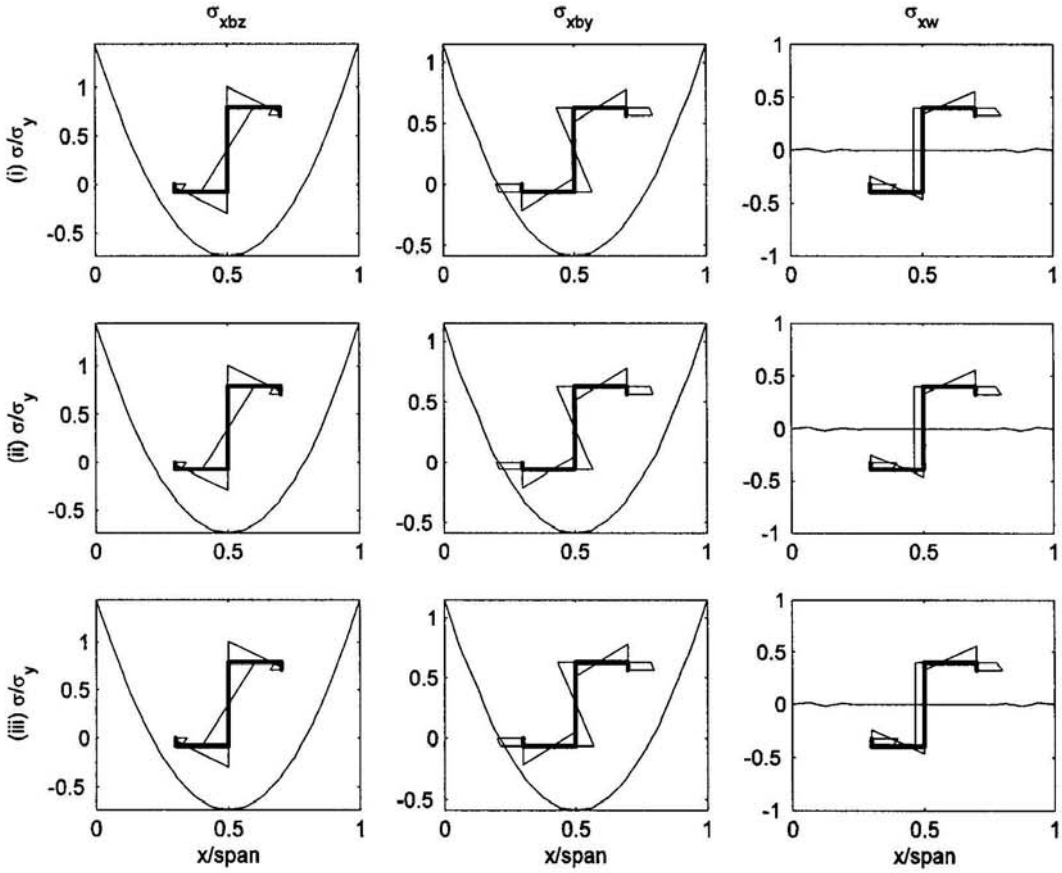


(b) Fixed beam ($y_q$=-d/2, $z_q$=b/2).

**Fig.3.9 Pre-buckling stress distribution for zed section beam when $k_z=\infty$ and $k_\phi=\infty$. (i) No anti-sag bars; (ii) One anti-sag bar; (iii) Two anti-sag bars.**

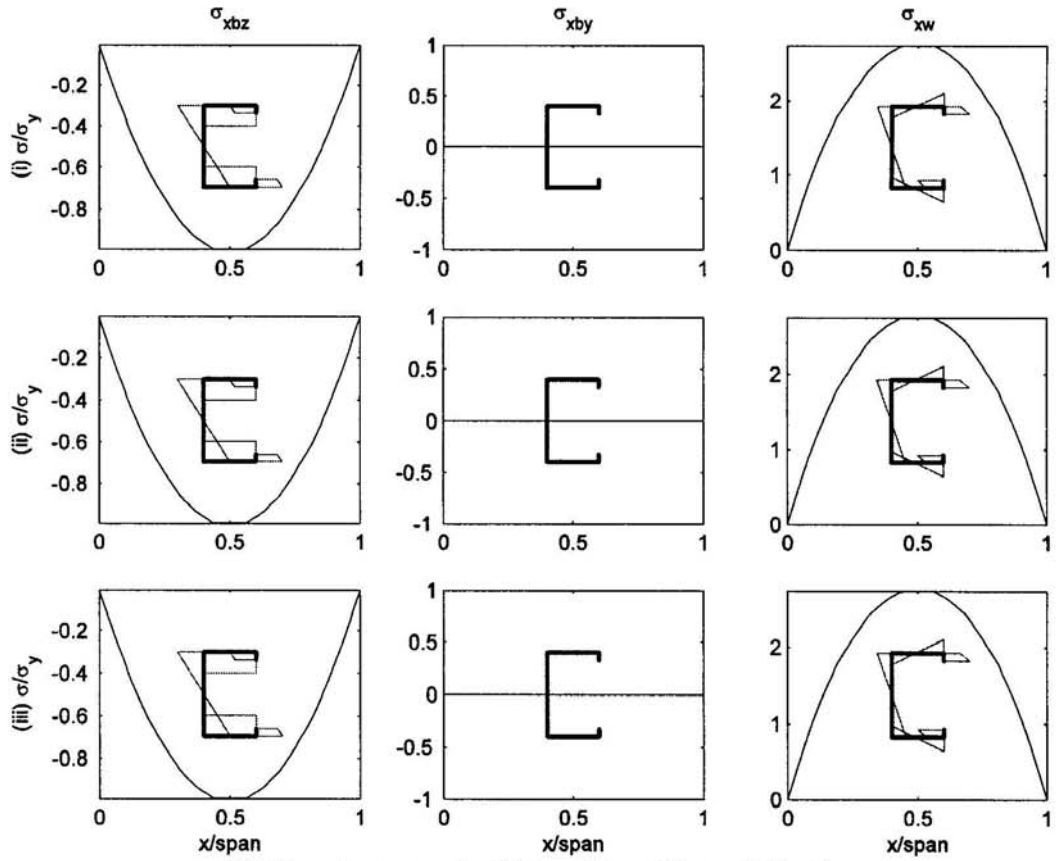


**(a) Simply supported beam ($y_q$=-d/2, $z_q$=b/2-$e_2$).**

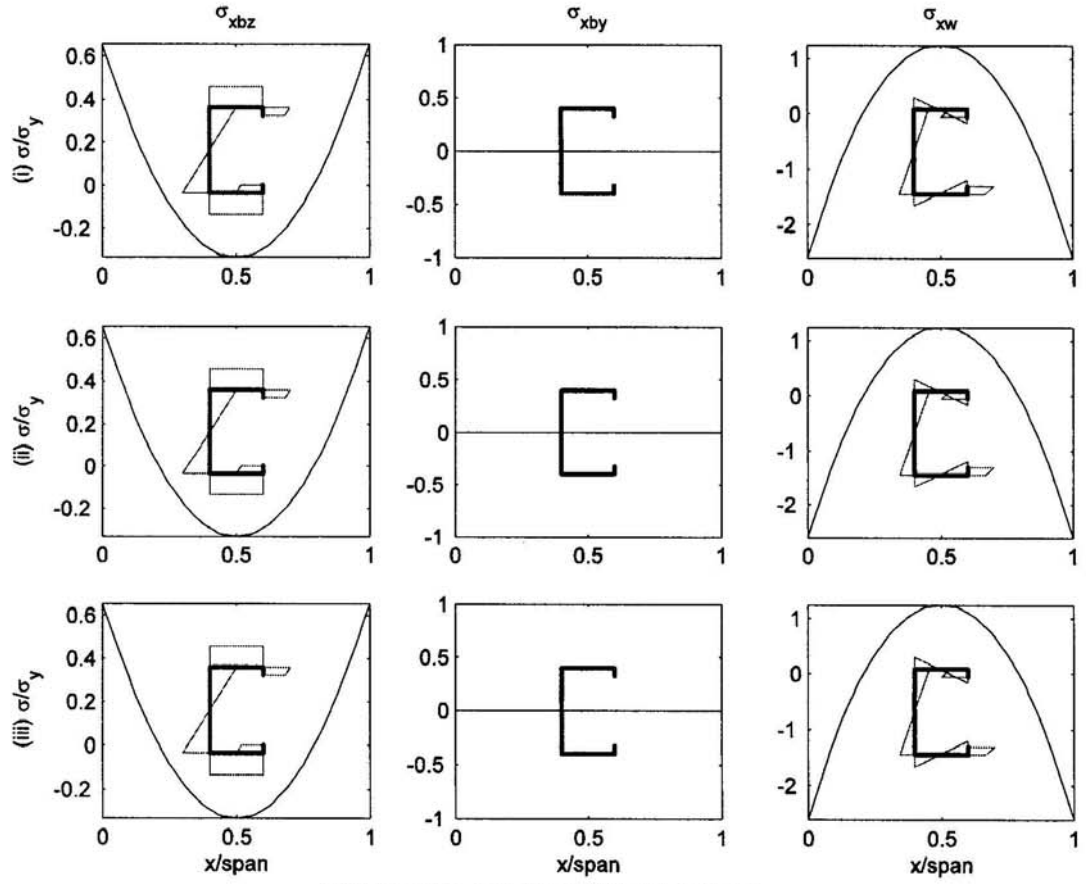


**(b) Fixed beam ($y_q$=-d/2, $z_q$=b/2-$e_2$).**

**Fig.3.10 Pre-buckling stress distribution for channel section beam when $k_z$=0 and $k_\phi$=0. (i) No anti-sag bars; (ii) One anti-sag bar; (iii) Two anti-sag bars.**

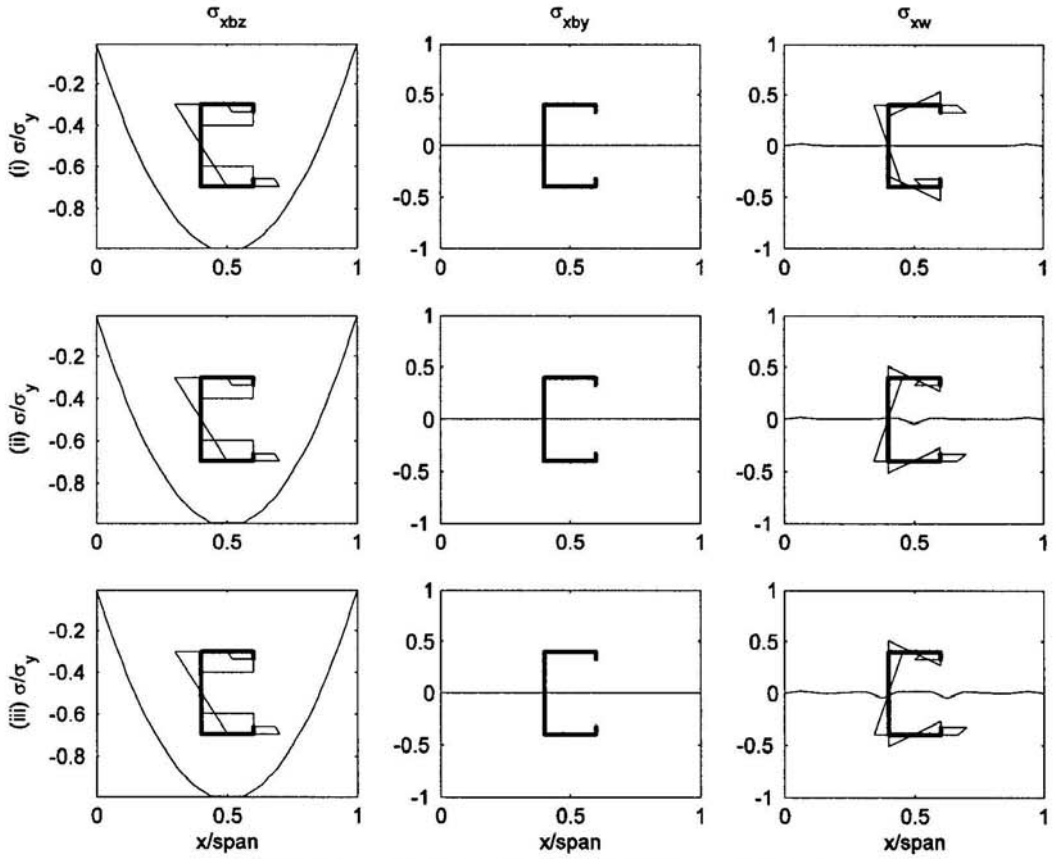


(a) Simply supported beam($y_q$=-d/2, $z_q$=b/2-$e_2$).

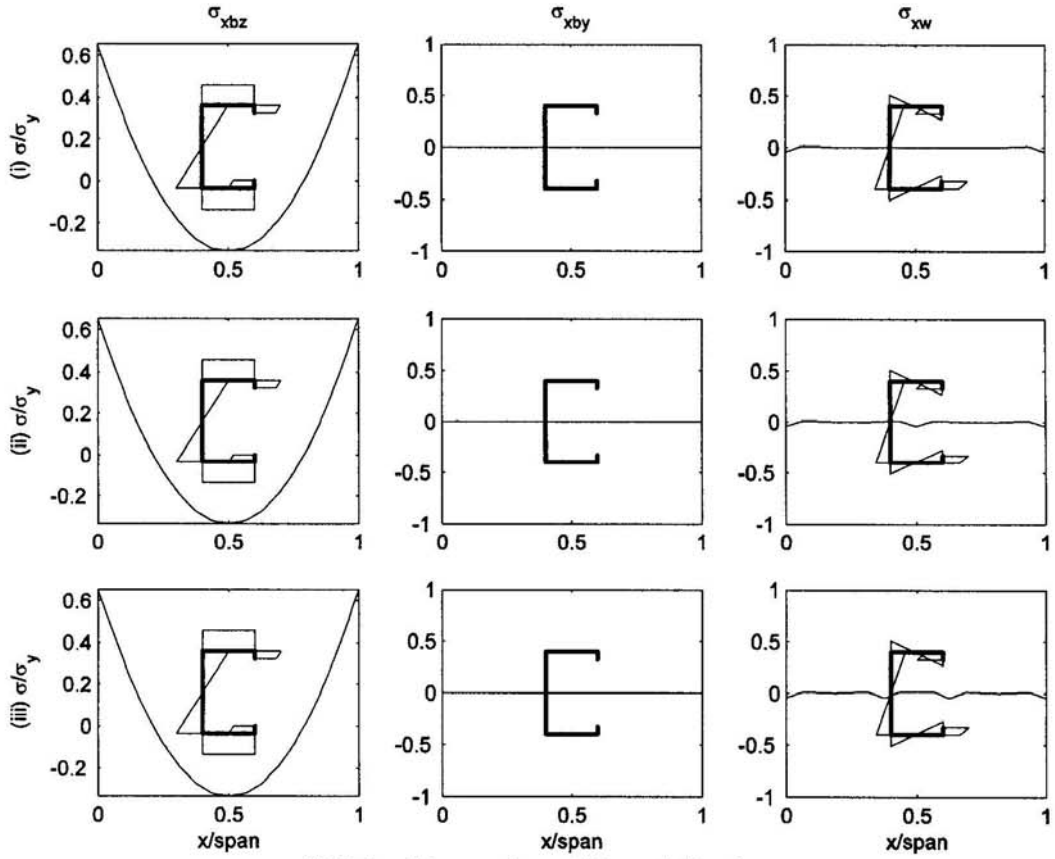


(b) Fixed beam ($y_q$=-d/2, $z_q$=b/2-$e_2$).

**Fig.3.11 Pre-buckling stress distribution for channel section beam when $k_z$=0 and $k_\phi$=∞. (i) No anti-sag bars; (ii) One anti-sag bar; (iii) Two anti-sag bars.**

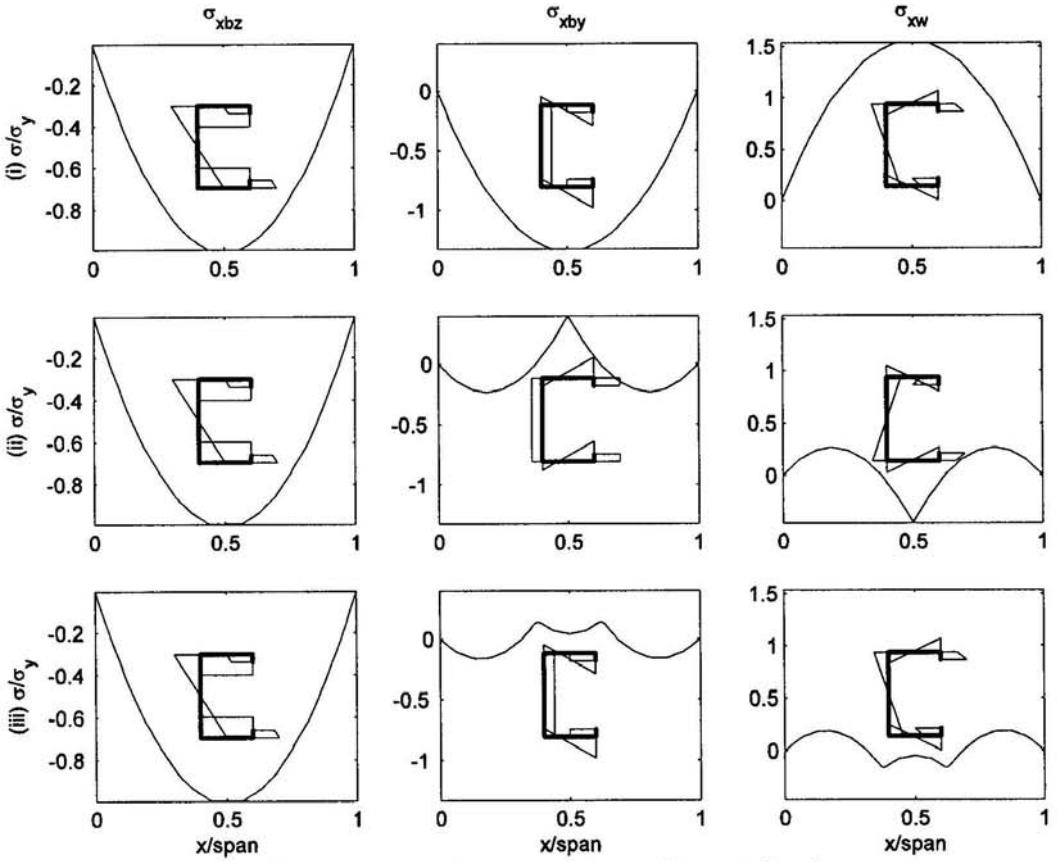


(a) Simply supported beam ($y_q$=-d/2, $z_q$=b/2-$e_2$).

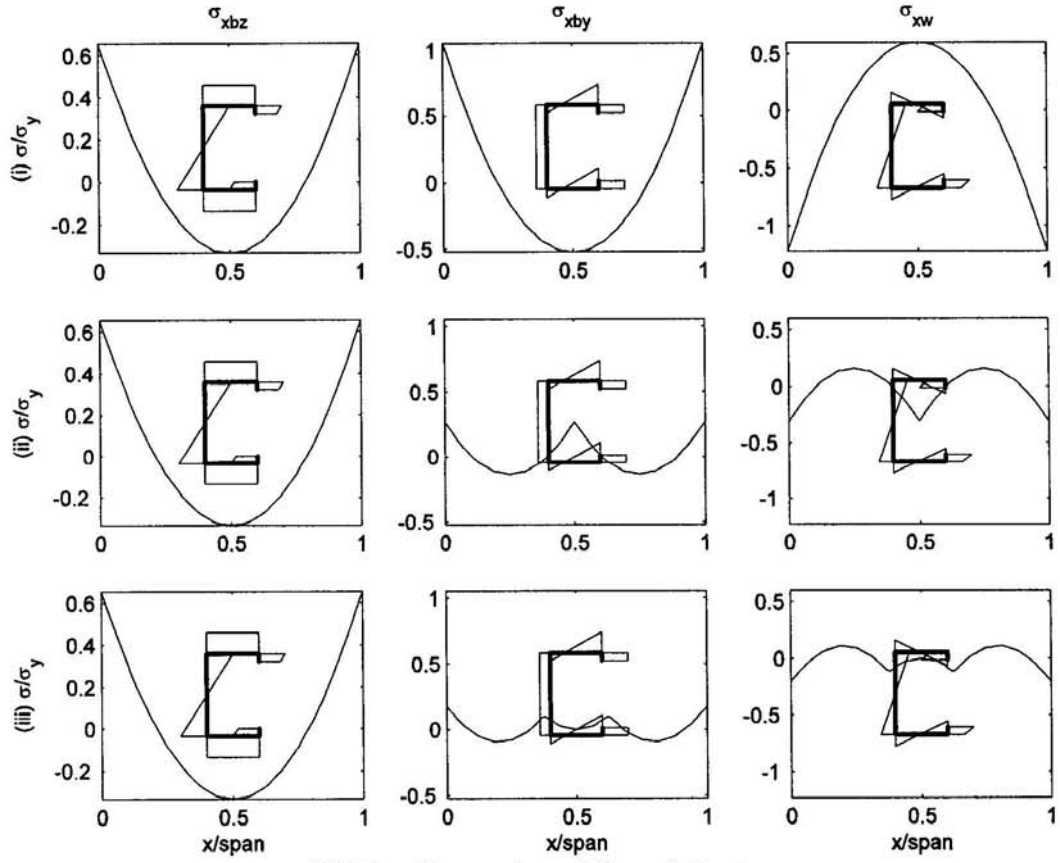


(b) Fixed beam ($y_q$=-d/2, $z_q$=b/2-$e_2$).

**Fig.3.12 Pre-buckling stress distribution for channel section beam when $k_z=\infty$ and $k_\phi$=0. (i) No anti-sag bars; (ii) One anti-sag bar; (iii) Two anti-sag bars.**

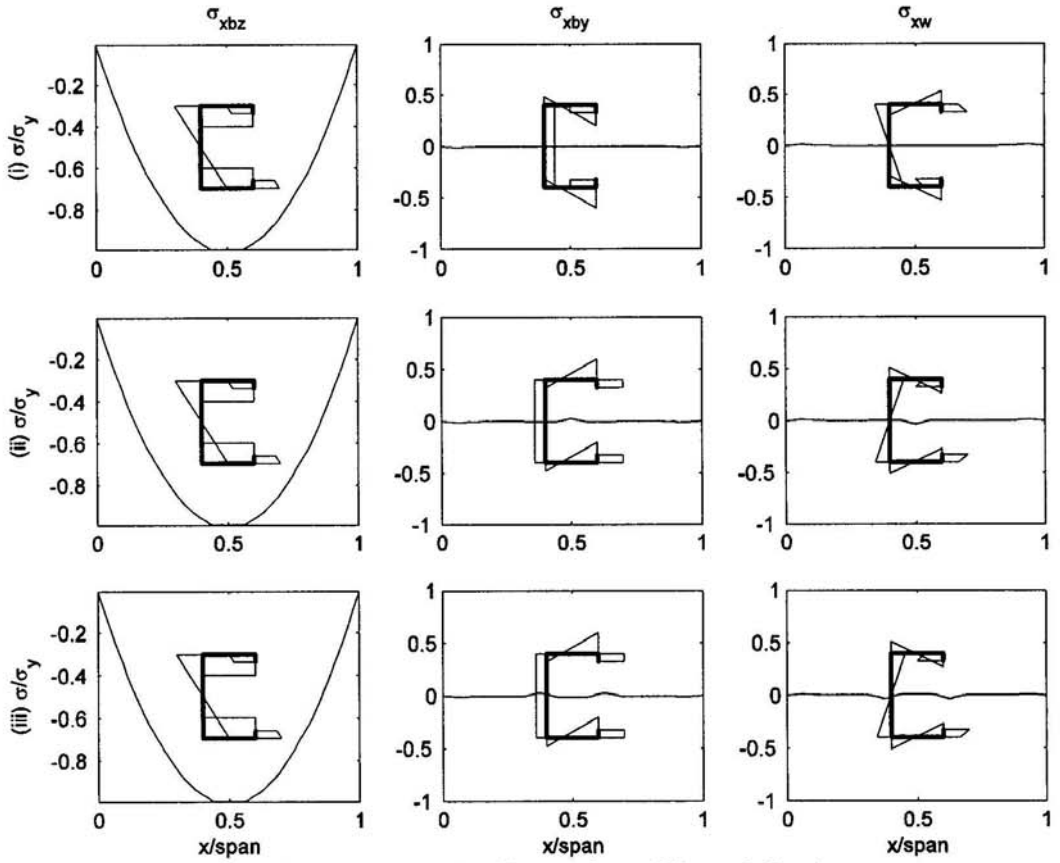


(a) Simply supported beam ($y_q$=-d/2, $z_q$=b/2-$e_2$).

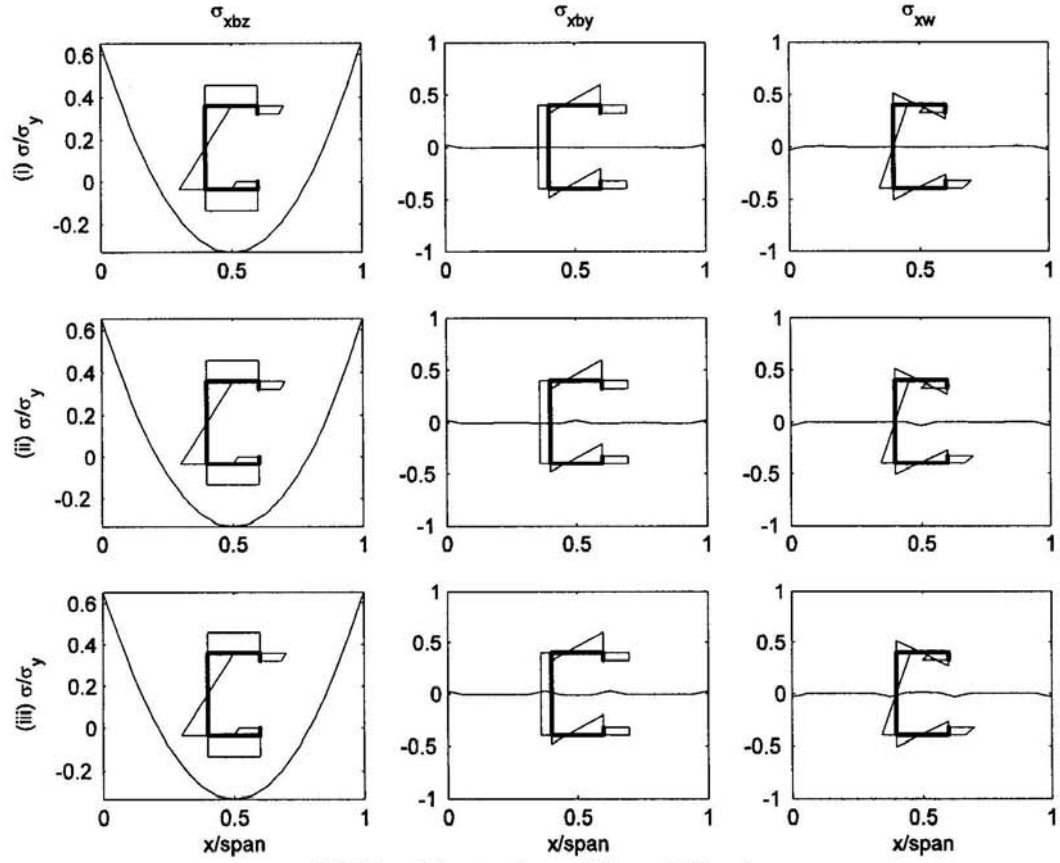


(b) Fixed beam ($y_q$=-d/2, $z_q$=b/2-$e_2$).

**Fig.3.13 Pre-buckling stress distribution for channel section beam when $k_z=\infty$ and $k_\phi=\infty$. (i) No anti-sag bars; (ii) One anti-sag bar; (iii) Two anti-sag bars.**

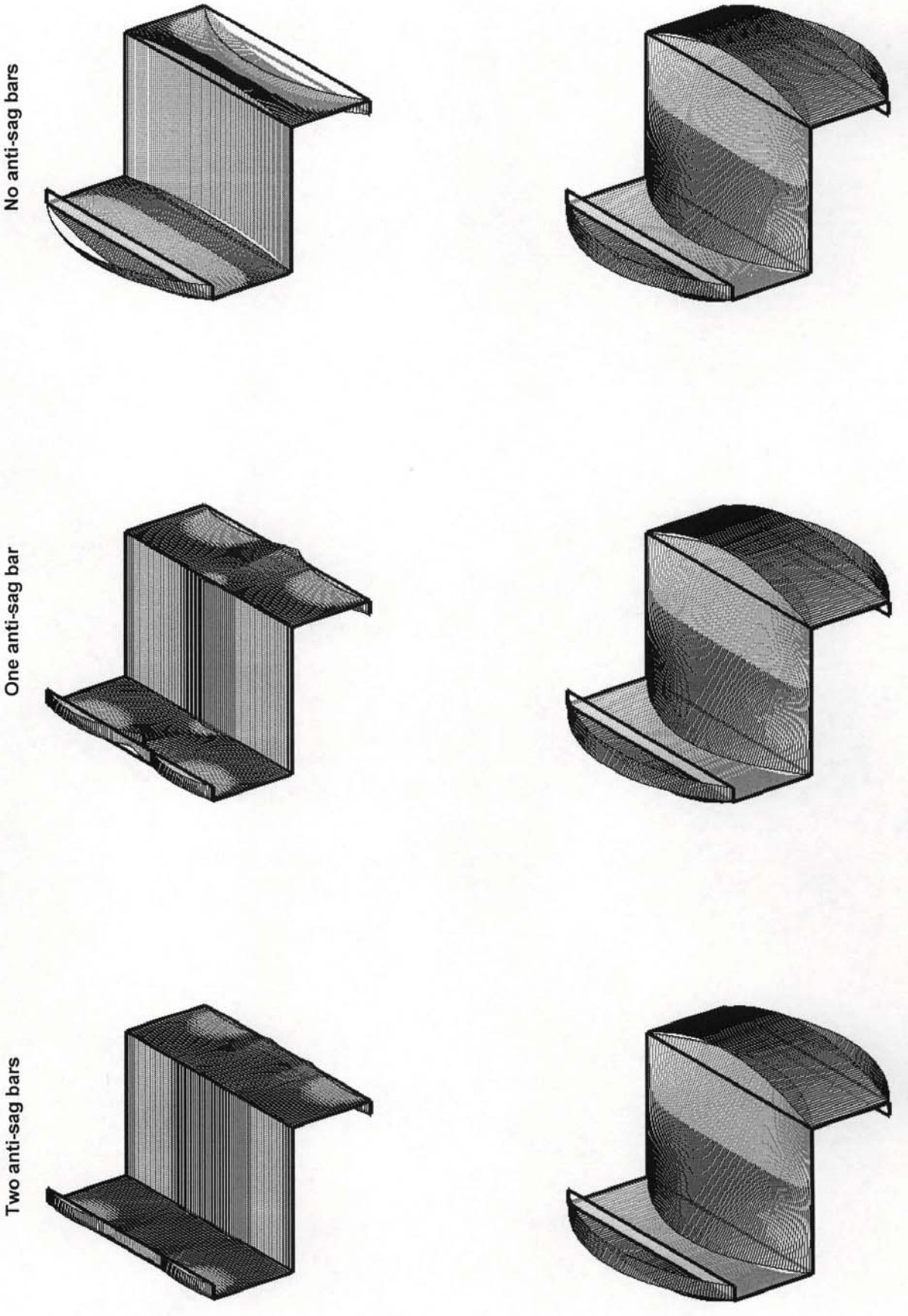


**Fig.3.14 The longitudinal stress distribution of zed section beams when $k_z=\infty$ and $k_\phi=0$. (a) Warping stress and (b) bending stress ($y_q$=-d/2, $z_q$=b/2).**

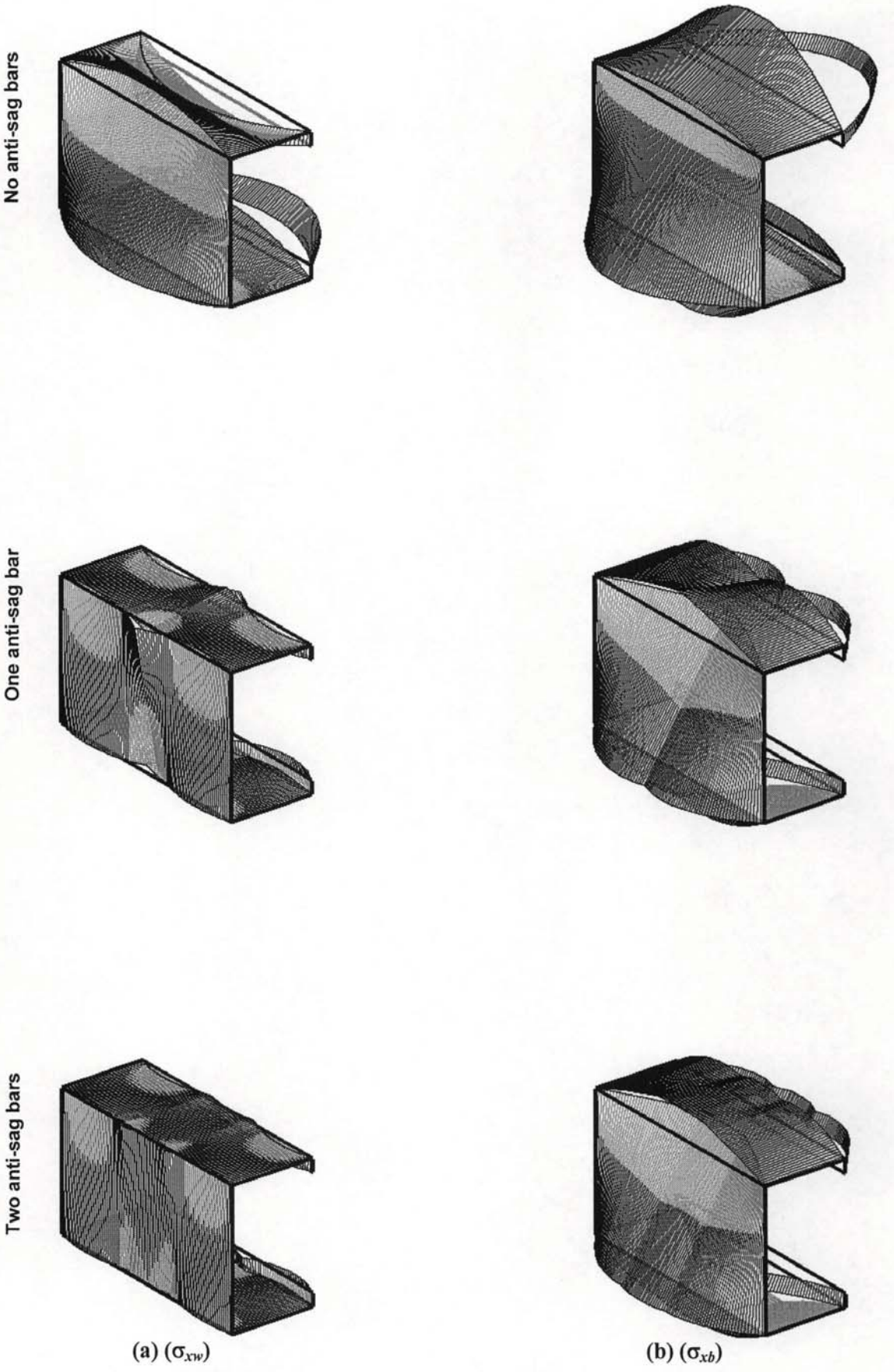


**Fig.3.15 The longitudinal stress distribution of channel section beams when $k_z=\infty$ and $k_\phi=0$. (a) Warping stress and (b) bending stress ($y_q$=-d/2, $z_q$=b/2-$e_2$).**

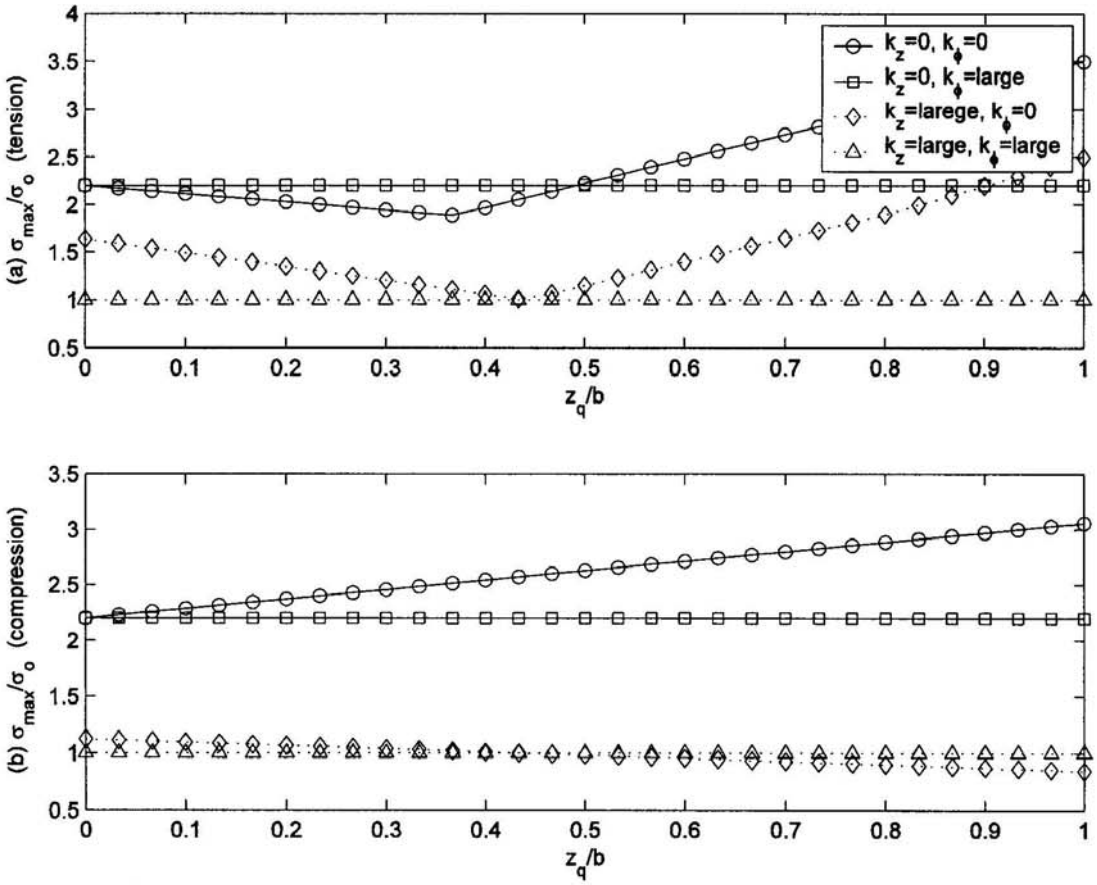


**Fig.3.16 Influence of the position of loading point on maximum stresses of zed section beams ($\sigma_o$ is the maximum stress when $k_z=k_\phi=\infty$, $y_q$=-d/2).**

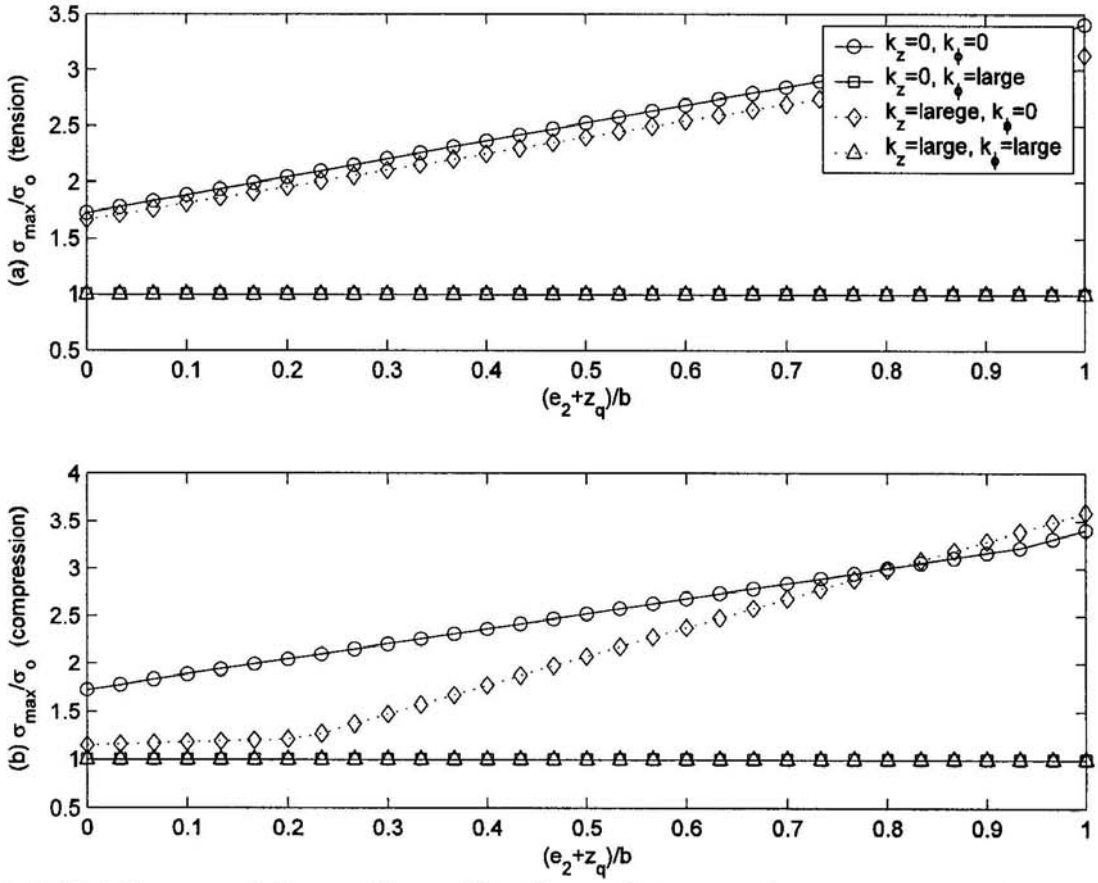


**Fig.3.17 Influence of the position of loading point on maximum stresses of channel section beams ($\sigma_o$ is the maximum stress when $k_z=k_\phi=\infty$, $y_q$=-d/2).**

**Table 3.1 Details of the analytical models.**

| | | |
|---|---|---|
| **Material Properties** | **Young's Modulus E (GPa)** | 205 |
| | **Poisson's ratio $\upsilon$** | 0.3 |
| | **Yield Stress $\sigma_y$ (MPa)** | 390 |
| **Boundary Conditions** | **Simply-supported (S)** | $v = v'' = 0;\ w = w'' = 0;\ \phi = \phi'' = 0$ |
| | **Fixed* (F)** | $\begin{cases} v = v' = 0; w = w' = 0; \phi = \phi' = 0; & \textit{for zed section} \\ v = v' = 0; w = w'' = 0; \phi = \phi'' = 0; & \textit{for channel section} \end{cases}$ |
| | **Anti-sag Bar** | $w = 0$; ***Note:*** *The position is assumed at the centre of the span for one bar or at 3/8 and 5/8 of the span length for two bars.* |
| **Loading Details** | **Loading Density $q_y$** | $8M_{yield}/l^2$ ($M_{yield}=2\sigma_y I_z/d_1$) |
| | **Loading Position** | $y_q$=-$d$/2, $z_q$=$b$/2 (Zed) $\quad$ $y_q$=-$d$/2, $z_q$=$b$/2-$e_2$ (Channel) |
| | | ***Note:*** *This is the case if without further illumination.* |

* The displacement conditions of fixed boundary are different for zed section and channel section, which is because they are assumed based on the practical engineering cases.

# Chapter 4

# 4 LOCAL BUCKLING BEHAVIOUR

## 4.0 CHAPTER SYNOPSIS

The following chapter describes the local buckling behaviour of cold-formed zed and channel section beams subjected to various loading conditions. A novel method is presented for analysing the elastic local buckling behaviour of cold-formed zed and channel section beams with partial-lateral restraint from metal sheeting when subjected to a uniformly distributed transverse load.

The focus of the study is to investigate the local buckling behaviour of cold-formed zed and channel section beams under pure bending and uniformly distributed transverse loading by using the available approaches, the individual influences of warping stress, partial lateral restraints from the sheeting and the dimensions of the cross section on the local buckling behaviour.

## 4.1 INTRODUCTION

It is well known that the effective width and the finite strip method are commonly used for studying the local buckling behaviour of cold-formed steel sections. However, by ignoring the interaction between the individual plate elements, the effective width method may be inaccurate, particularly when dealing with different stress conditions. In the finite strip method the stress distribution is assumed as constant along the half wavelength, while for the uniformly distributed transverse loading case the longitudinal stress varies along the span. Nevertheless, it is conceivable that, for a beam subjected to a varying stress distribution along its span, the local buckling will occur only at a worst place. The worst place should be where the compressive stress is the largest. Therefore, only the cross-sectional stresses with the largest compressive stress are used as the input to the finite strip analysis for carrying out the elastic local buckling analysis. The finite strip method has been shown to be a good approach to effectively analyse the local buckling of cold-formed members. The details of the finite strip method can be found in Section 2.8.5 and thus is not presented further here.

## 4.2 LOCAL BUCKLING OF THE MEMBERS UNDER PURE BENDING

The local bucking capacity of the simply-supported zed and channel section beams under pure bending are investigated using the effective width method based on BS 5950 (1998) and the finite strip program – CUFSM (Schafer, 2001c & 2003a). The stress distribution on the cross section is demonstrated in Fig.4.1, where $d_1$ is the overall depth of section, $b_1$ is the width of flange, $c_1$ is the length of stiffening lip and $t$ is the thickness.

Note, because the purlins investigated here are restrained both laterally and rotationally at the corner between the web and the flange subjected to tensile stress

and are subjected to pure bending, the results in Section 4.2 can be applied to both zed and channel section beams.

### 4.2.1 Effective Width Method Based On BS 5950-5

The procedure of the calculation of effective section based on BS 5950 (1998) is listed as follows,

⇨ Limiting compressive stress in the web:

$$p_0 = p_y \times \min(1, k) \tag{4.1}$$

$$\text{where } k = 1.13 - 0.0019(\frac{d_w}{t})\sqrt{\frac{\sigma_y}{280}} = 1.13 - 0.212(\frac{d}{100t}) \tag{4.2}$$

$d_w = \max(d, 2Y_m)$;

$d$ = depth of web (=$d_1$-$t$);

$\sigma_y$ = yield stress, given in Table 3.1.

$Y_m$ = depth of compression zone (=0.5$d$);

$t$ = thickness of web.

⇨ Effective width of the compressed flange (with stiffening lip)

$$\text{Local buckling stress: } p_{cr} = \frac{\pi^2 E}{12(1-\nu^2)} k_\sigma (\frac{t}{b})^2 = 0.904 E k_\sigma (\frac{t}{b})^2 \tag{4.3}$$

$$\text{where } k_\sigma = 5.4 - \frac{1.4(d/b)}{0.6 + d/b} - 0.02(\frac{d}{b})^3$$

$b$ = width of flange (=$b_1$-$t$)

$$\text{Compressive stress in the flange: } f_c = p_o \tag{4.4}$$

$$\text{Effective width of the flange: } b_{e1} = b_{e2} = 0.5 b_{eff} \tag{4.5}$$

where $b_{eff} = b$ if $f_c / p_{cr} \leq 0.123$;

$$b_{eff} = b\left[1+14\left(\sqrt{\frac{f_c}{p_{cr}}}-0.35\right)^4\right]^{-0.2} \quad \text{if } f_c / p_{cr} > 0.123$$

⇨ Effective length of the compressed stiffening lip

Local buckling stress: $p_{cr} = \frac{\pi^2 E}{12(1-\nu^2)} k_\sigma (\frac{t}{c})^2$ (4.6)

$$\text{where } k_\sigma = \frac{1.7}{3+f_{cs}/f_{cf}};\ f_{cs} = p_o;\ f_{cf} = f_{cs}\frac{Y_m - c}{Y_m};\ c = c_l\text{-}0.5t.$$

Compressive stress in the stiffening lip: $f_c = (f_{cf} + f_{cs})/2$ (4.7)

Effective length of the stiffening lip:

$$c_{eff} = c \quad \text{if } f_c / p_{cr} \leq 0.123$$

$$c_{eff} = c\left\{0.89\left[1+14\left(\sqrt{\frac{f_c}{p_{cr}}}-0.35\right)^4\right]^{-0.2}+0.11\right\} \quad \text{if } f_c / p_{cr} > 0.123 \quad (4.8)$$

⇨ Calculation of the new position of the neutral axis

$$Y_m = \frac{\frac{c_{eff}^2}{2}+\frac{d^2}{2}+bd+c(d-\frac{c}{2})}{c_{eff}+b_{eff}+d+b+c} \quad (4.9)$$

### 4.2.2 Elastic Buckling Based On Finite Strip Analysis

The buckling modes of cold-formed steel sections can be classified as local, distortional and global buckling modes. Some typical buckling curves calculated using CUFSM are shown in Fig.4.2.

The curve, 'd100_b60_c20_t20', is a 'standard' buckling curve, which provides the information about when and how the section buckles for a given length. There are three

regions in the curve, which correspond to the local buckling of short buckling wavelengths, the distortional buckling of medium buckling wavelengths and the lateral distortional buckling of long buckling wavelengths. The local minimum in each region provide the lowest possible critical load and the corresponding buckling wavelength for the particular type of the buckling.

Fig.4.3 shows the typical local buckling modes. The main local buckling mode is the combination of lip, flange and web buckling. However, due to the difference in the width for each element, the buckling is initiated by the longest element amongst the lip, the flange and the compression part of the web.

### 4.2.3 Comparison Of Local Buckling Capacity Calculated Using BS 5950-5 And Finite Strip Analysis

Fig.4.4 shows comparisons of the critical bending moments for local buckling calculated using the method shown in BS 5950 and the finite strip method, for the beam restrained both laterally and rotationally at the corner between web and the flange subjected to tensile stress. The results can be applied to both channel and zed sections. It can be seen from the figure that the values of the moment capacity calculated using BS 5950 increase with increase in the flange width $b$, web depth $d$ and the ratio of lip depth $c$ to flange width $b$. This is due to the fact that the effective area for the bigger cross section is larger than for the smaller cross section.

However, the results are more complicated for the moment capacity calculated using the finite strip method. It is found in Fig.4.4a that the moment capacity decreases with the increase of flange width $b$ when $d$=100mm, but increases with the flange when $d$=300mm; and in Fig.4.4b that the moment capacity reaches to the maximum value before it decreases with the increase of the web depth. The influence of the ratio of $c$ to $b$ was found only for the shallower section (d=100mm) when $c/b$ is larger than 0.3 (see Fig.4.4c). In general, it is the difference between the width of the flange and the compression part of the web that determines the elastic buckling capacity. When the width of the flange is larger than the depth of the compression part of the web, the buckling mode is flange buckling. The elastic local buckling capacity can be decreased by increasing the flange width $b$. On the other hand, when the width of the flange is less than the depth of the compression part of the web, the buckling mode

will be the web buckling. The elastic local buckling capacity can be increased by increasing either the flange width $b$ or the lip length $c$.

It is also apparent from Fig.4.4 that the results from the finite strip method and BS 5950 are closing when the web depth is deeper than 270mm, otherwise the results from the finite strip method are greater than those from BS 5950. This is due to the fact that local buckling is initiated in web when the section is deeper. Note that in BS 5950, the web element is assumed to be fully effective but the maximum compressive stress is limited; while in the finite strip method, the interaction of local buckling of the individual elements is considered.

Fig.4.5a shows the ratios of critical bending moments to yielding moments ($M_{cr}/M_{yield}$) calculated using the finite strip method and BS 5950. It can be seen that the results obtained from the finite strip method exceed yielding moments when d=100m, particularly when $b$ is small; while the results from BS 5950 are almost equal to the yielding moments. However, when d=300mm, both of the results are smaller than yielding moment, which means the local buckling occurs before the yielding.

Fig.4.5b shows the influences of the dimensions on the moment efficiency, which is defined as the ratio of the moment capacity to the gross area of the cross section. It is interesting to see that it gives different trends for d=100mm and d=300mm. The maximum value of moment efficiency is reached when the flange width is 60mm for the section with d=100mm and around 80mm for the section with d=300mm.

## 4.3 LOCAL BUCKLING OF PURLIN-SHEETING SYSTEMS

### 4.3.1 Limitation Of Design Specifications

As illustrated in Section 2.3.2.1, elastic local buckling is typically treated by ignoring any interaction between the elements (flanges and web) in the design specifications (EC3, Part 1.3, 1996; BS 5950, 1998). Each element is considered independently and

the classical plate buckling equations based on isolated free or simply supported plates are used. This approach, called the element model, can lead to rather conservative predictions.

Eurocode 3: Part 1.3 (1996) gives some comprehensive rules for the determination of the effective widths under different stress conditions. In principle, the effective widths of the individual plate elements may be combined to give an effective section and the member design can be completed using conventional techniques. However, this apparent simplicity conceals a number of difficulties. This is because individual plate elements do not buckle in isolation but interact with each other.

Furthermore, with modern, highly stiffened sections, the stiffeners may be partially effective so that stiffener buckling interacts with local plate buckling. Eurocode 3: Part 1.3 (1996) gives some design rules for more general situations but these are complicated to use and not particularly accurate (Kesti & Davies, 1999). Evidently, this is the situation where design based on an analysis of the whole section is to be preferred.

### 4.3.2 The Novel Model Based On Energy Methods And Finite Strip Analysis

The analytical model introduced in Section 3.2 is used to carry out pre-buckling stress analysis for the zed and channel section beams, which are partially restrained by the sheeting on the upper flange. The restraint of the sheeting can be simplified by a translational spring and a rotational spring, as shown in Fig.3.1.

The critical load for local buckling of the partially restrained zed and channel section members can be calculated using the finite strip method (Schafer, 2001c & 2003a). It should be mentioned here that, in this method the stress distribution is assumed as constant along the half wavelength, while in the present case the longitudinal stress varies along the span. However, it is conceivable that for a beam subjected to a varying stress distribution along its span, local buckling will only occur at a worst place. The worst place should be one at length in which the compressive stress is the largest. Therefore, only the cross-sectional stresses with the largest compressive stress are used as the input to the finite strip analysis for carrying out the elastic local

buckling analysis. The finite strip method has been proved to be a good approach to effectively analyse the local buckling of cold-formed members. The details of the finite strip method can be found in Section 2.8.5 and thus is not presented further here.

Also, in the finite strip method the local buckling analysis is performed with respect to the half wavelength of the buckling modes which is independent of the span length and the end boundary conditions. However, since the pre-buckling stress in the present study is calculated based on the particular member of a given span length and of prescribed boundary conditions, the critical load obtained from the finite strip analysis is thus only applicable to this particular member. Any change in the beam span length or the end boundary conditions will alter the pre-buckling stress and thus leads to different local buckling critical load.

### 4.3.3 Numerical examples

Table 3.1 gives the details of the analyzed zed and channel sections, such as material properties, definition of boundary conditions and loading details. Here the boundary conditions for the displacements are assumed as simply supported. The investigated beams have a span length of 8m.

For a given problem, one can solve variational Eq.(3.6) by using the numerical method to obtain pre-buckling displacements $v(x)$, $w(x)$ and $\phi(x)$ and the corresponding longitudinal stresses $\sigma_x$. The stress distribution in the cross-section with the largest compressive stress is then used for carrying out the local buckling analysis by using the finite strip method. The beams investigated are subjected to the uniformly distributed transverse load (that is, $\alpha = 90^o$).

#### 4.3.3.1 Influence of Translational and Rotational Spring Stiffness

The influences of the translational and rotational spring stiffnesses are studied for the zed and channel section beams without anti-sag bars when subjected to the uniformly distributed uplift load located at the middle of the top flange shown in Fig.3.1.

**Zed section beams** ($y_q$=-d/2; $z_q$=b/2)

Fig.4.6 show the influence of the translational and rotational spring stiffnesses on the local buckling load $q_{cr}/q_y$ for the simply-supported zed section beams without anti-sag bars subjected to the uniformly distributed uplift load (Zd202_b75_c20_t20 and Zd302_b75_c20_t20). Fig.4.6a is for a zero rotational spring stiffness ($k_\phi$=0) and Fig.4.6b is for an infinite rotational spring stiffness ($k_\phi = \infty$). It can be seen from Fig.4.6a ($k_\phi$=0) that the local buckling loads increase with the increase of translational spring stiffness and the influence of the translational spring stiffness on the local buckling load only occurs in the range $10^{-9}<k_z/E<10^{-7}$. Warping stress is much more obvious when $k_z/E$ is very small. As is to be expected, for the case of $k_\phi = \infty$, the warping stress is zero because the beam is fully restrained in the rotational degree. However, although the cross section is rotationally restrained, the critical loads still increase with the increase of the translational spring stiffness, which is due to the fact that coordinate axes are not coincident with the principle axe of the cross section; therefore, the pre-buckling stress caused by bi-moments can be influenced by the translational spring stiffness.

Fig.4.6c and 4.6d show the influence of the rotational spring stiffness on the local buckling load for the simply-supported zed section beams. Fig.4.6c is for a zero translational spring stiffness ($k_z$=0) and Fig.4.6d is for an infinite translational spring stiffness ($k_z = \infty$). It is clear that the local buckling loads decrease with the increase of the rotational spring stiffness when warping stress is considered, particularly when $k_z$=0.

It can also be seen from the results in Fig.4.6 that for most of the cases the critical loads increase when the warping stress is considered, the most obvious case being when $k_z$=0 and $k_\phi$=0. The local buckling loads for the beams Zd202_b75_c20_t20 are higher than those for the beams Zd302_b75_c20_t20. The warping stress has more effect on Zd202_b75_c20_t20 than on Zd302_b75_c20_t20.

**Channel section beams** ($y_q$=-d/2; $z_q$=b/2-$e_2$)

Fig.4.7 shows the influence of the translational and rotational spring stiffnesses on the local buckling load for the simply-supported channel section beams, without anti-sag bars, subjected to a uniformly distributed uplift load (Cd202_b75_c20_t20 and

Cd302_b75_c20_t20). Fig.4.7a is for a zero rotational spring stiffness ($k_\phi$=0) and Fig.4.7b is for an infinite rotational spring stiffness ($k_\phi = \infty$). It can be seen from Fig.4.7a ($k_\phi$=0) that the local buckling loads decrease with the increase of translational spring stiffness. Again, for the case of $k_\phi = \infty$, the warping stress is zero and the translational spring stiffness does not have any influence on the local buckling because the cross section is under the single moment bending. Figs.4.7c and 4.7d show the influence of the rotational spring stiffness. It can be seen that the loads increase with the increase of translational spring stiffness and the rotational spring stiffness has more influence than the translational spring stiffness.

It can also be seen from the results in Fig.4.7 that the critical loads decrease when warping stress is considered for most of the cases and the most obvious case is that when $k_z$=0 and $k_\phi$=0.

#### 4.3.3.2 Influence of the Dimensions of Cross Section

The influence of the dimensions of the cross section is studied for the zed and channel section beams without anti-sag bars when subjected to a uniformly distributed uplift load applied at the middle of the top flange as shown in Fig.3.1.

**Zed section beams** ($y_q$=-d/2; $z_q$=b/2)

Fig.4.8 shows the influence of the dimensions of the cross section on the critical loads for the simply-supported zed section beams. It is found in Fig.4.8a that the critical load decreases with the increase of flange width when $d$=100mm, but keeps almost constant when $d$=300mm. This is due to the fact that the wider flange tends to buckle locally for the shallow sections; while the compressed part of the web buckles locally for the deeper section. This is also the reason that the significant influence of the ratio of c to b only occurs for the shallow sections ($d$=100mm). It can be seen from Fig.4.8b that the critical loads decrease with the increase of the web depth for most cases except that when flange is wider and lip is longer (b=90mm and c/b=0.4) for which case the influence of section depth is almost neglected, which is also the only case showing the effect of c/b. Fig.4.8c shows that the effects of c/b on the local buckling are only for the shallow section (d=100mm) when c/b is at least 0.27.

**Channel section beams** ($y_q$=-d/2; $z_q$=b/2-$e_2$)

Fig.4.9 show influence of the dimensions of the cross section on the critical loads for the simply-supported channel section beams, subjected to a uniformly distributed uplift load. It can be seen that most of the features are similar to those found in Fig.4.8 for zed section beams, except that the ratio of $c$ to $b$ did not show any effect on the local bucking loads for the investigated examples.

#### 4.3.3.3 Influence of the position of the loading points

The influence of the position of the loading points ($z_q$) is studied for the zed and channel section beams without anti-sag bars when subjected to the uniformly distributed uplift load as shown in Fig.3.1.

**Zed section beams**

Figs.4.10a and 4.10b respectively show the influence of the position of loading point ($z_q$) on the local buckling loads for zed section beams Zd202_b75_c20_t20 and Zd250_b50_c20_t20.

Again, as is expected, for the fully rotational restrained cases ($k_\phi = \infty$) the local buckling loads do not vary with the position of loading point which can be explained by Eq. (3.5). The comparison of Fig.4.10a and 4.10b shows that deeper cross sections have lower local buckling loads. However, when the beam is not rotationally restrained ($k_\phi$=0), warping stresses are generated due to the torsion caused by eccentric loading and so the position of loading point does affect the loading results. For the case of $k_z = \infty$ and $k_\phi$=0, the local buckling loads increase with the increase of the distance $z_q$ between the loading point and the y axis until $z_q$ is around 0.5$b$ for Zd202_b75_c20_t20 and 0.7b for Zd250_b50_c20_t20 where the loads start to decrease, while in the case of $k_z$=0 and $k_\phi$=0, the critical loads are always to decrease with the increased $z_q$.

**Channel section beams**

Figs.4.11a and b respectively show the influence of the position of loading point on the local buckling loads for channel section beams Cd202_b75_c20_t20 and Cd250_b50_c20_t20.

Again, as is expected, for the fully rotational restrained cases ($k_\phi = \infty$) the local buckling loads do not vary with the position of loading point. For the case of $k_z$=0 and $k_\phi$=0, the local buckling loads slightly increase with increased $z_q$ while, in the case of $k_z = \infty$ and $k_\phi$=0, the critical loads decrease with increased $z_q$.

## 4.4 SUMMARY

In this chapter the local buckling behaviour has been investigated for cold-formed zed and channel section beams subjected to pure bending and uniformly distributed transverse loading. By using the presented novel method, the individual influences of warping stress, partial lateral restraints from the sheeting, the dimensions of the cross section and the position of the loading point are also investigated. The following major conclusions can be drawn based on the investigated examples:

⇨ For the beams restrained both translationally and rotationally, subjected to pure bending, the moment capacities calculated using BS 5950 and the finite strip method show the influence of the various cross-section dimensions, which indicate the importance of considering the interactions between the individual elements.

⇨ For the beams under a uniformly distributed transverse loading in a purlin-sheeting system:

- The local buckling loads $q_{cr}/q_y$ of the zed section beams increase with increase in the translational spring stiffness, but decrease with increase in the rotational spring stiffness. The influence of the translational and rotational spring stiffnesses occurs only over a limited range of stiffness values.

- The local buckling loads $q_{cr}/q_y$ of the channel section beams decrease with increase in the translational spring stiffness, but increase with increase in the rotational spring stiffness.

- Warping stress has a significant influence on the local buckling loads; however, the influence is reduced by increases of both the translational and rotational spring stiffnesses.

- As far as local buckling is concerned, the best location for fixing (that is, the loading line) is close to the centre of the flange for zed section beams and to the web line for channel section beams, which provides rather higher local buckling loads.

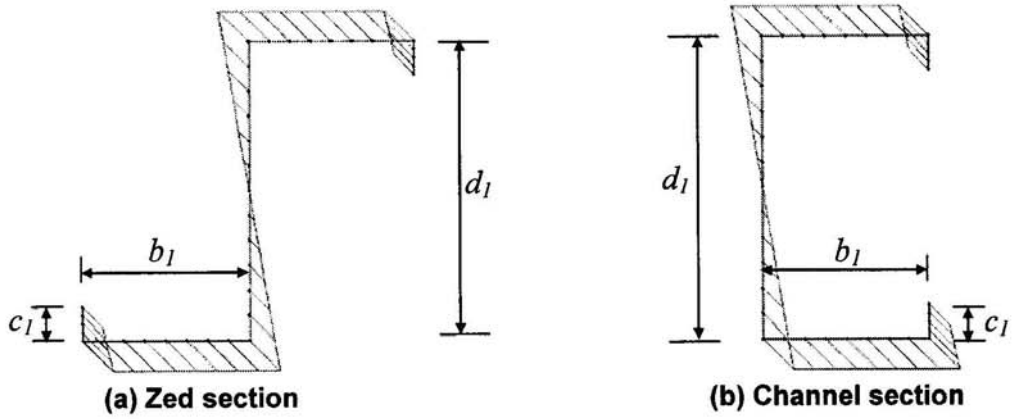


**Fig.4.1 Stress distribution under pure bending**

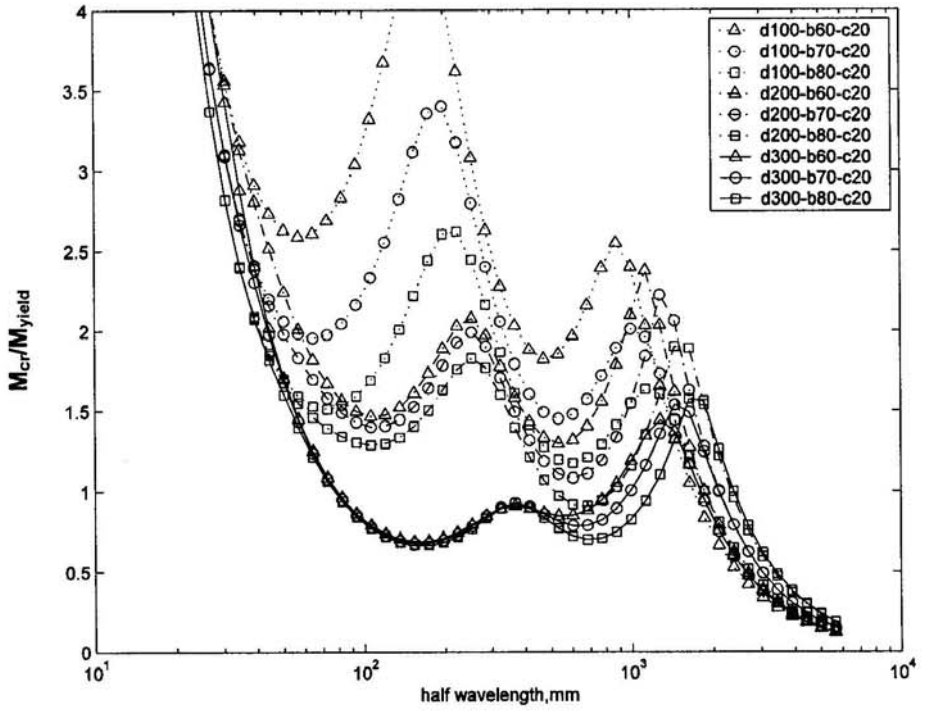


**Fig.4.2 Elastic buckling curves.**

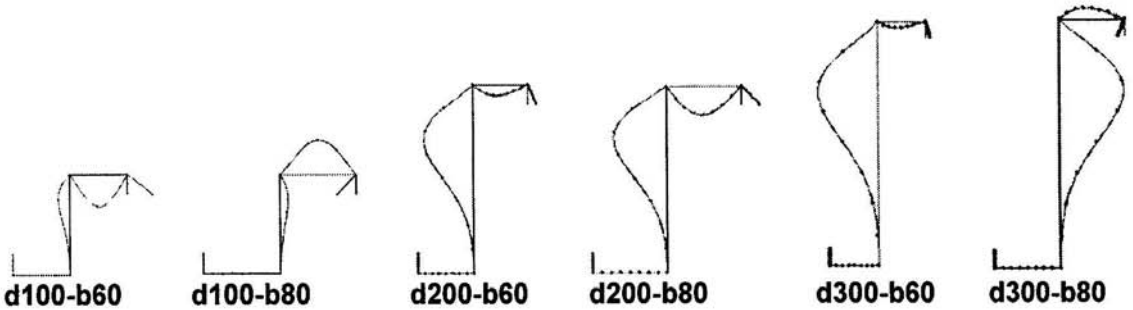


**Fig.4.3 Elastic local buckling modes.**

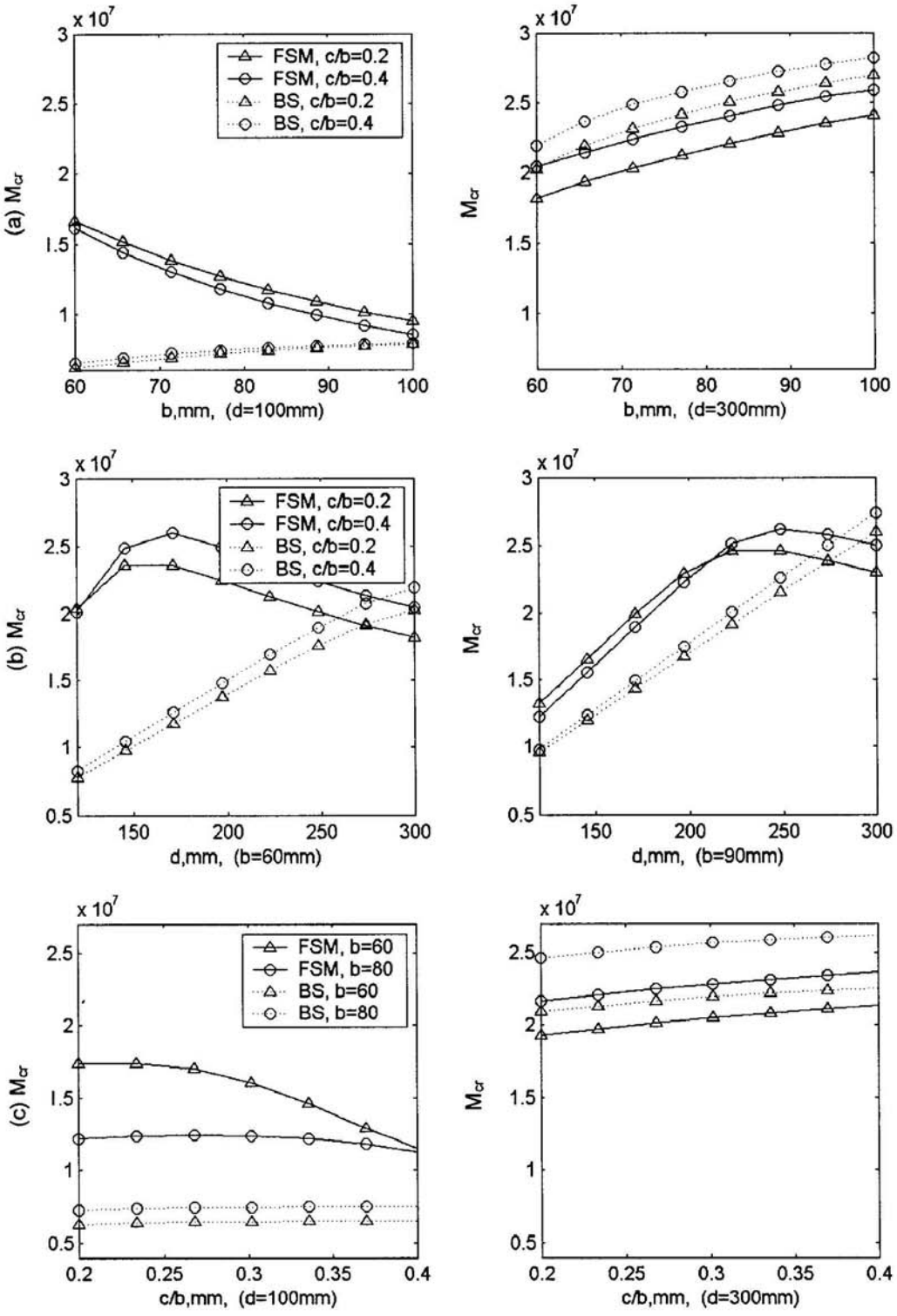


**Fig.4.4 Comparisons of bending moment of local buckling calculated using BS 5950 with those calculated by the finite strip method.**

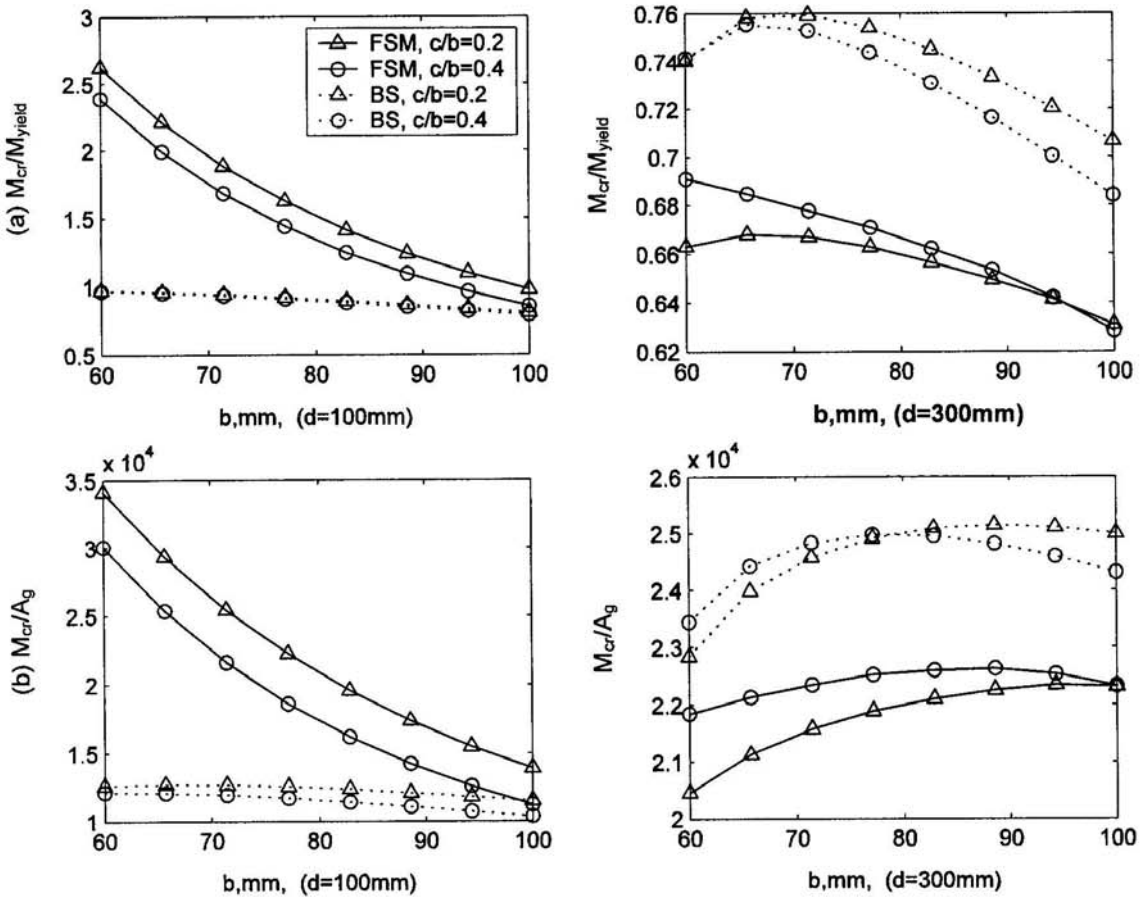


**Fig.4.5 Comparisons of bending moment of local buckling calculated using BS 5950 with those calculated by the finite strip method.**

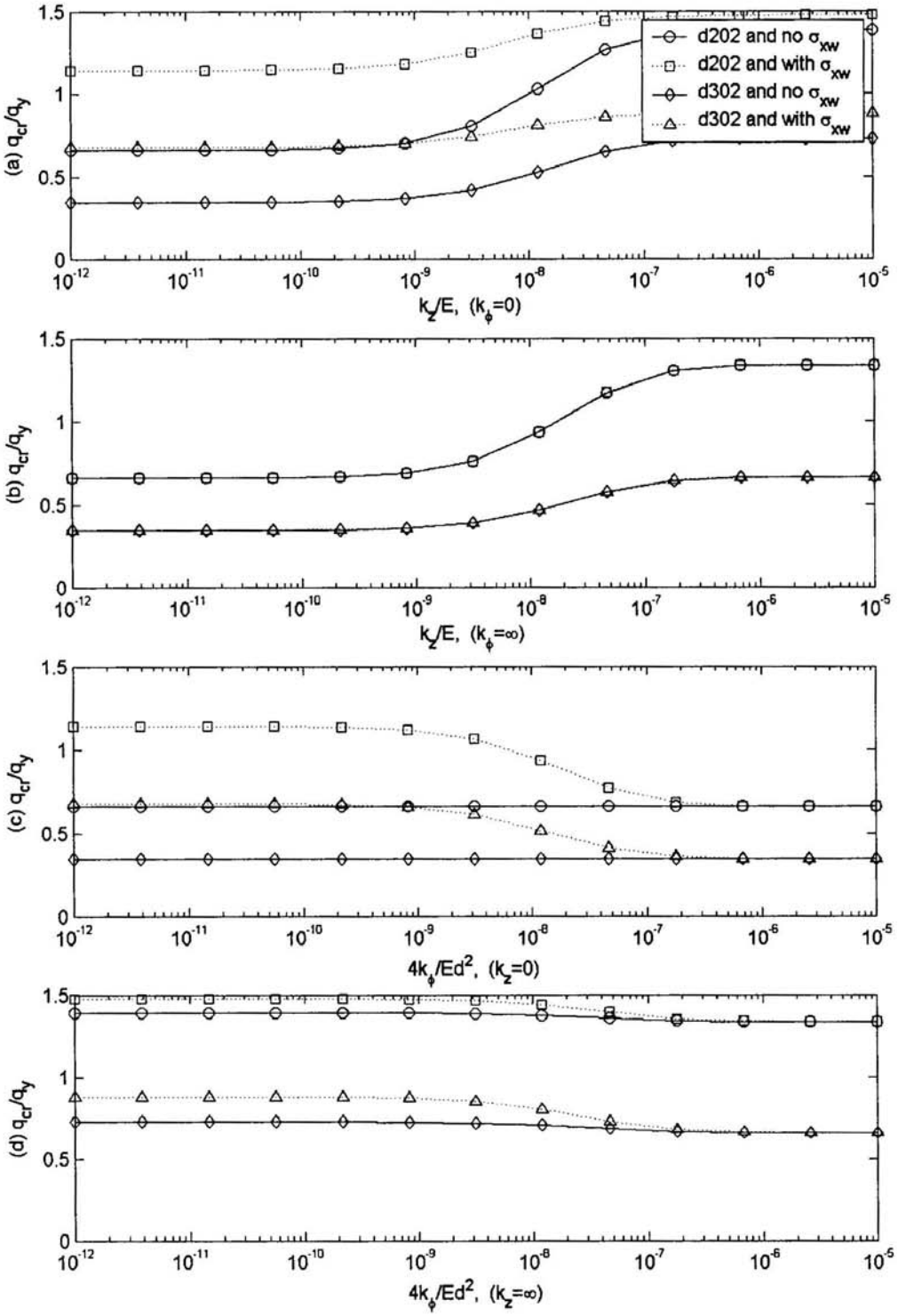


**Fig.4.6 Influence of translational and rotational spring stiffness on the local buckling loads for the simply-supported zed section beams subjected to uniformly distributed uplift load ($y_q$=-d/2, $z_q$=b/2).**

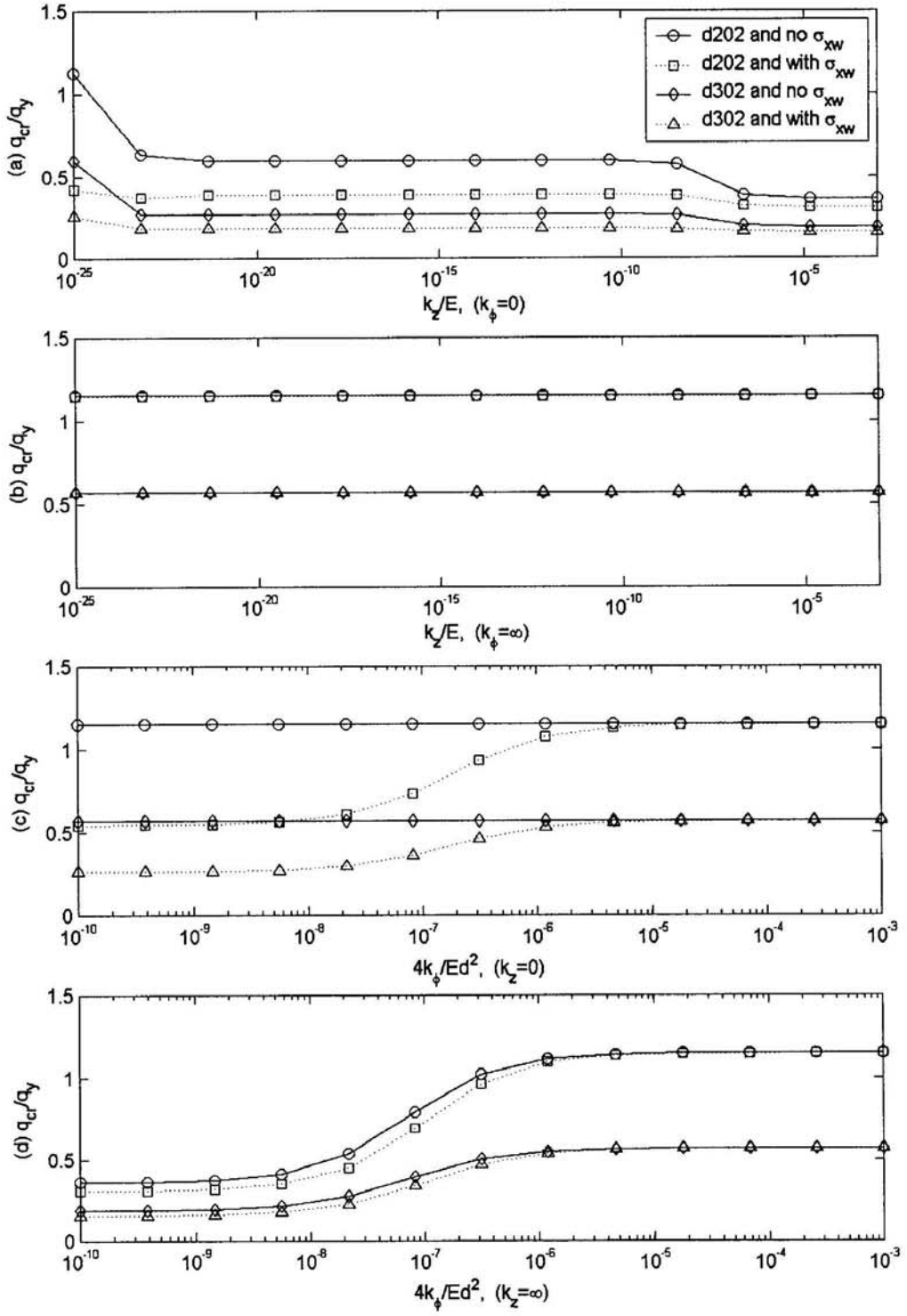


**Fig.4.7 Influence of translational and rotational spring stiffness on the local buckling loads for the simply-supported channel section beams subjected to uniformly distributed uplift load ($y_q$=-d/2, $z_q$=b/2-$e_2$).**

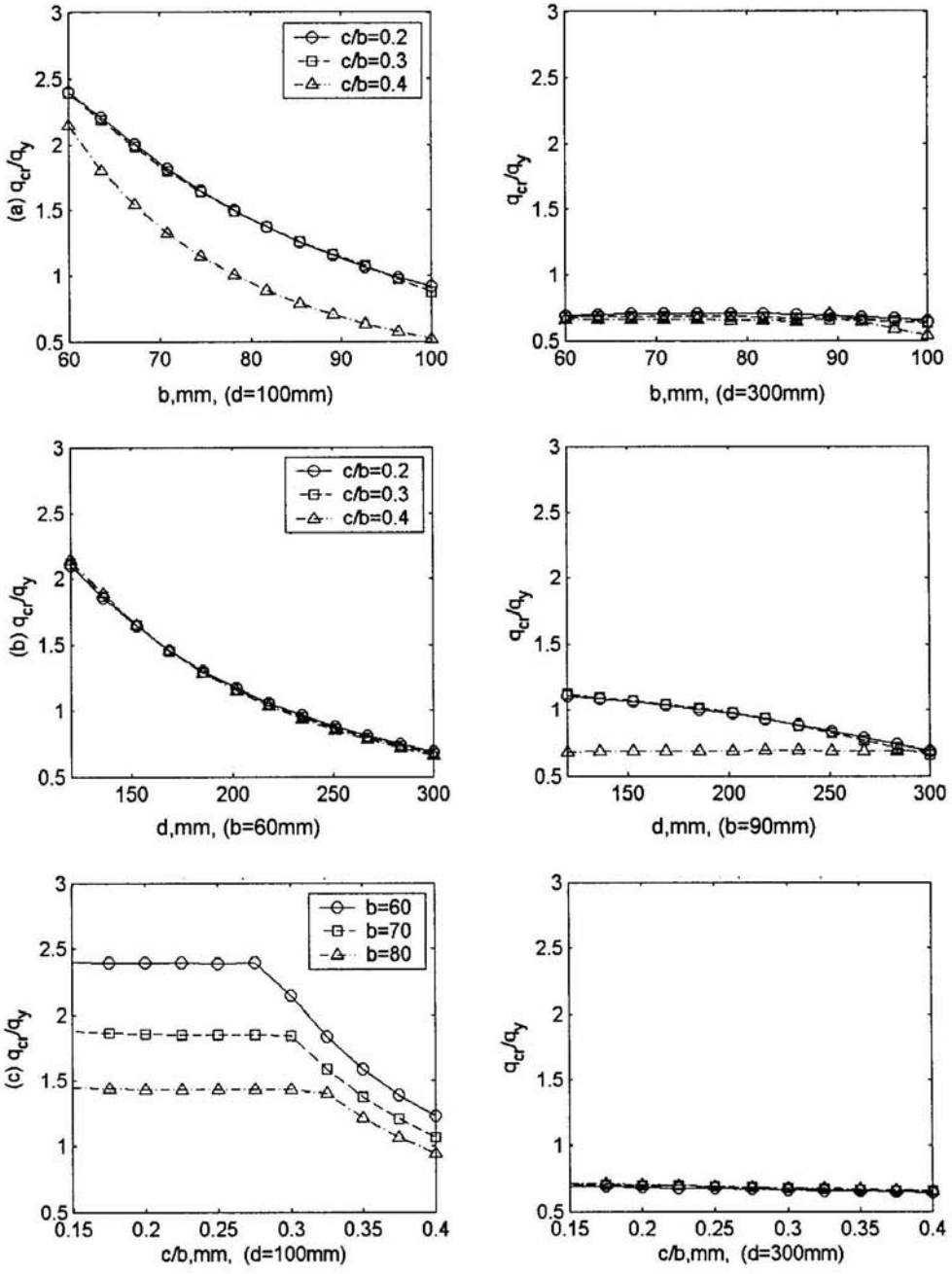


**Fig.4.8 Influence of the dimensions of cross section on the local buckling loads for the simply-supported zed section beams subjected to the uniformly distributed uplift load ($y_q$=-d/2, $z_q$=b/2).**

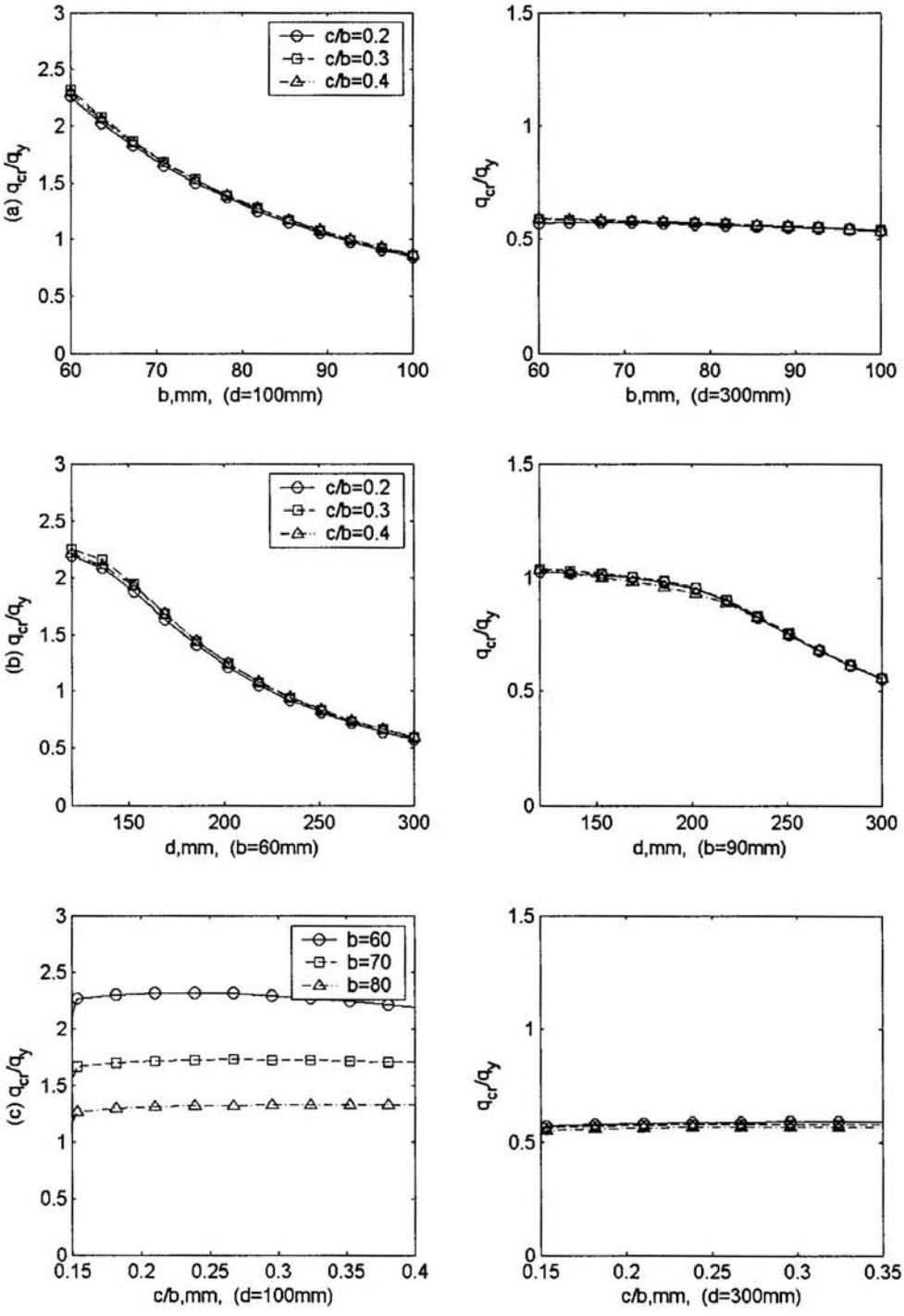


**Fig.4.9 Influence of the dimensions of cross section on the local buckling loads for the simply-supported channel section beams subjected to the uniformly distributed uplift load ($y_q$=-d/2, $z_q$=b/2-$e_2$).**

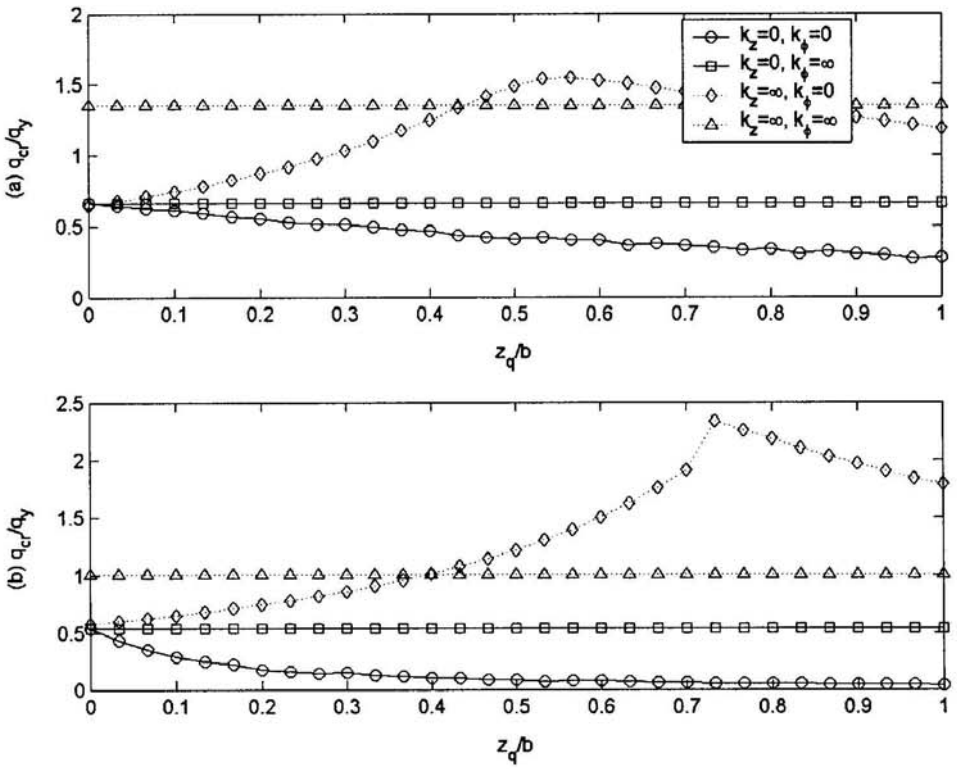


**Fig.4.10 Influence of the position of loading point on the local buckling loads for the simply-supported zed section beams.**

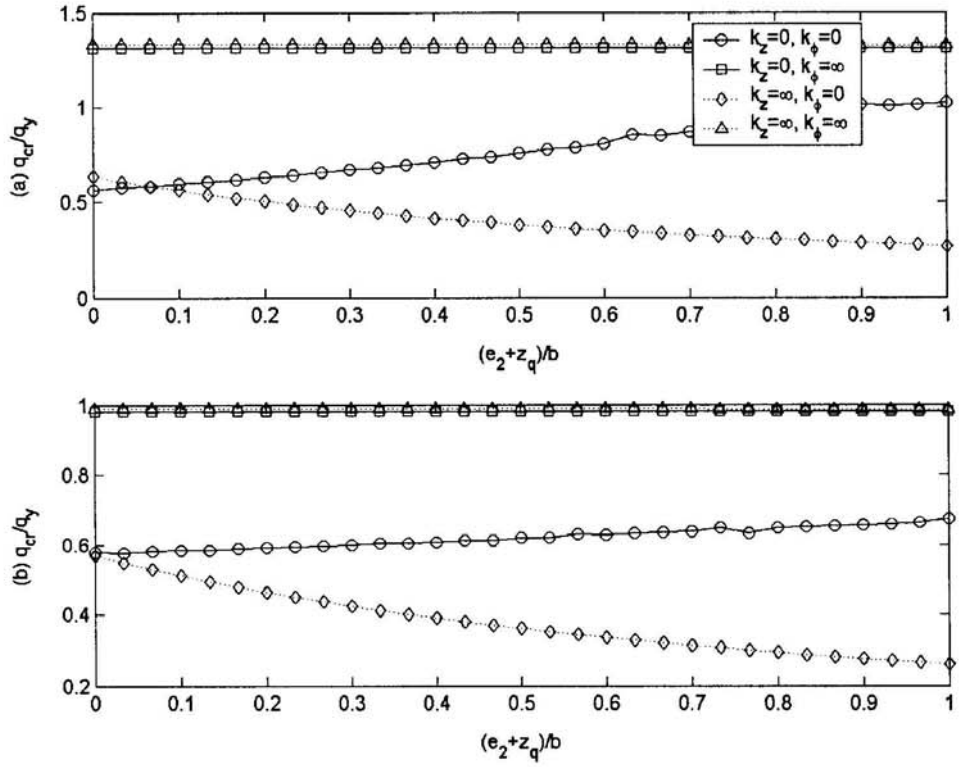


**Fig.4.11 Influence of the position of loading point on the local buckling loads for the simply-supported channel section beams.**

# Chapter 5

# 5 SEMI-ANALYTICAL FINITE STRIP METHOD

## 5.0 CHAPTER SYNOPSIS

A semi-analytical finite strip method is introduced in this chapter to investigate the buckling behaviour of the cold-formed steel zed and channel section beams when subjected to different loads. The focus of the study is on the local and distortional buckling, for which currently available results are only for sections subjected to pure compression and/or pure bending.

The results obtained from this study have shown that, for local buckling there is no practical difference in the critical loads between pure bending and uniformly distributed loading. For distortional buckling, however, remarkable difference exists. The critical load for the uniformly distributed load is generally higher than that for the pure bending. The difference between these two loading cases is found to decrease with the beam length.

# 5.1 INTRODUCTION

It is well known that beams made of cold-formed steel sections may exhibit local, distortional and lateral-torsional buckling. Most design methods used in current standards and specifications that account for local and distortional buckling are based on the effective width concept for stiffened and unstiffened elements. The effective width method was originally developed by Von Karman et al. (1932) and calibrated for cold-formed members by Winter (1968). The method was initially intended to account for local buckling but has now been extended to the distortional bucking of stiffened elements with an intermediate stiffener or edge stiffeners (Schafer, 2003b).

The key part in calculating the effective width is the selection of the technique to determine the critical loads related to local and distortional buckling. The common methods currently employed to calculate these critical loads include analytical methods (Rhodes and Lawson, 1993; Schafer and Pekoz, 1999a; Hancock, 2003), based on various simplified models, and the finite strip method (Hancock, 1997a; Schafer, 2001c & 2003a). However, most of these methods are limited to the members subjected to pure compression or pure bending or a combination of these two loading cases. In other words, the methods cannot be applied to the case where the compressive stresses vary along the longitudinal axis. Apart from these methods, there is one that may be applied to the case of varying stresses, which is the generalized beam theory (GBT) method (Camotim et al., 2004). It is, therefore, surprising that there is no published work regarding its application to the case of varying stresses.

Cold-formed steel sections are usually used as purlins or rails, the intermediate members between the main structural frame and the corrugated roof or wall sheeting in buildings for farming and industrial use. Therefore it is very common that the cold-formed member is subjected to a uniformly distributed transverse load, and so this creates a question - can the critical loads obtained from pure bending be applied to the uniformly distributed loading case? The objective of the chapter is to answer this

question. The chapter is only focused on the local and distortional buckling. The lateral-torsional buckling will be addressed in the next chapter.

## 5.2 SEMI-ANALYTICAL FINITE STRIP METHOD

This section addresses the modification that is incorporated into the conventional finite strip analysis procedure in order to perform the buckling analysis of beams under uniformly distributed loads. Similar to the finite strip method, we consider a strip shown in Fig.2.12. To be consistent with the notations used in the finite strip method addressed in Chapter 2, we use the local coordinate system in which the x- and y-axes are the two axes within the plane of the strip and the z-axis is normal to the plane of the strip. The three displacements of the strip at a point $(x,y)$ can be expressed in terms of the nodal displacements as follows (Schafer, 2003a; Boresi et al. 2002):

$$\begin{Bmatrix} u(x,y) \\ v(x,y) \end{Bmatrix} = \sum_{m=1} \begin{bmatrix} \sin\dfrac{m\pi y}{a_s} & 0 \\ 0 & \cos\dfrac{m\pi y}{a_s} \end{bmatrix} \begin{bmatrix} 1-\dfrac{x}{b_s} & 0 & \dfrac{x}{b_s} & 0 \\ 0 & 1-\dfrac{x}{b_s} & 0 & \dfrac{x}{b_s} \end{bmatrix} \begin{Bmatrix} u_{1m} \\ v_{1m} \\ u_{2m} \\ v_{2m} \end{Bmatrix} \tag{5.1}$$

$$w(x,y) = \sum_{m=1} \sin\frac{m\pi y}{a_s} \begin{bmatrix} 1-\dfrac{3x^2}{b_s^2}+\dfrac{2x^3}{b_s^3} & x-\dfrac{2x^2}{b_s}+\dfrac{x^3}{b_s^2} & \dfrac{3x^2}{b_s^2}-\dfrac{2x^3}{b_s^3} & \dfrac{x^3}{b_s^2}-\dfrac{x^2}{b_s} \end{bmatrix} \begin{Bmatrix} w_{1m} \\ \theta_{1m} \\ w_{2m} \\ \theta_{2m} \end{Bmatrix} \tag{5.2}$$

where $u(x,y)$ and $v(x,y)$ = the plane displacements;

$w(x,y)$ = the deflection;

$(u_{1m}, v_{1m}, w_{1m}, \theta_{1m})$ and $(u_{2m}, v_{2m}, w_{2m}, \theta_{2m})$ = the nodal displacements associated with wave number m;

$a_s$ and $b_s$ = the length and width of the strip, respectively.

The assumed displacement functions satisfy the simply supported boundary conditions. The strain energy of the strip can be expressed as

$$U = \frac{Et}{2(1-\nu^2)} \int_o^a \int_o^b [(\varepsilon_x + \varepsilon_y)^2 - 2(1-\nu)(\varepsilon_x \varepsilon_y - \frac{\gamma_{xy}^2}{4})]dxdy + \frac{Et^3}{24(1-\nu^2)} \int_o^a \int_o^b [(\kappa_x + \kappa_y)^2 - 2(1-\nu)(\kappa_x \kappa_y - \kappa_{xy}^2)]dxdy \tag{5.3}$$

where E = Young's modulus;

$\nu$ = Poisson's ratio;

t is the thickness of the strip.

The membrane and bending strains in Eq. (5.3) are defined as follows

$$\varepsilon_x = \frac{\partial u}{\partial x}, \quad \varepsilon_y = \frac{\partial v}{\partial y}, \quad \gamma_{xy} = \frac{\partial u}{\partial y} + \frac{\partial v}{\partial x}$$
$$\kappa_x = -\frac{\partial^2 w}{\partial x^2}, \quad \kappa_y = -\frac{\partial^2 w}{\partial y^2}, \quad \kappa_{xy} = -\frac{\partial^2 w}{\partial x \partial y} \tag{5.4}$$

The element stiffness matrix can be obtained by substituting Eqs. (5.1) and (5.2) into (5.4) and then into (5.3). Note that for each wave number the element stiffness matrix is independent and thus the global stiffness matrix consists of M sub-stiffness matrices sitting on the diagonal location (where M is the total number of waves).

The element geometric stiffness matrix can be derived based on the work done by the membrane stresses through the nonlinear strains of the buckling displacements as follows (Schafer, 2003a)

$$W = \frac{1}{2} \int_o^a \int_o^b f(y)[T_1 - (T_1 - T_2)\frac{x}{b}][(\frac{\partial u}{\partial y})^2 + (\frac{\partial v}{\partial y})^2 + (\frac{\partial w}{\partial y})^2]dxdy \tag{5.5}$$

where $T_1$ and $T_2$ = the tractions at nodes 1 and 2 (see Fig.2.13), respectively;

$f(y)$ = the function defining the variation of the compressive stress along the longitudinal axis.

Obviously, for either pure compression or pure bending $f(y)$=1. For beams subjected to a uniformly distributed load $f(y) = 4(ay - y^2)/a^2$. The element geometric stiffness matrix can be obtained by substituting Eqs. (5.1) and (5.2) into (5.5). Note,

because $f(y) \neq 1$, the element geometric stiffness matrix is coupled about the wave number. After the assembly of the element matrices, the following global matrix equation can be obtained:

$$\begin{bmatrix} [K_1] & 0 & \dots & 0 \\ & [K_2] & \dots & 0 \\ & & \dots & \dots \\ & & & [K_M] \end{bmatrix} \begin{Bmatrix} \{d_1\} \\ \{d_2\} \\ \\ \{d_M\} \end{Bmatrix} = \lambda \begin{bmatrix} [K_{g11}] & [K_{g12}] & \dots & [K_{g1M}] \\ & [K_{g22}] & \dots & [K_{g2M}] \\ & & \dots & \dots \\ & & & [K_{gMM}] \end{bmatrix} \begin{Bmatrix} \{d_1\} \\ \{d_2\} \\ \\ \{d_M\} \end{Bmatrix} \tag{5.6}$$

where $[K_m]$ and $[K_{gmm}]$ = the global stiffness matrix and global geometric stiffness matrix associated with wave number $M$; the expressions of which can be found in Appendix 1;

$[K_{gmn}](= [K_{gnm}])$ = the coupled global geometric stiffness matrix associated with wave number $m$ and $n$, the expression of which is given in the Appendix 1;

$\{d_m\}$ = the nodal displacement vector associated with wave number $m$;

$\lambda$ is the loading factor.

The critical load can be obtained by solving the eigen-value matrix Eq. (5.6).

## 5.3 NUMERICAL EXAMPLES

In this section, the buckling behavior of simply-supported cold-formed channel and zed section beams is investigated using the semi-analytical finite strip method addressed in Section 5.2.

In order to illustrate the application and to provide a better grasp of the capabilities of this approach, two numerical examples are presented and briefly discussed in this section. The first example relates to a section of depth d=250 mm, flange width b=50 mm, lip length c=20 mm and thickness t=1.9 mm (d250_b50_c20_t19), which is dominated by local buckling. In the second example the section has a depth of d=202 mm, flange width b=75 mm, lip length c=20 mm and thickness t=2.3 mm (d202_b75_c20_t23) and it is dominated by distortional buckling. Their material

properties are listed in Table 3.1. Two different loading cases, pure bending or uniformly distributed loading (applied at shear centre), are discussed.

### 5.3.1 Channel-section Beams

The bending moment diagrams and the corresponding stress distribution within the cross-section for these two different loading cases are plotted in Fig.5.1.

Fig.5.2 shows the typical buckling curves of the simply supported channel section beam (Cd250_b50_c20_t19) subjected to pure bending, in which $m$ is the number of half-waves. The buckling curve corresponding to $m$=1 exhibits two local minima associated with local buckling and distortional buckling, the features of which are well known and have been explained by many investigators (Hancock, 1997a; Schafer, 2003a). It can be seen that the critical load for local buckling is lower than that for distortional buckling. This is particularly so for deep channels with narrow flanges. Note that the buckling curve only provides information about how and when the beam buckles. The actual critical load of the beam for a given length should be taken as the lowest value from all of the buckling curves of the same length. The critical loads obtained in such a way are plotted in Fig.5.3. In order to identify the buckling mode associated with the critical load, the buckling curve corresponding to m=1 is also superimposed in the figure. It is seen from the figure that these two curves coincide in the two end regions, which indicates that the buckling modes of the beam in these two regions are essentially of a single wave. The difference between the two curves is apparent in the mid part, where the critical load curve is below the buckling curve and, except in the beginning part of the region where the critical load varies slightly, representing the interaction between different waves, in the majority of this central region the critical load is virtually constant, representing the local buckling mode of equal half-wavelengths. These features are clearly demonstrated by the buckling modes plotted in Fig.5.3.

The beam subjected to pure bending is an ideal case. In reality, particularly for cold-formed steel members, the beam is usually subjected to uniformly distributed transverse loading in which case the longitudinal stress varies not only within the cross-section but also along the longitudinal axis. When the longitudinal stress varies

along the longitudinal axis, the buckling modes associated with the wave number are coupled and therefore the conventional finite strip analysis method with a single wave can no longer be applied. Fig.5.4 shows the critical load curve of the channel-section beam (Cd250_b50_c20_t19), subjected to a uniformly distributed load, obtained by using the present semi-analytical method. In order to demonstrate the difference in buckling behaviour between pure bending and uniformly distributed loading, the buckling curves ($m$=1) for the two loading cases and the critical load curve for the pure bending are superimposed on the figure.

Comparing the two buckling curves it can be seen that both curves have a similar pattern although, for any beam length, significantly lower critical loads are associated with pure bending as opposed to uniformly distributed loading. The difference between the two buckling curves is attributed to the difference in the longitudinal stresses in the two loading cases. For pure bending, the longitudinal stress is constant along the longitudinal axis while, for uniformly distributed load, it varies parabolically. As a consequence of this variation, the buckling modes with different m values are coupled with each other. This indicates that the half-wavelengths would be different in different regions if the buckling mode has multiple half-waves. This is demonstrated by the critical load curve of the channel subjected to the uniformly distributed load, in Fig.5.4 which shows a further decrease after the local minima in the corresponding buckling curve is reached, which is clearly different from the critical load curve of the channel subjected to pure bending. Fig.5.4 shows that in both cases the critical load curve is close to the buckling curve for either very short or very long beams, indicating that, in either region the local or lateral-torsional buckling mode is dominated by the single half-wave. In the central region, the critical load, for uniformly distributed loading, decreases with increasing beam length. With the longer beams, this value approaches the corresponding critical load for local buckling for a similar beam subjected to pure bending, but it slightly exceeds this limiting value. This is attributed to the individual half-wavelengths being not equal when the beam buckles locally. For long beams, the dominant local buckling occurs in the central part where the moment is higher; as is demonstrated by the buckling mode plotted in Fig.5.4 which, compared to the whole beam length, is much shorter and so the variation of the longitudinal stress due to the moment gradient over this half-wavelength may be neglected. This implies that for most beams, which are longer

than 1 m, as shown in the figure, the critical loads for local buckling are very close for these two different loading cases.

The second example is for a similar channel but the section depth is slightly shallower and the flange is slightly wider than those in the first example (Cd202_b75_c20_t23). It is known that shallow channels with wide flanges can easily buckle distortionally (Schafer & Pekoz, 1999a; Schater, 2003a). This is demonstrated by the buckling curves of the channel subjected to a pure bending, shown in Fig.5.5, in which the second local minima, representing distortional buckling, is much lower than the first local minima, representing local buckling. The corresponding critical load curve for the channel is plotted in Fig.5.6, from which one can easily see three different buckling regions, local, distortional and lateral-torsional buckling, controlled by the beam length. In reality, local buckling would be highly unlikely as most practical beams are longer than 1 m. Nevertheless the figure shows how the buckling modes are influenced by the length of the beam.

The buckling behaviour of the same channel under a uniformly distributed load is shown in Fig.5.7. Again, in order to identify the difference in buckling behaviour between pure bending and uniformly distributed load, the corresponding results from pure bending are superimposed on the figure. Unlike the critical load curve for pure bending, the critical load curve for uniformly distributed loading does not have any clear buckling regions and the distortional buckling mode is highly influenced by the beam length. This leads the critical load to decrease continuously with beam length. Comparing the two critical load curves shown in Fig.5.7, it can be seen that the critical load for uniformly distributed loading is significantly greater than that for pure bending. The minimum difference between the two curves is about 17%, which is obviously not negligible.

The results shown in Fig.5.8 are for the channel restrained both laterally and rotationally at the corner between web and the flange subjected to tensile stresses. As the section is restrained, lateral-torsional buckling does not occur (Ye et al. 2002 & 2004) and so the difference between the two critical load curves for long beams still reveals the difference in distortional buckling for the two loading cases. This difference between the two curves is clearly present for beams up to 7 m long. For

example, the difference in the critical loads between the uniformly distributed load and pure bending is about 15% for a 3 m beam and 8% for a 7 m beam. It is also evident, from the buckling modes plotted in Fig.5.8, that distortional buckling is mainly located in the central region where the compressive stresses are the highest.

In conclusion, the comparison of the present results with the critical loads for the same channel sections subjected to pure bending has shown that, for local buckling, there is no practical difference in the critical loads between the two loading systems but, for distortional buckling, significant differences exist. The critical load for uniformly distributed loading is generally higher than that for pure bending. For most practical cases the difference in the critical loads between uniformly distributed loading and pure bending is not negligible although it decreases with the beam length. Finally, it should be pointed out that the approximation method presented here is only for the beam with simply-supported boundary conditions which, however, are sufficient to investigate the behaviour of local and distortional buckling. For other boundary conditions the displacement functions expressed in Eqs.(5.1) and (5.2) have to be modified.

### 5.3.2 Zed-section Beams

For zed-section beams two different loading cases, pure bending and uniformly distributed transverse loading (applied at the shear centre), are discussed here. For each loading case two different stress distributions are investigated which are with respect to when the section is (a) fully restrained in its lateral and rotational degrees and (b) entirely unrestrained. The stress distributions in the cross-section corresponding to these two cases are shown in Fig.5.9 and can be mathematically expressed as (Ye et al. 2002 & 2004),

$$\text{(a) } \sigma_x(y,z) = \frac{M_{yield}\, y}{I_z} \qquad \text{for the restrained section} \qquad (5.7)$$

$$\text{(b) } \sigma_x(y,z) = \frac{M_{yield}}{I_y I_z - I_{yz}^2}(I_y y - I_{yz} z) \qquad \text{for the unrestrained section} \qquad (5.8)$$

where $M_{yield} = 2\sigma_y I_z / d$ is the yield moment.

Fig.5.10 shows the typical buckling curves of the simply supported zed-section beam (Zd250_b50_c20_t19) subjected to the pure bending stress shown in Fig.5.9a. It is seen that the buckling curves for different wave numbers, m, exhibit very similar features, in which the local minima are associated with local buckling and distortional buckling, as demonstrated by the plotted buckling modes. These features are well known and have been explained by many investigators (Hancock, 1997a; Schafer, 2001c & 2003a). Since the section is fully restrained the lateral-torsional buckling is replaced by a secondary distortional buckling. Note that the buckling curves only provide information about how and when the beam buckles. The actual critical load of the beam for a given length should be taken as the lowest value from all of the buckling curves of the same length, that is, the critical load curve which is plotted by the solid line in Fig.5.10. It is seen from the critical load curve that, the critical load associated with local buckling undergoes an initial decrease followed by a ripple area before it reaches constant. The critical load of the constant value for different beam lengths implies that the local buckling modes in beams of different lengths have almost equal wavelength. This can be demonstrated by examining the buckling modes of 135 m and 270 m beams.

As mentioned before, the beam subjected to pure bending is an ideal case. In reality, particularly for cold-formed steel members, the beam is normally subjected to a uniformly distributed transverse load in which case the longitudinal stress varies not only within the cross-section but also along the longitudinal axis. Fig.5.11 shows the critical load curve and the corresponding buckling modes of the same zed-section beam subjected to a uniformly distributed load (stress distribution (a) in Fig.5.9), obtained by using the present semi-analytical method. In order to demonstrate the difference in buckling behaviour between pure bending and uniformly distributed loading, the critical load curve for the pure bending is also superimposed in the figure.

Comparing the two critical load curves one can see two significant differences between the two curves. The first difference is that the critical load is higher in the uniformly distributed loading case than in the pure bending case. The second difference is that the critical load for local buckling in the uniformly distributed loading case decreases continuously with the beam length. In additional to the local

buckling, Fig.5.11 also shows the significant difference between the two loading cases in relating to the secondary distortional buckling. These differences may be explained by examining their buckling modes. For pure bending beam the local buckling exhibits an equal-wavelength multi-waves mode, as is shown in Fig.5.10, while for uniformly distributed loading beam the local buckling exhibits a multi-waves mode of unequal wavelengths, as is shown in Fig.5.11. As it is mentioned before, the critical load is mainly dominated by the shortest wavelength. The stress gradient along the shortest wavelength, which is located in the central part of the beam, is dependent on the span length of the beam. The longer the beam is, the smaller the stress gradient will be. This is why the critical loads related to local buckling for the two different loading cases become close when the beam length increases.

Fig.5.12 shows the buckling curves of the same zed-section beam subjected to the pure bending stress shown in Fig.5.9b. Interestingly, for the section with no lateral and rotational restraints the beam buckles only locally or lateral-torsionally; there is no distortional buckling. The critical load curve shown in Fig.5.12 has the similar feature as that shown in Fig.5.10 and thus is not discussed further here.

The comparison of the critical loads between pure bending and uniformly distributed loading for this unrestrained beam (that is, the stress distribution (b) shown in Fig.5.9) is shown in Fig.5.13. Again, it can be seen that the critical load is higher in the uniformly distributed case than in the pure bending case. The difference (for the local buckling) between the two loading cases decreases quickly with the beam length. For example, the difference is less than 5% for a 2 m long beam. This indicates that, as far as local buckling is concerned, there is no practical difference in the critical loads between the two loading cases.

Fig.5.14 shows the buckling curves of the second zed-section beam (Zd202_b75_c20_t23) under the pure bending stress shown in Fig.5.9a. The pattern of the buckling curves shown here is similar to that shown in Fig.5.10 except for that the critical load corresponding to local buckling is now higher than that corresponding to distortional buckling. This is particularly so for shallow sections with large flange widths. The critical load curve shown in Fig.5.14 indicates that the beam will exhibit

either a local buckling (if it is extremely short) or distortional buckling. The buckling modes for different beam lengths are also plotted in the figure.

The comparison of critical loads between the pure bending and uniformly distributed loading for the unrestrained section is shown in Fig.5.15. It is evident that the critical load corresponding to uniformly distributed loading is significantly higher than that corresponding to pure bending, although for both local and distortional buckling, the differences between the two loading cases decrease with the beam length. For example, for a 5 m long beam, the critical load of a uniformly distributed loading beam is 12% higher than that of the pure bending beam.

Fig.5.16 shows the buckling curves and corresponding critical load curve for the second zed-section beam when subjected to the pure bending stress shown in Fig.5.9b. Similar to that shown in Fig.5.12, the unrestrained beam buckles only locally or lateral-torsionally. The critical load corresponding local buckling varies slightly for very short beams, representing the change in wavelength, and then becomes constant for long beams, representing the constant wavelength in multiple-waves buckling modes. The difference in critical loads between pure bending and uniformly distributed loading is shown in Fig.5.17. Again, the difference reduces quickly with the increase of beam length. For example, for a 2 m long beam, the difference between the two loading cases is only about 3%.

## 5.4 SUMMARY

The local and distortional buckling behaviour of the cold-formed steel zed and channel section beams subjected to a uniformly distributed load has been investigated using a semi-analytical method. The results obtained from this study have shown that:

- For local buckling there is no practical difference in the critical loads for the same cross section between pure bending and uniformly distributed loading. Thus, the approach introduced in Chapter 4 is still valid.

- For distortional buckling, however, remarkable difference between the two loading cases was found. The critical load corresponding to uniformly distributed loading is higher than that corresponding to pure bending. Their difference decreases with the increase of beam length.

- For either local buckling or distortional buckling, the beam subjected to pure bending exhibits the multi-wave buckling mode of equal wavelength, while the beam subjected to uniformly distributed loading exhibits the multi-wave buckling mode of unequal wavelengths.

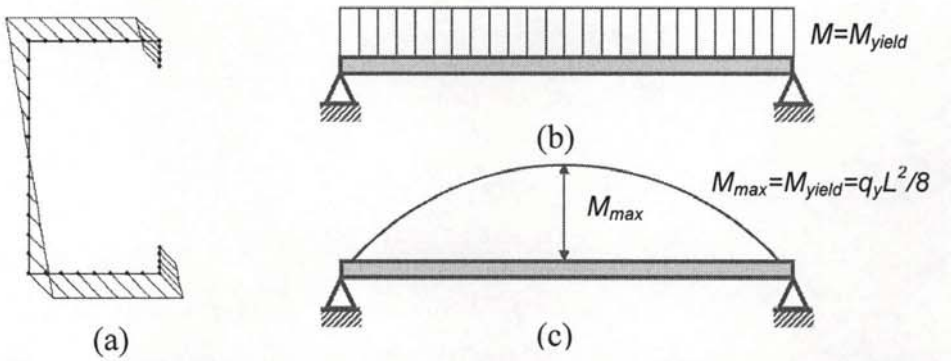


**Fig.5.1 (a) Stress distribution within cross-section, (b) bending moment diagram for pure bending and (c) bending moment diagram for uniformly distributed loading. ($M_{yield}$ is the yield moment and $q_y$ is the yield distributed load).**

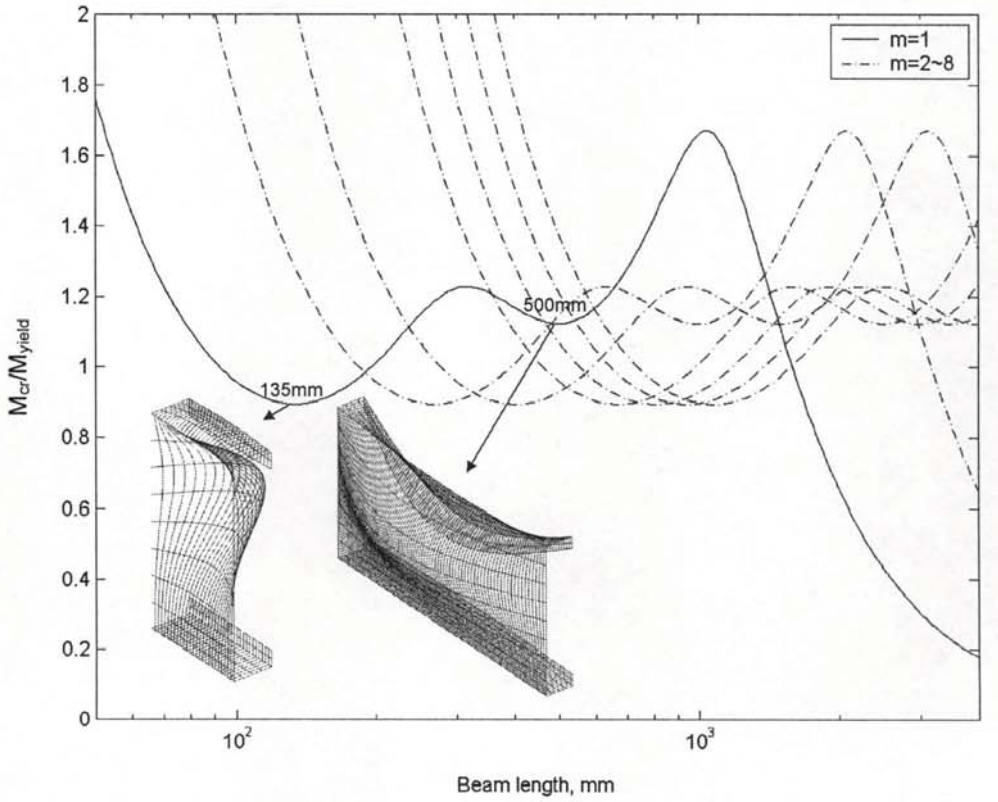


**Fig.5.2 Buckling curves of simply supported channel under pure bending (d=250mm, b=50mm, c=20mm, t=1.9mm).**

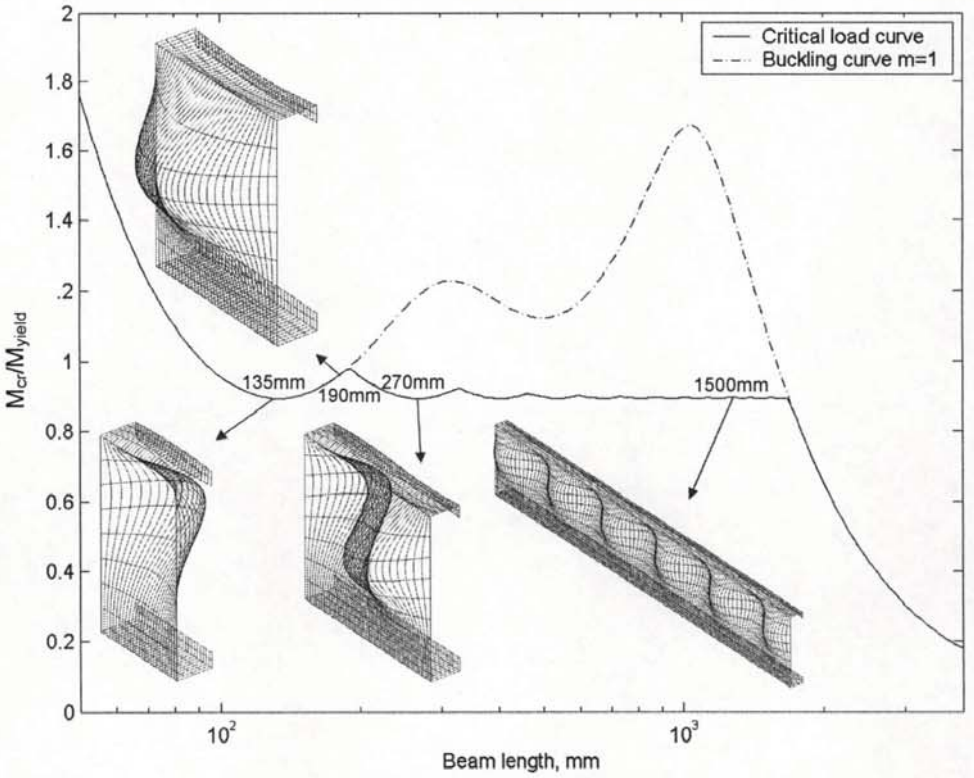


**Fig.5.3 Critical load curve of simply supported channel under pure bending (d=250mm, b=50mm, c=20mm, t=1.9mm).**

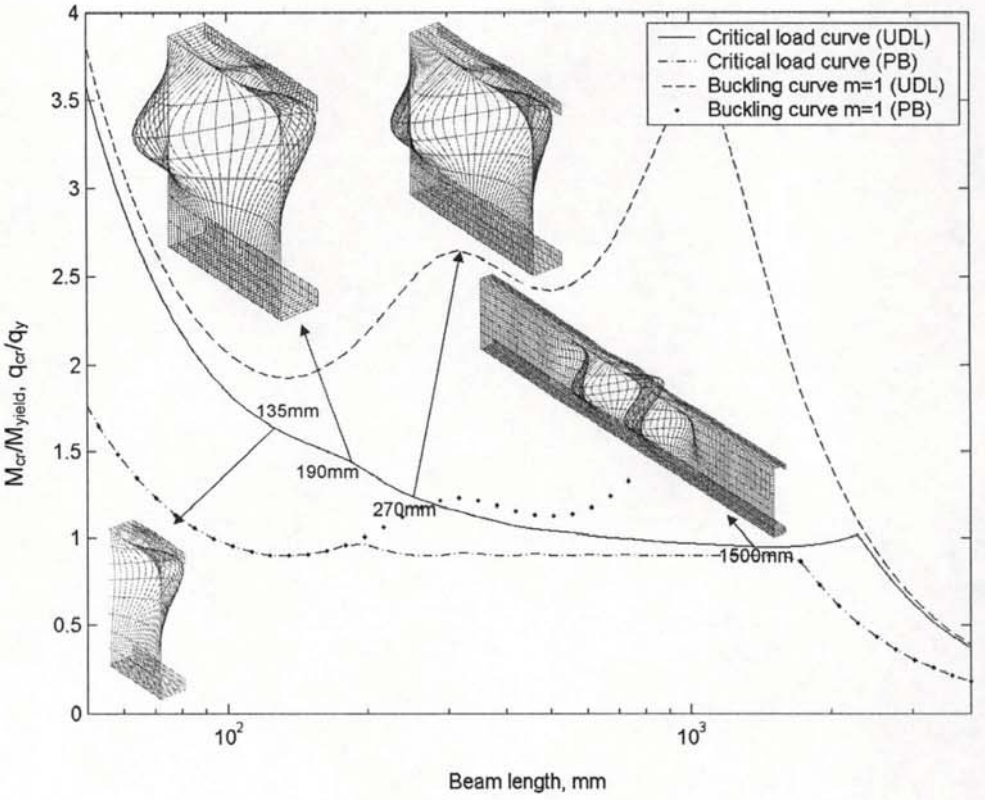


**Fig.5.4 Critical load curve of simply supported channel under a uniformly distributed transverse load (d=250mm, b=50mm, c=20mm, t=1.9mm).**

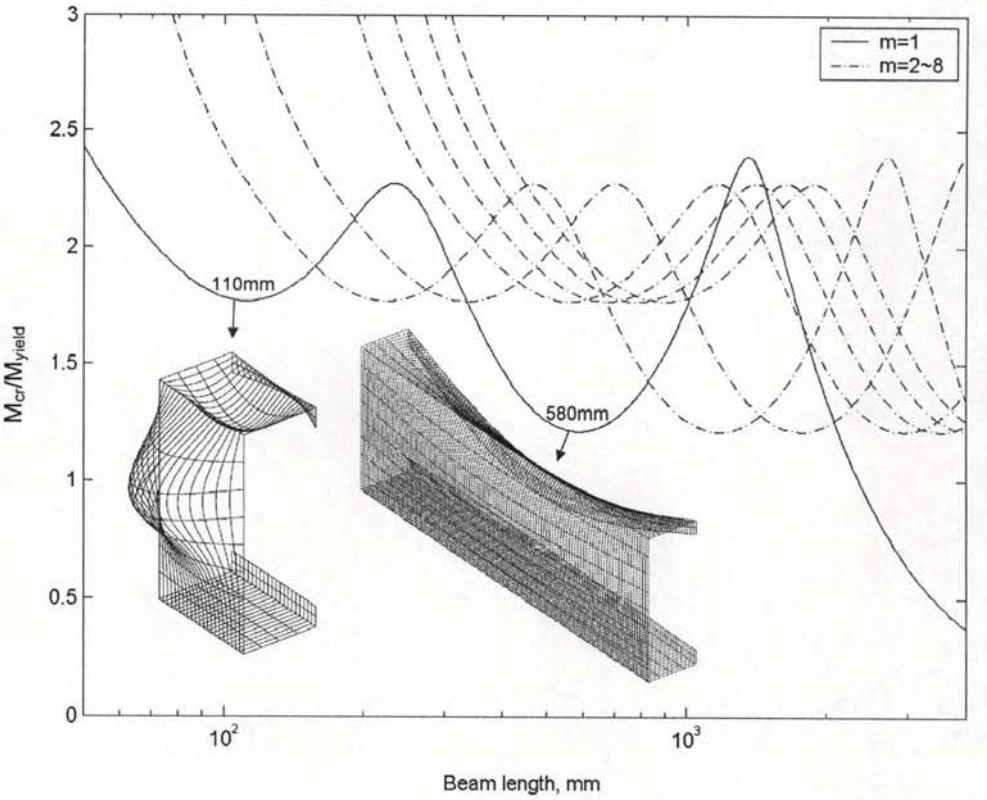


**Fig.5.5 Buckling curves of simply supported channel under pure bending (d=202mm, b=75mm, c=20mm, t=2.3mm).**

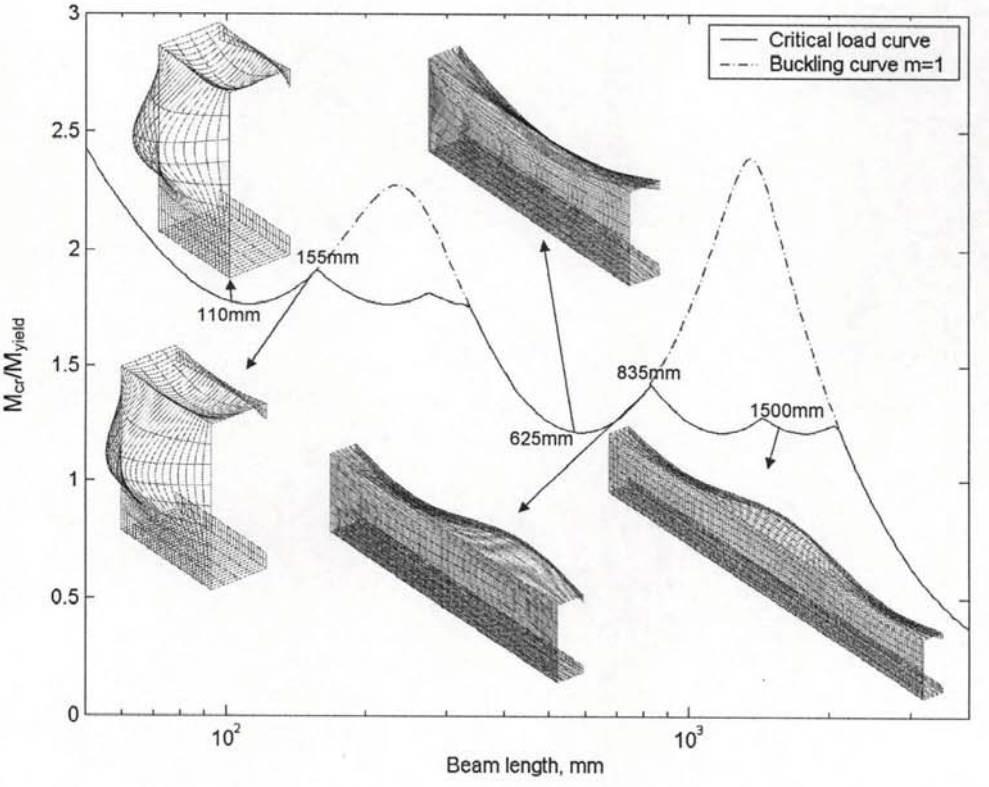


**Fig.5.6 Critical load curve of simply supported channel under pure bending (d=202mm, b=75mm, c=20mm, t=2.3mm).**

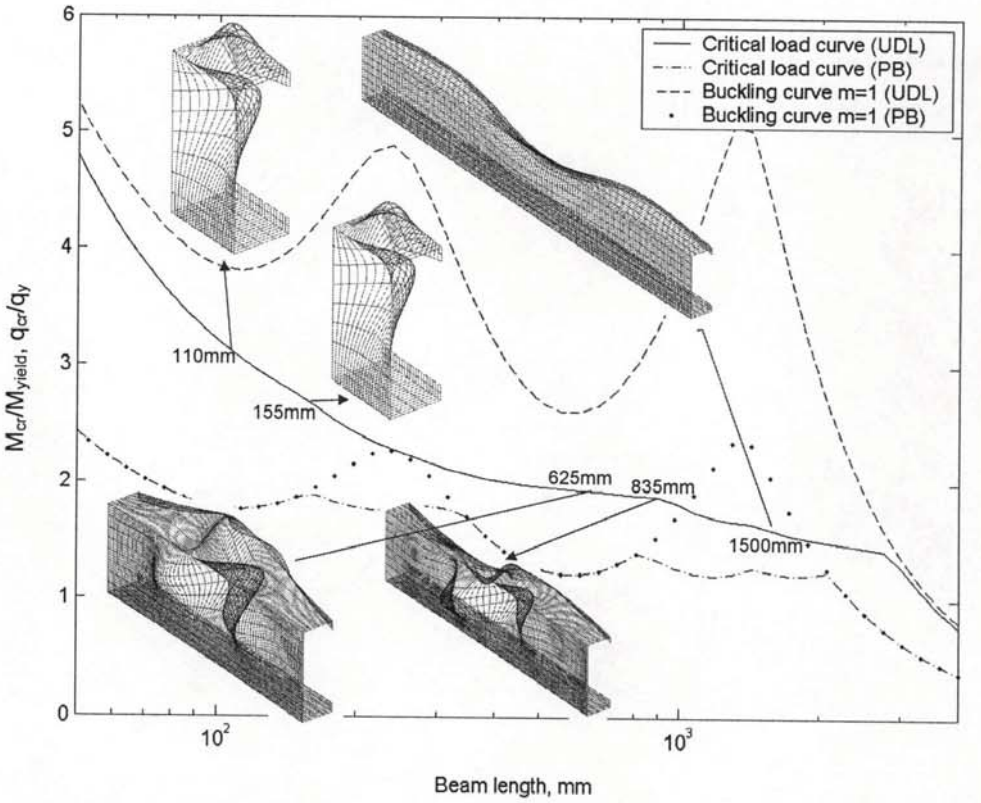


**Fig.5.7 Critical load curve of simply supported channel under a uniformly distributed transverse load (d=202mm, b=75mm, c=20mm, t=2.3mm).**

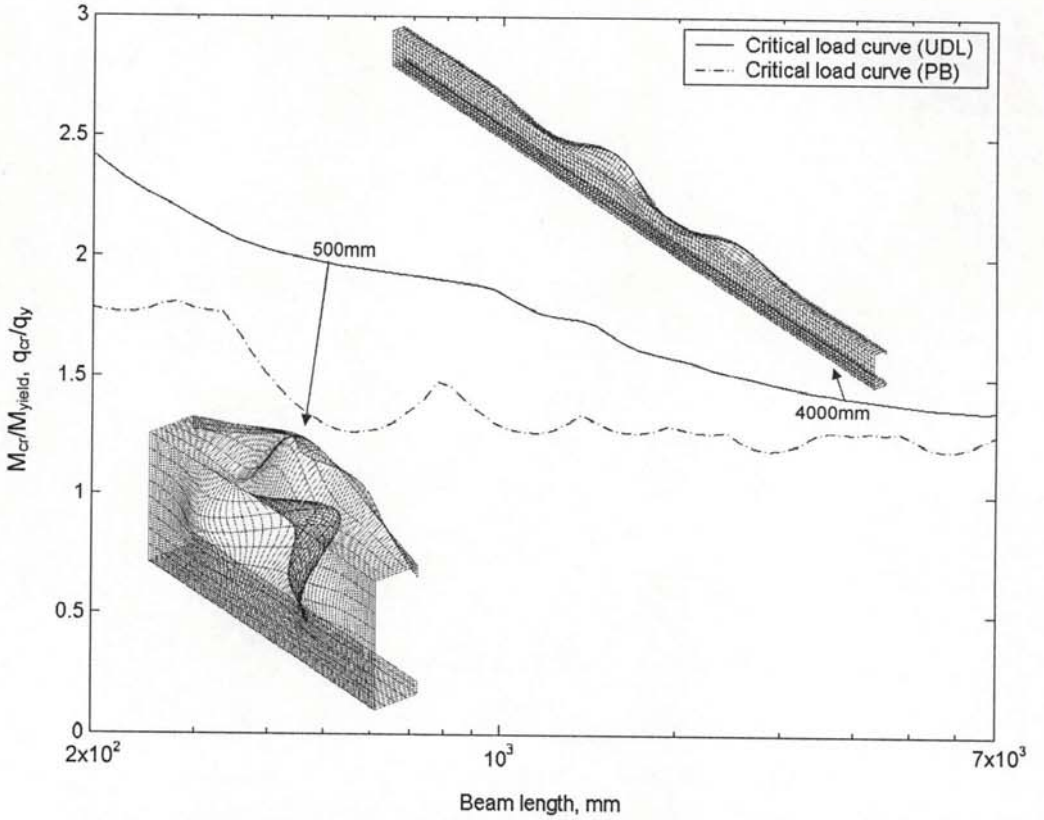


**Fig.5.8 Critical load curve of simply supported channel restrained both laterally and rotationally under a uniformly distributed transverse load (d=202mm, b=75mm, c=20mm, t=2.3mm).**

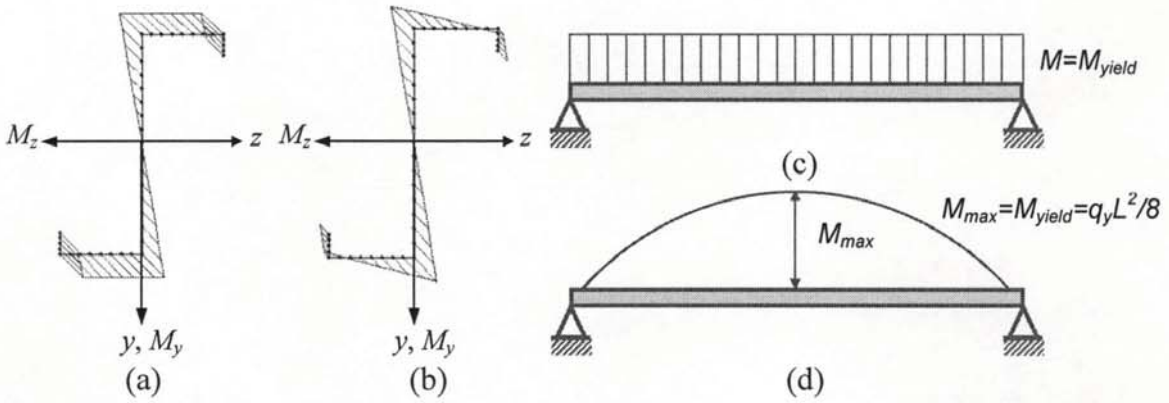


**Fig.5.9 (a) Cross-section stress distribution for restrained section. (b) Cross-section stress distribution for unrestrained section. (c) Bending moment diagram for pure bending. (d) Bending moment diagram distribution for uniformly distributed loading.**

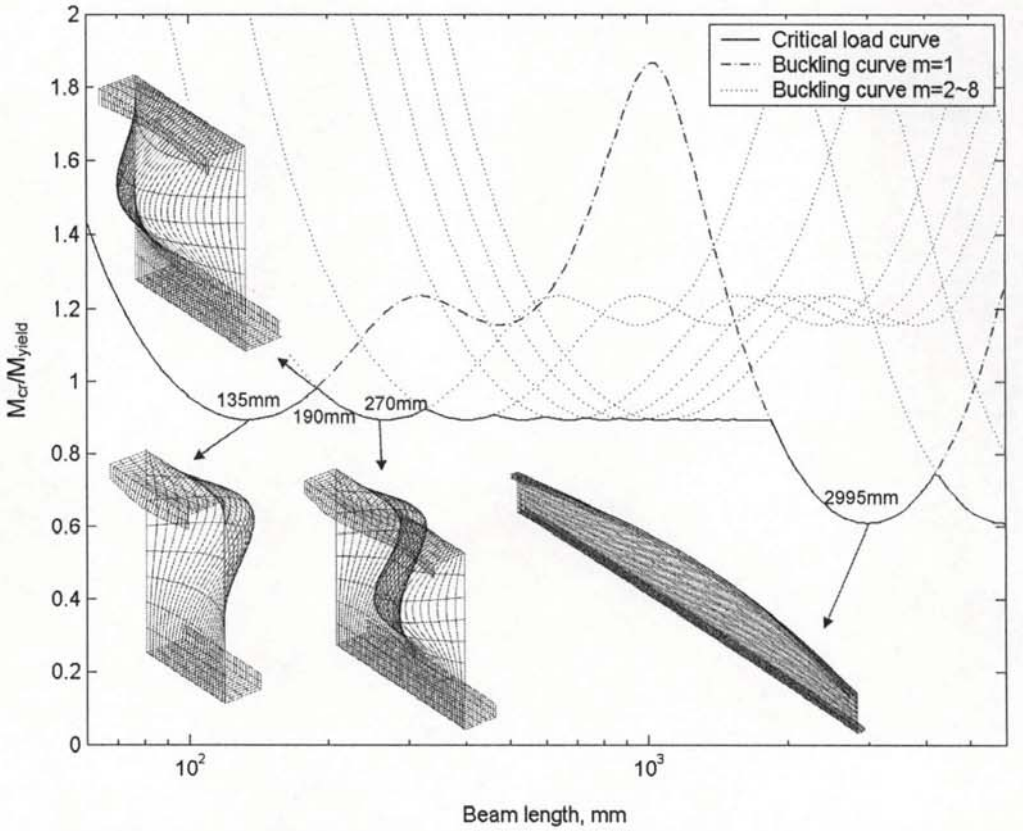


**Fig.5.10 Buckling curves of simply supported, restrained beam under pure bending (d=250mm, b=50mm, c=20mm, t=1.9mm).**

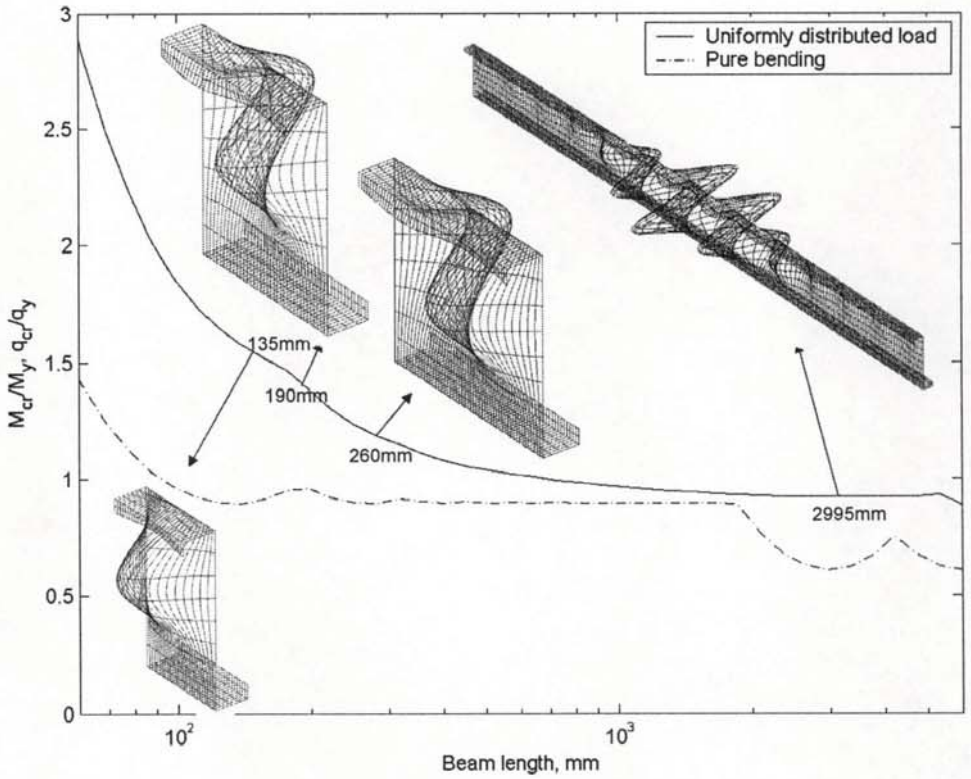


**Fig.5.11 Critical load curve of simply supported, restrained beam under uniformly distributed loading (d=250mm, b=50mm, c=20mm, t=1.9mm).**

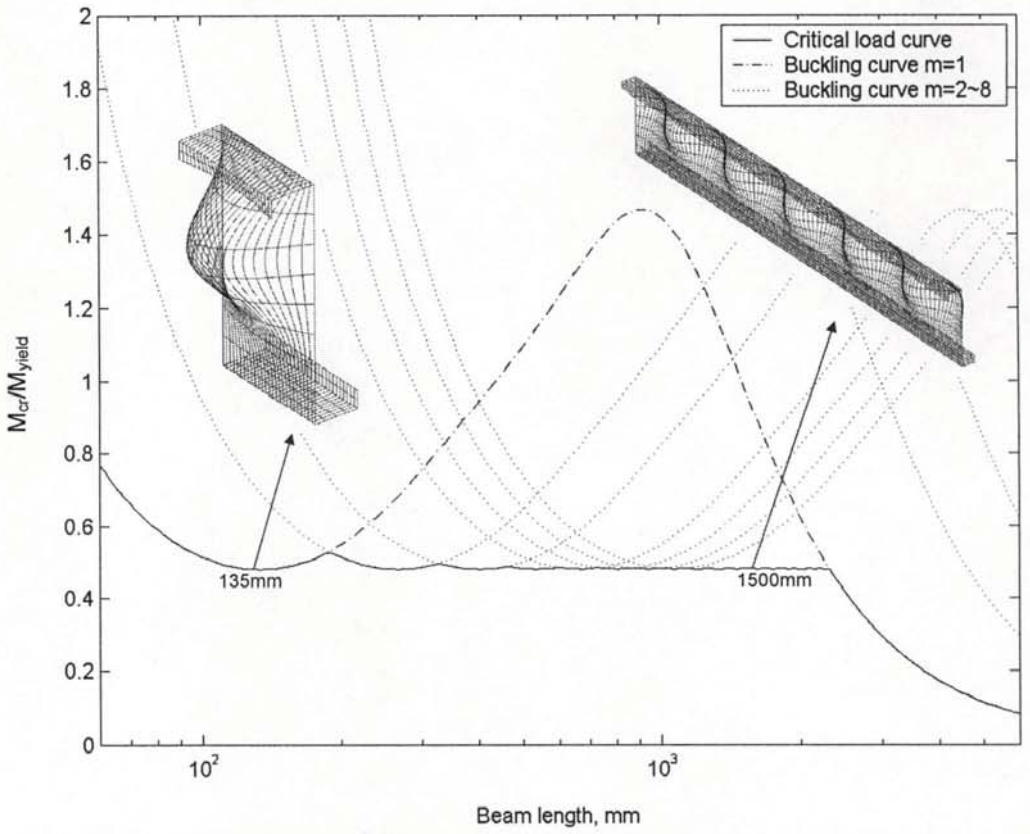


**Fig.5.12 Buckling curves of simply supported, unrestrained beam under pure bending (d=250mm, b=50mm, c=20mm, t=1.9mm).**

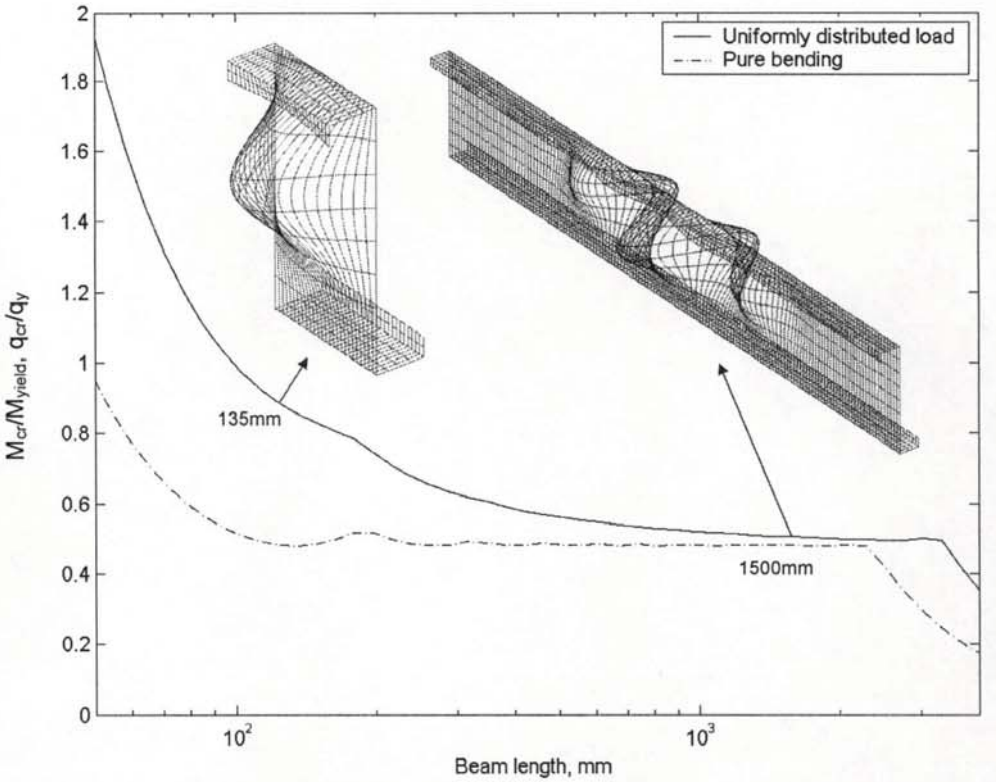


**Fig.5.13 Critical load curve of simply supported, unrestrained beam under uniformly distributed loading (d=250mm, b=50mm, c=20mm, t=1.9mm).**

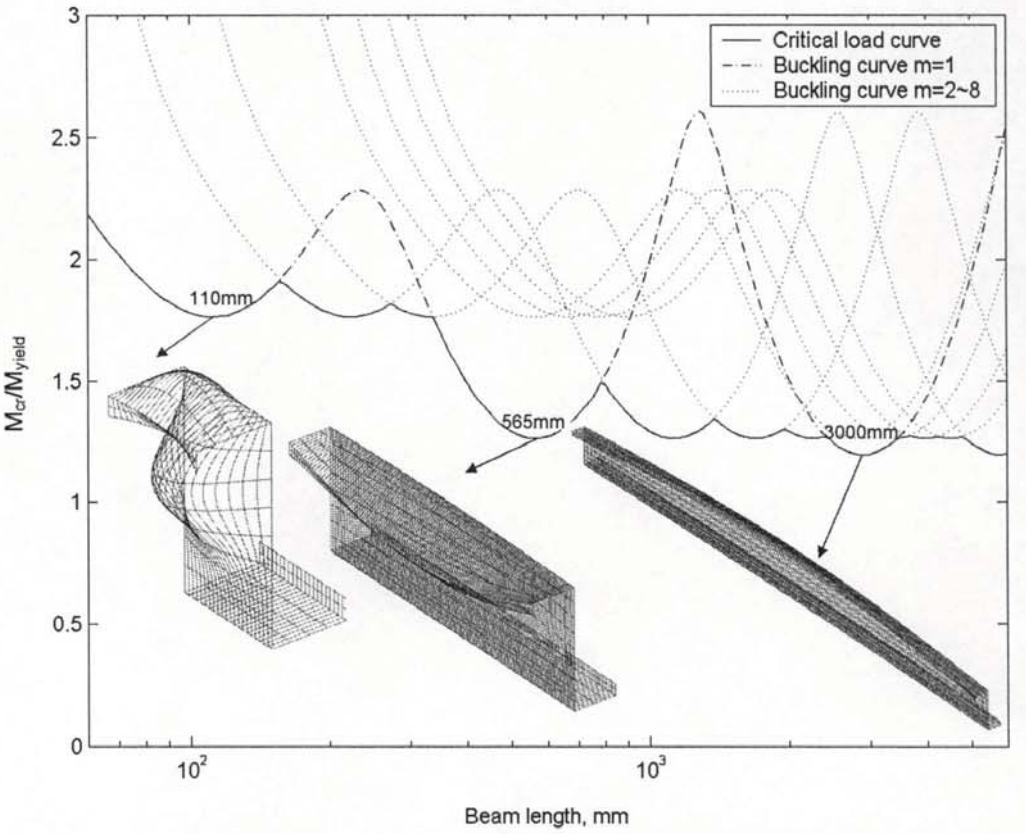


**Fig.5.14 Buckling curves of simply supported, restrained beam under pure bending (d=202mm, b=75mm, c=20mm, t=2.3mm).**

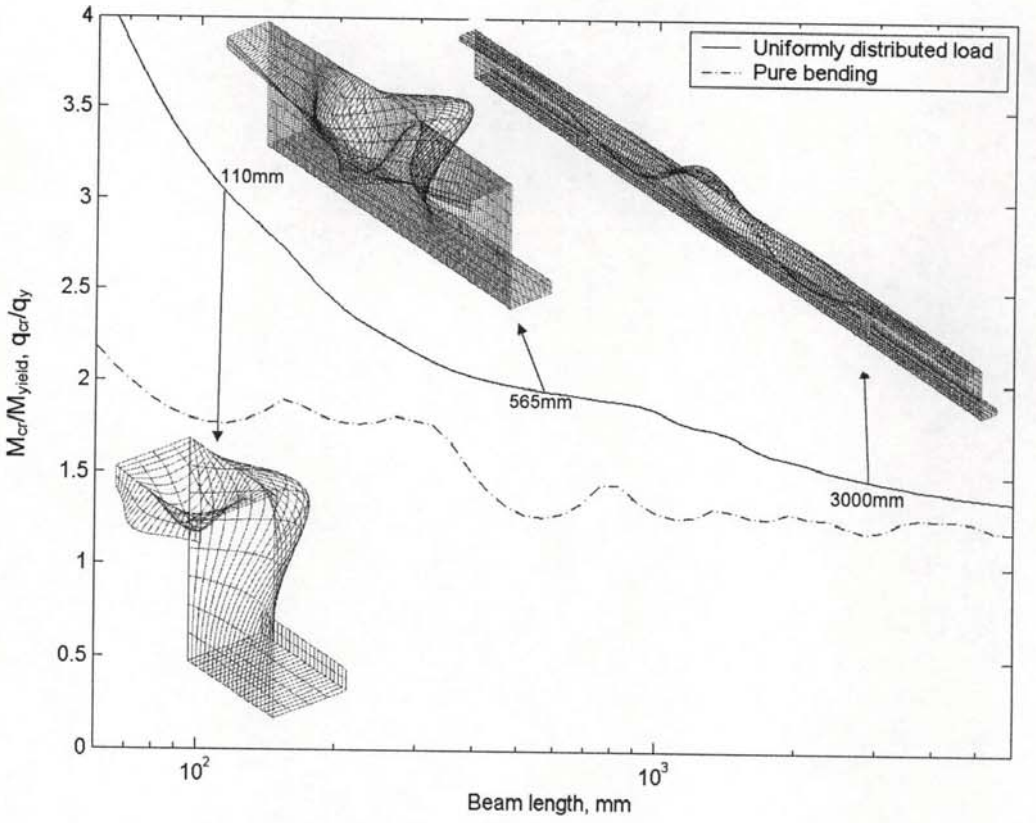


**Fig.5.15 Critical load curve of simply supported, restrained beam under uniformly distributed loading (d=202mm, b=75mm, c=20mm, t=2.3mm).**

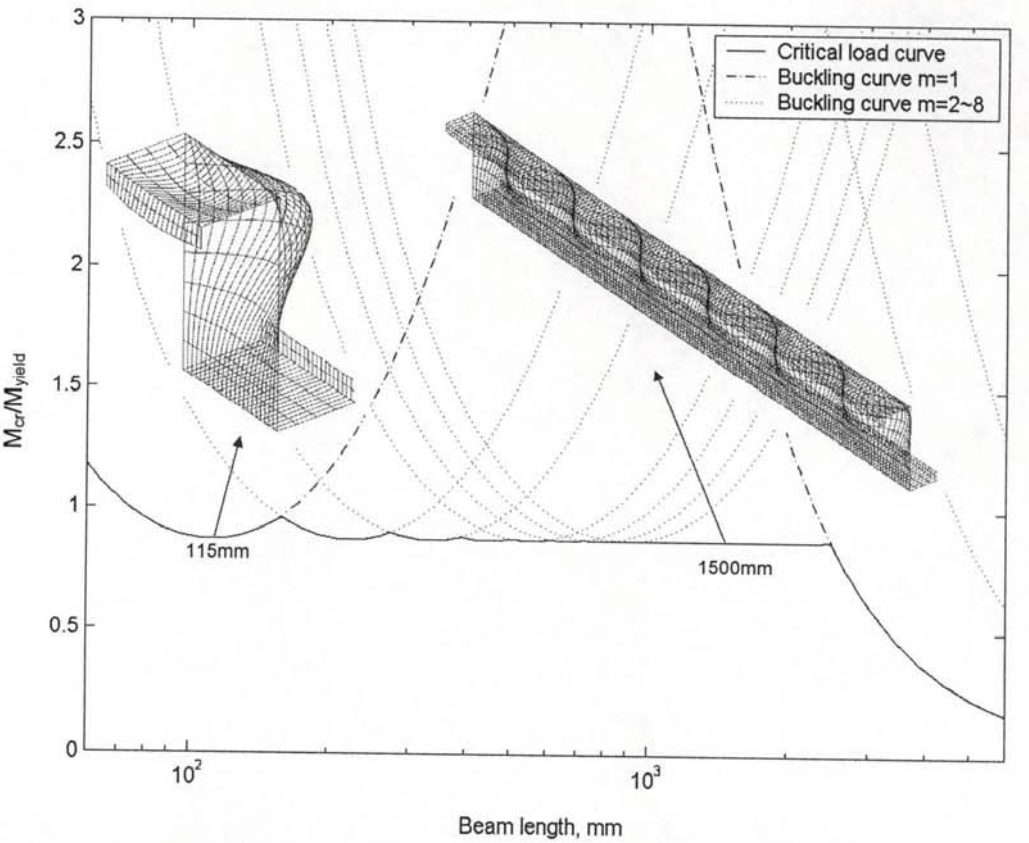


**Fig.5.16 Buckling curves of simply supported, unrestrained beam under pure bending (d=202mm, b=75mm, c=20mm, t=2.3mm).**

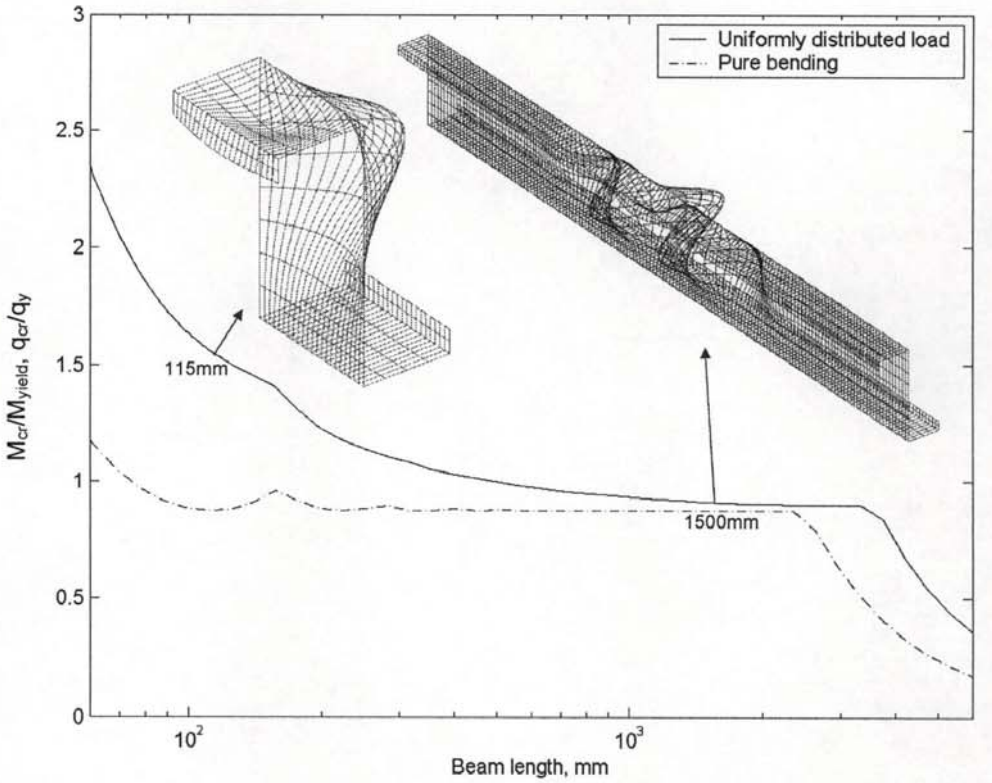


**Fig.5.17 Critical load curve of simply supported, unrestrained beam under uniformly distributed loading (d=202mm, b=75mm, c=20mm, t=2.3mm).**

# Chapter 6

# 6 LATERAL-TORSIONAL BUCKLING

## 6.0 CHAPTER SYNOPSIS

This chapter presents an analytical model for predicting the lateral-torsional buckling of cold-formed zed and channel section beams, with partial lateral restraint provided by the metal sheeting, subjected to uniformly distributed transverse loading.

The focus of the study is to investigate the individual influences of the restraint provided by the sheeting and the interval anti-sag bars, the boundary conditions, warping stress, loading position and the dimensions of the cross section on the lateral-torsional buckling behaviour of the beams. These are of practical interests to design engineers but have not previously been investigated.

## 6.1 INTRODUCTION

The phenomenon of lateral-torsional buckling is not new to structural engineers. However, due to the nature of the problem, most existing studies have been on detached beams with symmetric cross-sections, subjected to bending loads in the direction of their greatest flexural rigidity (Singer et al., 1998; Trahair, 1993). The recently developed finite strip analysis packages are aimed at more accurately predicting the elastic buckling stresses related to the local, distortional, and lateral-torsional buckling of thin-walled beams with various lateral restraints. The method itself is very effective. However, at present, these packages can only deal with the case where the member is subjected to pure bending and/or pure compression (Li, 2004; Ye et al, 2002 & 2004). Recently, Li (2004) has developed an analytical model for predicting the lateral-torsional buckling of cold-formed zed-purlins, with partial-lateral restraint from the cladding, with various end boundary conditions and interval restraints provided by anti-sag bars, subjected to any lateral and transversal distributed loads.

In this chapter, we use Li's model to analyze the lateral-torsional buckling of zed sections (Chu et al., 2004) and channel sections (Chu et al., 2004), which also repeats a further development of the analytical model for the stress analysis of purlin-sheeting system addressed in Section 3.2.

## 6.2 ANALYTICAL MODEL

The beam may exhibit a lateral-torsional buckling when the resultant longitudinal stress is in compression. The critical load of the beam, when lateral-torsional buckling occurs, can be calculated using a similar energy method as the stress analysis introduced in Section 3.2. The expression of the strain energy of the beam, when buckling occurs, is the same as Eqs.(3.3) and (3.4) except for that the deflections and the angle of twist are now the buckling deflections and the buckling angle of twist, that is,

$$U_1 = U_{1\_beam} + U_{1\_spring}$$
$$= \frac{E}{2}\int_o^l [I_y(\frac{d^2w_b}{dx^2})^2 + 2I_{yz}\frac{d^2w_b}{dx^2}\frac{d^2v_b}{dx^2} + I_z(\frac{d^2v_b}{dx^2})^2]dx$$
$$+ \int_o^l [\frac{GJ}{2}(\frac{d\phi_b}{dx})^2 + \frac{EI_\omega}{2}(\frac{d^2\phi_b}{dx^2})^2 - EI_{\omega z}\frac{d^2v_b}{dx^2}\frac{d^2\phi_b}{dx^2}]dx + \frac{k_z}{2}\int_o^l (w_b + y_k\phi_b)^2 dx + \frac{k_\phi}{2}\int_o^l \phi_b^2 dx \quad (6.1)$$

where $v_b$ and $w_b$ = the buckling deflections of the beam in the $y$ and $z$ directions;

$\phi_b$ = the buckling angle of twist.

The buckling deflections of the beam at any point $(x,y,z)$ during buckling can be expressed in terms of the buckling displacements of the beam centroidal axis, $v_b$, $w_b$ and $\phi_b$, as follows (Ressner, 1989; Li, 2004):

$$\bar{v}(x,y,z) = v_b - z\sin\phi_b + y(\cos\phi_b - 1) \approx v_b - z\phi_b - \frac{1}{2}y\phi_b^2$$
$$\bar{w}(x,y,z) = w_b + z(\cos\phi_b - 1) + y\sin\phi_b \approx w_b + y\phi_b - \frac{1}{2}z\phi_b^2 \quad (6.2)$$

where $\bar{v}(x,y,z)$ and $\bar{w}(x,y,z)$ = the deflections of the beam at point $(x,y,z)$ during buckling.

The longitudinal displacement at point (x,y,z) can be expressed as follows:

$$\bar{u}(x,y,z) = u_b - (y\cos\phi_b - z\sin\phi_b)\frac{dv_b}{dx} - (z\cos\phi_b + y\sin\phi_b)\frac{dw_b}{dx} + \beta(y,z)\frac{d\phi_b}{dx}$$
$$\approx u_b - y\frac{dv_b}{dx} - z\frac{dw_b}{dx} + \beta\frac{d\phi_b}{dx} + z\phi_b\frac{dv_b}{dx} - y\phi_b\frac{dw_b}{dx} \quad (6.3)$$

where $\beta(y,z)$ = the warping function of St. Venant torsion;

$\bar{u}(x,y,z)$ and $u_b(x)$ = the longitudinal displacements of the beam at points $(x,y,z)$ and $(x,o,o)$, respectively.

The longitudinal strain and shear strains generated by the buckling displacements can be calculated by

$$\varepsilon_x(x,y,z)=\frac{\partial\overline{u}}{\partial x}+\frac{1}{2}[(\frac{\partial\overline{v}}{\partial x})^2+(\frac{\partial\overline{w}}{\partial x})^2]$$
$$\gamma_{xy}(x,y,z)=\frac{\partial\overline{u}}{\partial y}+\frac{\partial\overline{v}}{\partial x}+\frac{\partial\overline{w}}{\partial x}\frac{\partial\overline{w}}{\partial y} \tag{6.4}$$
$$\gamma_{xz}(x,y,z)=\frac{\partial\overline{u}}{\partial z}+\frac{\partial\overline{w}}{\partial x}+\frac{\partial\overline{v}}{\partial x}\frac{\partial\overline{v}}{\partial z}$$

Substituting Eqs.(6.2) and (6.3) into (6.4) and splitting them into linear and nonlinear terms of the buckling displacements, it leads to the following second-order nonlinear strains:

$$\varepsilon_{x2}(x,y,z)=\frac{1}{2}[(\frac{dv}{dx})^2+(\frac{dw}{dx})^2+(y^2+z^2)(\frac{d\phi}{dx})^2]+z\phi\frac{d^2v}{dx^2}-y\phi\frac{d^2w}{dx^2}$$
$$\gamma_{xy2}=0 \tag{6.5}$$
$$\gamma_{xz2}=0$$

The strain energy caused by the pre-buckling stresses can be calculated separately as those caused by the longitudinal bending stresses and by the longitudinal warping stress as follows:

$$W_{\sigma xb}=-\int_0^l\int_A\sigma_{xb}(x,y,z)\varepsilon_{x2}(x,y,z)dAdx$$
$$W_{\sigma xw}=-\int_0^l\int_A\sigma_{xw}(x,y,z)\varepsilon_{x2}(x,y,z)dAdx \tag{6.6}$$

The negative sign in Eq.(6.6) is because $\sigma_x$ and $\varepsilon_{x2}$ are in opposite directions. Substituting Eq.(6.5) into Eq.(6.6) and noting that the zed purlin is symmetric about its centroid

$$\int_A\sigma_{xb}dA=\int_A y^2\sigma_{xb}dA=\int_A z^2\sigma_{xb}dA=0$$
$$\int_A\sigma_{xw}dA=\int_A y\sigma_{xw}dA=\int_A z\sigma_{xw}dA=0 \tag{6.7}$$

and for the channel section that is monosymmetric about z axis

$$\int_A \sigma_{xb} dA = \int_A \sigma_{xw} dA = 0$$
$$\int_A y\sigma_{xw} dA = \int_A z\sigma_{xw} dA = 0 \tag{6.8}$$
$$\int_A (y^2 + z^2)\sigma_{xbz} dA = \int_A (y^2 + z^2)\sigma_{xw} dA = 0$$

the following equation is obtained for the zed section,

$$W_{\sigma xb} = -\int_o^l \int_A \sigma_{xb}[\phi_b(z\frac{d^2v_b}{dx^2} - y\frac{d^2w_b}{dx^2})]dAdx = \int_o^l \phi_b(M_{zo}\frac{d^2w_b}{dx^2} - M_{yo}\frac{d^2v_b}{dx^2})dx$$
$$W_{\sigma xw} = -\frac{1}{2}\int_o^l \int_A \sigma_{xw}[(y^2 + z^2)(\frac{d\phi_b}{dx})^2]dAdx = -\frac{ED_w}{2}\int_o^l \frac{d^2\phi}{dx^2}(\frac{d\phi_b}{dx})^2 dx \tag{6.9}$$

where $D_w = \int_A (\overline{\omega} - \omega)(y^2 + z^2)dA$ is a section property given in the Appendix 2;

And for the channel section

$$W_{\sigma xb} = -\int_o^l \int_A [\frac{\sigma_{xby}}{2}(y^2 + z^2)(\frac{d\phi_b}{dx})^2 + \sigma_{xb}\phi_b(z\frac{d^2v_b}{dx^2} - y\frac{d^2w_b}{dx^2})]dAdx$$
$$= -\int_A \frac{z(y^2 + z^2)}{2I_y} dA \int_o^l M_y(\frac{d\phi_b}{dx})^2 dx + \int_o^l \phi_b(M_z\frac{d^2w_b}{dx^2} - M_y\frac{d^2v_b}{dx^2})dx \tag{6.10}$$
$$W_{\sigma xw} = 0$$

It is interesting to notice from Eq.(6.10) that the warping stress does not do work during the lateral-torsional buckling of the channel section beams. This indicates that as far as lateral-torsional buckling is concerned, the warping stress has no influence on the critical buckling load for channel section beams.

The strain energy caused by the load due to the load that is acting above the shear centre can be expressed as (Timoshenko & Gere, 1961; Li, 2004):

$$W_q = -\frac{y_q}{2}\int_o^l (q\sin\alpha)\phi_b^2 dx - \frac{z_q}{2}\int_o^l (q\cos\alpha)\phi_b^2 dx \tag{6.11}$$

Hence, the total strain energy generated during lateral-torsional buckling is

$$W_1 = W_{\sigma xb} + W_{\sigma xw} + W_q \tag{6.12}$$

The minimum buckling critical load and corresponding buckling modal displacements can thus be determined by the conventional variational equation:

$$\delta(U_1 - \lambda W_1) = 0 \tag{6.13}$$

where $\lambda$ = the critical load factor. If the stain energy generated by the warping stress, $W_{\sigma xw}$, is neglected in Eq.(6.12) then the present model reduces to the conventional lateral buckling models (Li, 2004; Tarnai, 1979; Reissner 1989; Lee & Kim, 2002).

The variation of Eq.(6.13) results in three simultaneous, linear homogeneous ordinary differential equations from which the minimum eigenvalue representing the critical load factor and corresponding eigenvector representing the buckling displacements, that is the buckling modes, $v_b$, $w_b$ and $\phi_b$, can be determined.

## 6.3 NUMERICAL IMPLEMENTATION

In the present study, both variational Eqs.(3.6) and (6.13) are solved using a numerical procedure in which the horizontal and vertical deflections and the angle of twist are constructed using cubic splines. It is well known that cubic polynomials are widely used to approximate the curve between each pair of data points. Since a straight line is uniquely defined by two points, an infinite number of cubic polynomials can be used to approximate a curve between two points. Therefore, in cubic splines, additional constraints are required on the cubic polynomials to make sure the result is unique. Constraining the continuity of the first and second derivatives of each cubic polynomial at internal points will define all internal cubic polynomials. The first and last cubic polynomials, however, do not have adjoining cubic polynomials beyond the first and last points. As a result, two more constrains must be added at the two end points in order to define these two end polynomials. In the present study, the first derivatives at each end point are chosen as the two required constrains. Therefore, for each to-be-determined function, if there are $n$ nodes, we will end up $n+2$ unknowns, in which $n$ unknowns are the functional values at $n$ nodes and the other two unknowns are the first derivatives at two end nodes. The horizontal and vertical deflections and the angle of twist can thus be expressed in terms of their

$(n+2)$ nodal unknowns by using the cubic interpolation function. The buckling deflections and buckling angle of twist can be treated in a similar manner. By using this approach, Eqs.(3.6) and (6.13) reduce to the following two sets of algebra equations, in which one is inhomogeneous and the other is homogeneous,

$$\begin{bmatrix} A_{11} & A_{12} & A_{13} \\ A_{12} & A_{22} & A_{23} \\ A_{13} & A_{23} & A_{33} \end{bmatrix} \begin{bmatrix} \{v\} \\ \{w\} \\ \{\phi\} \end{bmatrix} = \begin{bmatrix} f_1 \\ f_2 \\ f_3 \end{bmatrix} \tag{6.14}$$

$$\begin{bmatrix} A_{11} & A_{12} & A_{13} \\ A_{12} & A_{22} & A_{23} \\ A_{13} & A_{23} & A_{33} \end{bmatrix} \begin{bmatrix} \{v_b\} \\ \{w_b\} \\ \{\phi_b\} \end{bmatrix} = \lambda \begin{bmatrix} B_{11} & B_{12} & B_{13} \\ B_{12} & B_{22} & B_{23} \\ B_{13} & B_{23} & B_{33} \end{bmatrix} \begin{bmatrix} \{v_b\} \\ \{w_b\} \\ \{\phi_b\} \end{bmatrix} \tag{6.15}$$

where $A_{ij}$ = the coefficient matrices obtained from the calculation of the strain energy from Eqs.(3.3) and (3.4) or (6.1);

$f_i$ and $B_{ij}$ = the coefficient columns and matrices obtained from the calculations of work done by the externally applied load through the pre-buckling and buckling displacements, that is, Eqs.(3.5) and (6.12).

The solution of Eq.(6.14) gives the pre-buckling displacements from which the pre-buckling longitudinal stress can be calculated and thus the coefficient matrices $B_{ij}$ can be evaluated. The solution of Eq.(6.15) gives the eigenvalue and eigenvector, which represent the critical load factor and the corresponding buckling modes. The use of spline interpolations provides great convenience in simulating the various displacement boundary conditions and the interval displacement restraints provided by anti-sag bars.

## 6.4 NUMERICAL EXAMPLES

Table 3.1 gives the details of the analyzed zed and channel sections, such as material properties, definition of boundary conditions and internal supports.

Here, the considered beams are restrained by translational and rotational springs at the top corner of the section and subjected to a uniformly distributed load. Since the beam

buckles easily when the compressed flange is not laterally restrained, only the uplift load is considered here.

### 6.4.1 Comparison Of Present Model With Other Approaches

Fig.6.1 shows the critical load factors of simply supported zed section beams with and without lateral restraint ($k_\phi$=0), subjected to pure bending about the $z$-axis and the corresponding stress distribution is shown in Fig.5.9a (Zd302_b75_c20_t25). The results are compared with those obtained from the finite strip method (Schafer, 2001c & 2003a). As is to be expected, the present solutions provide exactly the same results as the finite strip method. It is interesting to notice from the figure that, for pure bending, the critical loads for the beams with and without lateral restraint are very close, which indicates that the lateral restraint has almost no influence on the lateral-torsional buckling of the beam subjected to pure bending. The reason for this is because buckling is only caused by the compressive stress. In the present two cases, the assumed pure bending is such that it causes the bottom flange of the section to be in compression. While, for the laterally restrained purlin, the restraint provided by the cladding is on the top flange which is actually in tension. Thus it has very little influence on the critical load when the lateral-torsional buckling occurs. Significant differences will be expected if the moment is applied in an opposite direction (top flange in compression), for in this case the lateral restraint will constrain the lateral movement of the top flange and thus increase the critical load.

Fig.6.2 is the demonstration on how the lateral restraint influences the lateral-torsional buckling of a simply supported zed section beam under pure compression. In the figure the results are also compared with those obtained using the Euler buckling theory for the laterally unrestrained beam and the finite strip method for the laterally restrained beam. Again, it can be seen that the present solutions are exactly the same as those provided by the Euler buckling theory and by the finite strip method. The results show that the laterally restrained beam has significantly higher critical loads than the laterally unrestrained beam. This is because the buckling modes for the laterally restrained and laterally unrestrained beams are different. For the laterally unrestrained beam, the beam buckles in the principal plane with minor flexural rigidity whereas, for the laterally restrained beam, the beam is unable to buckle in that

principal plane because of the lateral restraint imposed at the top flange. In other words, the laterally restrained beam can only take the higher buckling mode, which, of course, results in a higher critical load.

The common point for the pure bending and pure compression is that the pre-buckling stresses are exactly the same for laterally restrained and laterally unrestrained beams. Thus the increase in critical loads caused by the lateral restraint purely reflects its influence on the restriction of the buckling modes. In reality, most purlins are subjected to a uniformly distributed transverse load. Because of the asymmetry of the cross-section of the zed-purlin, the vertical transverse load generates not only a vertical deflection but also a horizontal deflection. If it is not acting at the shear centre the load may also cause the beam to twist about its longitudinal axis. For the purlin that is laterally restrained at its top flange the constraining provides an additional horizontal force, which also causes the beam to bend and twist. Thus, the pre-buckling stresses of the laterally restrained beam will be different from those of the laterally unrestrained beam although they both are subjected to the same external load.

### 6.4.2 Influence Of Boundary Conditons And Internal Support

#### 6.4.2.1 Zed Section Beams

The comparison of the critical loads for the simply supported zed section (Zd202_b75_c20_t20) beams laterally restrained in the translational direction but free in the rotational direction ($k_z=\infty$, $k_\phi=0$) with and without considering the influence of warping stress is shown in Fig.6.3, in which the beams are subjected to the uniformly distributed uplift load at the middle of the top flange ($y_q$=-d/2, $z_q=b/2$). As is to be expected, the warping stress has almost no influence on the critical lateral torsion-buckling load for purlins with and without anti-sag bars. This is simply due to the warping stress not being significant when the purlin is simply supported as is demonstrated in Chapter 3.

Practically, purlins are often used as continuous beams over two or more spans, in which case the boundary conditions of the beam can be simplified as simply supported at one end and fixed at the other end. The influence of the warping stress on the critical loads for the same zed section beam (Zd202_b75_c20_t20) simply

supported at one end and fixed at the other end are shown in Fig.6.4 ($k_z=\infty$, $k_\phi=0$, $y_q$=-d/2, $z_q=b/2$). It is seen from this figure that the main influence of the warping stress is when the purlin has no anti-sag bars, in which case the critical load is slightly lower when the warping stress is considered. For purlins with either one or two anti-sag bars the influence of the warping stress on the critical load is almost negligible. This can be explained by the results of the pre-buckling stress analysis where the region with the highest warping stresses tends to be very narrow when one or more anti-sag bars are present.

The critical loads for fixed zed section beams (Zd202_b75_c20_t20, $k_z=\infty$, $k_\phi=0$, $y_q$=-d/2, $z_q=b/2$) with and without considering the influence of warping stress can be compared in Fig.6.5 and, similarly, the main influence of the warping stress on the critical load occurrs when the purlin has no anti-sag bars. The shorter the purlin, the stronger the influence of the warping stress. For example, for a 3m span purlin, the critical load is reduced by some 28% when the warping stress is considered.

Fig.6.6 shows the critical load factors of simply supported zed section beams with zero, one and two anti-sag bars, subjected to a uniformly distributed uplift load (Zd302_b75_c20_t25, $k_\phi=0$, $y_q$=-d/2, $z_q=0$). It can be seen from the figure that the lateral restraint has a remarkable influence on the lateral-torsional buckling of the beam, particularly when there are two anti-sag bars. The influence is found to decrease with the increase in the beam length.

Fig.6.7 shows the critical load factors of the zed section beam simply supported at one end and fixed at the other end (Zd302_b75_c20_t25, $k_\phi=0$, $y_q$=-d/2, $z_q=0$). The figure shows that there is a significant increase in critical load when the top flange is fully laterally restrained. Compared to the pinned-pinned beam, the pinned-fixed beam also appears sensitive to the lateral restraint.

#### 6.4.2.2 Channel Section Beams

The critical loads for the simply supported channel section beams (Cd202_b75_c20_t20), subjected to the uniformly distributed uplift load at the middle of the top flange ($y_q$=-d/2, $z_q=b/2-e_2$) and laterally restrained in the translational

direction but free in the rotational direction ($k_z=\infty$, $k_\phi=0$), without considering the influence of warping stress are shown in Fig.6.8. As is to be expected, the critical load increases with the number of anti-sag bars used and decreases with the span length.

Fig.6.9 shows the comparison of critical loads for the channels with 0, 1 and 2 anti-sag bars when its one end is simply supported and the other end is fixed (Cd202_b75_c20_t20, $k_z=\infty$, $k_\phi=0$, $y_q$=-d/2, $z_q=b/2-e_2$). It is clear that the critical loads shown in this figure are much higher than the corresponding one shown in Fig.6.8. This indicates that the boundary condition of the beam has significant influence on the lateral-torsional buckling of the beam. This is further demonstrated by the results shown in Fig.6.10 for the beams with both ends fixed. It is interesting to notice from both Figs.6.9 and 6.10 that, the influence of the mid anti-sag bar seems to be less significant when the boundary of the beam becomes to be fixed. This is probably due to the combined influence of the fixed boundary on the pre-buckling stress and buckling modal displacements, which makes the mid anti-sag bar be less effective.

Fig.6.11 shows the critical load factors of simply supported channel section beams with zero, one and two anti-sag bars, subjected to a uniformly distributed uplift load (Cd302_b75_c20_t25, $k_\phi$=0, $y_q$=-d/2, $z_q$=-e2). It can be seen from the figure that the lateral restraint has a remarkable influence on the lateral-torsional buckling of the beam when there are two anti-sag bars. The influence is found to decrease with the increase of the beam length.

Fig.6.12 shows the critical load factors of the channel section beam simply supported at one end and fixed at the other end (Cd302_b75_c20_t25, $k_\phi$=0, $y_q$=-d/2, $z_q$=-e2). Again, the figure shows that there is a significant increase in critical load when the top flange is fully laterally restrained. Compared to the pinned-pinned beam, the pinned-fixed beam also appears sensitive to the lateral restraint.

### 6.4.3 Influence Of Loading Position

#### 6.4.3.1 Zed Section Beams

In this section the influence of various loading positions on the critical loads of the zed section beam (Zd302_b75_c20_t25, $k_\phi$=0) under a uniformly distributed uplift load is investigated. Fig.6.13 is for the load acting along the web central line ($z_q$=0) but with different vertical distance ($y_q$) from the z-axis for the simply-supported beam with or without lateral restraints. It is shown that, the highest critical load is related to the load that is applied at the top, while the lowest critical load corresponds to the load applied at the bottom. This feature appears to be consistent with those found earlier in I beams (Timoshenko & Gere, 1961). The influence of the lateral restraint on the critical load seems not very remarkable when the load is applied below the z-axis.

Fig.6.14-6.16 show the influence of the loading position on the critical load where the load is acting vertically on the top flange but with different horizontal distance ($z_q$) from the y-axis (Zd202_b75_c20_t20, $k_z=\infty$, $k_\phi$=0, $y_q$=-d/2). From these figures, the critical load is seen to decrease with the increase in the distance between the loading point and web central line. The worst case, that is, associated with the lowest critical load factor, is when the load is placed at the corner between the flange and the lip, whereas the highest critical load factor occurs when the load is applied through the central line of the web. The influence of the warping stress on the critical load factor is variable. When the warping stress is considered, the critical load factor is reduced for $z_q$=$b$/2 and $z_q$=b, but is increased when $z_q$=0.

#### 6.4.3.2 Channel Section Beams

The influence of various different loading positions ($y_q$) on the critical loads of the channel section beam (Cd302_b75_c20_t25, $k_\phi$=0, $z_q$=0) under a uniformly distributed uplift load is investigated and the corresponding results are provided in Fig.6.17. Again, it is clear that the highest critical load occurs when the load is applied at the top, while the lowest critical load corresponds to the load applied at the bottom, which is consistent with those found earlier in I beams (Timoshenko & Gere, 1961). The influence of the lateral restraint on the critical load seems not very remarkable when the load is applied below the z-axis.

Figs.6.18-6.20 show the influence of loading position ($z_q$) on the critical load of the channel-section beam for different boundary conditions (Cd202_b75_c20_t20, $k_z=\infty$, $k_\phi=0$, $y_q$=-d/2). The loading positions shown in these figures include one above the shear centre ($z_q$ =*-e1-e2*) and four on the top flange; along the web central line ($z_q$=*-e2*), above the centroid ($z_q$=*0*), along the mid of the flange ($z_q$=*b/2-e2*) and along the lip central line ($z_q$=*b-e2*). It is surprisingly found that the lowest critical load is corresponding to the case where the load is applied at the position above the shear centre, whereas the highest critical load is in the case where the load is applied at the top of the lip. This indicates that, the closer the loading point is to the shear centre, the lower the critical load. Since the warping stress does not do work during lateral-torsional buckling, the lower the critical load means that less work done by the two bending stresses. However, the bending stress $\sigma_{xbz}$ generated by the bending moment about z-axis is not affected by the loading position. This implies that during the lateral-torsional buckling the work done by the bending stress $\sigma_{xby}$ is opposite to the work done by the bending stress $\sigma_{xbz}$.

### 6.4.4 Influence Of Spring Stiffnesses

The influence of the translational and rotational spring stiffnesses on the lateral-torsional buckling is studied for the zed and channel section beams without anti-sag bars for beams subjected to a uniformly distributed uplift load at the top of the web line.

#### 6.4.4.1 Zed Section Beams

Fig.6.21a and b show the influence of the translational spring stiffness on the lateral-torsional buckling load $q_{cr}/q_y$ for simply-supported zed section beams subjected to the uniformly distributed uplift load (Zd202_b75_c20_t20 and Zd302_b75_c20_t20) when $k_\phi$=0. It can be seen that the critical loads slightly increase with the increase of translational spring stiffness and the influence of the translational spring stiffness on the critical load primarily occurs in the range $10^{-9}<k_z/E<10^{-6}$. The influence of the beam length on the critical loads is also shown in Fig.6.21 from which it is evident that the longer the beam the lower the critical load.

Fig.6.21c and d show the influence of the rotational spring stiffness on the critical buckling load for simply-supported zed section beams subjected to a uniformed distributed uplift load when $k_z$=0. It is shown that the critical loads significantly increase with the increase of the rotational spring stiffness, particular in the region where $k_\phi/(Ey_k^2)$ is greater than $10^{-7}$.

Fig.6.22 shows the influence of the translational and rotational spring stiffnesses on the lateral-torsional buckling load $q_{cr}/q_y$ for zed section beams simply-supported at one end and fixed at the other end, subjected to a uniformly distributed uplift load (Zd202_b75_c20_t20 and Zd302_b75_c20_t20). The figure shows that the influences of the two springs on the critical loads are different. For increasing translational spring the critical load initially decreases then increases, whereas for the rotational spring the critical load increases continuously with the increase of the spring stiffness.

Fig.6.23 shows the influence of the translational and rotational spring stiffnesses on the lateral-torsional buckling load for zed section beams with both ends fixed (Zd202_b75_c20_t20 and Zd302_b75_c20_t20). Comparing Fig.6.23 and Fig.6.22, it seems that the influence of the translational spring stiffness is more remarkable on fixed beams than on simply supported beams.

#### 6.4.4.2 Channel Section Beams

Fig.6.24 shows the influence of the translational and rotational spring stiffnesses on the lateral-torsional buckling load $q_{cr}/q_y$ for simply-supported channel section beams subjected to a uniformly distributed uplift load (Cd202_b75_c20_t20 and Cd302_b75_c20_t20). Again, it can be seen that the critical load slightly increases with increase in the translational spring stiffness in the range $10^{-9}<k_z/E<10^{-6}$. In contrast, the increase in the critical load with increase in the rotational spring stiffness is significant, particularly for the region where $k_z/(Ey_k^2)>10^{-7}$.

Fig.6.25 shows the influence of the translational and rotational spring stiffnesses on the lateral-torsional buckling load $q_{cr}/q_y$ for channel section beams simply-supported at one end and fixed at the other end, subjected to a uniformly distributed uplift load (Cd202_b75_c20_t20 and Cd302_b75_c20_t20). Again, it can be seen from the figure

that the increase of the critical loads is more significant with the increase of rotational spring stiffness than the translational spring stiffness.

Fig.6.26 shows the influence of the translational and rotational spring stiffnesses for channel section beams with both ends fixed. Most of the features shown in this figure are similar to those shown in Fig.6.24 and 6.25.

### 6.4.5 Influence Of The Dimensions Of Cross Section

The influence of the sectional dimensions on the critical loads of lateral-torsional buckling is studied for zed and channel section beams, 8m in length, without anti-sag bars when subjected to the uniformly distributed uplift load at the middle of the top flange, as is shown in Fig.3.1.

Figs.6.27 and 6.28 respectively show the results of the simply-supported zed and channel section beams. It is found from these figures that, for the zed section the critical buckling load increases with the increase of web depth, flange width and lip depth whereas, for the channel section, the critical buckling load increases with the increase of flange width and lip depth, but decreases slightly with the increase of web depth.

## 6.5 SUMMARY

In this chapter an analytical model is presented for predicting the lateral-torsional buckling of cold-formed zed and channel section beams subjected to partial-lateral restraint by the metal sheeting and subjected to a uniformly distributed transverse loading. The focus of the study is to investigate the individual influences of the restraints provided by the sheeting and the interval anti-sag bars, the boundary conditions, warping stress, loading position and the dimensions of cross section on the lateral-torsional buckling behaviour of the beams. The following conclusions can be drawn from the investigation:

- The use of interval anti-sag bars is a very effective way to increase the buckling resistance of the beam. However the position of the anti-sag bars to be used should take into account the influence of the boundary condition. In general, it is more effective to use the anti-sag bars in the simply supported beams than in the fixed beams.

- The warping stress is found to have a significant influence on the critical load for lateral-torsional buckling of the partial-laterally restrained zed section beams only when the purlin is fixed at least at one end and no anti-sag bars are present. For a simply supported purlin or a purlin with anti-sag bars, the effect of the warping stress on the critical load for lateral-torsional buckling is almost negligible. Warping stress does not have influence on the lateral-torsional buckling of the channel section beams.

- The loading position has remarkable influence on the critical buckling load. The highest critical load is found when the loading point is closer to the shear centre for zed section. For channel section, however, the lowest critical load is found when the loading point is closer to the shear centre.

- Rotational spring stiffness has more influence on the lateral-torsional buckling loads than translational spring stiffness. The influence of translational spring stiffness on the critical load occurs only in a small range of stiffness value, while that of rotational spring stiffness occurs when $k_\phi/(Ey_k^2)$ is larger $10^{-7}$.

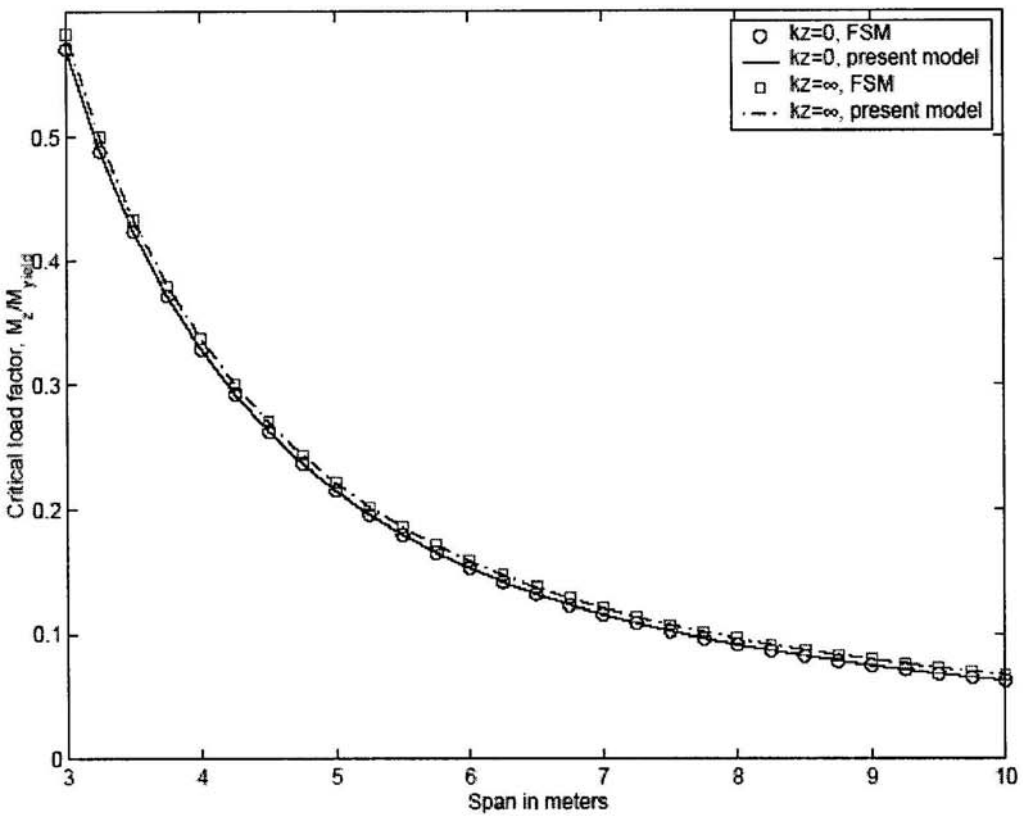


**Fig.6.1 Critical loads of simply supported zed section beams under pure bending ($k_\phi$=0).**

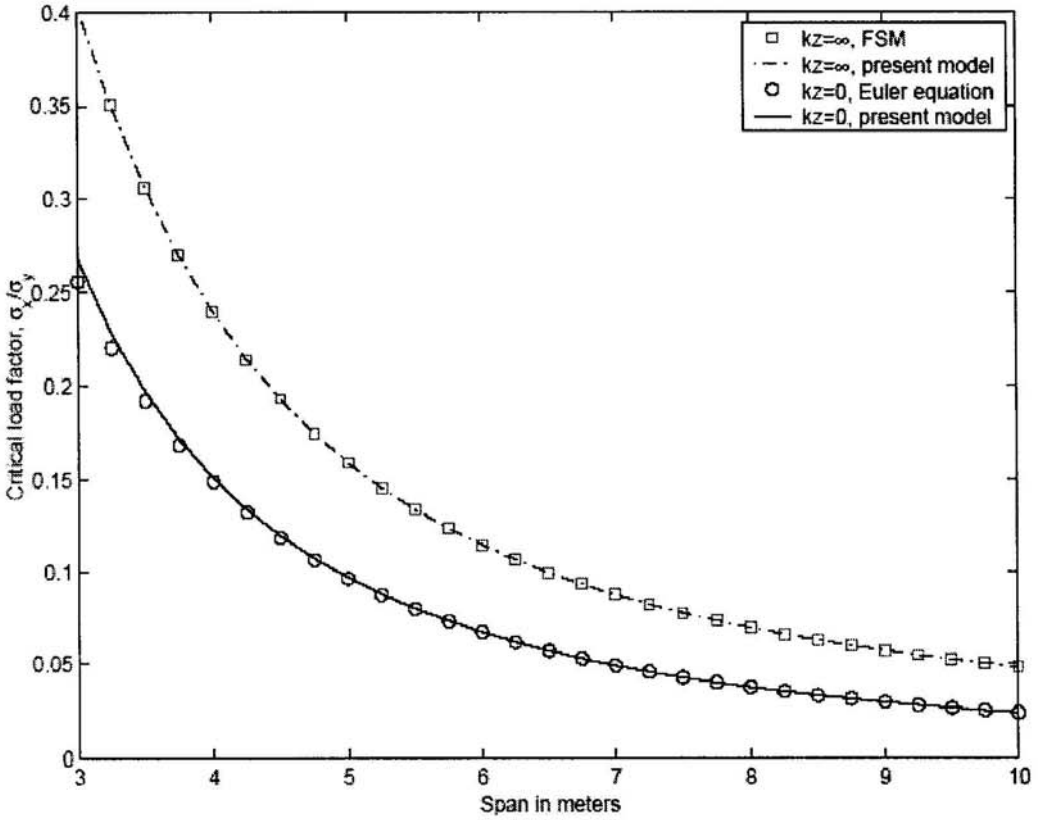


**Fig.6.2 Critical loads of simply-supported zed section beams under pure compression ($k_\phi$=0).**

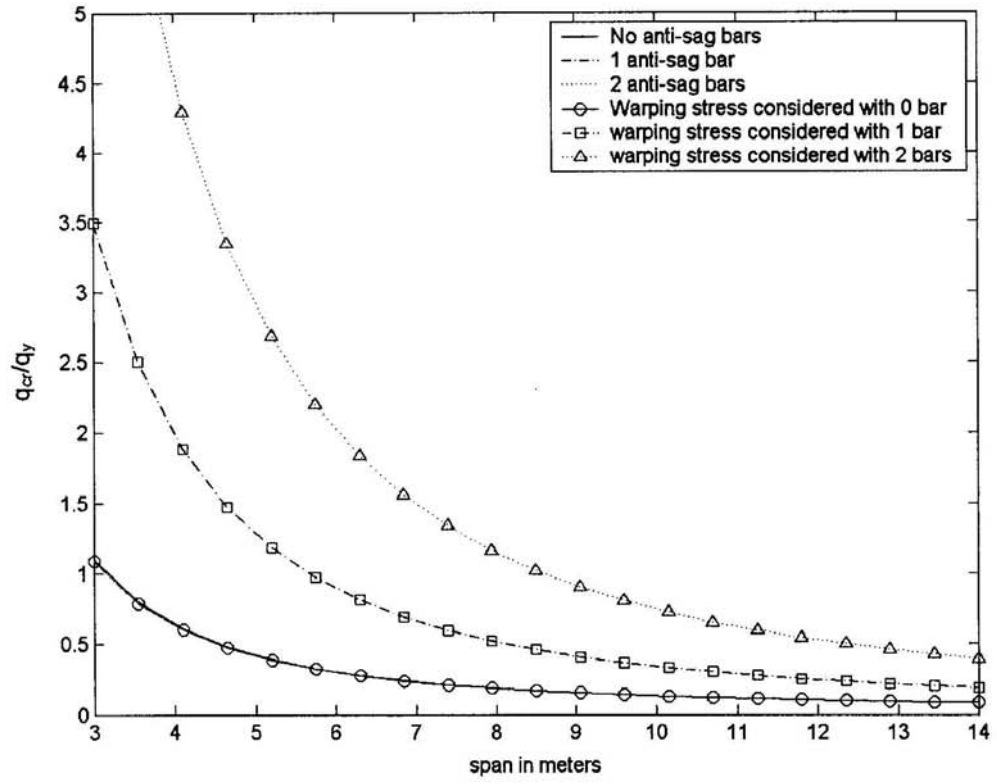


**Fig.6.3 Critical loads of the simply supported zed section beams ($k_z=\infty$, $k_\phi=0$, $y_q=-d/2$, $z_q=b/2$).**

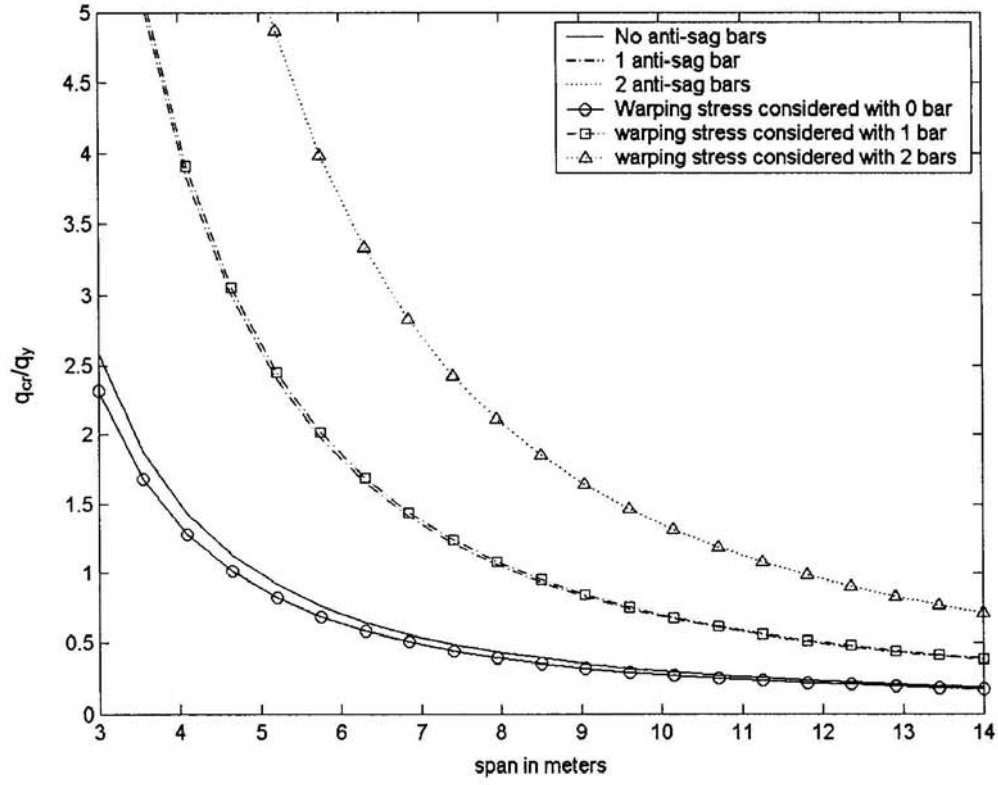


**Fig.6.4 Critical loads of zed section beams with one end simply supported and the other end fixed ($k_z=\infty$, $k_\phi=0$, $y_q=-d/2$, $z_q=b/2$).**

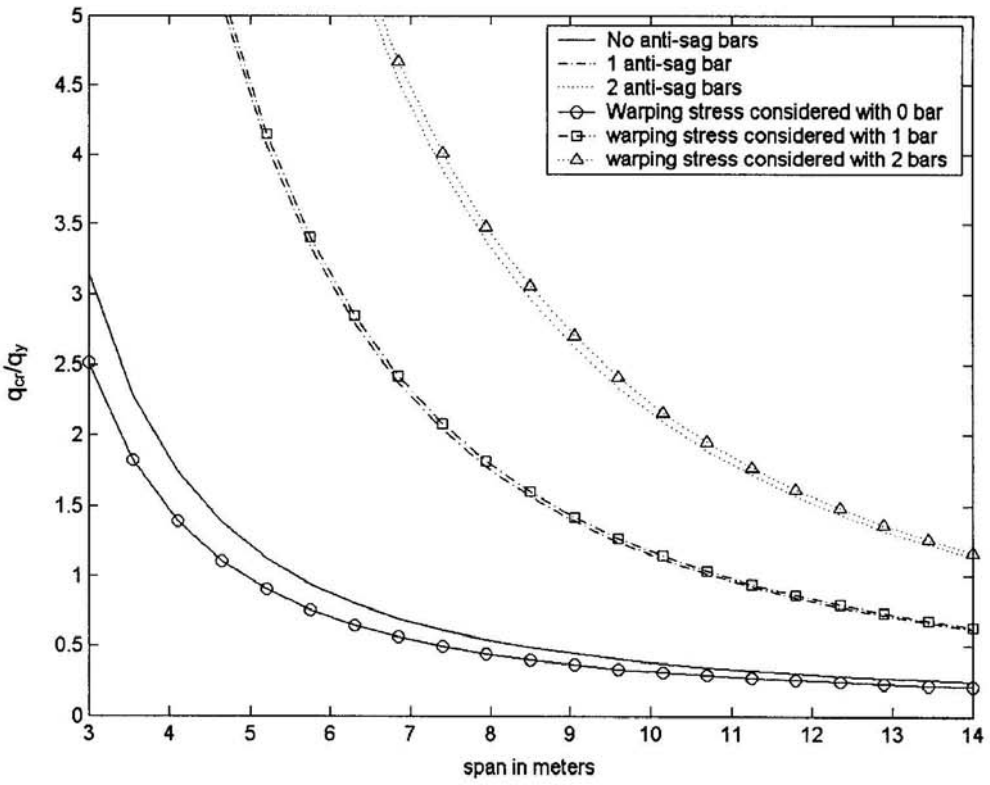


**Fig.6.5 Critical loads of the fixed zed section beams ($k_z=\infty$, $k_\phi=0$, $y_q$=-d/2, $z_q$=b/2).**

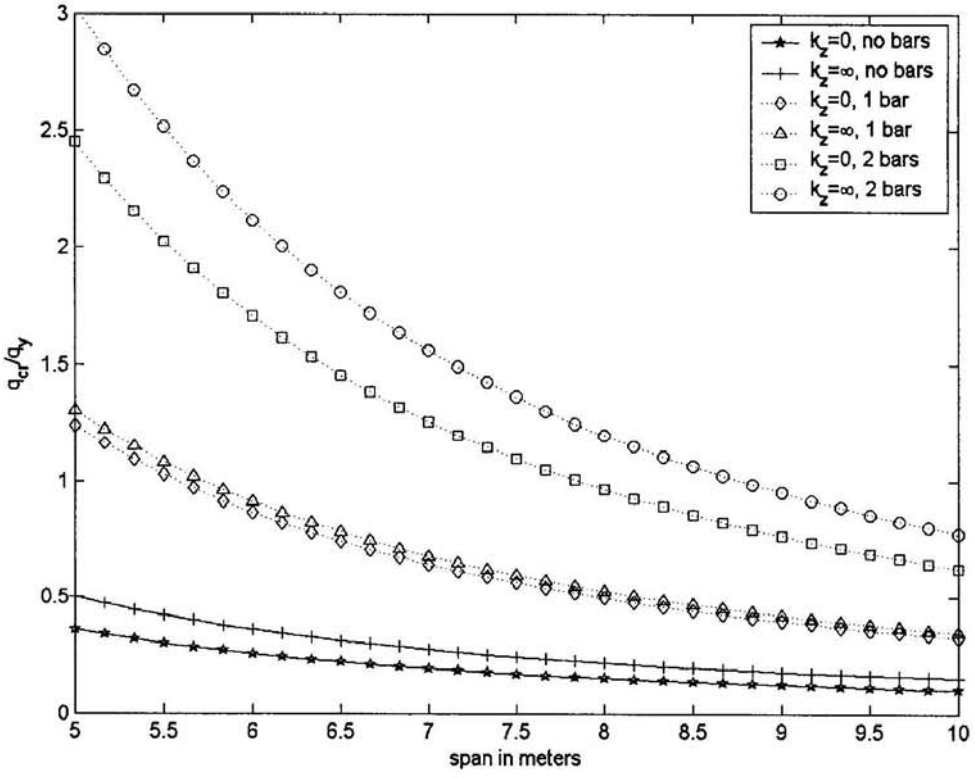


**Fig.6.6 Critical loads of the simply-supported zed section beams ($k_\phi=0$, $y_q$=-d/2, $z_q$=0).**

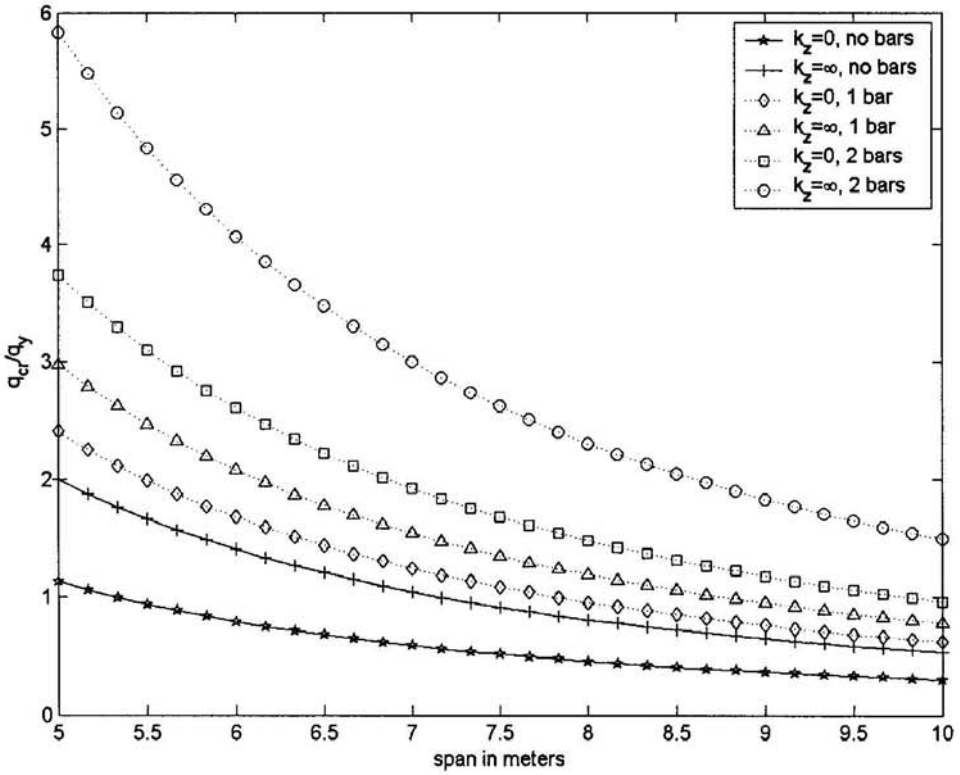


**Fig.6.7 Critical loads of zed section beams with one end simply supported and the other end fixed ($k_\phi$=0, $y_q$=-d/2, $z_q$=0).**

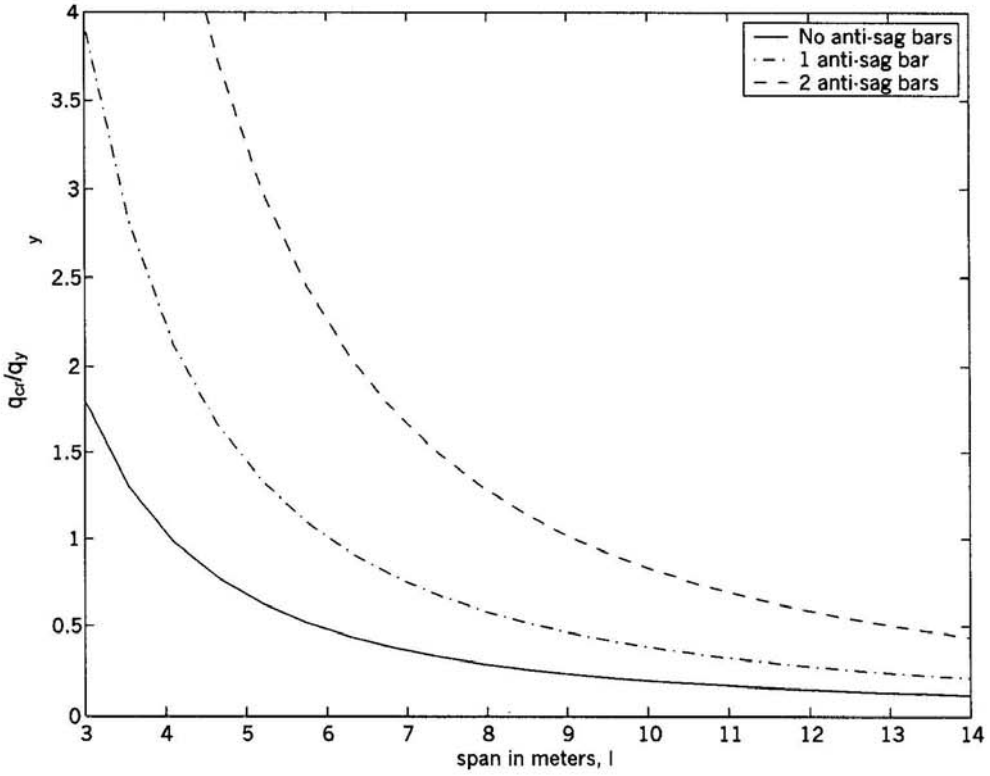


**Fig.6.8 Critical loads of the simply supported channel section beams ($k_z$= ∞, $k_\phi$=0, , $y_q$=-d/2, $z_q$=b/2-$e_2$).**

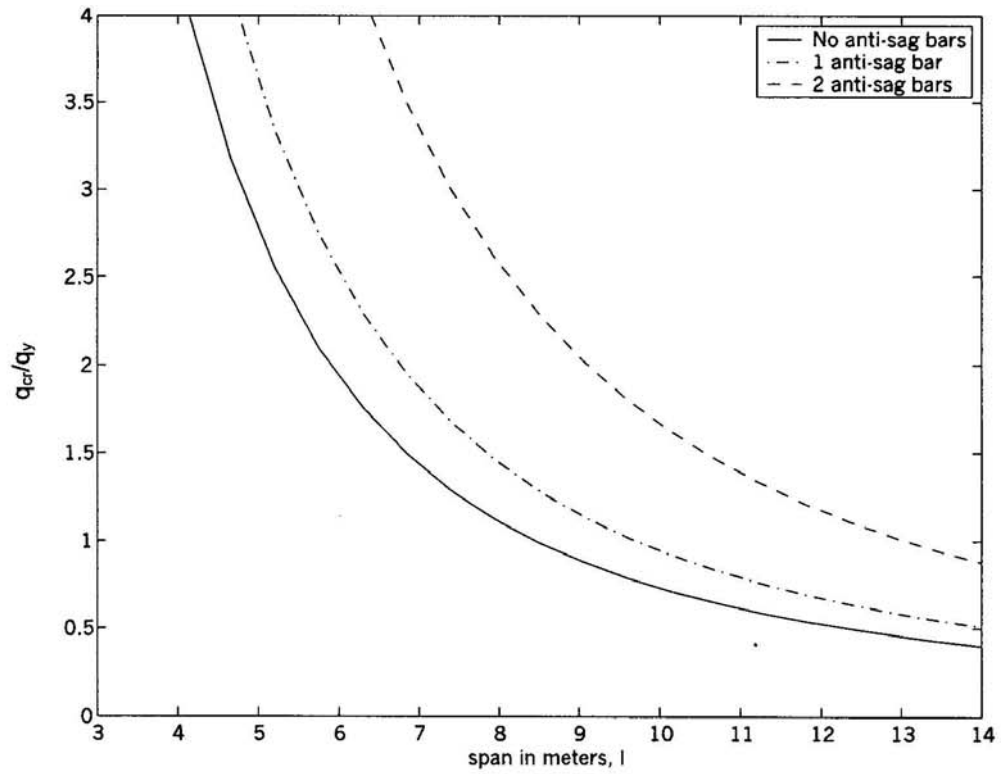


**Fig.6.9 Critical loads of channel section beams with one end simply supported and the other end fixed ($k_z=\infty$, $k_\phi=0$, $y_q=-d/2$, $z_q=b/2-e_2$).**

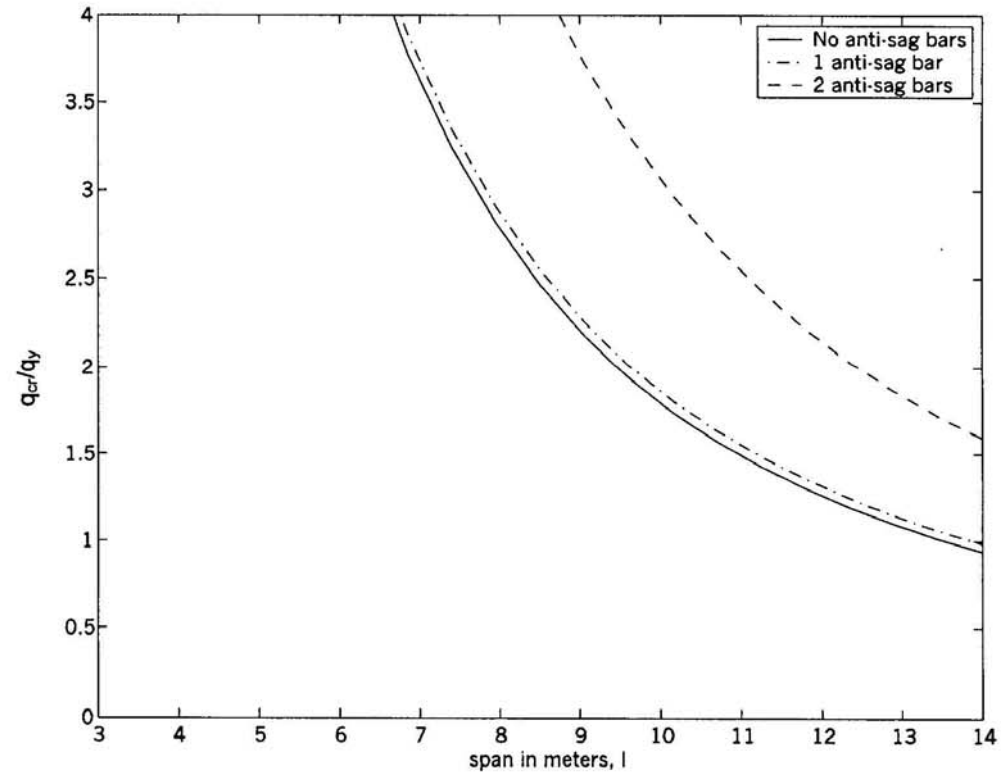


**Fig.6.10 Critical loads of the fixed channel section beams ($k_z=\infty$, $k_\phi=0$, $y_q=-d/2$, $z_q=b/2-e_2$).**

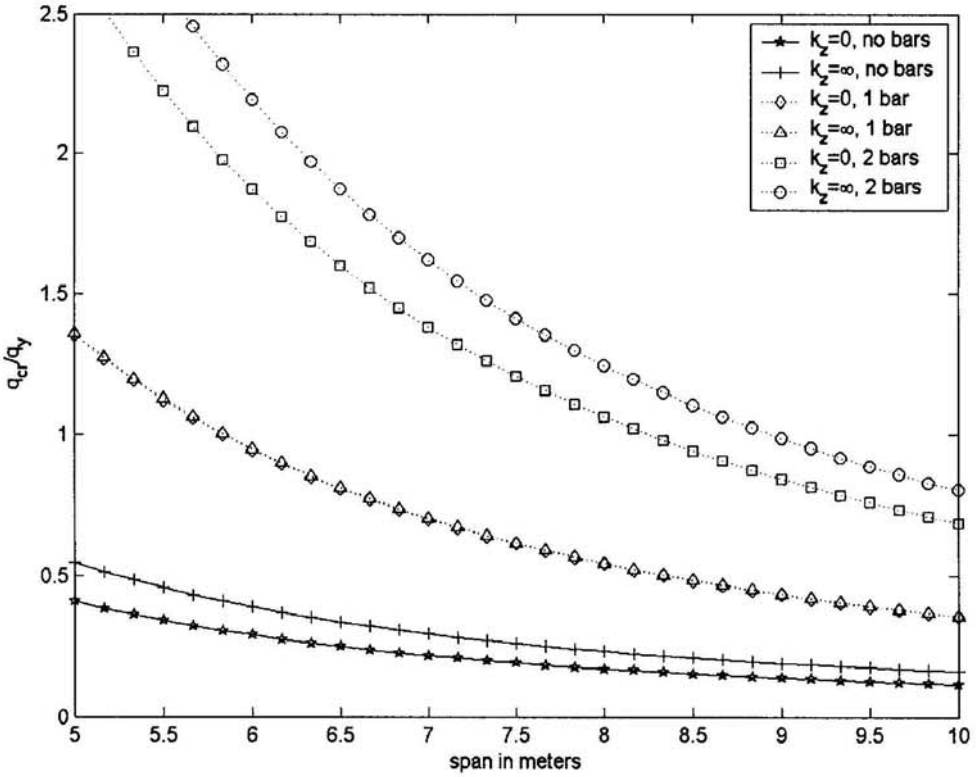


**Fig.6.11 Critical loads of the simply-supported channel section beams ($k_\phi$=0, $y_q$=-d/2, $z_q$=-$e_2$).**

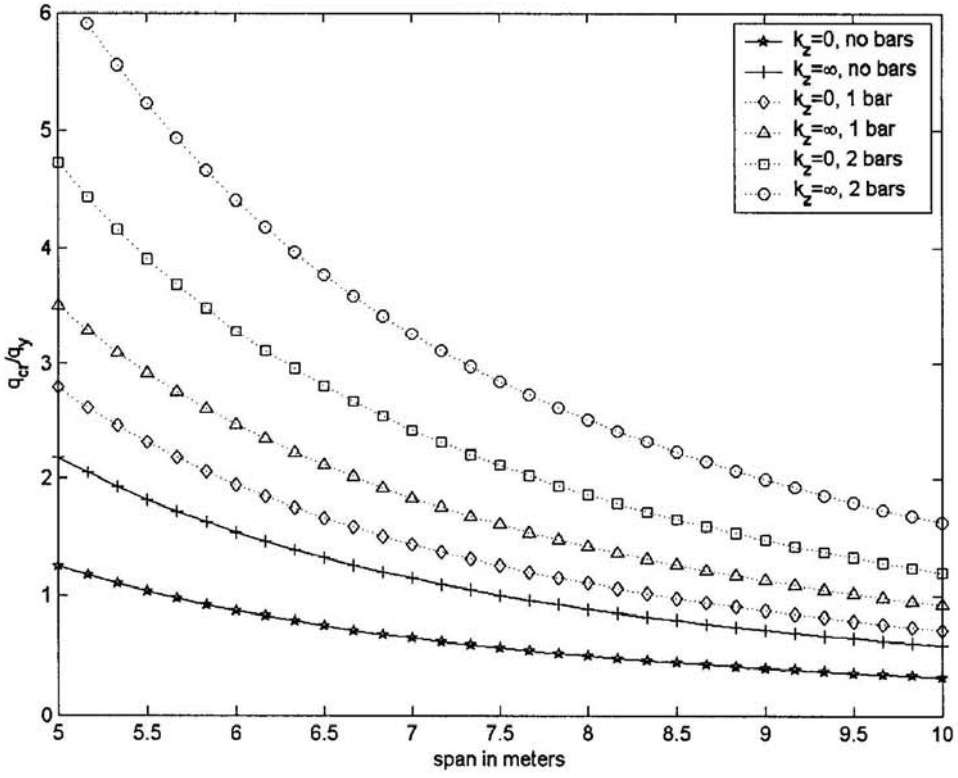


**Fig.6.12 Critical loads of channel section beams with one end simply supported and the other end fixed ($k_\phi$=0, $y_q$=-d/2, $z_q$=-$e_2$).**

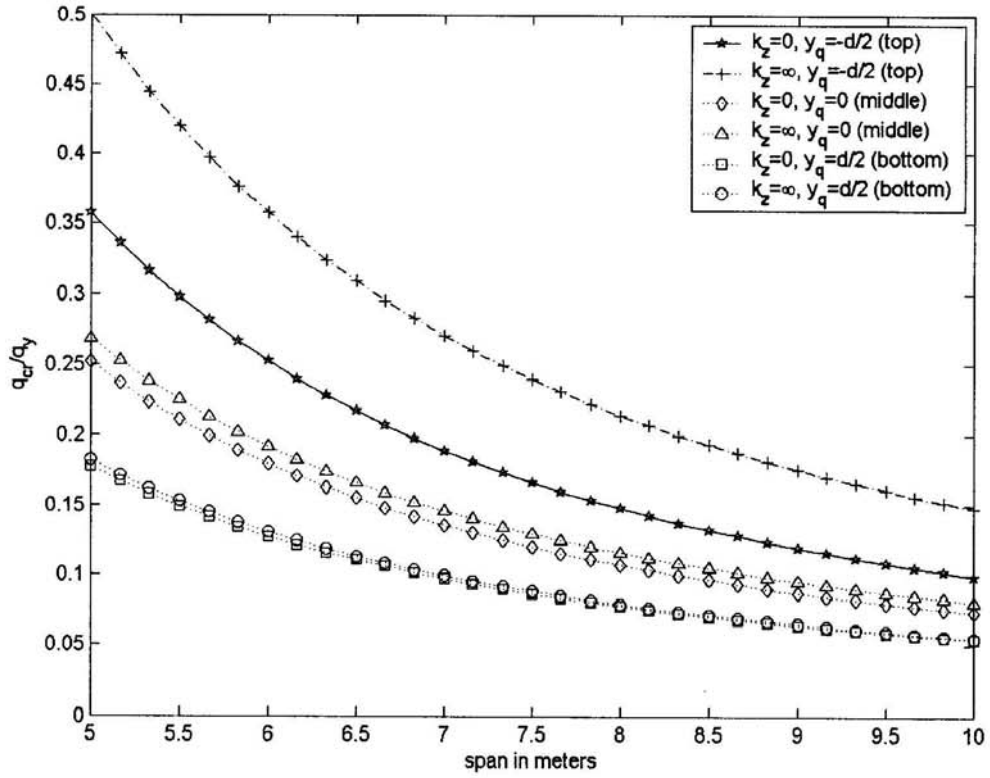


**Fig.6.13 Critical loads of simply-supported zed section beams under different loading positions ($k_\phi$=0, $z_q$=0).**

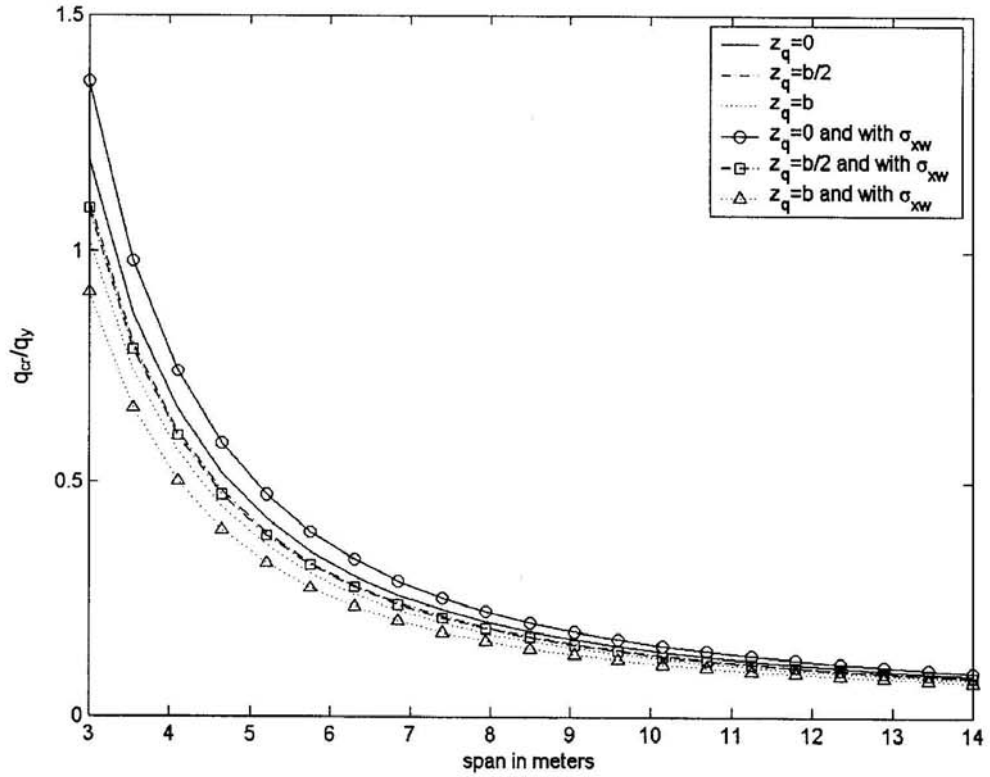


**Fig.6.14 Influence of loading position on the critical load of simply supported zed section beams ($k_z$= ∞ , $k_\phi$=0, $y_q$=-d/2).**

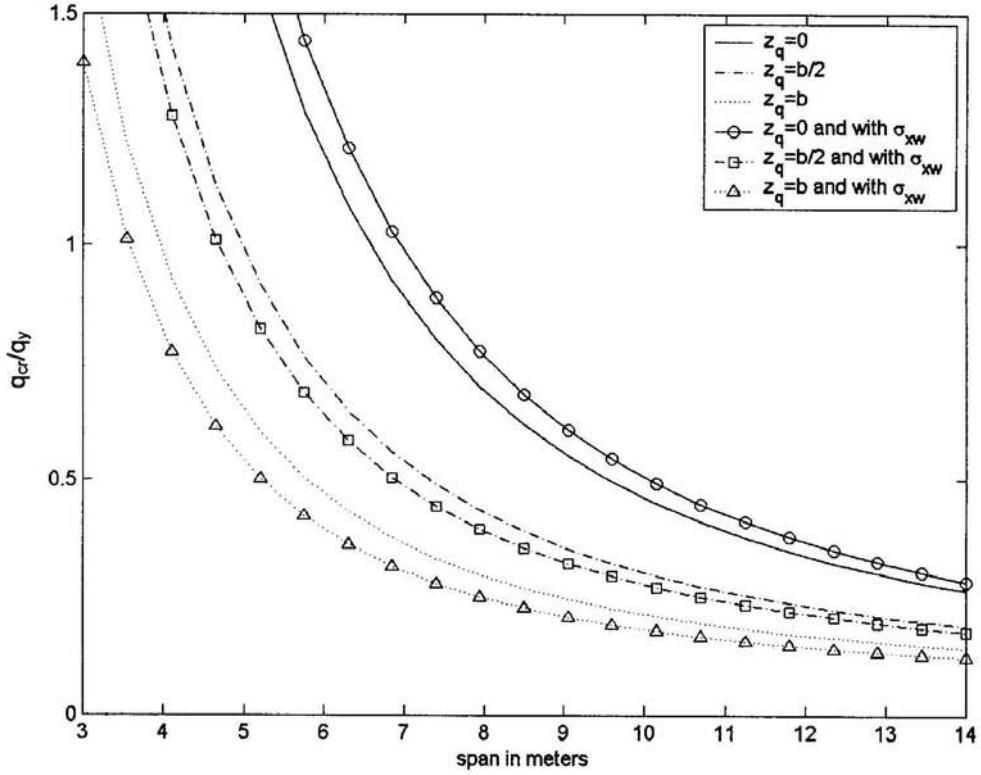


**Fig.6.15 Influence of loading position on the critical load of zed section beams with one end simply supported and other end fixed ($k_z=\infty$, $k_\phi=0$, $y_q$=-d/2).**

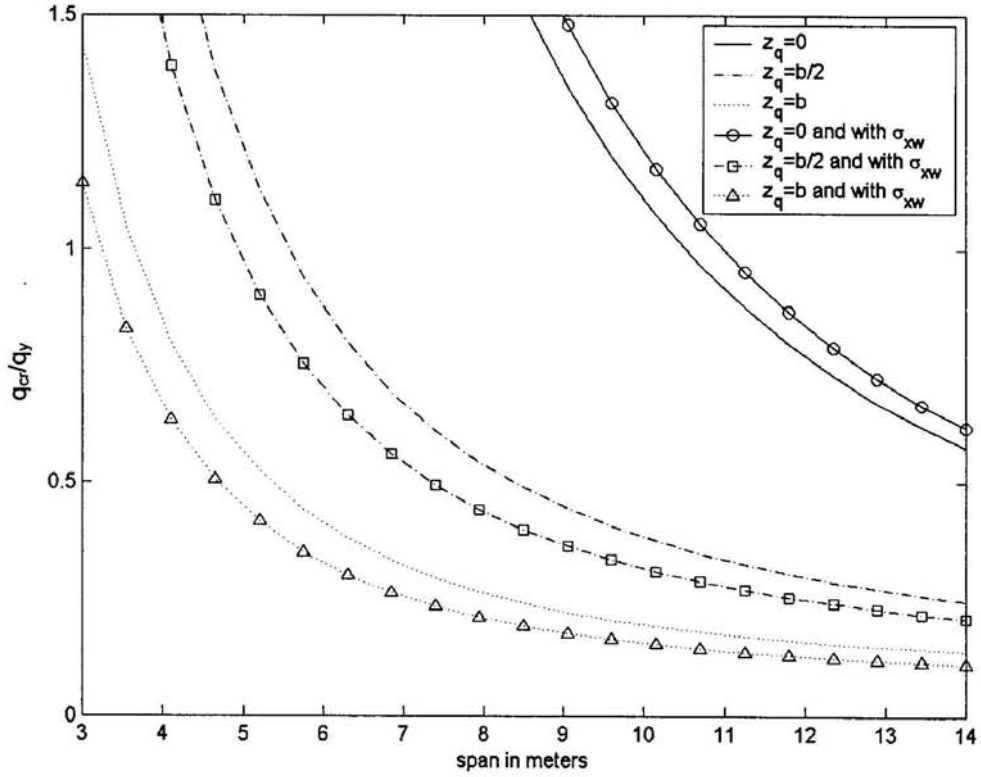


**Fig.6.16 Influence of loading position on the critical load of fixed zed section beams ($k_z=\infty$, $k_\phi=0$, $y_q$=-d/2).**

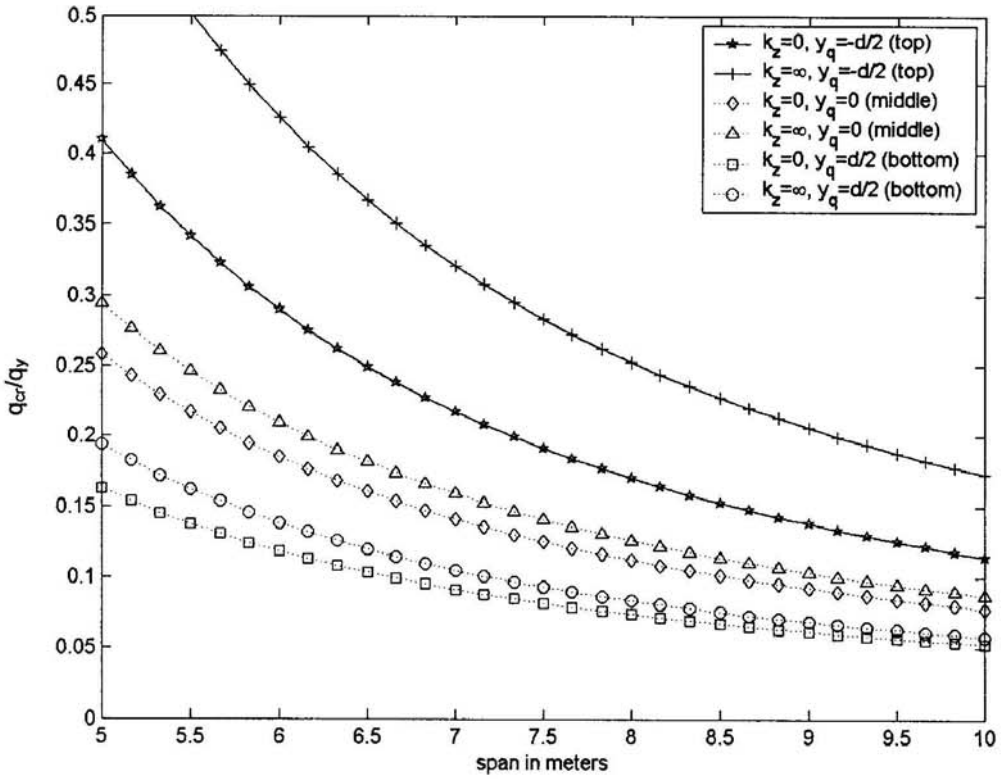


**Fig.6.17 Critical loads of simply-supported channel section beams under different loading positions ($k_\phi$=0, $z_q$=-$e_2$).**

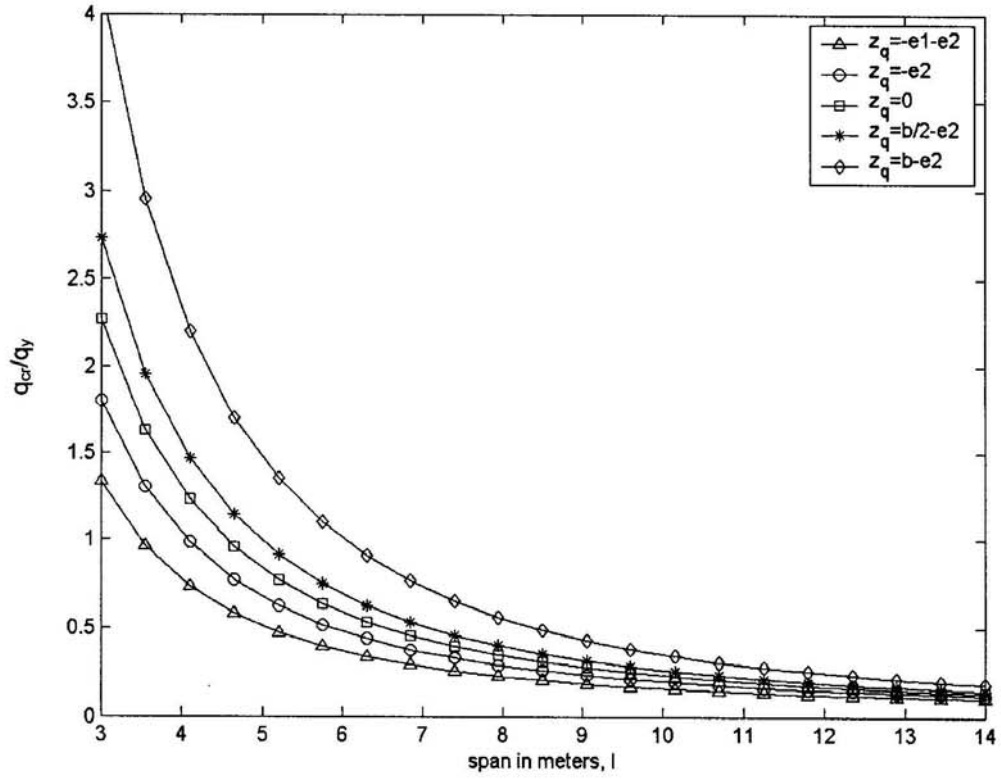


**Fig.6.18 Influence of loading position on the critical load of simply supported channel section beams ($k_z$= ∞ , $k_\phi$=0, $y_q$=-d/2).**

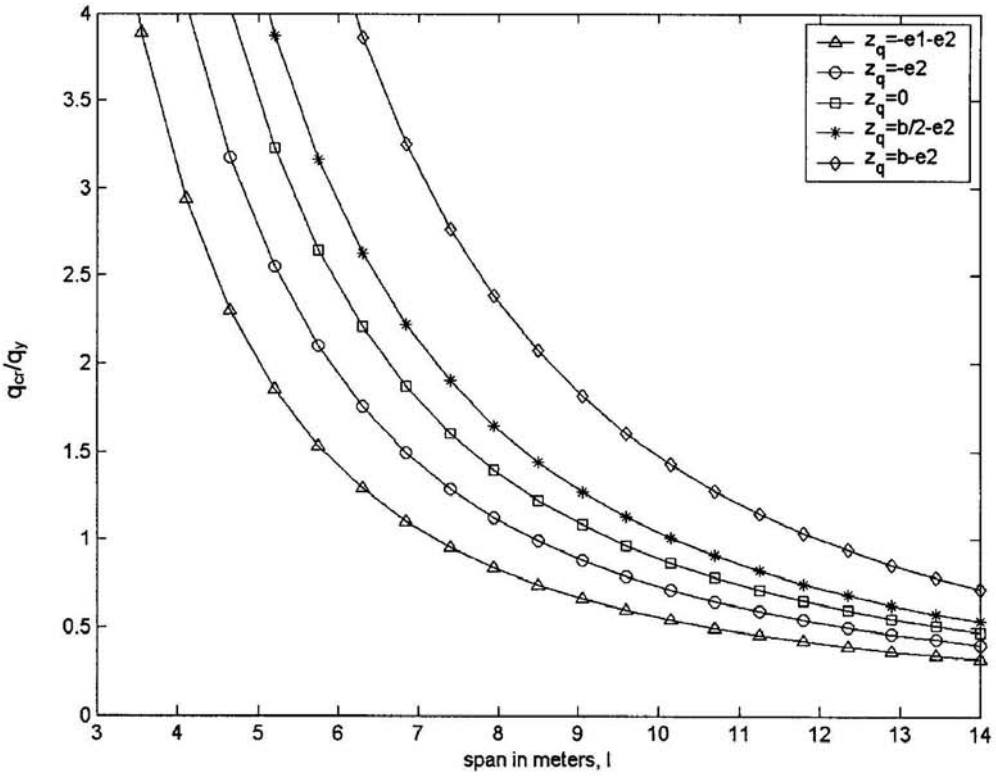


**Fig.6.19 Influence of loading position on the critical load of channel section beams with one end simply supported and other end fixed ($k_z=\infty$, $k_\phi=0$, $y_q$=-d/2).**

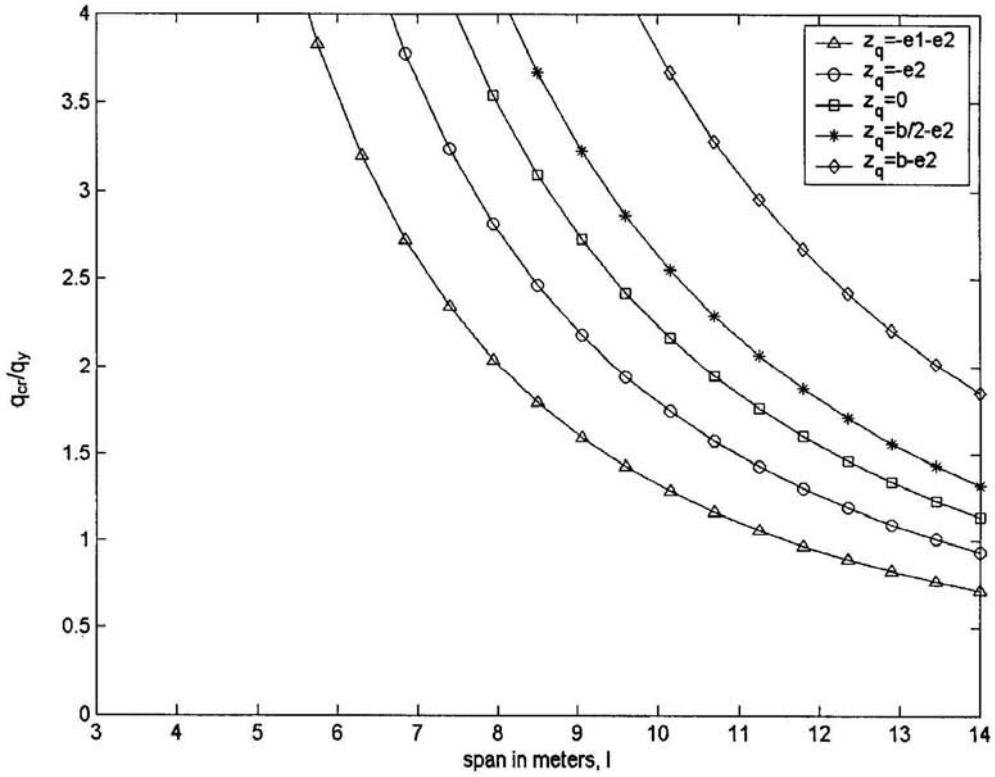


**Fig.6.20 Influence of loading position on the critical load of fixed channel section beams ($k_z=\infty$, $k_\phi=0$, $y_q$=-d/2).**

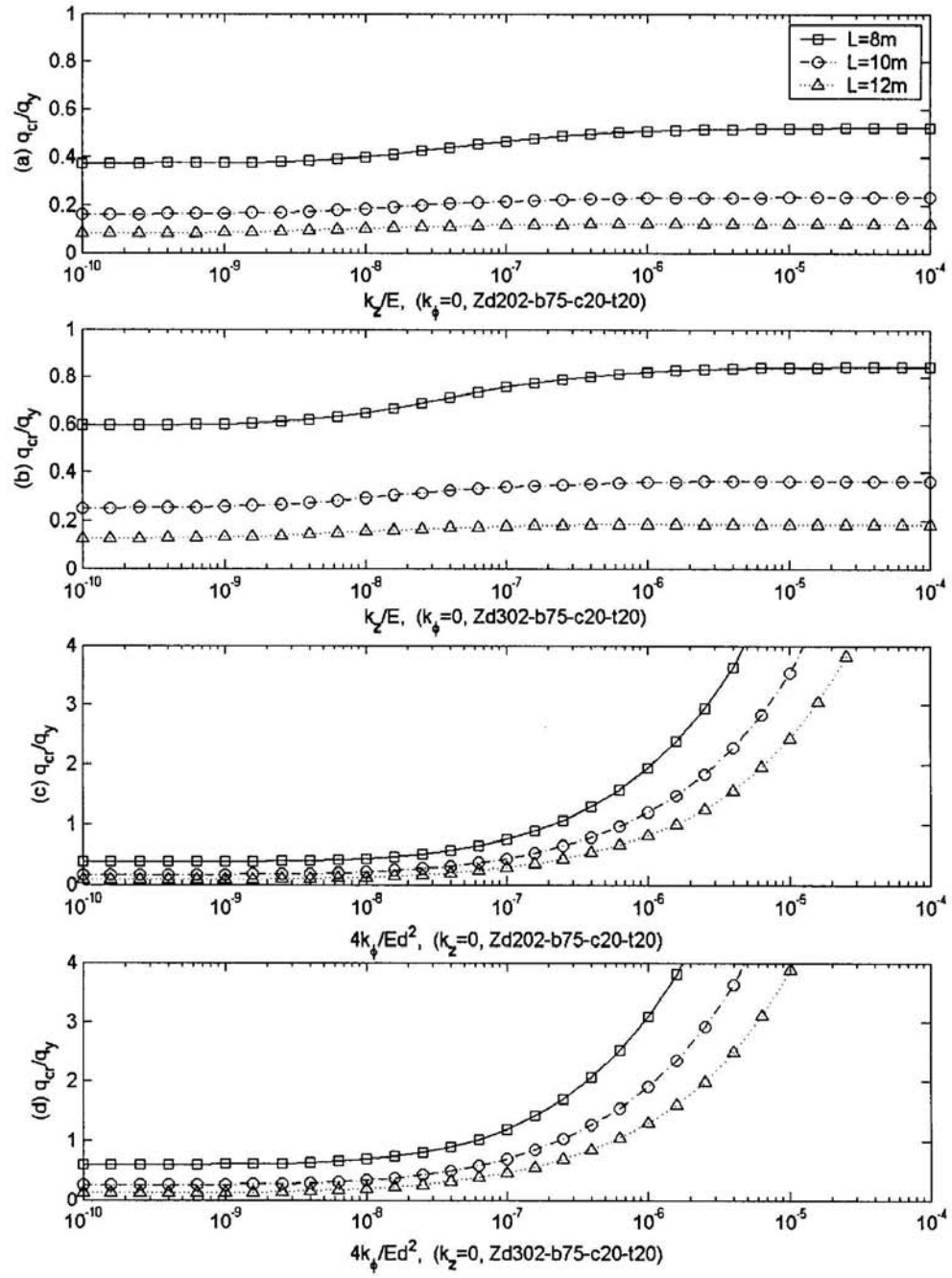


**Fig.6.21 Influence of spring stiffnesses on the critical load of simply supported zed section beam ($y_q$=-d/2, $z_q$=0).**

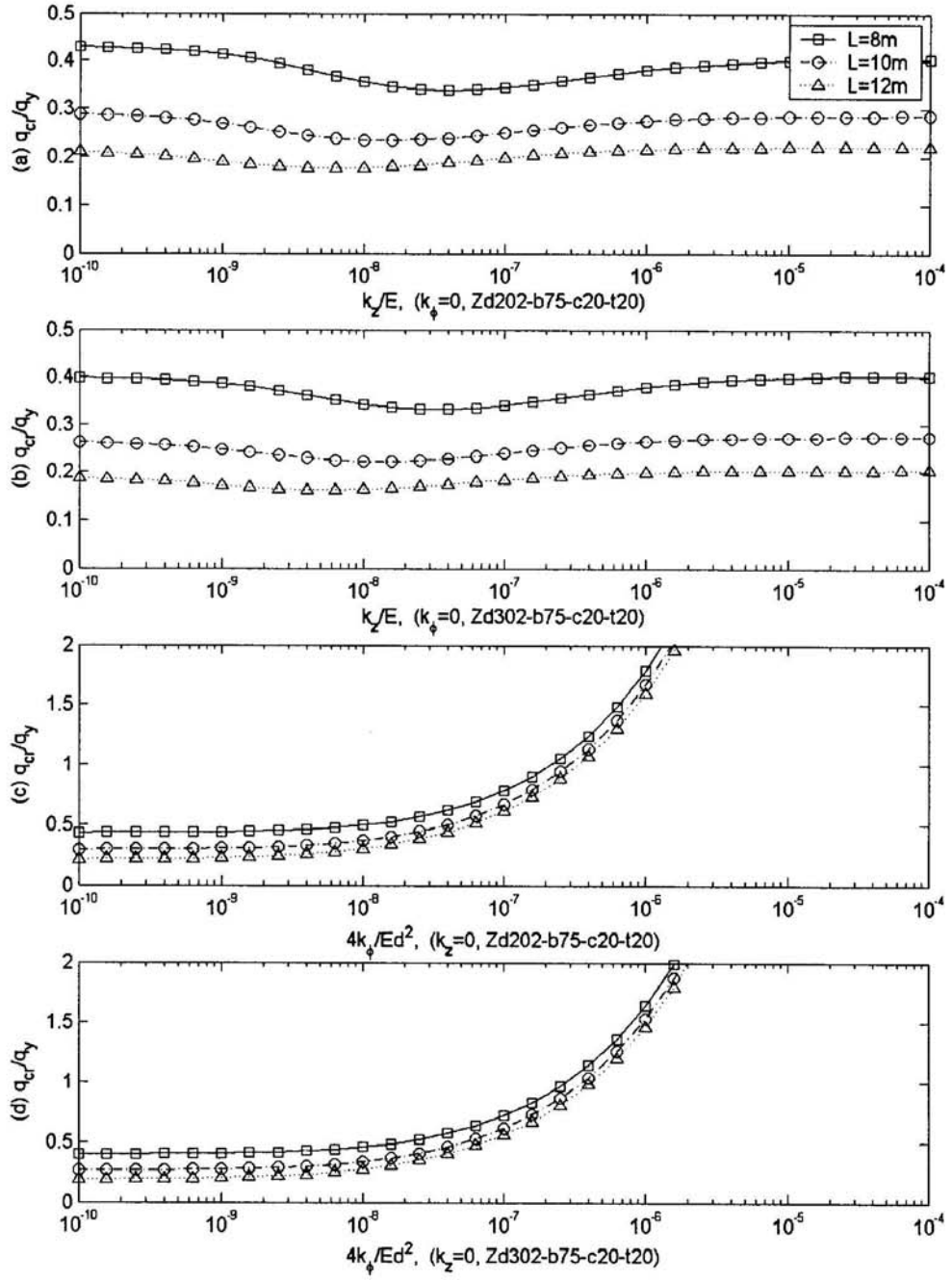


**Fig.6.22 Influence of spring stiffnesses on the critical load of zed section beam with one end simply supported and other end fixed ($y_q$=-d/2, $z_q$=0).**

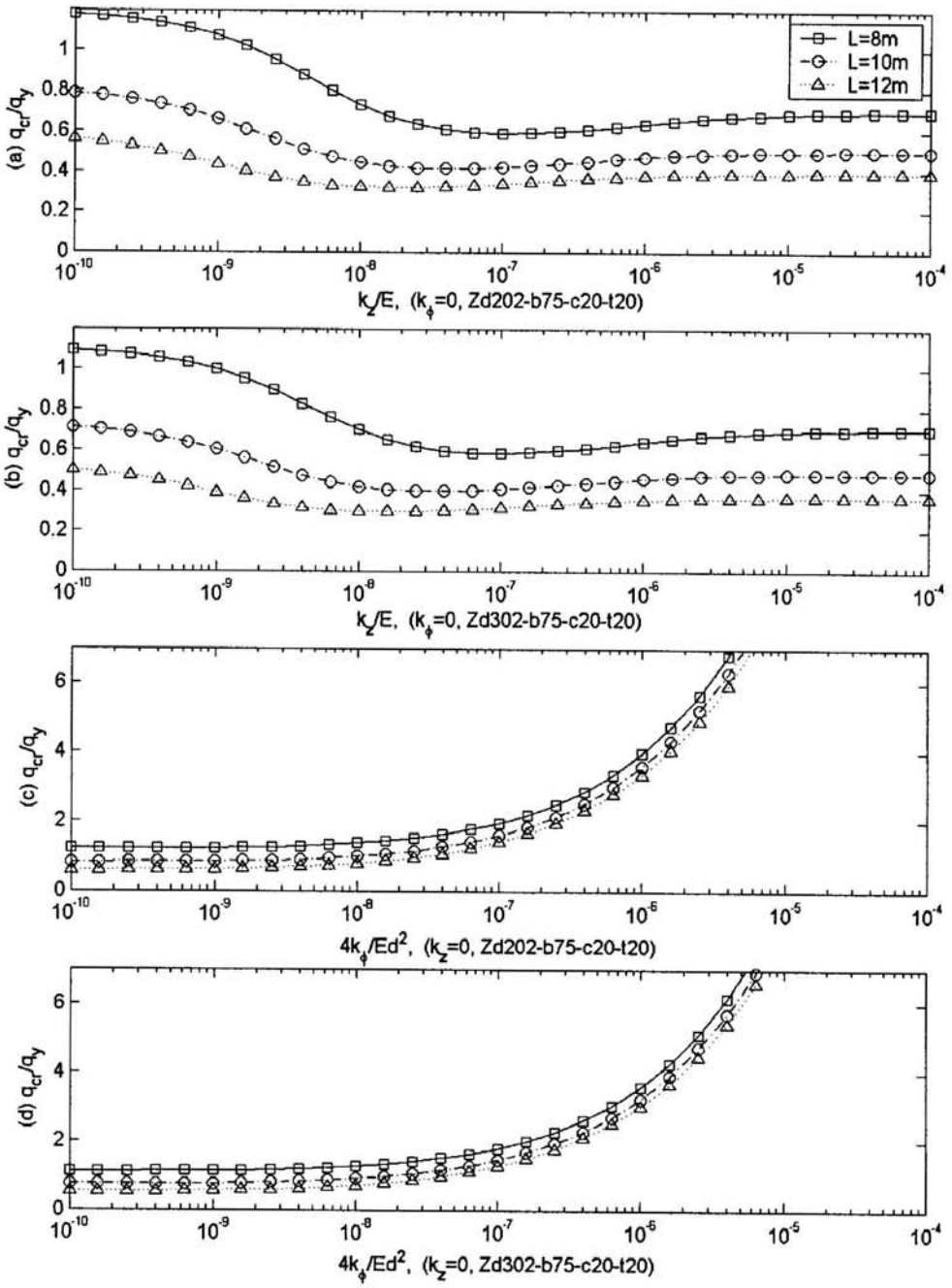


**Fig.6.23 Influence of spring stiffnesses on the critical load of fixed zed section beam ($y_q$=-d/2, $z_q$=0).**

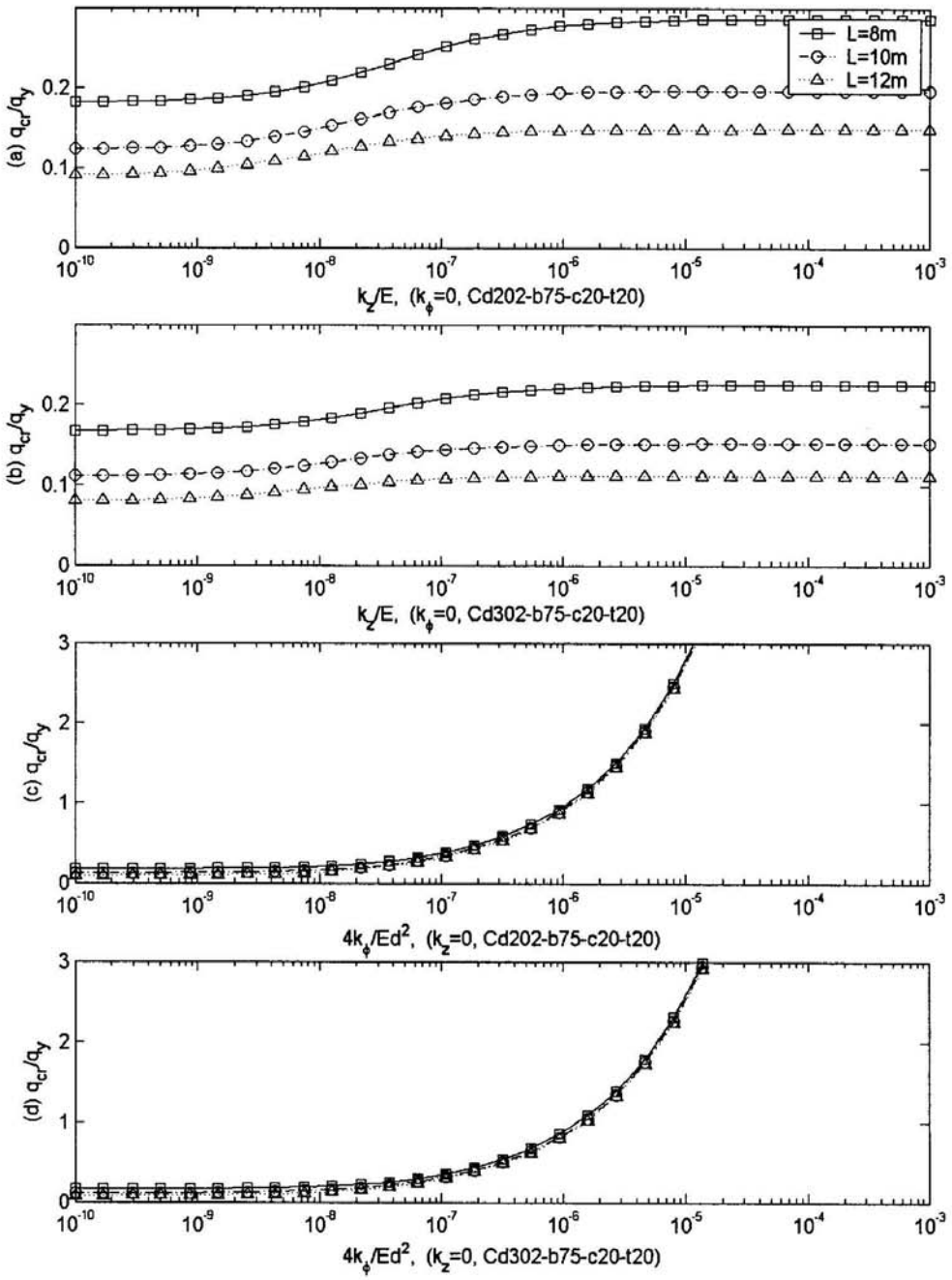


**Fig.6.24 Influence of spring stiffnesses on the critical load of simply supported channel section beam ($y_q$=-d/2, $z_q$=-e2).**

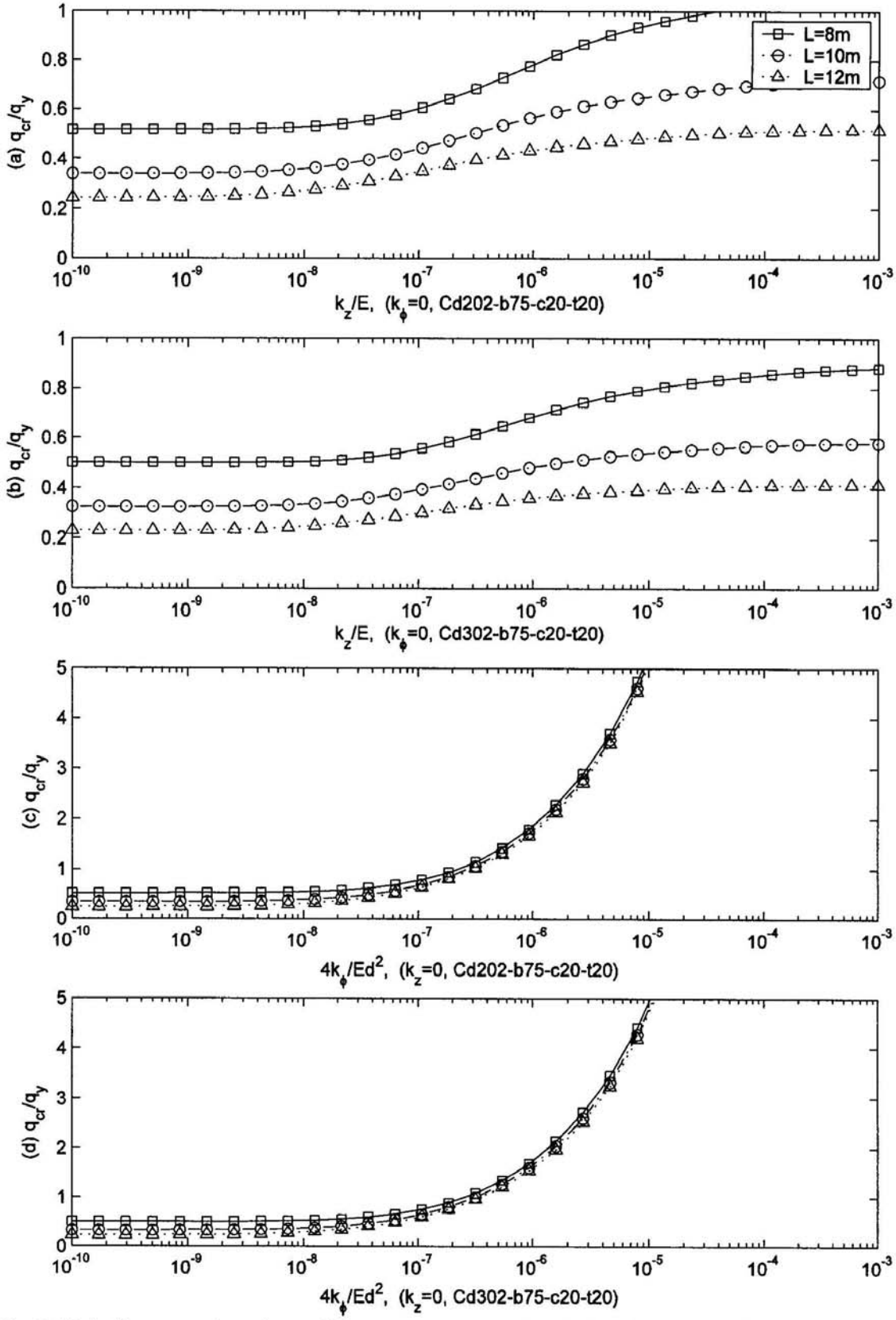


**Fig.6.25 Influence of spring stiffnesses on the critical load of channel section beam with one end simply supported and other end fixed ($y_q$=-d/2, $z_q$=-e2).**

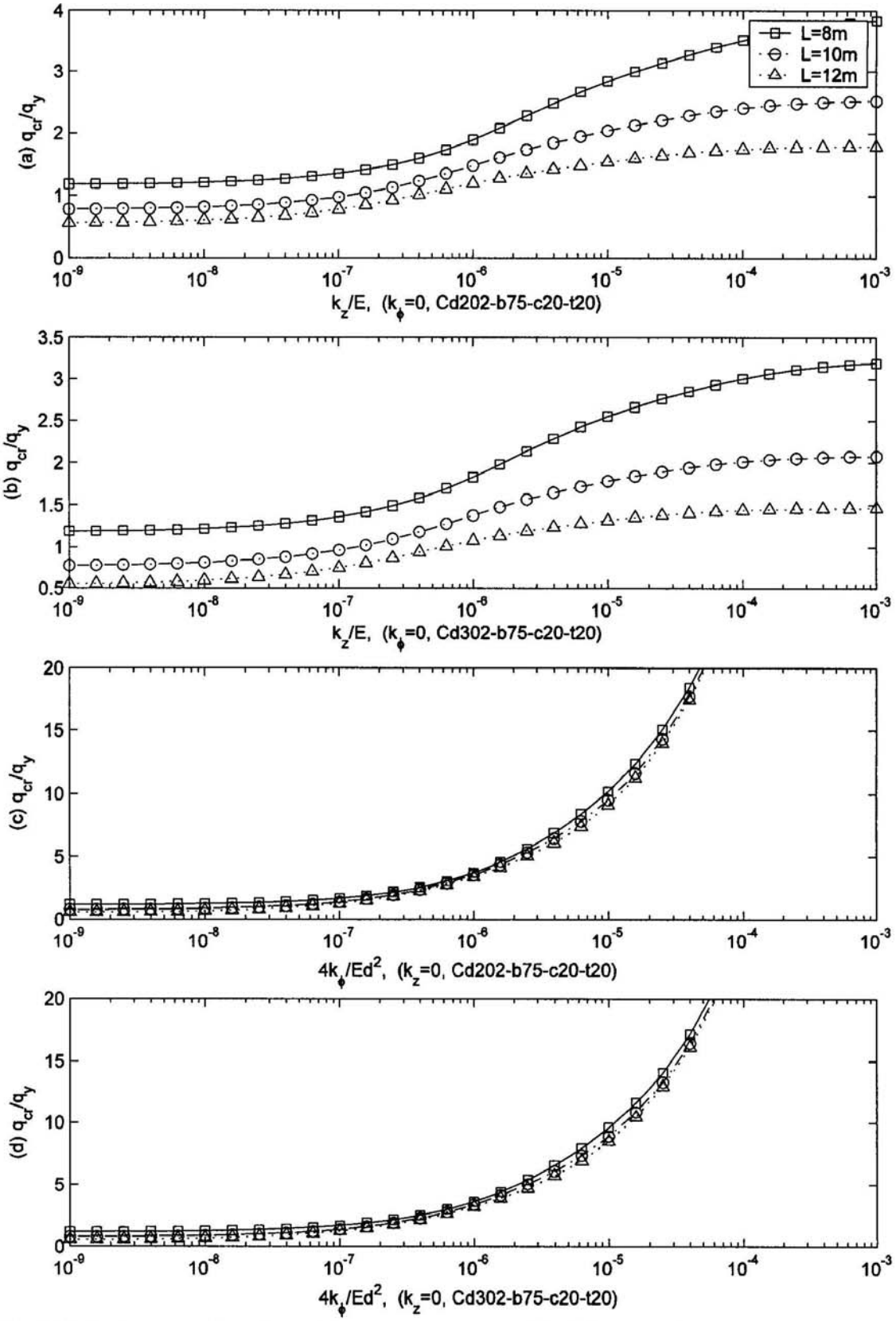


**Fig.6.26 Influence of spring stiffnesses on the critical load of fixed channel section beam ($y_q$=-d/2, $z_q$=-e2).**

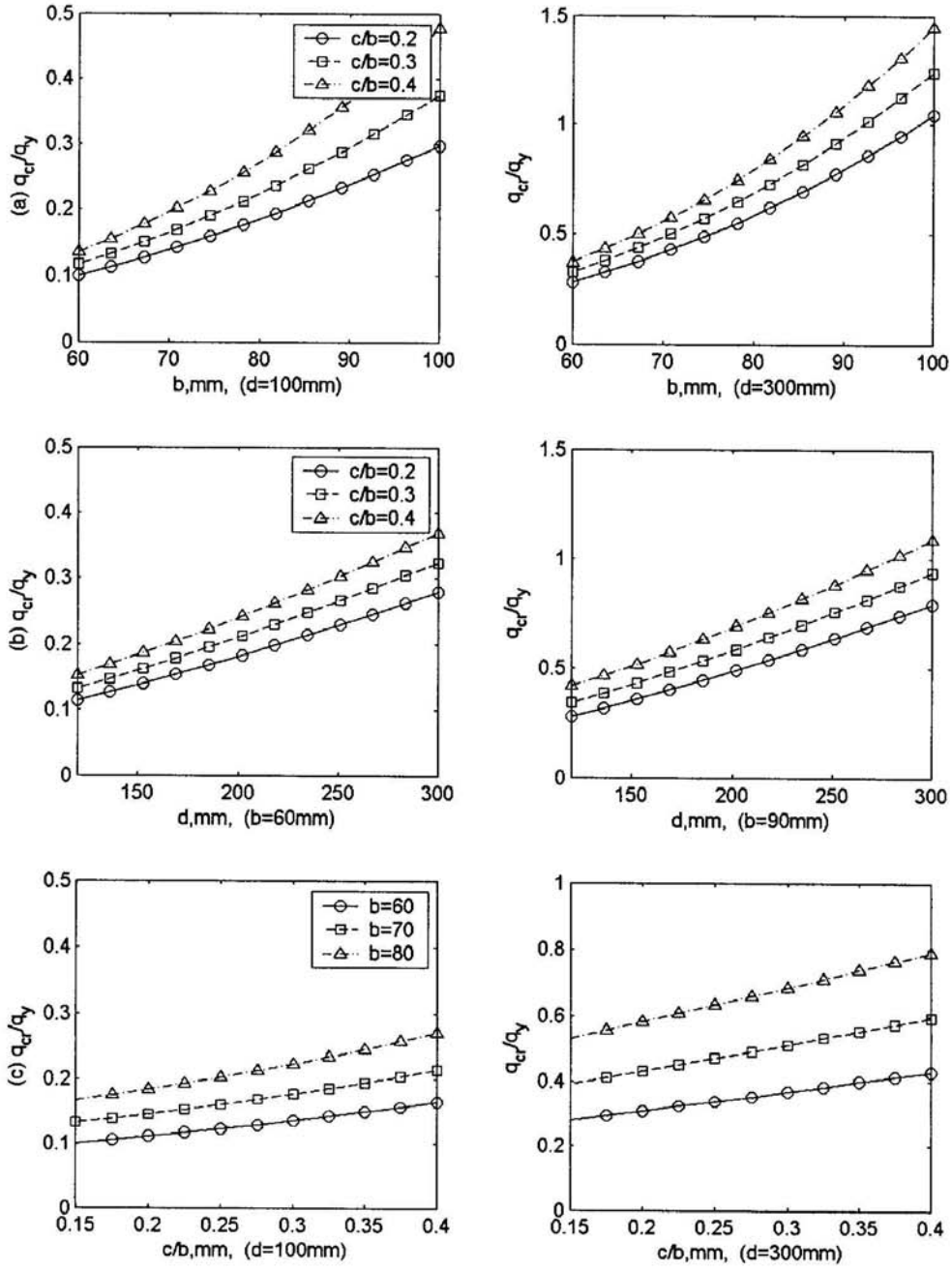


**Fig.6.27 Influence of the dimensions of cross section on the local buckling loads for the simply supported zed section beams ($k_z$=0, $k_\phi$=0, $y_q$=-d/2, $z_q$=b/2).**

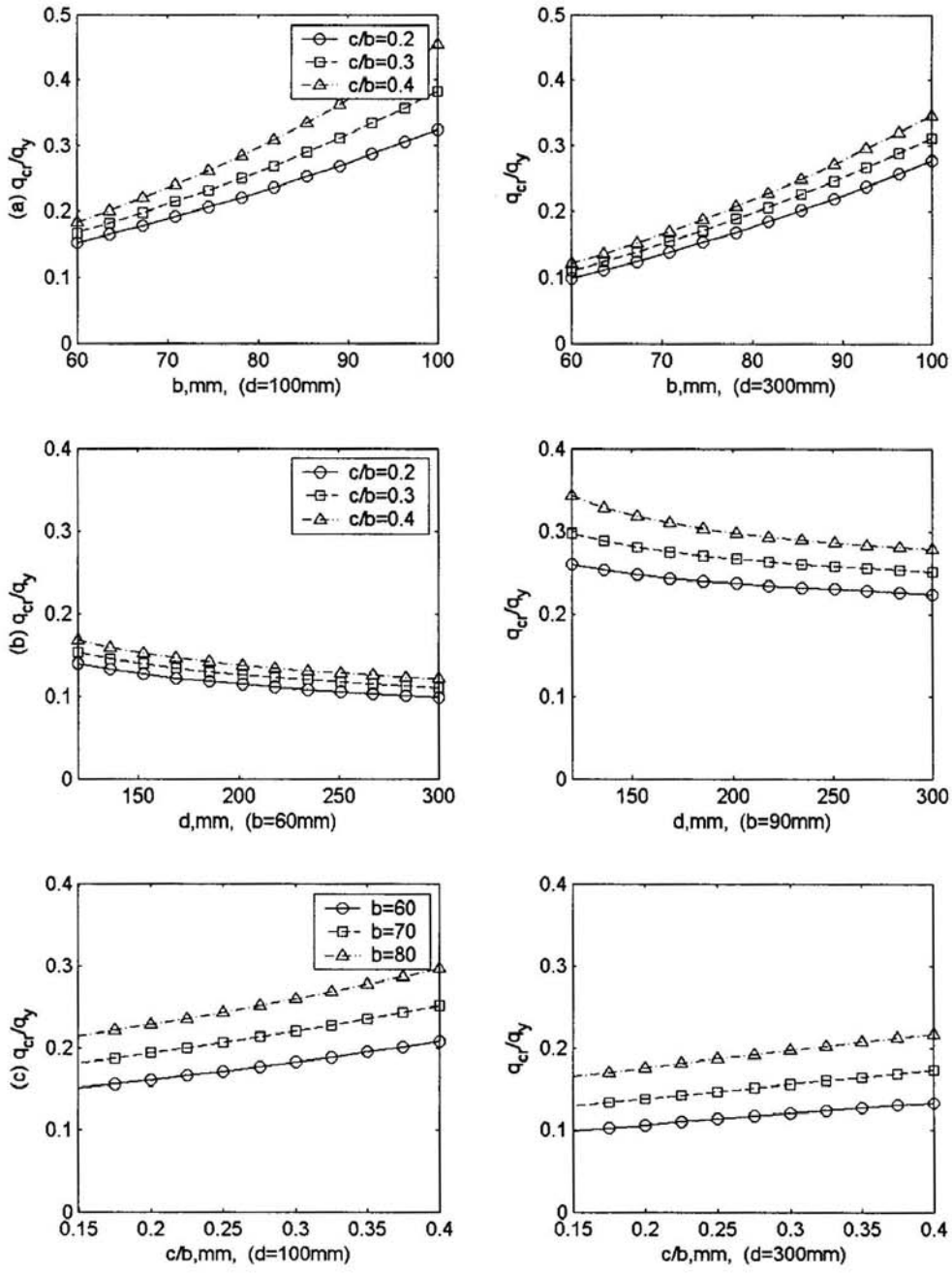


**Fig.6.28 Influence of the dimensions of cross section on the local buckling loads for the simply supported channel section beams ($k_z$=0, $k_\phi$=0, $y_q$=-d/2, $z_q$=b/2-e2).**

# Chapter 7

# 7 INTERACTION BETWEEN LATERAL-TORSIONAL BUCKLING AND LOCAL BUCKING

## 7.0 CHAPTER SYNOPSIS

This chapter presents a novel analytical model for determining the load capacity for the lateral-torsional buckling of statically indeterminate zed purlins (single span beams with one or two ends fixed), with partial lateral restraint from metal sheeting, when subjected to a uniformly distributed uplift load. The model takes account of the influence of the "softening" of the section stiffness due to local buckling and/or local material yielding. The analytical model developed in this paper, together with the numerically or experimentally obtained moment-rotation curves describing the local stiffness softening, can be used to determine the critical load for lateral-torsional buckling of the statically indeterminate purlin.

## 7.1 INTRODUCTION

Structural members made with cold-formed sections are widely used as purlins or rails, the intermediate members between the main structural frame and the corrugated roof or wall sheeting in light gauge steel construction. These members are produced in a variety of forms, such as zed, channel and sigma, which are inherently sensitive to local, distortional and lateral-torsional buckling (Hancock, 1997a; Davies, 2000). The modes corresponding to these different types of buckling are well defined in the paper of Hancock (1997a). In the literature, local buckling has been extensively addressed but, in contrast, lateral-torsional buckling has not been considered by many investigators. This is probably because cold-formed steel members are usually used together with metal sheeting which restrains the lateral movement of the members and so reduces the possibility of the occurrence of lateral-torsional buckling. However, with the increasing use of various new composite cladding systems that offer little rotational restraint to the purlin, the consideration of lateral-torsional buckling becomes necessary.

In current design codes such as BS 5950 (1998) and EC3 (1996) the lateral-torsional buckling of cold-formed members is treated by using the theory of the lateral buckling of detached beams, but this does not take into account either the lateral restraint of the sheeting or the torsion produced by the loading that is not applied at the shear centre. The analytical model for predicting the lateral-torsional buckling of cold-formed zed-purlins partially restrained by the sheeting, originally presented by Li (2004), has been developed in Chapter 6. However, the model considers only elastic buckling with no interaction with the other buckling modes. Experience has shown that, if a purlin is not very long and if it is fixed at one or both ends, local material yielding near the fixed end(s) will take place before lateral-torsional buckling occurs. A problem previously recognized is that of the exploitation of the inelastic bending strength reserve that seems to exist, as well as the associated problem of bending moment redistribution. The main objection to the existence of such a strength reserve is based on the fact that thin-walled cross-sections are not compact enough for significant plastic strain to develop. The high width to thickness ratios of the elements of the

cross-section and the consequent existence of local buckling corroborate in favour of this objection. Experimental and theoretical research has shown that some inelastic strength reserve in bending does indeed exist. This reserve mainly depends on the width to thickness ratio of the compressed part of the cross-section and the degree of longitudinal restraint at the member's walls. This indicates that the analysis of lateral-torsional buckling has to take into account the influence of the local softening of the section stiffness due to this local buckling and/or local material yielding.

Previous attempts have been made to consider the influence of the local buckling and/or local material yielding on the load capacity of purlin systems. Recently, EC 3 (1996) provides a simple trial and error method to deal with the interaction of local and lateral-torsional buckling for two-equal-span continuous beams. However, the application of this method to continuous, arbitrary multi-span beams is limited. In addition to this trial and error method, there is a simplified method, namely the moment redistribution method, which was very popular in past (Rhodes & Lawson, 1993). The main reservations for the application of moment redistribution are the unfamiliar form of the $M$-$\theta$ diagram caused by cracking and plasticization of some regions of the structure and the strong dependence of $M$-$\theta$ on the shearing forces that develop near the support points. The form of this non-linear $M$-$\theta$ diagram is due to the combination of material non-linearity with severe local buckling, the softening branch being its main trait (Grundy, 1990). Laine and Tuomala (1999) investigated experimentally the utilization of a softening moment resistance and described an ideally plastic calculation method which defines the bending moment at the internal support as a function of the plastic rotation. Softening behaviour of continuous thin-walled steel beams was also studied numerically by Thomopoulos et al (1996).

## 7.2 A SPRING MODEL OF ANALYZING LATERAL-TORSIONAL BUCKLING

For a statically determinate purlin, its corresponding moment distribution diagram when lateral-torsional buckling occurs is illustrated in Fig.7.1. However, for a statically indeterminate purlin, with one end simply supported and the other fixed, the

initial moment distribution diagram has different format as is shown in Fig.7.2. It is well known that, the purlin will undergo lateral-torsional buckling if it has a long span. But if the purlin is not very long, it will buckle locally in the region near the fixed end before lateral-torsional buckling takes place since the moment in the region close to the fixed end is the largest. After the local buckling occurs, the purlin is still able to sustain the load. However, the moment at the fixed support will decrease because of the local buckling, while the span moment increases as usual. With further increase of the load, the beam will undergo overall lateral-torsional buckling. This indicates that the analysis of lateral-torsional buckling has to take into account the influence of the local softening of the section stiffness due to the local buckling.

### 7.2.1 Analytical Model

Consider a statically indeterminate zed section beam (fixed at both ends), subjected to a uniformly distributed transverse load, the section of which is shown in Fig.7.3a. It is assumed that the section is laterally restrained in the translational direction but free in the rotational direction ($k_z=\infty$, $k_\phi=0$), which is of most practical applications. The model representing the lateral-torsional buckling when there has been some softening at the supports for the statically indeterminate purlin is illustrated in Fig.7.3b, in which the statically indeterminate beam is simplified to a simply supported beam with two rotational springs over the two indeterminate supports.

The critical buckling load of the simplified beam with rotational spring supports, as shown in Fig.7.3, can be determined by using a similar energy method based on the analytical method addressed in Chapter 2, 3 and 6, in which the analysis involves two steps. The first is *the stress analysis*, which determines the pre-buckling stress distribution in the member. The second is *the buckling analysis,* which determines the critical buckling load when lateral-torsional buckling occurs.

Similarly, the strain energy of the beam due to deflections and rotation can be expressed as:

$$U_{o\_beam} = \frac{E}{2}\int_o^l [I_y(\frac{d^2w}{dx^2})^2 + 2I_{yz}\frac{d^2w}{dx^2}\frac{d^2v}{dx^2} + I_z(\frac{d^2v}{dx^2})^2]dx + \int_o^l [\frac{GJ}{2}(\frac{d\phi}{dx})^2 + \frac{EI_\omega}{2}(\frac{d^2\phi}{dx^2})^2 - EI_{\omega z}\frac{d^2v}{dx^2}\frac{d^2\phi}{dx^2}]dx \tag{7.1}$$

The strain energy stored in the two distributed springs due to the deformation of the beam can be expressed by

$$U_{o\_spring} = \frac{k_z}{2}\int_o^l (w + y_k\phi)^2 dx + \frac{k_\phi}{2}\int_o^l \phi^2 dx \tag{7.2}$$

where $k_z$ and $k_\phi$ = the per-unit length stiffness constants of the translational and rotational springs.

The strain energy stored in the two rotational springs over the supports can be expressed by

$$U_{o\_k} = \frac{1}{2}[k_1(\frac{dv}{dx}\Big|_{x=0})^2 + k_2(\frac{dv}{dx}\Big|_{x=l})^2] \tag{7.3}$$

where $\frac{dv}{dx}\Big|_{x=0}$ and $\frac{dv}{dx}\Big|_{x=l}$ = the rotational angles about $z$ axis over two supports;

$k_1$ and $k_2$ = the constants of the two rotational springs applied at the ends of the purlin.

For a purlin that is subjected only to a uniformly distributed transverse load at the point $(y_q, z_q)$, the potential energy generated by the load can be expressed by

$$W_o = \int_o^l q(v - z_q\phi)dx \tag{7.4}$$

The deflections, $v(x)$ and $w(x)$, and the angle of twist $\phi(x)$ due to the externally applied loads can be determined by employing the stationary principle as follows:

$$\delta(U_o - W_o) = \delta(U_{o\_beam} + U_{o\_spring} + U_{o\_k} - W_o) = 0 \tag{7.5}$$

After the deflections and rotation are determined the pre-buckling moment distributions along the longitudinal axis can then be calculated using Eq. (3.1). Then the pre-buckling longitudinal stresses can be calculated as follows:

$$\sigma_x(x,y,z) = \sigma_{xb} + \sigma_{xw} \tag{7.6}$$

where $\sigma_{xb}$ and $\sigma_{xw}$ = the longitudinal stresses generated by the bending and twisting moments, respectively, which are expressed by

$$\sigma_{xb} = \sigma_{xbz} + \sigma_{xby} = M_z \frac{I_y y - I_{yz} z}{I_y I_z - I_{yz}^2} + M_y \frac{I_z z - I_{yz} y}{I_y I_z - I_{yz}^2} \tag{7.7}$$

$$\sigma_{xw} = E(\overline{\omega} - \omega - y\frac{I_{\omega z}}{I_z})\frac{d^2\phi}{dx^2} = E(\overline{\omega}_s - \omega_s)\frac{d^2\phi}{dx^2} \tag{7.8}$$

The pre-buckling longitudinal stresses generated by the pre-buckling bending and twisting moments can be calculated, which are then used to calculate the strain energy generated by the membrane stresses through the buckling displacements as follows:

$$\begin{aligned} W_{\sigma xb} &= -\int_o^l \int_A \sigma_{xb}(x,y,z)\varepsilon_{x2}(x,y,z)dAdx \\ W_{\sigma xw} &= -\int_o^l \int_A \sigma_{xw}(x,y,z)\varepsilon_{x2}(x,y,z)dAdx \end{aligned} \tag{7.9}$$

The strain energy generated by the load due to the load acting above the shear centre can be expressed as:

$$W_q = -\frac{y_q}{2}\int_o^l q\phi_b^2 dx \tag{7.10}$$

The expression used for calculating the strain energy generated by the buckling displacements is the same as Eqs.(7.1)-(7.3),

$$\begin{aligned} U_1 = {} & \frac{E}{2}\int_o^l [I_y(\frac{d^2w_b}{dx^2})^2 + 2I_{yz}\frac{d^2w_b}{dx^2}\frac{d^2v_b}{dx^2} + I_z(\frac{d^2v_b}{dx^2})^2]dx \\ & + \frac{GJ}{2}\int_o^l (\frac{d\phi_b}{dx})^2 dx + \frac{EC_w}{2}\int_o^l (\frac{d^2\phi_b}{dx^2})^2 dx + \frac{1}{2}[k_1(\frac{dv_b}{dx}\Big|_{x=0})^2 + k_2(\frac{dv_b}{dx}\Big|_{x=l})^2] \end{aligned} \tag{7.11}$$

The minimum critical buckling load and the corresponding buckling mode displacements can thus be determined by the use of the following variational equation:

$$\delta(U_1 - \lambda W_1) = \delta(U_{1\_beam} + U_{1\_spring} + U_{1\_k} - W_{\sigma xb} - W_{\sigma xw} - W_q) = 0 \qquad (7.12)$$

where $\lambda$ = the loading proportional factor, i.e., the critical buckling load factor.

The details of the numerical treatment can be found in Chapter 2 and 6 and thus are not presented further here.

### 7.2.2 Bucking Load Of Spring Model

For given $k_1$ and $k_2$ values the above model can be used to calculate the critical buckling load. Figures 7.4 and 7.5 plot the critical buckling load against the spring stiffness $k$ for a zed section beam (Zd202_b75_c20_t20) subjected to the uniformly distributed uplift load applied at the middle of top flange, for the material properties listed in Table 3.1. The results are presented for three different span lengths – 3, 5 and 8 m – representing short, intermediate and long beams, respectively. As is expected, the critical load increases with the spring constant but reduces as the length of the beam increases. The critical load corresponding to $k_1=k_2=0$ represents the critical load of the purlin with both ends simply supported, whereas the critical load corresponding to $k_1 = k_2 = \infty$ represents the critical load of the purlin with both ends fixed. For the case of $k_1 = 0, k_2 = \infty$ it represents the purlin with one end simply supported and the other end fixed.

## 7.3 LATERAL-TORSIONAL BUCKLING OF STATICALLY INDETERMINATE PURLINS

Analysis of the lateral-torsional buckling of statically indeterminate thin-walled beams is very difficult as it is usually required to consider local influences such as local buckling or local material yielding unless the particular beam is very long, in

which case local buckling or local material yielding does not occur before the beam buckles lateral-torsionally. Although the occurrence of local buckling or local material yielding may not cause the failure of the beam, it alters the distribution of internal forces in the beam and so conventional analysis of the eigen-value type cannot be applied directly.

Strictly speaking, the analysis of the lateral-torsional buckling of statically indeterminate beams involving local buckling or local material yielding has to be nonlinear, using the load increment method (Zienkiewicz & Taylor, 2000). The analysis takes account of local post-buckling and/or local post-yielding behavior of the section if either occurs before the beam undergoes an overall lateral-torsional buckling. The local post-buckling and local post-yielding behaviour of the beam can be obtained by using experimental or numerical methods (finite element analysis) (Laine & Tuomala, 1999).

### 7.3.1 $M$-$\theta$ Relationship Of Local Buckling

Fig.7.6a shows typical curves of moment-to-angle of rotation at the loading point for a cantilever purlin with a point load applied at its free end, which were idealized from experimental results (Li, 1999). The corresponding curves of moment-to-angle of rotation at the fixed end are plotted in Fig.7.6b.

These curves describe the softening behaviour of the section due to local buckling and can be used to describe the post-buckling relationship between the moment and the angle of rotation at the fixed support for the statically indeterminate beam when it is loaded, although their exact value when lateral-torsional buckling occurs is also dependent upon the properties of the section, the length of the beam and the load applied.

### 7.3.2 $M$-$\theta$ Relationship Of The Spring Model

Consider a statically indeterminate beam, one end simply supported and the other end fixed, subjected to a uniformly distributed uplift load. If the load is small, neither local nor overall buckling occurs. When the load increases to a certain value, this beam will suffer local buckling which takes place in the region close to the fixed end

since it is in that region that the moment is the largest. After the local buckling occurs the angle of rotation at the fixed support increases while the actual moment decreases, as shown by the curves in Fig.7.6b.

With further increase of the load, the beam will undergo overall lateral-torsional buckling, with $M_{sup}$ and $\theta_{sup}$ assumed to be the moment and angle of rotation at the fixed end when the beam experiences overall lateral-torsional buckling. It is conceivable that the pre-buckling moment distribution of the beam is dependent only on the final values of $M_{sup}$ and $\theta_{sup}$. The stiffness of the rotation spring thus should be $k=M_{sup}/\theta_{sup}$.

Note that for the simply supported beam with a rotation spring at its one end ($k_i$), the analytical model presented in Section 7.2 can be used to calculate the critical load ($q_i$) of the lateral-torsional buckling of the beam (see in Fig.7.4 and 7.5), which can be used to calculate the end angle of rotation ($\theta_i$) by using conventional stress analysis method. The corresponding moment at the support can thus be calculated from the obtained angle of rotation. The curve of $M_{sup}$~$\theta_{sup}$ obtained in this way is plotted in Fig.7.7. It can be seen that the moment reduces with the increase of the angle of rotation. The rotational spring stiffness is zero at the bottom end of the curve, where the support can be regarded as being simply supported; whereas at the top of the curve, the rotational spring stiffness is very large and the corresponding support can be regarded as a fixed support.

### 7.3.3 Determination Of $M_{sup}$ And $\theta_{sup}$ When Lateral-Torsional Buckling Occurs

Figs.7.8 and 7.9 show the re-plotted curves of Figs.7.4 and 7.5. The re-plotted $M_{sup}$~$\theta_{sup}$ curves provide the relationship between $M_{sup}$ and $\theta_{sup}$ when lateral-torsional buckling is taking place. These curves together with the numerically or experimentally determined $M$~$\theta$ curves describing the section stiffness softening can be used to determine the exact values of $M_{sup}$ and $\theta_{sup}$ at which the lateral-torsional buckling actually occurs. In order to demonstrate this, the worst $M_{sup}$~$\theta_{sup}$ curve (with the steepest slope) shown in Fig.7.6b describing the local post-buckling behaviour of

the section is superimposed in Figs.7.8 and 7.9 (the dot straight line). Examination of Figs.7.8 and 7.9 shows that there are three different cases:

- ⇨ The first one is for the long span purlin ($l$=8m) in which lateral-torsional buckling occurs first and thus there is no rotation at the support before the lateral-torsional buckling occurs and therefore $k = \infty$.
- ⇨ The second case is for the intermediate span purlin ($l$=5m) in which local buckling occurs initially and so there is some rotation at the fixed support when the subsequent lateral-torsional buckling occurs. The intersection point of the two curves provides the values of $M_{\text{sup}}$ and $\theta_{sup}$ for lateral-torsional buckling. From $M_{\text{sup}}$ and $\theta_{sup}$ the value of $k$ and thus the critical load $q_{cr}$ can be determined, which presents the interaction between the local buckling and the overall lateral-torsional buckling.
- ⇨ The third one is for the short span purlin ($l$=3m) in which case local buckling again occurs initially. However, it is apparent that when the subsequent lateral-torsional buckling occurs, the beam has already had a large rotation at the fixed support and therefore the value of $k$ is rather small. This indicates that for the short span purlin when lateral-torsional buckling occurs the fixed support has almost lost its rotational resistance. Consequently, for the sake of simplicity the critical load of the lateral-torsional buckling for short beams can be calculated simply based on the beam with simply supported boundaries.

## 7.4 NUMERICAL RESULTS

Figs.7.10 and 7.11 shows the critical loads of lateral-torsional buckling for the zed-purlin beams obtained by using the approach introduced in Section 7.3. Fig.7.10 is for beams with one end simply supported and the other end fixed, while Fig.7.11 is for the beams with both ends fixed. In order to examine the feature of the results, two curves obtained from the same beam but without considering the influence of local buckling are also superimposed in the figure.

From Figs.7.10 it is interesting to notice that, for long beams, the curve that considers local buckling is very close to that for the beam having fixed support. This indicates

that the interaction between the local and lateral-torsional buckling is not important in long beams. For very short beams, the curve that considers local buckling is close to that for the beam with both ends simply-supported. This indicates that the local buckling occurs much earlier and when the lateral-torsional buckling takes place the fixed support has almost no rotational resistance. Therefore, only for the intermediate span purlins, the analysis needs to consider the interaction between the local and lateral-torsional buckling. Similar conclusions can be obtained by examining the results shown in Fig.7.11 for the beams with both end fixed.

## 7.5 SUMMARY

In this chapter a novel analytical model is presented for predicting the lateral-torsional buckling of statically indeterminate zed section purlins. The model together with experimentally or numerically obtained stiffness softening curves for local buckling or local material yielding can be used to determine the critical load of lateral-torsional buckling of the purlin with statically indeterminate boundary conditions.

Conclusions from the present study can be summarised as follows:

- For long span purlins lateral-torsional buckling occurs first and so the local stiffness softening need not be considered when analyzing the lateral-torsional buckling.

- For intermediate span purlins, local buckling occurs first and thus the analysis of lateral-torsional buckling needs to consider the local stiffness softening.

- For short span purlins, local buckling occurs much earlier than the lateral-torsional buckling and so the moment resistance at the fixed support becomes very weak when the subsequent lateral-torsional buckling occurs. Therefore for the sake of simplicity the fixed beam may be regarded as the simply supported beam for the lateral-torsional buckling analyses.

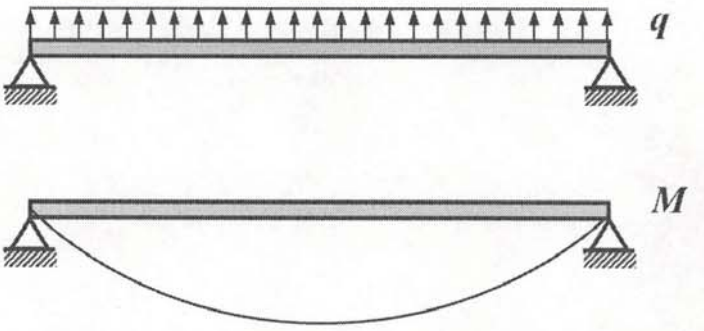


**Fig.7.1 Moment distribution of the statically determinate purlin.**

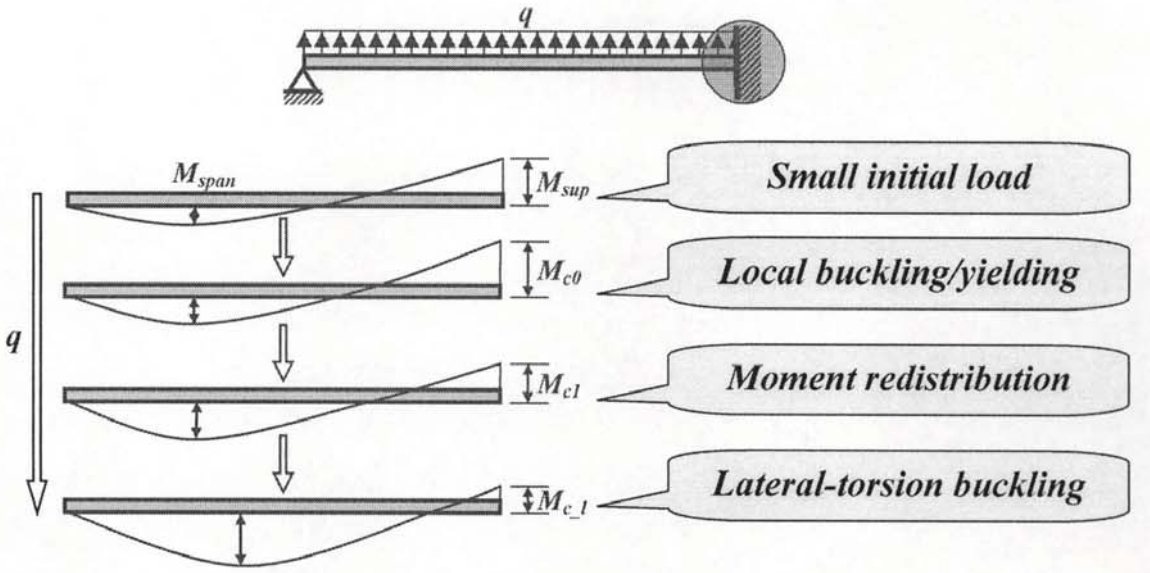


**Fig.7.2 Interaction of lateral-torsional buckling and local buckling.**

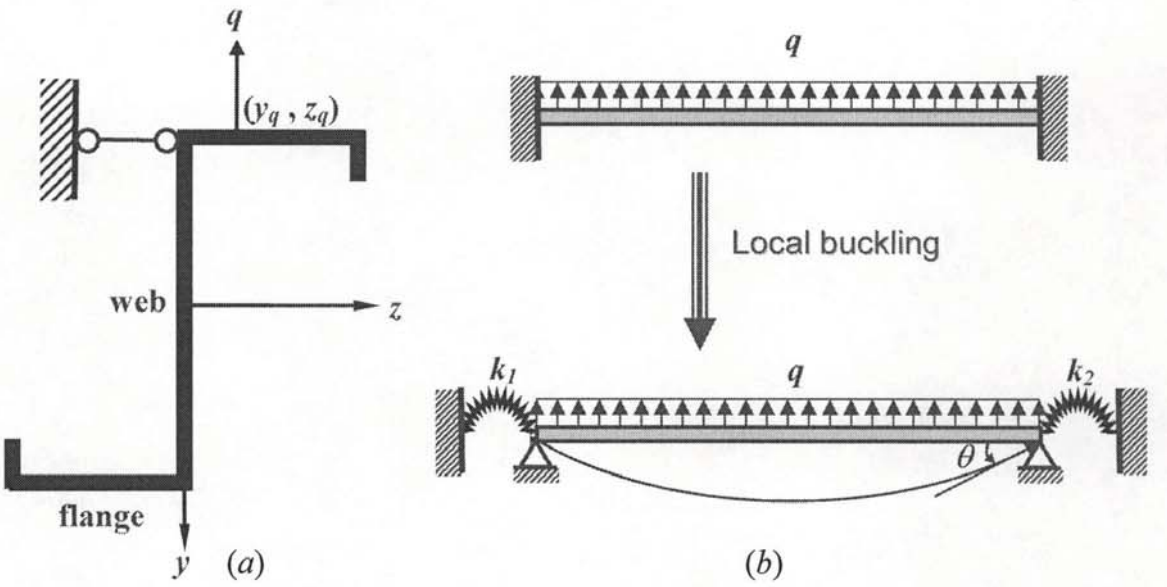


**Fig.7.3 Analytical model for the statically indeterminate purlin.**

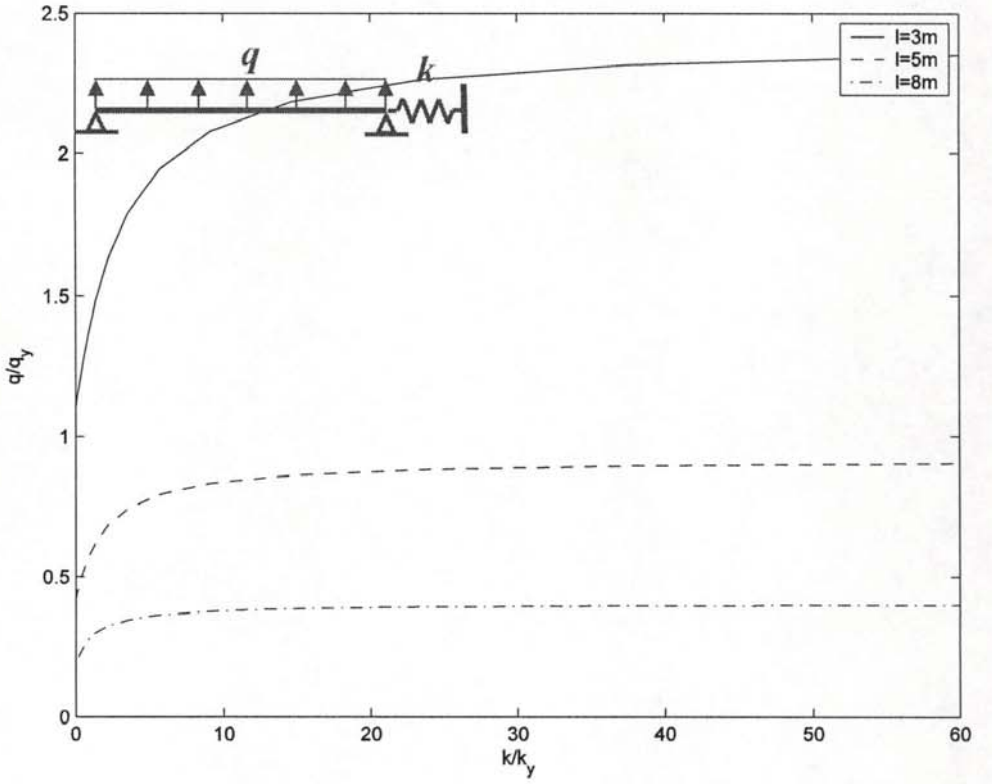


**Fig.7.4 Lateral-torsional buckling curves for one spring beam ($k_1$=0, $k_2$=$k$, $q_y = \frac{8M_{yield}}{l^2}$, $k_y = \frac{EI_z}{l}$).**

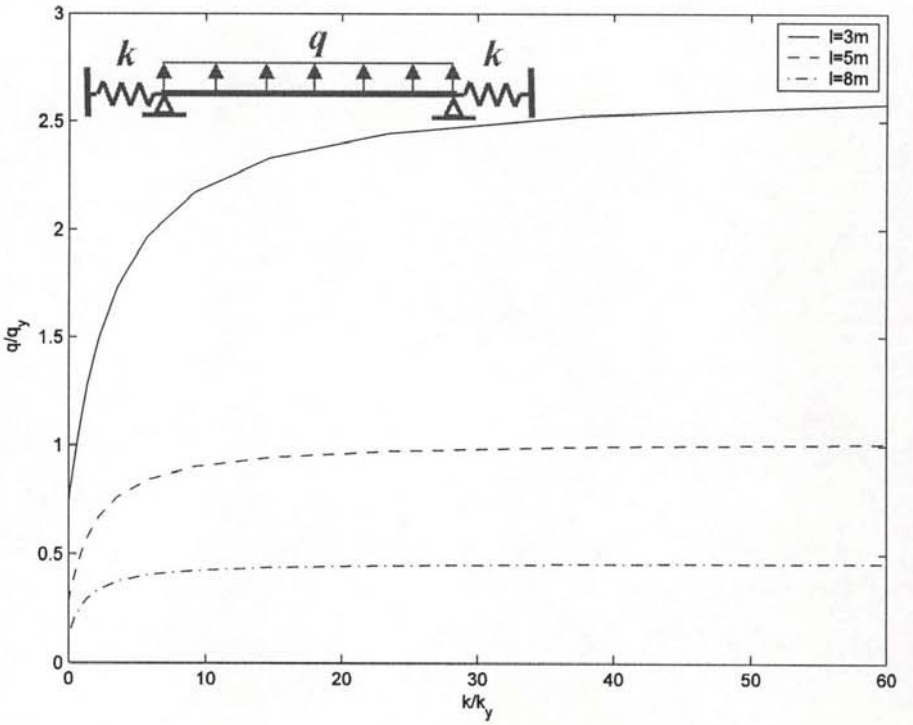


**Fig.7.5 Lateral-torsional buckling curves for two spring beam ($k_1$=$k_2$=$k$, $q_y = \frac{12M_{yield}}{l^2}$, $k_y = \frac{EI_z}{l}$).**

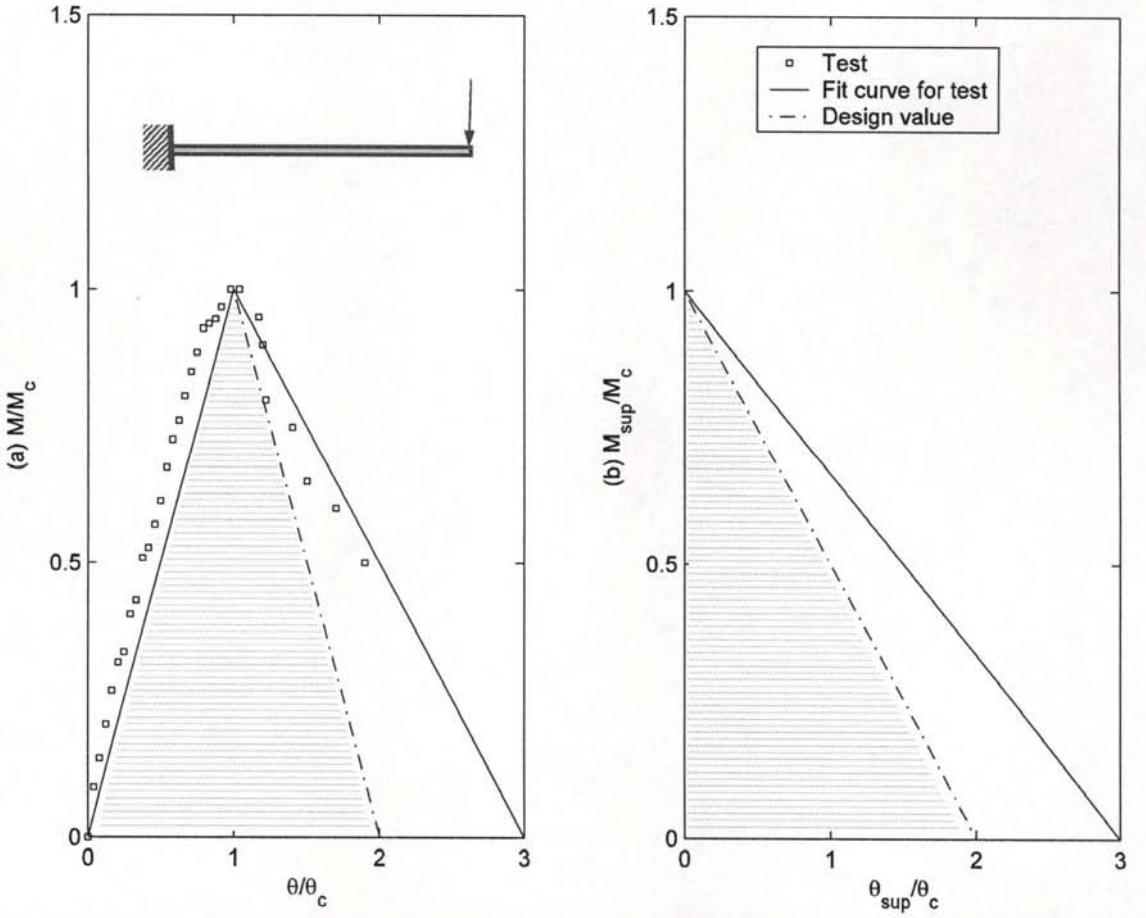


**Fig.7.6 Load-displacement curves. (a) $M$-$\theta$ curves. (b) $M_{sup}$-$\theta_{sup}$ curves. ($M$=$M_{sup}$ =$Pl$, $M_c$=local bucking moment, $\theta$=slope at loading point, $\theta_{sup}$=slope at support).**

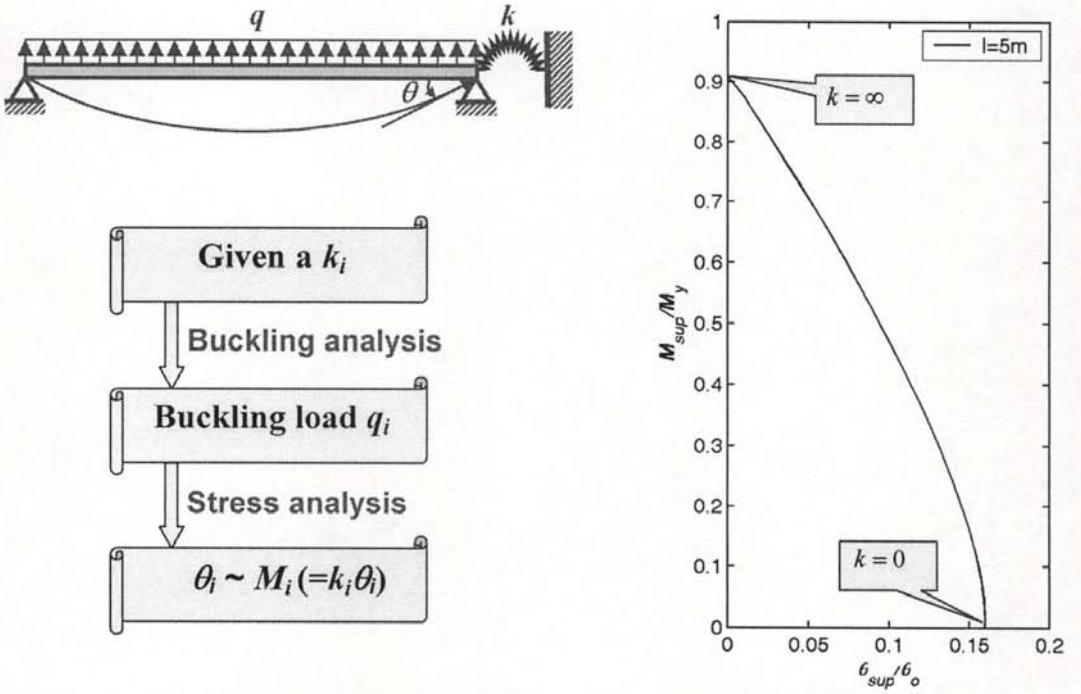


**Fig.7.7 Demonstration of *M*-$\theta$ relationship of the one spring beam model.**

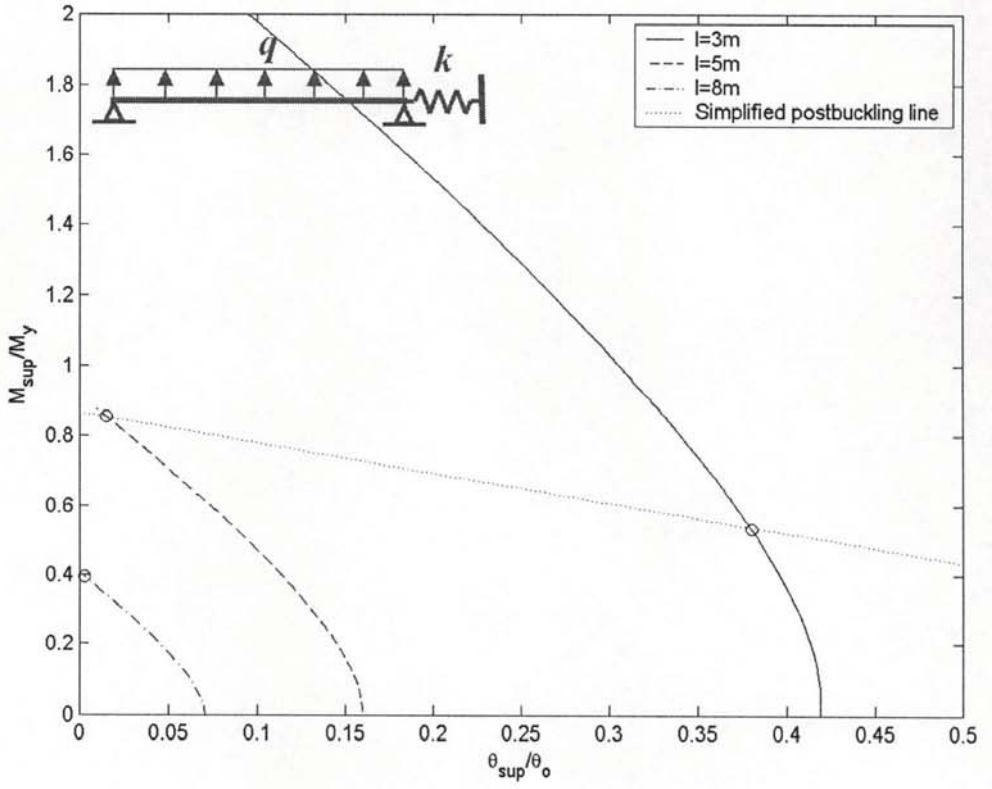


**Fig.7.8 Re-plotted buckling curves for one spring beam ($k_1$=0, $k_2$=k, $\theta_o = \frac{M_c l}{EI_z}$).**

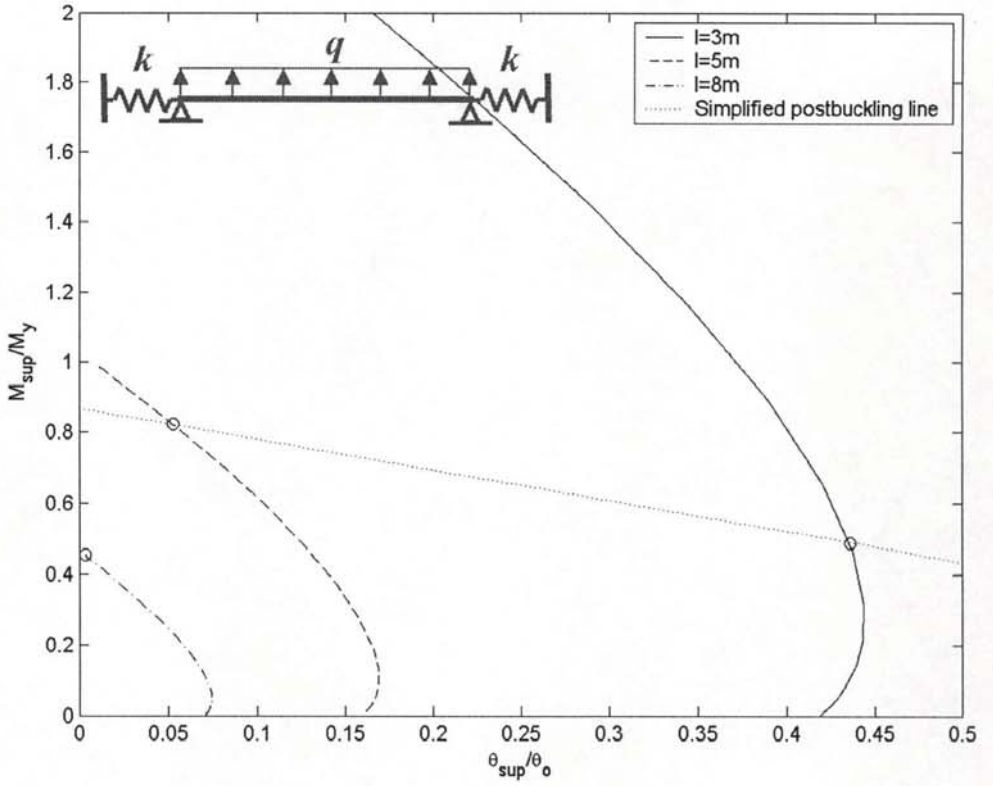


**Fig.7.9 Re-plotted buckling curves for two spring beam ($k_1$=0, $k_2$=k, $\theta_o = \frac{M_c l}{EI_z}$).**

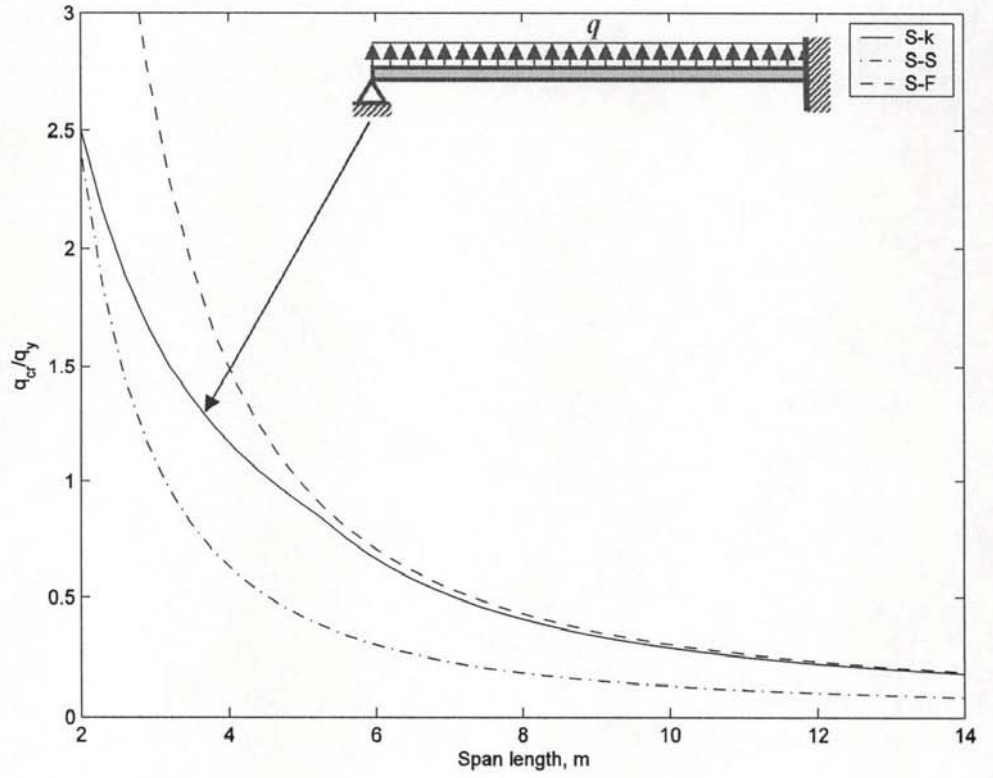


**Fig.7.10 Critical loads for the beam with one end simply supported and the other fixed ($q_y=8M_{yield}/l$).**

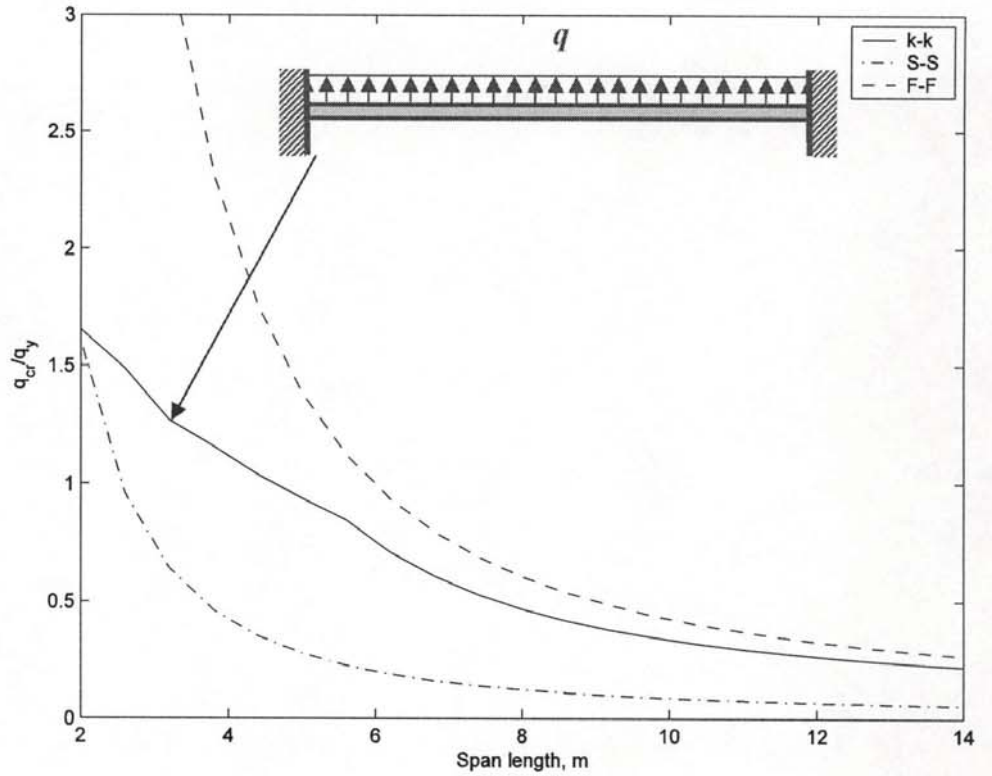


**Fig.7.11 Critical loads of for the fixed beam ($q_y=12M_{yield}/l$).**

# Chapter 8

# 8 CONCLUSIONS AND FUTURE RESEARCH

## 8.0 CHAPTER SYNOPSIS

This thesis has investigated the behaviour of cold-formed steel zed and channel section beams in purlin-sheeting systems. **The main aim was to develop an approach to investigate cold-formed zed and channel section beams with partial-lateral restraint from metal sheeting when subjected to a uniformly distributed transverse load,** which has not been extensively studied by other researchers.

Since the project has been predominately theoretical, the main methodology to perform the analysis for the cold formed steel purlins is via computer programs, which has involved an extensive range of theory developments, equation derivations, and substantial set of numerical analysis (MATLAB) on cold-formed zed and channel section beams. The programming schemes are presented in Appendix 1 and 3.

## 8.1 LITERATURE REVIEW

Chapter 2 examined the history of cold-formed structural technology, the characteristics of cold-formed structures, structural behaviour of cold-formed purlin-sheeting systems and the current approaches in design standards. The most significant findings in the literature review were:

- Developments in technology and applications make demands for a more sophisticated treatment of local, distortional and global buckling and their interactions between these different buckling modes.

- The finite strip method is the best known of the numerical methods developed for relatively short half wave-length buckling (local buckling) analysis of thin-walled beams. However, the current version of the approach becomes inaccurate when dealing with the distorsional and global buckling of long half wave-lengths for beams subjected to uniformly distributed loadings.

- Channel and Zee (Zed) sections are the most common members used as purlins and girts in roof and wall systems with sheeting attached and so the effect of the sheeting in preventing torsion and lateral-torsional buckling needs to be quantified.

## 8.2 STRESS ANALYSIS OF PURLIN-SHEETING SYSTEMS

An analytical model for the stress analysis of cold-formed zed and channel section beams, subjected to a uniformly distributed transverse load, has been developed in which the restraint actions of the sheeting are modelled by using two springs representing the translational and rotational restraints. The following conclusions are drawn:

- Both translational and rotational spring stiffnesses have significantly different influences on the stresses in the beams. The influence of the two springs has also been found to depend on the presence of anti-sag bar and the position of the loading line.

- For most of the cases, the maximum tensile and compressive stresses decrease with the increase in the translational and rotational spring stiffness. The influence of translational and rotational spring stiffness on the maximum tensile and compressive stresses occurs only in small range of stiffness value.

- As far as the maximum tensile and compressive stresses are concerned, for zed section beams the rotational spring stiffness has less influence than translational spring stiffness, while for channel section beams the rotational spring stiffness has more influence.

- The translational and rotational spring stiffnesses have more significant influence on the bending stress $\sigma_{xby}$ and warping stress $\sigma_{xw}$ than on the bending stress $\sigma_{xbz}$, particularly for the case where no bi-moments are generated by the external load.

- When there is no rotational restraint ($k_\phi$=0), the warping stress makes a significant contribution to the pre-buckling stress. However, its contribution is reduced by the presence of anti-sag bars. The bending stress of zed section beams is less sensitive to anti-sag bars than those of channel section beams.

- The influence of the two spring stiffnesses on the stress and its distribution is influenced to be interfered by anti-sag bars. The influence range for the spring stiffness moves from a low value to a high value when the anti-sag bars are present. The maximum stresses for beams with anti-sag bars are smaller than those for beams without anti-sag bars, particularly when the translational and rotational spring stiffnesses are very small.

- In terms of the generated stresses, it appears that the best location for fixing (that is, the loading line) is close to the centre of the flange for zed section beams and on the web central line for channel section beams, which provide the lowest tensile and compressive stresses.

## 8.3 LOCAL BUCKLING BEHAVIOUR

The local buckling behaviour of cold-formed zed and channel section beams, under pure bending and a uniformly distributed transverse load, has been investigated using the available approaches. A novel method is presented for analysing the elastic local buckling behaviour of cold-formed zed and channel section beams with partial-lateral restraint from the metal sheeting when subjected to a uniformly distributed transverse load. The following major conclusions can be drawn based on the investigated examples:

- For beams restrained both translationally and rotationally, subjected to pure bending, the moment capacities calculated using both BS 5950 and the finite strip method show the influence of the cross-section dimensions, hereby indicating the importance of considering the interactions between the individual elements.

- For beams under a uniformly distributed transverse load in the purlin-sheeting system, the local buckling loads $q_{cr}/q_y$ of the zed section beams increase with increase in the translational spring stiffness, but decrease with the increased rotational spring stiffness. Furthermore the influence of the translational and rotational spring stiffnesses occurs only over a limited range of stiffness values. The local buckling loads $q_{cr}/q_y$ of the channel section beams decrease with the increase of translational spring stiffness, but increase with increased rotational spring stiffness. Warping stress has significant influence on the local buckling loads; however, the influence is reduced by the increase of both translational and rotational spring stiffnesses. As far as local buckling is concerned, the best location for fixing (that is, the loading line) is close to the

centre of the flange for zed section beams and on the web central line for channel section beams, hereby providing the highest local buckling loads.

## 8.4 SEMI-ANALYTICAL FINITE STRIP METHOD

The local and distortional buckling behaviour of the cold-formed steel zed and channel section beams, subjected to a uniformly distributed load, has been investigated using a semi-analytical method. The focus of the study is on the local and distortional buckling, for which the existing results are only for sections subjected to pure compression and/or pure bending.

The results from this study have shown that for local buckling there is no practical difference in the critical loads for the same cross section between pure bending and uniformly distributed loading. Thus, the approach introduced in Chapter 4 is still valid. For distortional buckling, however, remarkable differences were found between the two loading cases. The critical load for uniformly distributed loading is higher than that for the corresponding pure bending. This difference decreases with increase in the beam length. Furthermore, for either local buckling or distortional buckling, the beam subjected to pure bending exhibits the multi-wave buckling mode of equal wavelength, while the beam subjected to uniformly distributed loading exhibits a multi-wave buckling mode of unequal wavelengths.

## 8.5 LATERAL-TORSIONAL BUCKLING

An analytical model is presented for predicting the lateral-torsional buckling of cold-formed zed and channel section beams partially-laterally restrained by metal sheeting and subjected to uniformly distributed transverse loading. The following conclusions can be drawn from the investigation:

- The use of interval anti-sag bars is a very effective way of increasing the buckling resistance of the beam. However the position of the anti-sag bars should take into account the influence of the boundary condition. In general, it

is more effective to use anti-sag bars in the simply supported beams than in the fixed beams.

- The warping stress is found to have a significant influence on the critical load for lateral-torsional buckling of the partially-laterally restrained zed section beams when the purlin is fixed at least at one end and no anti-sag bars are present. For a simply supported purlin or a purlin with anti-sag bars, the effect of the warping stress on the critical load for lateral-torsional buckling is almost negligible. Warping stress does not have influence on the lateral-torsional buckling of channel section beams.

- Loading position has a remarkable influence on the critical buckling load. The highest critical load is found when the loading point is closer to the shear centre for zed sections. For channel section, however, the lowest critical load is found when the loading point is closer to the shear centre.

- The rotational spring stiffness has more influence on the lateral-torsional buckling loads than the translational spring stiffness. The influence of the translational spring stiffness on the critical load only occurs over a limited range of stiffness values, while that of the rotational spring stiffness occurs when $k_\phi/(Ey_k^2)$ is larger $10^{-7}$.

## 8.6 INTERACTION BETWEEN LATERAL-TORSIONAL BUCKLING AND LOCAL BUCKLING

A novel analytical model is developed for determining the load capacity for the lateral-torsional buckling of statically indeterminate zed purlins (a single span beam with one or two ends fixed), with partial lateral restraint from metal sheeting, when subjected to a uniformly distributed uplift load. The model takes account the influence of the "softening" of the section stiffness due to local buckling and/or local material yielding. The analytical model together with the numerically or experimentally obtained curves describing the local stiffness softening, can be used to determine the

critical load for lateral-torsional buckling of the statically indeterminate purlin. The study has reached to the following conclusions:

- For long span purlins lateral-torsional buckling occurs first and so the local stiffness softening need not be considered when analyzing the lateral-torsional buckling.

- For intermediate span purlins, local buckling occurs first and thus the analysis of lateral-torsional buckling needs to consider the local stiffness softening, that is, there is an interaction between the local and lateral-torsional buckling.

- For short span purlins, local buckling occurs much earlier than the lateral-torsional buckling and so the moment resistance at the fixed support becomes very weak when the lateral-torsional buckling occurs. Therefore for the sake of simplicity the fixed beam may be regarded as a simply supported beam for carrying out the analysis of lateral-torsional buckling without considering the local buckling.

## 8.7 SUGGESTIONS FOR FUTURE STUDY

The work conducted in this thesis has identified several areas where further research may be required:

**Various cross sections**

The introduced analytical model based on the energy method can only be applied to the beams with zed or channel sections with straight corners. Further study can be carried out for the cold-formed steel beams with various cross sections considering the effects of details, like round corners.

**Local buckling/yielding relationship between the moment and the angle of rotation**

One of the most important findings of this investigation was the analysis of the interaction of lateral-torsional buckling and local buckling/yielding. It is

recommended that there should be further examination of the local buckling/yielding relationship between the moment and the angle rotation for cold-formed steel beams, which may involve more related experiments and finite element analyses, to make more general conclusions that can improve the performance of the presented approach.

**Friendly interface computer program**

The full study has been coded into a computer-based analysis program (MATLAB) that can be used to analysis local, distortional and lateral-torsional buckling of zed and channel section beams. It is suggested that the performance of the program can be further improved by upgrading to a friendly interface computer program-stand alone version, which would become a more efficient tool for design engineers.

**Optimum design of cold-formed steel beams**

An important advantage of cold-formed steel is the great flexibility of cross-sectional shapes and sizes available to the structural steel designer. However, the lack of standard optimized shapes makes the selection of the most economical shape very difficult. Therefore, it is suggested that the optimization of cold-formed steel beams should be carried out using the approaches developed in this thesis together with an optimization tool so that a set of optimum sections that can be easily accessed for structural steel designers and steel manufacturers.

# REFERENCE


1. American Iron and Steel Institute. 1996. Specification for the design of cold-formed steel structural members; Washington.

2. American Iron and Steel Institute. 1999. Specification for the design of cold-formed steel structural members with commentary, 1996 (Suppl. 1).

3. American Iron and Steel Institute. 2001. North American Specification for the design of cold-formed steel structural members. November 9 draft ed.

4. American Iron and Steel Institute. 2004. Specification for the design of cold-formed steel structural members with commentary, Appendix 1: Design of Cold-Formed Steel Structural Members Using the Direct Strength Method.

5. American Iron and Steel Institute. Undated. Residential Steel Framing Manual. American Iron and Steel Institute. Chestertown, MD 21690, USA.

6. AS/NZS 4600. 1996. Standards Australia/Standards New Zealand. Cold-formed steel structures.

7. Badway Abu-Sena AB, Chapman JC and Davidson PC. 2001. Interaction between critical torsional flexural and lip buckling in channel sections. Journal of Constructional Steel Research 57(8):925-44.

8. Barsoum R and Gallagher R. 1970. Finite element analysis of torsional and torsional-flexural stability problems. International Journal of Numerical Methods in Engineering 2:335-52.

9. Beshara B and LaBoube RA. 2001. Pilot study: lateral braced C-sections under bending. Thin-Walled Structures 39(10):827-39.

10. Boresi AP, Chong KP and Saigal S. 2002. Approximate Solution Methods in Engineering Mechanics (2nd Edition). Wiley, New York.

11. Bradford MA. 2000. Strength of compact steel beams with partial restraint. Journal of Constructional Steel Research 53(2): 183-200.

12. BS 5950-5. 1998. Structural use of steelwork in building: Code of practice for the design of cold formed sections,BSI: Part 5. London: British Standards Institution.

13. Camotim D, Silvestre N, Goncalves R. and Dinis BP. 2004. GBT analysis of thin-walled members: new formulations and applications. International Workshop on Advances and Future Trends in Thin-Walled Structures Technology. Loughborough University, UK. 25 June, 137-68.

14. Chu XT, Li LY and Kettle R. 2004. The effect of warping stress on the lateral-torsion buckling of cold-formed zed purlins. Journal of Applied Mechanics 71(5):742-44.

15. Chu XT, Kettle R and Li LY. 2004. Lateral-torsion buckling analysis of partial-laterally restrained thin-walled channel-section beams. Journal of Constructional Steel Research 60(8):1159-75.

16. Cheung YK. 1976. Finite Strip Method in Structural Analysis, Pergramon Press.

17. Davies JM. 1998. Light gauge steel cassette wall construction. In: Nordic Steel Construction Conference. Bergen, 427-40.

18. Davies JM. 2000. Recent research advances in cold-formed steel structures. Journal of Constructional Steel Research 55(1-3):267-88.

19. Davies JM and Jiang C. 1996a. Design of thin-walled beams for distortional buckling. In: 13th Int. Specialty Conf. on Cold-Formed Steel Structures, St. Louis, Missouri, 141-53.

20. Davies JM and Jiang C. 1996b. Design of thin-walled purlins for distortional buckling, In: TWS Bicentenary Conf. on Thin-Walled Structures, Strathclyde, Glasgow.

21. Davies JM, Jiang C and Leach P. 1994a. The analysis of restrained purlins using generalised beam theory, in: 12th Int. Speciality Conf. on Cold-formed Steel Structures. St. Louis, Missouri, Oct. 18-19:109-20.

22. Davies JM and Leach P. 1994. First-order generalised beam theory. Journal of Constructional Steel Research 31:221-41.

23. Davies JM, Leach P and Heinz D. 1994b. Second-order generalized beam theory. Journal of Constructional Steel Research 31:221-41.

24. Davies JM, Leach P and Kelo E. 1995. The use of light gauge steel in low and medium rise modular buildings. In: Proc. 3rd Int. Conf. on Steel and Aluminum Structures, ICSAS'95. Istanbul.

25. Davies R, Pedreschi R and Sinha BP. 1996. The shear behavior of press-joining in cold-formed steel structures. Thin-Walled Structures 25(3):153-70.

26. EC 3 part 1.3. 1996. Design of steel structures: general rules. European Committee for Standardization (CEN). ENV 1993-1-3.

27. Ghosn AA and Sinno RR. 1995. Governing stresses in Z-purlin lap joints. Journal of Structural Engineering, ASCE 121(12):1735-41.

28. Gotluru BP, Schafer BW and Pekoz T. 2000. Torsion in thin-walled cold-formed steel beams. Thin-Walled Structures 37(2)127-45.

29. Grundy P. 1990. Effect of pre- and post-buckling behaviour on load capacity of continuous beams. Thin-Walled Structure 9(1-4):407-15.

30. Hancock GJ. 1994. Design of cold-formed steel structures (To Australia Standard AS 1538-1988), 2nd ed. North Sydney, Australia: Australia Institute of Steel Construction.

31. Hancock GJ. 1995. Design for distortional buckling of flexural members, In: Proc. 3rd Int. Conf. on Steel and Aluminum Structures, Istanbul. (also in Thin-walled Structures 1997;27:3-12).

32. Hancock GJ. 1997a. The behaviour and design of cold-formed purlins. Journal of Constructional Steel Research 15(3):2-16.

33. Hancock GJ. 1997b. Light gauge construction. Prog Struct Engng Mater 1(1):25-30.

34. Hancock GJ. 2003. Cold-formed steel structures. Journal of Constructional Steel Research, 59(4): 473-487.

35. Hoglund T. 1995. Strength of butt welds in extra high strength steel. In: Proc. 3rd Int. Conf. on Steel and Aluminum Structures. Istanbul.

36. Hoglund T. 1998. Design of light gauge studs with perforated webs. In: Nordic Steel Conference, Bergen.

37. Jönsson J. 1999a. Distortional warping functions and shear distributions in thin-walled beams. Thin-Walled Structures 33(4):245-68.

38. Jönsson J. 1999b. Distortional theory of thin-walled beams. Thin-Walled Structures 33(4):269-303.

39. Karren KW. 1967. Corner Properties of Cold-Formed Steel Shapes. ASCE, Journal of the Structural Division, Vol.93, ST1.

40. Karren KW. And Winster G. 1967. Effects of Cold-forming on Light-Gage Steel Members. ASCE, Journal of the Structural Division, Vol.93, ST1.

41. Kesti J. and Davies JM. 1999. Local and distortional buckling of thin-walled short columns. Thin-Walled Structures 34(2):115-34.

42. Kesti J. and Makelainen P. 1998. Design of gypsum-sheathed perforated wall studs. In: Second World Conf. on Steel in Construction. San Sebastian.

43. Kitipornchai S and Trahair NS. 1980. Buckling properties of monosymmetric I-beams. Journal of Structural Division, ASCE 106(ST5): 941-57.

44. LaBoube RA, Yu WW, Deshmukh SU and Uphoff CA. 1999. Crippling capacity of web elements with openings. Journal of Structural Engineering 125(2):137-41.

45. Laine M and Tuomala M. 1999. Testing and design of gravity loaded steel purlins restrained by sheeting. Journal of Constructional Steel Research 49(2):129-38.

46. Lau SCW and Hancock GJ. 1987. Distortional buckling formulas for channel columns. Journal of Structural Division, ASCE 113(5):1063-78.

47. Leach P and Robinson P. (1993). The behaviour of purlins subjected to wind uplift. The Structural Engineers 72(14):250-2.

48. Lee J and Kim SE. Lateral buckling analysis of thin-walled laminated channel-section beams. Composite Structures. 56:391-99.

49. Li LY. (1999). Test reports of cold-formed steel sections. Department of Civil Engineering, Aston University, Birmingham.

50. Li LY. (2004) Lateral-torsional buckling of cold-formed zed-purlins partial laterally restrained by metal sheeting. Thin-Walled Structures. 42(7):995-1011.

51. Lindner J and Aschinger R. 1994. Load-carrying capacity of cold-formed beams subjected to overall lateral-torsional buckling and local plate buckling. Journal of Constructional Steel Research 31(2-3): 267-87.

52. Loughlan J. 1996. The buckling of composite stiffened box sections subjected to compression and bending. Composite Structures 35:101-16.

53. Loughlan J. 2004. Thin-Walled Structures Advances in Research, Design and Manufacturing Technology. Proceedings of the Fourth International Conference on Thin-Walled Structures in Loughborough, UK, 22-24 June.

54. Loughlan J. 2004. Thin-Walled Structures Recent Advances and Future Trends in Thin-Walled Structures Technology. International Workshop in Loughborough, UK, 25 June.

55. Lucas RM, Al-Bermani FGA and Kitipornchai S. 1997a. Modeling of cold-formed purlin-sheeting systems. Part 1: Full model. Thin-Walled Structures 27(3):223-43.

56. Lucas RM, Al-Bermani FGA and Kitipornchai S. 1997b. Modeling of cold-formed purlin-sheeting systems. Part 2: Simplified model. Thin-walled Structures 27(4):263-86.

57. Makelainen P. and Kesti J. 1999. Advanced method for lightweight steel joining. Journal of Constructional Steel Research 49:107-16.

58. Moore DB. 1988. Load tests on full scale cold formed steel roofs. Part 1 – Sigma purlin system (BR 122); Part 2 – Zed purlin system (BR 123); Part 3 – Zeta purlin system (BR 124), Building Research Establishment.

59. Oden JT. 1967. Mechanics of Elastic Structures. McGraw-Hill Book Company, New York.

60. Pasternak H. and Komann S. 1999. Shear behavior of rosette joints - Tests and finite element analysis. In: Proc. Conf. Eurosteel '99. CVUT Prague, 479-82.

61. Pekoz T. 1999. Possible future developments in the design and application of cold-formed steel. Keynote lecture, "ICSAS'99", 4th Int. Conf. Light-weight Steel and Aluminum Structures. Espoo, Finland 20-23 June.

62. Pekoz T and Soroushian P. 1982. Behaviour of C- and Z-purlins under wind uplift, Report No.81-2, Department of Civil Engineering, Cornell University, Ithaca, NY.

63. Pi YL, Put BM and Trahair NS. 1998. Inelastic lateral buckling of cold-formed channel and z-section beams. Second International Conference on Thin-walled Structures. Singapore: Research and development; 205-12.

64. Put BM, Pi YL, Trahair NS. 1998. Lateral buckling tests on cold-formed channel beams. Research Report No R767, Centre for Advanced Structural Engineering, Department of Civil Engineering, the University of Sydney, Australia.

65. Put BM, Pi YL and Trahair NS. 1999. Bending and torsion of cold-formed channel beams. Journal of Structural Engineering 25(5):540-6.

66. Reissner E. 1989. Lateral buckling of beams. Computer & Structures 33(5):1289-1306.

67. Rhodes J. 1991. Design of Cold Formed Steel Members. Elsevier Applied Science.

68. Rhodes J and Lawson RM. 1993. Design of structures using cold formed steel sections. SCI Publication, 089. The Steel Construction Institute.

69. Rondal J. 2000. Cold formed steel members and structures-general report. Journal of Constructional Steel Research 55(1-3):155-8.

70. Rusch A and Lindner J. 2001. Remarks to the direct strength method. Thin-Walled Structures 39:807-20.

71. Schardt R. 1982. Cold Formed Thin Walled Purlins, Concluding Report, Institut fur Staik, Technische Hochschule, Darmstadt.

72. Schafer BW. 2001a. Thin-walled column design considering local, distortional and euler buckling. Structural Stability Research Council, Annual Technical Session and Meeting.

73. Schafer BW. 2001b. Experiments on braced thin-walled cold-formed steel C and Z beams in flexure. Recent Advances in Stability of Structural Components and Systems Combined ASCE-EMD and ASME Summer Conference, San Diego, California.

74. Schafer BW. 2001c. Elastic buckling analysis of thin-walled members using the classical finite strip method, CUFEM Version 2. Johns Hopkins Univerisity.

75. Schafer BW. 2003a. Elastic buckling analysis of thin-walled members using the classical finite strip method, CUFSM Version 2.6, Johns Hopkins University.

76. Schafer BW. 2003b. Advances in Direct Strength Design of Thin-Walled Members, Proceedings, Advances in Structures Conference, ASSCCA03, 22-25 June, Sydney, Australia.

77. Schafer BW and Pekoz T. 1998. Direct strength prediction of cold-formed steel members using numerical elastic buckling solutions. In: Thin-walled Structures, Research and Development. Proc. 2nd International Conf on Thin-walled Structure, Singapore, Dec. Elsevier, 137-44.

78. Schafer BW and Pekoz T. 1999a. Local and distortional buckling of cold-formed steel members with edge stiffeners flanges. ICSAS'99, 4th International Conference on Light-weight Steel Aluminum Structures, Espoo, Finland, 20-23 June, 89-97.

79. Schafer BW and Pekoz T. 1999b. Laterally braced cold-formed steel flexural members with edge stiffened flanges. Journal of Structural Engineering 125(2):118-27.

80. Singer J, Arbocz J and Weller T. 1998. Buckling Experiments. John Wiley & Sons, Chichester.

81. Sokol L. 1979. Calcul des panes en section Z. Construction Metallique (1):34-52.

82. Sokol L. 1996. Stability of cold formed purlins braced by steel sheeting. Thin-Walled Structures 25(4):247-68.

83. Tarnai T. 1979. Variational methods for analysis of lateral buckling of beams hung at both ends. International Journal of Mechanical Science. 21:329-37.

84. Thomopoulos KT, Mistakidis ES, Koltsakis EK and Panagiotopoulos PD. 1996. Softening behaviour of continuous thin-walled steel beams. Two numerical methods. Journal of Constructional Steel Research 36(I):1-13.

85. Timoshenko SP and Gere JM. 1961. Theory of Elastic Stability. McGraw-Hill Book Company, New York.

86. Toma T and Soetens F. 1987. Research for the mechanical behaviour of cold-formed sections and drafting of design rules: final report. BI-87-100/63.5.5481. TNO Building and Construction Research, Delft.

87. Toma T and Wittenmann K. 1994. Design of cold-formed purlins and rails restrained by sheeting. Journal of Constructional Steel Research 31(2/3):149-68.

88. Trahair NS. 1993. A survey of tests on cold formed purlins. International Workshop on Cold Formed Steel Structures, University of Sydney.

89. Trahair NS and Bradford MA. 1998. The behavior and design of steel structures to AS4100 (3rd ed.), E & FN Spon, London.

90. Vlasov VZ. 1961. Thin-Walled Elastic Beams. Israel Program for Scientific Translations. Jerusalem. Israel.

91. Von Karman T, Sechler EE and Donnell LH. 1932. The strength design of thin plates in compression. Transactions ASME 54:54-5.

92. Walker AC. 1995. Design and Analysis of Cold-formed Sections. International Textbook Company Ltd., London.

93. Williams FW and Jemah AK. 1987. Buckling curves for leatically supported columns with varying axial force, to predict lateral buckling of beams. Journal of Constructional Steel Research 72: 133-47.

94. Winter G. 1947. Strength of thin steel compression flanges. Cornell University Engineering Experimental Station. Print No.32.

95. Winter G. 1968. Thin-Walled Structures- Theoretical Solutions and Test Results. Preliminary Publications of the Eight Congress of IABSE:101-12.

96. Ye ZM, Kettle R, Li LY and Schafer B. 2002. Buckling behaviour of cold-formed zed-purlins partially restrained by steel sheeting. Thin-Walled Structures 40(10):853-64.

97. Ye ZM, Kettle R and Li LY. 2004. Strength analysis of cold-formed zed-purlins partially restrained by steel sheeting. Computer & Structures 82(9-10): 731-9.

98. Young B and Hancock GJ. 2001. Design of cold-formed channels subjected to web crippling. Journal of Structural Engineering 127(10):1137-44.

99. Yu WW. 1985. Cold-Formed Steel Design. J. Wiley and Sons, New-York.

100. Zienkiewicz OC and Taylor RL. 2000. The Finite Element Method (5th Edition). Butterworth Heinemann, Oxford.

# APPENDIX

## A.1 FINITE STRP METHOD

### A.1.1 Plane Stress Stiffness Matrix

$$[K_{uv}] = t\begin{bmatrix} \left(\frac{a_s E_1}{2b_s} + \frac{a_s b_s k_m^2}{6}\right) & & & & \textit{symmetric} \\ \left(\frac{a_s k_m \nu_x E_2}{4} - \frac{a_s k_m G}{4}\right) & \left(\frac{a_s b_s k_m^2 E_2}{6} + \frac{a_s G}{2b_s}\right) & & & \\ \left(-\frac{a_s E_1}{2b_s} + \frac{a_s b_s k_m^2 G}{12}\right) & \left(-\frac{a_s k_m \nu_x E_2}{4} - \frac{a_s k_m G}{4}\right) & \left(\frac{a_s E_1}{2b_s} + \frac{a_s b_s k_m^2 G}{6}\right) & & \\ \left(\frac{a_s k_m \nu_x E_2}{4} + \frac{a_s k_m G}{4}\right) & \left(\frac{a_s b_s k_m^2 E_2}{12} - \frac{a_s G}{2b_s}\right) & \left(-\frac{a_s k_m \nu_x E_2}{4} + \frac{a_s k_m G}{4}\right) & \left(\frac{a_s b_s k_m^2 E_2}{6} + \frac{a_s G}{2b_s}\right) \end{bmatrix}$$

where: $k_m = \frac{m\pi}{a_s}$ $E_1 = \frac{E_x}{1-\nu_x \nu_y}$ $E_2 = \frac{E_y}{1-\nu_x \nu_y}$

### A.1.2 Bending Stiffness Matrix

$$[K_{w\theta}] = \begin{bmatrix} \left(\frac{13a_s b_s}{70}k_m^4 D_y + \frac{12a_s}{5b_s}k_m^2 D_{xy} + \frac{6a_s}{5b_s}k_m^2 D_1 + \frac{6a_s}{b_s^3}D_x\right) & & & \textit{symmetric} \\ \left(\frac{3a_s}{5}k_m^2 D_1 + \frac{a_s}{5}k_m^2 D_{xy} + \frac{3a_s}{b_s^2}D_x + \frac{11a_s b_s^2}{420}k_m^4 D_y\right) & \left(\frac{a_s b_s^3}{210}k_m^4 D_y + \frac{4a_s b_s}{15}k_m^2 D_{xy} + \frac{2a_s b_s}{15}k_m^2 D_1 + \frac{2a_s}{b_s^3}D_x\right) & & \\ \left(\frac{9a_s b_s}{140}k_m^4 D_y - \frac{12a_s}{5b_s}k_m^2 D_{xy} - \frac{6a_s}{5b_s}k_m^2 D_1 - \frac{6a_s}{b_s^3}D_x\right) & \left(\frac{13a_s b_s^2}{840}k_m^4 D_y - \frac{a_s}{5}k_m^2 D_{xy} - \frac{a_s}{10}k_m^2 D_1 - \frac{3a_s}{b_s^2}D_x\right) & \left(\frac{13a_s b_s}{70}k_m^4 D_y + \frac{12a_s}{5b_s}k_m^2 D_{xy} + \frac{6a_s}{5b_s}k_m^2 D_1 + \frac{6a_s}{b_s^3}D_x\right) & \\ \left(-\frac{13a_s b_s^2}{840}k_m^4 D_y + \frac{a_s}{5}k_m^2 D_{xy} + \frac{a_s}{10}k_m^2 D_1 + \frac{3a_s}{b_s^2}D_x\right) & \left(\frac{3a_s b_s^3}{840}k_m^4 D_y - \frac{a_s b_s}{15}k_m^2 D_{xy} - \frac{a_s b_s}{30}k_m^2 D_1 + \frac{a_s}{b_s}D_x\right) & \left(-\frac{11a_s b_s^2}{420}k_m^4 D_y - \frac{a_s}{5}k_m^2 D_{xy} - \frac{3a_s}{5}k_m^2 D_1 - \frac{3a_s}{b_s^2}D_x\right) & \left(\frac{a_s b_s^3}{210}k_m^4 D_y + \frac{4a_s b_s}{15}k_m^2 D_{xy} + \frac{2a_s b_s}{15}k_m^2 D_1 + \frac{2a_s}{b_s}D_x\right) \end{bmatrix}$$

where: $k_m = \frac{m\pi}{a_s}$

### A.1.3 Geometric Stiffness Matrix (CUFSM)

$$[K_g] = C\begin{bmatrix} 70(3T_1+T_2) & 0 & 70(T_1+T_2) & 0 & 0 & 0 & 0 & 0 \\ & 70(3T_1+T_2) & 0 & 70(T_1+T_2) & 0 & 0 & 0 & 0 \\ & & 70(T_1+3T_2) & 0 & 0 & 0 & 0 & 0 \\ & & & 70(T_1+3T_2) & 0 & 0 & 0 & 0 \\ & & & & 8(30T_1+9T_2) & 2b(15T_1+7T_2) & 54(T_1+T_2) & -2b(7T_1+6T_2) \\ & \textit{symmetric} & & & & b^2(5T_1+3T_2) & 2b(6T_1+7T_2) & -3b^2(T_1+T_2) \\ & & & & & & 24(3T_1+10T_2) & -2b(7T_1+15T_2) \\ & & & & & & & b^2(3T_1+5T_2) \end{bmatrix}$$

where: $C = \dfrac{b_s(m\pi)^2}{1680a_s}$;

### A.1.4 Coupled Geometric Stiffness Matrix Of Semi-Analytical Finite Strip Method

$$[K_{gmn}] = C\begin{bmatrix} 70(3T_1+T_2)k_c & 0 & 70(T_1+T_2)k_c & 0 & 0 & 0 & 0 & 0 \\ & 70(3T_1+T_2)k_s & 0 & 70(T_1+T_2)k_s & 0 & 0 & 0 & 0 \\ & & 70(T_1+3T_2)k_c & 0 & 0 & 0 & 0 & 0 \\ & & & 70(T_1+3T_2)k_s & 0 & 0 & 0 & 0 \\ & & & & 8(30T_1+9T_2)k_c & 2b(15T_1+7T_2)k_c & 54(T_1+T_2)k_c & -2b(7T_1+6T_2)k_c \\ & & symmetric & & & b^2(5T_1+3T_2)k_c & 2b(6T_1+7T_2)k_c & -3b^2(T_1+T_2)k_c \\ & & & & & & 24(3T_1+10T_2)k_c & -2b(7T_1+15T_2)k_c \\ & & & & & & & b^2(3T_1+5T_2)k_c \end{bmatrix}$$

where: $C = \dfrac{b_s(mn)\pi^2}{210a_s}$; $k_c = \dfrac{1}{a_s^3}\int_0^{a_s}(a_s y - y^2)\cos\dfrac{m\pi y}{a_s}\cos\dfrac{n\pi y}{a_s}dy = \begin{cases} \dfrac{1}{12} - \dfrac{1}{(m+n)^2\pi^2} & \text{if } (m-n)=0 \\ -\dfrac{1}{\pi^2}\left[\dfrac{1}{(m+n)^2} + \dfrac{1}{(m-n)^2}\right] & \text{if } (m-n) \text{ is even} \\ 0 & \text{if } (m-n) \text{ is odd} \end{cases}$

$$k_s = \frac{1}{a_s^3}\int_0^{a_s}(a_s y - y^2)\sin\frac{m\pi y}{a_s}\sin\frac{n\pi y}{a_s}dy = \begin{cases} \dfrac{1}{12} + \dfrac{1}{(m+n)^2\pi^2} & \text{if } (m-n)=0 \\ \dfrac{1}{\pi^2}\left[\dfrac{1}{(m+n)^2} - \dfrac{1}{(m-n)^2}\right] & \text{if } (m-n) \text{ is even} \\ 0 & \text{if } (m-n) \text{ is odd} \end{cases}$$

### A.1.5 Finite Strip Program Scheme

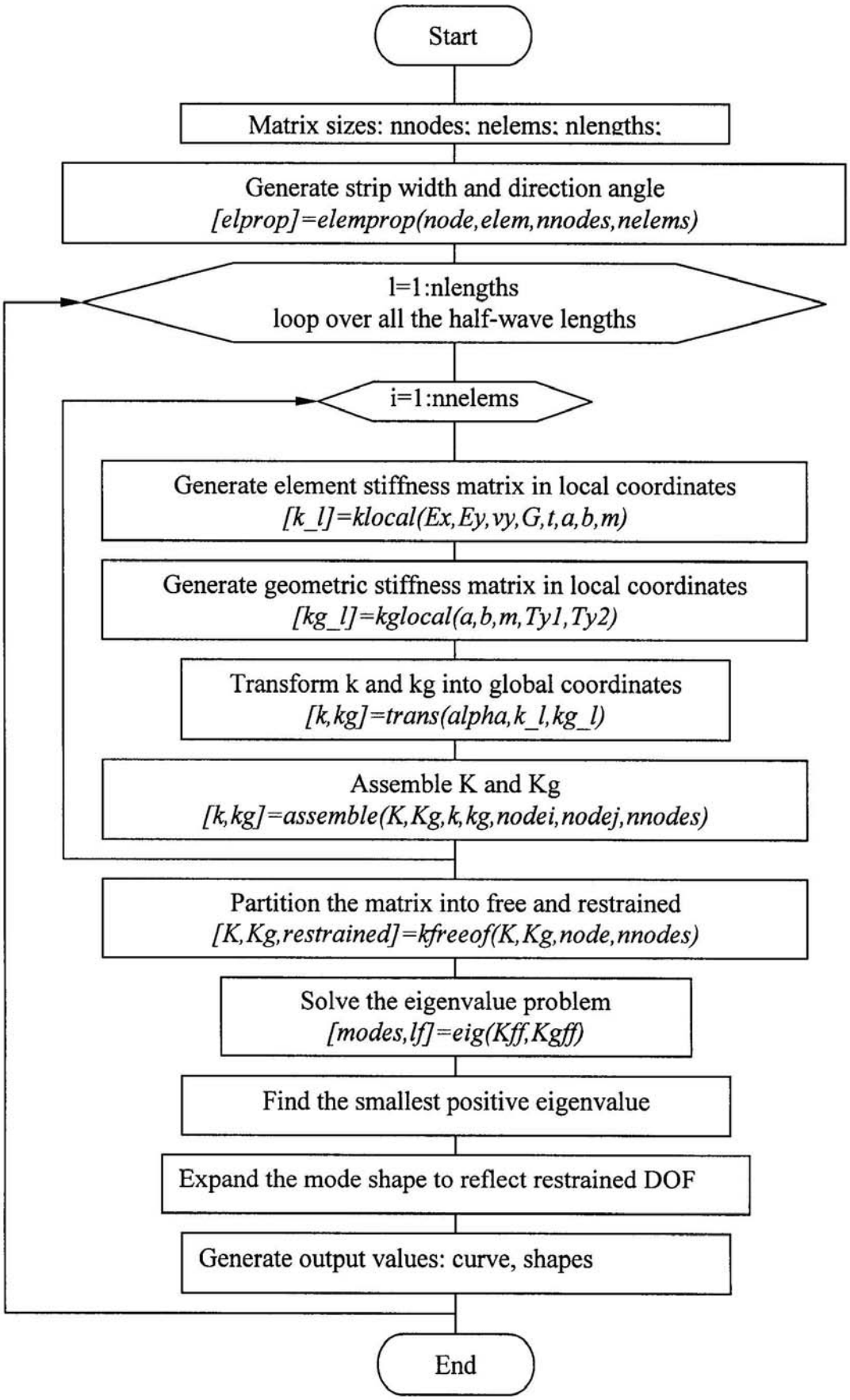

# A.2 EXPRESSIONS OF SECTION PROPERTIES

## A.2.1 Zed Sections

⇨ $\omega$ **and** $\overline{\omega}(=\frac{1}{k}\int_0^k \omega ds = \sum_{i=1}^{5}\overline{\omega}_i)$

| Plane Element $A_i$ | $s$ | $\omega_i$ | $\overline{\omega}_i$ |
|---|---|---|---|
| $A_1$ | $[0\ \ c]$ | $bs$ | $\frac{bc^2}{2}$ |
| $A_2$ | $[c\ \ c+b]$ | $bc+\frac{d}{2}(s-c)$ | $b^2(c+\frac{d}{4})$ |
| $A_3$ | $[c+b\ \ c+b+d]$ | $bc+\frac{db}{2}$ | $\frac{bd}{2}(2c+d)$ |
| $A_4$ | $[c+b+d\ \ c+2b+d]$ | $bc+\frac{db}{2}-\frac{d}{2}[s-(c+b+d)]$ | $b^2(c+\frac{d}{4})$ |
| $A_5$ | $[c+2b+d\ \ 2c+2b+d]$ | $bc-b[s-(c+2b+d)]$ | $\frac{bc^2}{2}$ |

Note: $A_i$ = the individual plane element of the cross section; $b,c,d$ = flange, lip and web width along the middle line respectively; $\omega$ = the sectorial co-ordinate; $k = 2b+2c+d$;

$$\overline{\omega} = \sum_{i=1}^{5}\overline{\omega}_i = bc + \frac{b}{2}\frac{d^2-2c^2+db}{2c+2b+d}.$$

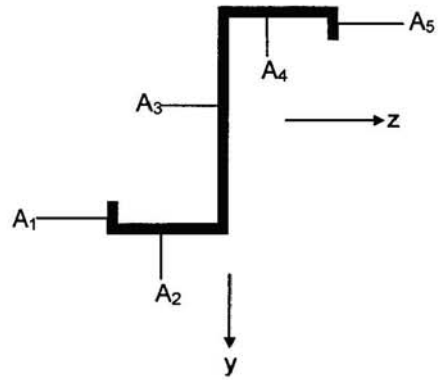

⇨ **Expression of $\mathbf{D_w}(=\sum_{i=1}^{5} D_{wi})$**

| | Plane Element | | $D_{wi} = \int_{A_i} (\overline{\omega} - \omega_i)(y^2 + z^2) dA_i$ |
|---|---|---|---|
| $A_i$ | $y$ | $z$ | |
| $A_1$ | [d/2-c d/2] | $b$ | $\frac{tbc}{24}[2c^2(c-d) + (12b^2 + 3d^2 - 6dc + 4c^2)\frac{d^2 + db + 2bc + dc}{2c + 2b + d}]$ |
| $A_2$ | $d/2$ | [-b 0] | $\frac{tb^2}{48}[2db^2 + (3d^2 + 4b^2)\frac{d^2 - 4c^2 - 2dc}{2c + 2b + d}]$ |
| $A_3$ | [-d/2 -d/2] | 0 | $-\frac{tbd^3}{24}\frac{2c^2 + 2dc + db}{2c + 2b + d}$ |
| $A_4$ | -d/2 | [0 b] | $\frac{tb^2}{48}[2db^2 + (3d^2 + 4b^2)\frac{d^2 - 4c^2 - 2dc}{2c + 2b + d}]$ |
| $A_5$ | [-d/2 -d/2+c] | $b$ | $\frac{tbc}{24}[2c^2(c-d) + (12b^2 + 3d^2 - 6dc + 4c^2)\frac{d^2 + db + 2bc + dc}{2c + 2b + d}]$ |

Note: $D_w$ is a constant in Eq.(6.9).

### A.2.2 Channel Sections

⇨ **Section Properties**

| | |
|---|---|
| Centroid $e_2$ | $b\dfrac{2c+b}{2c+2b+d}$ |
| Second moment about $y$ axis $I_y$ | $t[2b'^2c+\dfrac{2}{3}b'^3+\dfrac{2}{3}e_2^3+e_2^2d]$ |
| Second moment about $z$ axis $I_z$ | $\dfrac{t}{12}(8c^3-12dc^2+6d^2c+6d^2b+d^3)$ |
| Shear centre $e_1$ | $\dfrac{tbcd^2}{I_z}(\dfrac{1}{2}+\dfrac{b}{4c}-\dfrac{2}{3}\dfrac{c^2}{d^2})$ |
| Torsion constant $J$ | $\dfrac{t^3}{3}(2b+2c+d)$ |
| Warping constant about shear centre $C_w$ | $\dfrac{tb^2}{6}(4c^3+3d^2c+6dc^2+bd^2)-I_ze_1^2$ |
| Warping constant about centroid $I_\omega=\int_A(\bar{\omega}-\omega)^2dA$ | $C_w+I_{\omega z}/I_z$ |
| Sectorial product of inertia about $z$ axis $I_{\omega z}=-\int_A\omega ydA$ | $t[-bd(\dfrac{d^2}{4}-d'^2)+\dfrac{2b'}{3}(\dfrac{d^3}{8}-d'^3)-\dfrac{bd^2}{4}(b+2e_2)-\dfrac{e_2d^3}{12}]$ |

Note: $b,c,d$ = flange, lip and web width along the middle line respectively;
$b'=b\text{-}e_2$; $d'=d/2\text{-}c$; $e=e_1+e_2$;
$A=t(2b+2c+d)$;
$\omega$ and $\bar{\omega}$ are given next.

⇨ $\omega$, $\overline{\omega}$ **and** $\omega_s$, $\overline{\omega}_s$

| $A_i$ | Plane Element $s$ | $\omega_i$ | $\overline{\omega}-\omega_i$ | $\omega_{si}$ | $\overline{\omega}_s-\omega_{si}$ |
|---|---|---|---|---|---|
| $A_1$ | [0 c] | $-b's$ | $-bd+b'y$ | $-b''s$ | $-bd+b''y$ |
| $A_2$ | [c c+b] | $-b'c-\frac{d}{2}(s-c)$ | $-de_2-\frac{d}{2}z$ | $-b''c-\frac{d}{2}(s-c)$ | $\frac{d}{2}(e_1-e_2)-\frac{d}{2}z$ |
| $A_3$ | [c+b c+b+d] | $-b'c-\frac{db}{2}-e_2[s-(b+c)]$ | $-e_2y$ | $-b''c-\frac{db}{2}+e_1[s-(b+c)]$ | $e_1y$ |
| $A_4$ | [c+b+d c+2b+d] | $-b'c-e_2d-\frac{d}{2}[s-(c+d)]$ | $de_2+\frac{d}{2}z$ | $-b''c+e_1d-\frac{d}{2}[s-(c+d)]$ | $-\frac{d}{2}(e_1-e_2)+\frac{d}{2}z$ |
| $A_5$ | [c+2b+d 2c+2b+d] | $-2e_2d-b'(s-2b)$ | $bd+b'y$ | $2e_1d-b''(s-2b)$ | $bd+b''y$ |

Note: $A_i$ = the individual plane element of the cross section;

$b''=b+e_1$; $k=2b+2c+d$;

$\overline{\omega}=-b'c-\frac{d}{2}(b+e_2)$; $\overline{\omega}_s=-b''c-\frac{d}{2}(b-e_1)$.

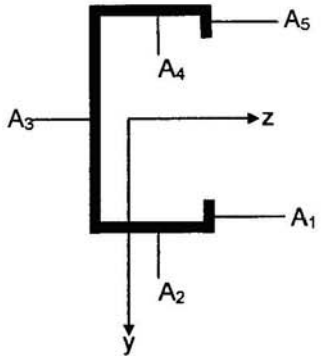

## A.3 MATLAB PROGRAMMING SCHEME OF ENERGY METHOD

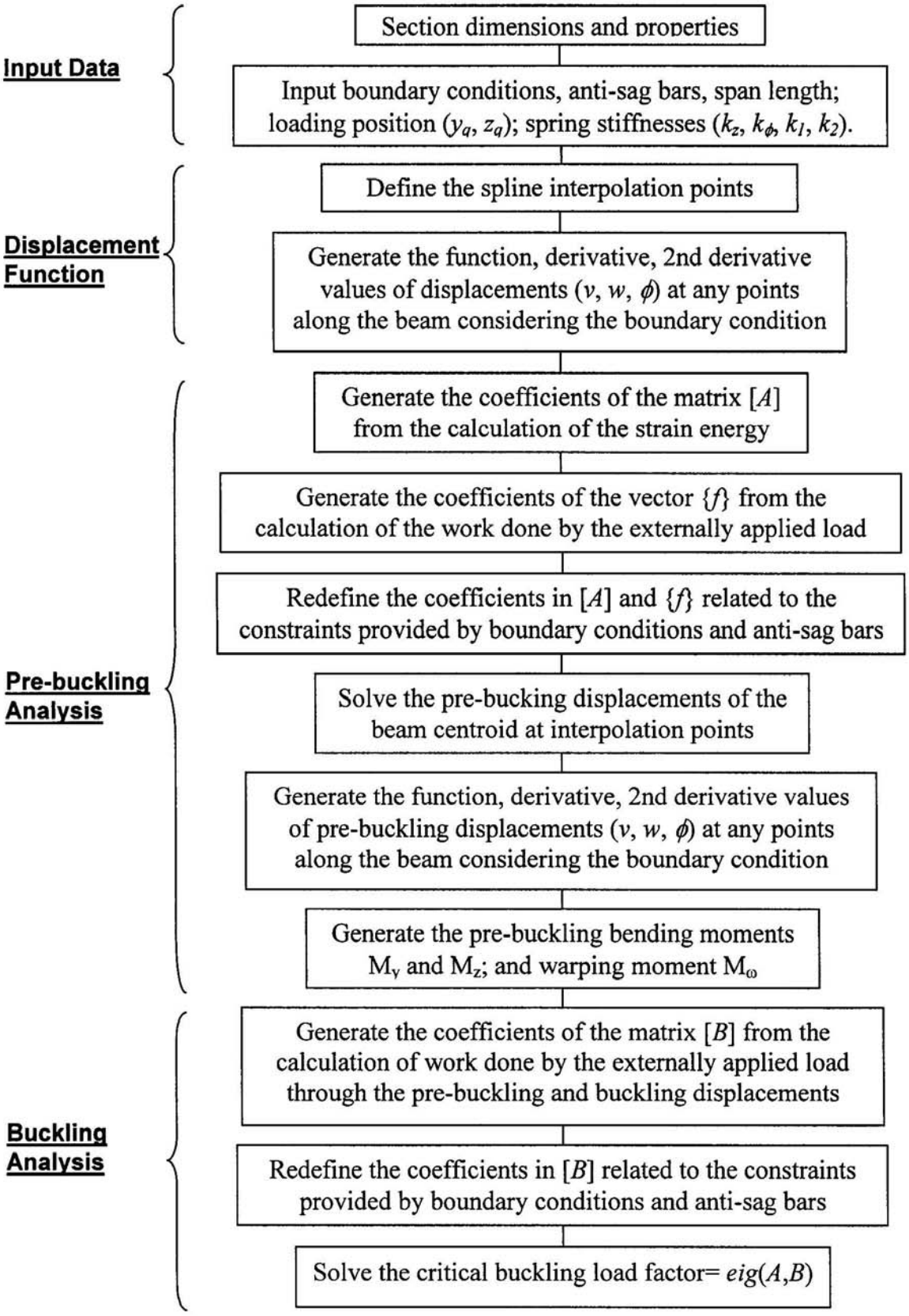

## A.4 PUBLICATIONS

1. Xiao-ting Chu, Zhi-ming Ye, Roger Kettle and Long-yuan Li, Local and distortional buckling of cold-formed zed-section beams under uniformly distributed transverse loads.

2. Xiao-ting Chu, Zhi-ming Ye, Roger Kettle and Long-yuan Li, Buckling behaviour of cold-formed channel sections under uniformly distributed loads, Thin-Walled Structures.(in press).

3. Xiao-ting Chu, Jamie Rickard and Long-yuan Li, Influence of lateral restraint on lateral-torsional buckling of cold-formed steel purlins. Thin-Walled Structures. (Submitted in Jun 2004)

4. Xiao-ting Chu, Long-yuan Li, Roger Kettle and Dinh-Tuan Tran, Local buckling behaviour of partially restrained cold-formed steel sections. Building and Environment. (Submitted in Jul 2004)

5. Xiao-ting Chu, Long-yuan Li and Roger Kettle, Lateral-torsion buckling of cold-formed steel purlins with partial restraint. 4th International Conference on Thin-Walled Structures (ICTWS 4). Loughborough University, Loughborough, Leicestershire, UK, 2004:265-72.

6. Xiao-ting Chu, Long-yuan Li and Roger Kettle, The effect of warping stress on the lateral-torsion buckling of cold-formed zed purlins. Journal of Applied Mechanics. 2004;71(5):742-44.

7. Xiao-ting Chu, Roger Kettle and Long-yuan Li, Lateral-torsion buckling analysis of partial-laterally restrained thin-walled channel-section beams. Journal of Constructional Steel Research. 2004;60(8):1159-75.